



Critical Review of Subsea Structures in the Gulf of Guinea

**“Finite Element Analysis to Predict the Behaviour of a
Multi-Layer Non-Bonded Flexible Pipe Under Hydrate Plug
in a Static Application”**

A thesis submitted to the University of Strathclyde

In partial fulfilment of the requirement for the award of a degree of Doctor of
Philosophy (PhD)

By

OWOLABI, GBENGA AYODELE

Department of Mechanical & Aerospace Engineering,

University of Strathclyde

Glasgow, UK

ABSTRACT

The concept of blockages in a non-bonded flexible pipe during oil and gas mining operations have over the years shown to be a persistent problem, and the need for a standardized remediation approach is paramount. This research work studies the behaviour of non-bonded flexible pipes with methane hydrate blockage under the influence of diverse loading conditions. Nonlinear tri-dimensional finite element models were used on two (2) scenarios, blocked and unblocked conditions. These models recreate a seven-layer flexible pipe with two tensile armour layers, an external polymeric sheath, high strength tape, orthotropic equivalent carcass, and pressure armour layers with an internal polymeric sheath. With these models, several studies were conducted to verify the influence of key parameters on the instability phenomenon when the flexible pipe is under hydrate blockage. The internal pressure and compressive loads can be considered one of these parameters, and their variation causes a significant change in the stability response of the pipe layers. This work includes a detailed description of the finite element model and a case study where the non-bonded flexible pipe is blocked by methane hydrate. The procedure of this analysis is here described, along with the results.

For in-depth knowledge of hydrate formation and its consequences in flexible pipes, this thesis used ABAQUS, a standard finite element (FE), in modelling, simulating, and investigating a hydrate blocked and unblocked non-bonded flexible pipe. It is divided into two Samples, A and B, respectively, under the influence of various load conditions. FE model was adopted to investigate the effects of hydrate on the layers as were not detailed in America Petroleum Institute codes [1]. This was carried out under various conditions such as pipe with and without blockage at various pressure, forces (longitudinal and compressive) values, different hydrate lengths, coefficients of friction and stiffness constants.

In addition to the FE analysis, an experimental investigation was carried out on the samples and where necessary mathematical analyses were undertaken to reverify results. The studies carried out were to determine the non-bonded flexible pipes responses under certain load conditions. This determines the deformation, stress concentration on individual layers, making sure the results are within the recommended API standards, hoop, axial and radial stresses, reactive force, and contact pressure between the layers.

A simplified model was employed and a finer mesh to resolve the issue with the FE model. And progress the effect of the hydrate on the pipe layers.

Importantly, this present work considered and investigated a 7-layers 6" diameter non-bonded flexible pipe as a case study. The results were obtained from the numerical and experimental investigations, analysed, and presented accordingly. Obtained results showed a significant influence of methane hydrate on Sample A, while Sample B behaves normally under various load conditions. The detailed outcome and further research works are presented in this thesis.

ACKNOWLEDGEMENTS

Most notably, I give glory to almighty God for his infinite mercy upon me to enable the conclusion of this work.

My special sincere gratitude goes to Professor David Nash (supervisor) for his guides, unalloyed support, and clarity throughout the research works. I am very grateful to Dr Asraf Uzzaman for his continuous support in the review and advice often rendered.

Moreover, I would like to thank all the MSc interns that contributed directly and indirectly during the research work.

Lastly, I would like to give my gratitude to my wife, Mrs Owolabi Yetunde, my children Miss Owolabi Oluwabukunmi; Mr Owolabi Oluwaferanmi; and Mr Owolabi Toluwani for the special encouragement given during the PhD period. And, to my entire families, friends and colleagues, most especially Engr. Abba Yakubu (CEng), Engr. Akanni Adedayo (CEng), John Okoli and other numerous persons for their advices and laughs we have had together, the tough times we have made it through together, and for their continuous support throughout the rough time.

DECLARATION

I hereby sincerely declare that this thesis represents my work conducted under my supervisors, except where due acknowledgement is made, and that it has not been previously included in a thesis, dissertation or report submitted to this University or to any other institutions of higher learning for a degree, or other qualification whatsoever.

A handwritten signature in blue ink, appearing to be 'OWOLABI GBENGA AYODELE', enclosed within a circular scribble.

Signed.....

OWOLABI GBENGA AYODELE

PUBLICATIONS

TABLE OF CONTENTS

| | |
|--|--------------|
| ABSTRACT | II |
| ACKNOWLEDGEMENTS | III |
| DECLARATION | IV |
| PUBLICATIONS | V |
| TABLE OF FIGURES | X |
| LIST OF TABLES | XV |
| LIST OF EQUATIONS | XVII |
| NOTATIONS | XVIII |
| CHAPTER 1: INTRODUCTION | 1 |
| 1.1 BACKGROUND | 1 |
| 1.2 FLEXIBLE PIPE AND ITS LAYERS | 1 |
| 1.2.1 Carcass Layer | 2 |
| 1.2.2 Pressure Sheath | 3 |
| 1.2.3 Pressure Armour | 3 |
| 1.2.4 Tensile Armour | 4 |
| 1.2.5 High Strength Tape (HST) | 5 |
| 1.2.6 External Sheath | 6 |
| 1.3 FLEXIBLE PIPE APPLICATIONS AND HYDRATE FORMATION | 8 |
| 1.4 INTERNATIONAL OUTLOOK OF THE FLEXIBLE PIPE | 9 |
| 1.5 STATEMENT OF THE PROBLEMS | 10 |
| 1.6 RESEARCH AIM AND OBJECTIVES | 12 |
| 1.7 RESEARCH SCOPE AND ITS SIGNIFICANCE | 12 |
| 1.8 THESIS OUTLINE | 13 |
| CHAPTER 2: LITERATURE REVIEW | 14 |
| 2.1 INTRODUCTORY REMARKS | 14 |
| 2.2 RESEARCH REVIEW ON NON-BONDED FLEXIBLE PIPE AND STATE OF THE ART | 14 |
| 2.2.1 Numerical Analysis | 15 |
| 2.2.2 Analytical Analysis | 25 |
| 2.2.3 Experimental analysis | 33 |
| 2.3 RESEARCH REVIEW ON HYDRATE FORMATION | 37 |
| 2.3.1 Samim, Soroush Zarinabadi and Amir | 39 |
| 2.4 SUBSEA SYSTEM CONFIGURATION AND TECHNOLOGY | 41 |
| 2.4.1 Installation and maintenance of the structures | 44 |
| 2.4.2 General Subsea Challenges | 45 |
| 2.5 CONCLUDING REMARKS | 48 |
| CHAPTER 3: FLEXIBLE PIPE NUMERICAL MODELLING | 49 |
| 3.1 INTRODUCTION | 49 |
| 3.2 TYPES OF FLEXIBLE PIPE | 49 |

| | | |
|---------|---|-----------|
| 3.3 | CODES AND STANDARD PRACTICES | 49 |
| 3.3.1 | Failure mode and recommended practices API RP | 50 |
| 3.3.2 | Failure mode and recommended allowable degradation | 52 |
| 3.4 | FINITE ELEMENT ANALYSIS SUITABILITY | 52 |
| 3.5 | GEOMETRY AND ELEMENT | 54 |
| 3.6 | MATERIAL PROPERTIES | 58 |
| 3.7 | DEVELOPING THE METALLIC PARTS | 58 |
| 3.7.1 | TENSILE ARMOURS | 58 |
| 3.7.2 | Carcass and Pressure Armour | 64 |
| 3.8 | DEVELOPING THE NON-METALLIC PARTS | 67 |
| 3.8.1 | Pressure sheath, High Strength Tape, and Outer sheath layers | 67 |
| 3.9 | DEVELOPING THE HYDRATE BLOCKAGE | 68 |
| 3.9.1 | Hydrate Plug Properties and Dimension | 68 |
| 3.10 | GENERAL MESH | 68 |
| 3.11 | ASSEMBLY OF NON-BONDED FLEXIBLE PART LAYERS | 70 |
| 3.11.1 | Assembled Layers | 70 |
| 3.12 | INTERACTIONS AND CONSTRAINTS | 71 |
| 3.13 | LOAD AND BOUNDARY CONDITIONS | 72 |
| 3.13.1 | Load Cases and Boundary Conditions | 72 |
| 3.14 | SIMULATION AND EFFECT OF BLOCKAGE | 72 |
| 3.15 | MODEL RESULTS VALIDATION | 73 |
| 3.16 | CONCLUSION | 76 |
| | CHAPTER 4: EXPERIMENTAL INVESTIGATIONS | 77 |
| 4.1. | INTRODUCTORY REMARKS | 77 |
| 4.2. | TEST SPECIMENS | 77 |
| 4.2.1 | Description of non-bonded flexible pipe makeup and flexible pipe design basis | 77 |
| 4.3 | ANALYSIS OF THE TEST SPECIMENS | 78 |
| 4.3.1 | Operating History of the Sample | 79 |
| 4.4 | MATERIALS PROPERTIES | 80 |
| 4.5 | GENERAL TEST PROCEDURE | 81 |
| 4.6 | TENSILE TESTS OF NON-METALLIC LAYERS | 83 |
| 4.6.1 | Test specimen-pressure sheath | 83 |
| 4.6.2 | Test specimen-external sheath | 84 |
| 4.6.3 | Test specimen-high strength tapes (HST) | 85 |
| 4.7 | TENSILE TESTS OF METALLIC LAYERS | 86 |
| 4.7.2 | First armour layer | 87 |
| 4.7.2.1 | RESULTS – LAYER 4 (FIRST ARMOUR) | 87 |
| 4.7.2.3 | RESULTS – LAYER 5 (SECOND ARMOUR) | 88 |
| 4.7.3 | Test Specimen-Zeta layer (Pressure Armour) | 88 |
| 4.7.4 | Test Specimen-Carcass | 90 |
| 4.8 | CONCLUSION | 92 |
| 4.10 | FURTHER EXPERIMENTAL INVESTIGATION ON A 9-LAYER FLEXIBLE PIPE | 93 |
| 4.10.1 | Sample Specifications | 94 |

| | | |
|---|--|------------|
| 4.11 | EXPERIMENTAL INVESTIGATION | 95 |
| 4.11.3 | Tensile Testing Machine - Instron 8802 (250 kN) Fatigue Testing System | 97 |
| 4.11.4 | Instron – Fast Track 8800 | 98 |
| 4.11.5 | RDP Electronics Spring Transducer | 98 |
| 4.12 | METHODOLOGY AND OBSERVATIONS | 99 |
| 4.12.1 | Procedure for Compression Test | 99 |
| 4.13.1 | Compression Test Results | 100 |
| 4.12.2 | Tensile Test | 103 |
| 4.13.2 | Tensile Test Results | 104 |
| CHAPTER 5: NUMERICAL INVESTIGATIONS | | 107 |
| 5.1 | INTRODUCTORY REMARKS | 107 |
| 5.2 | CASE STUDY | 108 |
| 5.3 | APPLIED BOUNDARY FACTORS AND LOAD VALUES | 112 |
| 5.3.1 | Applied boundary factors | 112 |
| 5.3.2 | Applied load values | 112 |
| 5.4 | BLOCKAGE SIMULATION | 117 |
| 5.5 | CONCLUSION | 118 |
| CHAPTER 6: RESULTS AND DISCUSSIONS | | 120 |
| 6.1 | RESULTS | 120 |
| 6.2 | NUMERICAL INVESTIGATION RESULTS ANALYSIS | 121 |
| 6.2.1 | Load case 1: Internal Pressure | 121 |
| 6.2.2 | Load case 2: External Pressure | 132 |
| 6.2.3 | Load case 3: Internal Pressure and Compressive Force | 133 |
| 6.2.4 | Load Case 4: (a) Compressive Force (b) Pulling Force | 136 |
| 6.2.5 | Load Case 5: Variation of co-efficient of friction | 137 |
| 6.3 | EXPERIMENTAL INVESTIGATION RESULTS ANALYSIS | 137 |
| 6.4 | VALIDATION AND VERIFICATION | 142 |
| 6.4.1 | Interlocked Carcass | 142 |
| 6.5.2 | Tensile wires | 146 |
| 6.5.3 | Behaviours of Flexible Pipe Layers when subjected to a combined Load | 146 |
| 6.6 | EFFECTS OF REACTION FORCE ON THE FLEXIBLE PIPE LAYERS | 152 |
| 6.7 | CONCLUSIONS | 154 |
| CHAPTER 7: CONCLUSION AND RECOMMENDATION FOR FURTHER WORKS | | 156 |
| 7.1 | CONCLUSION | 156 |
| 7.2 | EXPERIMENTAL INVESTIGATION | 157 |
| 7.3 | NUMERICAL INVESTIGATION | 158 |
| 7.4 | RECOMMENDATION | 159 |
| 7.5 | SUGGESTION FOR FUTURE WORKS | 159 |
| REFERENCES | | 160 |
| APPENDIX A | | 164 |
| THE OUTLOOK OF FLEXIBLE PIPES USAGE GLOBALLY AND ON A CONTINENT BASIS | | 164 |
| Flexible pipe usage | | 164 |

| | |
|--|------------|
| Flexible pipe annual usage | 164 |
| Flexible pipe size distribution and usage | 165 |
| Flexible pipe usage based on Companies | 165 |
| Flexible pipe usage in Africa | 166 |
| Flexible pipe usage in Asia | 166 |
| Flexible pipe usage in Australia | 167 |
| Flexible pipe usage in Europe | 167 |
| Flexible pipe usage in North America | 168 |
| Flexible pipe usage in South America | 168 |
| APPENDIX B | 169 |
| ADOPTED APPROACH- FLOW CHART | 169 |
| APPENDIX C | 170 |
| LOAD CONDITIONS CONSIDERED | 170 |
| Load case 1: Internal Pressure | 170 |
| Load case 2: External Pressure | 171 |
| Load case 3: Internal Pressure and Compressive Force | 171 |
| Load Case 4: Compressive Force | 173 |
| APPENDIX D | 174 |
| VALIDATION OF JOURNALS | 174 |
| APPENDIX E | 184 |
| DATASHEET | 184 |
| SUMMARY OF THE RESEARCH ANALYSES ON NON-BONDED FLEXIBLE PIPE | 185 |

TABLE OF FIGURES

| | |
|--|----|
| Figure 1-1: Non-bonded flexible pipe | 2 |
| Figure 1-2: Conventional carcass structure for a non-bonded flexible pipe | 3 |
| Figure 1-3: Showing the Pressure Sheath layer | 3 |
| Figure 1-4: Typical pressure armour layer-interlocking wire profiles..... | 4 |
| Figure 1-5: Tensile Armour layer | 5 |
| Figure 1-6: High Strength Tape | 5 |
| Figure 1-7: External Sheath layer | 6 |
| Figure 1-8: Typical non-bonded flexible pipe structure | 7 |
| Figure 1-9: Conventional and new proposed technology, L-R..... | 8 |
| Figure 1-10: Model of Hydrate in Multiphase Flow | 9 |
| Figure 2-1: Bending Hysteresis loop obtained from Constitutive model | 16 |
| Figure 2-2: Ten layer's Riser | 17 |
| Figure 2-3: Section and model of carcass layer | 18 |
| Figure 2-4: Displacement vs Pulling load for normal contact stiffness variation..... | 20 |
| Figure 2-5: Displacement vs Pulling load for frictional coefficient variation | 21 |
| Figure 2-6: Axial Shortening of Flexible Pipe Under Axial Compression..... | 22 |
| Figure 2-7: Schematic diagram of curved and straight beams models | 24 |
| Figure 2-8: Critical load in different coefficient of friction at a pressure of 2MPa..... | 24 |
| Figure 2-9: Critical load in different pressure at a coefficient of friction of 0.04 | 25 |
| Figure 2-10: Pipe section load and deformation convention | 26 |
| Figure 2-11: Load applied to the boundaries of a generic plastic layer | 27 |
| Figure 2-12: Typical Design of Carcass Layers | 28 |
| Figure 2-13: Stress-Strain curve of the carcass..... | 29 |
| Figure 2-14: Sensitivity analysis maximum Von Misses Stress..... | 29 |
| Figure 2-15: Curved beam equilibrium..... | 30 |
| Figure 2-16: Carcass and Pressure reinforcement layers | 32 |
| Figure 2-17: Cross-section analysis: Axial force/Elongation curve | 33 |
| Figure 2-18: Assembly of prototype layers and specimen for bending test | 34 |
| Figure 2-19: Predicted bending moment (N.m)-curvature (1/m)..... | 35 |
| Figure 2-20: Bending characterization test-Sketch instrumentation..... | 36 |

| | |
|---|----|
| Figure 2-21: Characterization Test-Instrumentation..... | 37 |
| Figure 2-22: Three common hydrate unit crystal structures..... | 38 |
| Figure 2-23: Gas Hydrate Build-up in Pipeline and Eclipse pipes | 39 |
| Figure 2-24: Hydrate formation in natural gas pipeline..... | 40 |
| Figure 2-25: (a) Burst pipes on hydrate formation (b) Eliminating clogging in pipes | 41 |
| Figure 2-26: Eliminating clogging pipes with time | 41 |
| Figure 2-27: Typical Subsea layout | 42 |
| Figure 2-28: Manifold and the Subsea trees | 42 |
| Figure 2-29: Subsea production manifolds, flow lines and risers on the seabed..... | 43 |
| Figure 2-30: Configuration of deep-water subsea system | 43 |
| Figure 2-31: Typical Subsea Connection-Exxon Mobil, Nigeria..... | 44 |
| Figure 2-32: Blockage inside a flexible pipe suspected to be a pig..... | 46 |
| Figure 2-33: Bird cage' failure caused by excessive axial compression load | 47 |
| Figure 2-34: Riser base jumper-spool trenching and diagrammatic representation | 47 |
| Figure 3-1: Process flow chart | 54 |
| Figure 3-2: Schematic of a typical seven-layer flexible flowline..... | 55 |
| Figure 3-3: 8-Nodes linear brick Element (C3D8R)..... | 55 |
| Figure 3-4: 4-Nodes Shell Element (S4R)..... | 56 |
| Figure 3-5: Geometry of the Flexible Pipe | 57 |
| Figure 3-6: 40 tendons of first tensile and 44 tendons of second tensile wire..... | 60 |
| Figure 3-7: Tensile wires | 61 |
| Figure 3-8: Complete tensile wire armour | 61 |
| Figure 3-9: Tensile Wire Pitch..... | 62 |
| Figure 3-10: Tensile Wire with Orientation..... | 63 |
| Figure 3-11: The pitch and orientation of the tensile wire..... | 63 |
| Figure 3-12: Stress-Strain relationship | 65 |
| Figure 3-13: Modelling of Carcass Layer | 67 |
| Figure 3-14: The non-metallic part..... | 68 |
| Figure 3-15: Meshed Solid Elements..... | 70 |
| Figure 3-16: Meshed Shell Elements | 70 |
| Figure 3-17: Assembled meshed parts..... | 71 |

| | |
|---|----|
| Figure 3-18: Assembled parts | 71 |
| Figure 3-19: Application of constrained points RP-1 and RP-2 | 72 |
| Figure 3-20: Meshed and unmeshed blockage/plug | 73 |
| Figure 3-21: Displacement vs Pulling load for normal contact stiffness variation..... | 75 |
| Figure 3-22: Stress distribution on 9-layer's pipe | 75 |
| Figure 3-23: Stress distribution on 9-layer's pipe with blockage..... | 76 |
| Figure 4-1: 7-Layers non-bonded flexible pipes..... | 78 |
| Figure 4-2: Gas injection line segmentation and Schematic of the dissection | 79 |
| Figure 4-3: Subsea structural overview with ROV of flexible pipe failure | 80 |
| Figure 4-4: Dissection of the flexible pipe specimen | 81 |
| Figure 4-5: Tensile test Configuration and Setup | 81 |
| Figure 4-6: Flexible pipe sectional view of layers during analysis | 82 |
| Figure 4-7: Sample description of the investigated flexible pipe | 82 |
| Figure 4-8: Pressure Sheath assessment | 83 |
| Figure 4-9: Specimen location and orientation on the sheath..... | 83 |
| Figure 4-10: External Sheath stress | 84 |
| Figure 4-11: Shown the torn External Sheath..... | 85 |
| Figure 4-12: Overview of external layers damage..... | 85 |
| Figure 4-13: High Strength Tape assessment | 86 |
| Figure 4-14: Overview of Armour layer damage, bird cage and torsion..... | 86 |
| Figure 4-15: First armour layer assessment | 87 |
| Figure 4-16: First Armour Thickness Comparison..... | 87 |
| Figure 4-17: Second armour layer analysis | 87 |
| Figure 4-18: First Armour Thickness Comparison..... | 88 |
| Figure 4-19: Zeta Thickness Comparison..... | 89 |
| Figure 4-20: Pressure armour layer analysis..... | 89 |
| Figure 4-21: Zeta layer assessment..... | 90 |
| Figure 4-22: Carcass layer assessment | 90 |
| Figure 4-23: Damaged and Twisted Carcass | 91 |
| Figure 4-24: New Carcass Configuration | 91 |
| Figure 4-25: The flexible pipe with calliper | 94 |

| | |
|--|-----|
| Figure 4-26: Original Pipe Seal Solution..... | 95 |
| Figure 4-27: Annotated Original 3D Solution | 96 |
| Figure 4-28: Tensile test bar | 97 |
| Figure 4-29: Tensile Testing Machine - Instron 8802 (250 kN) Fatigue Test System..... | 97 |
| Figure 4-30: INSTRON - Fast Track 8800..... | 98 |
| Figure 4-31: RDP Electronic Spring Transducer..... | 99 |
| Figure 4-32: Transducer Setup for Recovery Strain..... | 100 |
| Figure 4-33: 100 kN Compression Test- Axial Compression Displacement | 101 |
| Figure 4-34:100 kN Compression Test - Hoop Expansion Displacement..... | 101 |
| Figure 4-35: 250 kN Compression Test 1 - Axial Compression Displacement | 102 |
| Figure 4-36: 250 kN Compression Test 2 - Hoop Expansion Displacement..... | 102 |
| Figure 4-37: Unloaded Compression Strain Recovery | 103 |
| Figure 4-38: Tensile testing arrangement before loading | 104 |
| Figure 4-39: 100 kN Tension Test - Axial Tension Displacement..... | 105 |
| Figure 4-40: Attempt at 250 kN Tensile Loading – Axial Tension Displacement..... | 105 |
| Figure 4-41: Reloading Up Until Failure After One Set of Bolts Sheared..... | 106 |
| Figure 5-1: Case Study sketched flexible pipe sample | 109 |
| Figure 5-2: Schematic diagram of the flexible pipe under investigation..... | 109 |
| Figure 5-3: Applied pressure during pigging..... | 109 |
| Figure 5-4: Application of constrained at points RP-1 and RP-2..... | 112 |
| Figure 5-5: Stress Contours under Operating Conditions - 3D Model..... | 114 |
| Figure 5-6: Stress Contours under Factory Test Pressure from the end - 3D Model..... | 114 |
| Figure 5-7: Stress contours under damage pull and comprehensive forces..... | 116 |
| Figure 5-8: Reaction Force and Displacement in Samples A and B..... | 119 |
| Figure 6-1: Pipe deformations-blocked (a), (c), (e) & (g); unblocked layers; (b), (d), (f) &(h)..... | 126 |
| Figure 6-2: Pipe Understudy-Similar deformation with Sample A and B..... | 127 |
| Figure 6-3: Samples A and B: Stress Distribution in Carcass layer | 129 |
| Figure 6-4: Samples A and B: Stress Distribution in Zeta layer..... | 131 |
| Figure 6-5: Sample A and B: Stress Distribution in First Tensile Wire layer | 133 |
| Figure 6-6: Sample A and B: Stress Distribution in Second Tensile Wire layer..... | 134 |
| Figure 6-7: Samples A and Sample B: Stress distribution-Carcass/External Pressure (EP) | 136 |

| | |
|---|-----|
| Figure 6-8: Samples A & B: Stress Distribution in Second Tensile Wire layer..... | 137 |
| Figure 6-9: Stress vs Time showing an increase in stress value over the set time duration | 138 |
| Figure 6-10: The deformation when applied a compressive force | 139 |
| Figure 6-11: The deformation of the flexible when pulling force was applied | 140 |
| Figure 6-12: Experimental value of stress and strain for pressure sheath layer | 142 |
| Figure 6-13: Experimental Value of stress and strain for Pressure Sheath layer..... | 143 |
| Figure 6-14: Experimental value of stress and strain for external sheath layer..... | 144 |
| Figure 6-15: Experimental Value of stress and strain for external sheath layer..... | 144 |
| Figure 6-16: Carcass layer with axial displacement | 148 |
| Figure 6-17:Sample A- Stress distribution in Second Tensile Wire layer..... | 150 |
| Figure 6-18: Sample A- Stress distribution in High Strength Tape (HST) layer..... | 150 |
| Figure 6-19: Sample A- Stress distribution in Pressure Sheath layer..... | 151 |
| Figure 6-20: Sample A- Stress distribution in External Sheath layer..... | 151 |
| Figure 6-21: Sample A- Stress distribution in Zeta or Pressure Armour Wire layer..... | 152 |
| Figure 6-22: Sample A- Stress distribution in First Tensile Wire layer | 152 |
| Figure 6-23: Sample A- Stress distribution in Carcass layer | 153 |
| Figure 6-24: Sample B- Stress distribution in Second Tensile Wire layer..... | 153 |
| Figure 6-25: Sample B- Stress distribution in Carcass layer | 154 |
| Figure 6-26: Sample B- Stress distribution in First Tensile Wire layer | 154 |
| Figure 6-27: Stress vs Time showing an increase in stress value over set time duration..... | 155 |
| Figure 6-28: Reaction Force vs Displacement of the Flexible Pipe | 157 |
| Figure 6-29: General effects of Plug in the investigated pipe | 158 |

LIST OF TABLES

| | |
|--|-----|
| Table 2-1: The specification of the riser layers used by J.Y Li and others..... | 18 |
| Table 2-2: 10-layers flexible pipe model stress results..... | 19 |
| Table 2-3: Subsea structure maintenance | 45 |
| Table 3-1: Checklist of failure modes for non-bonded flexible pipe; API17B..... | 51 |
| Table 3-2: Recommended allowable degradation for non-bonded flexible pipes; API 17B | 52 |
| Table 3-3: Non-bonded Flexible Parts, Model 1-C3D8R..... | 56 |
| Table 3-4: Non-bonded Flexible Parts, Model 2- S4R | 56 |
| Table 3-5: Flexible Layers geometry Properties..... | 57 |
| Table 3-6: Flexible Pipe material data | 58 |
| Table 3-7: Blockage (plug) properties | 68 |
| Table 3-8: Mesh sensitivity analyses- Problem Size | 69 |
| Table 3-9: Load Cases and Boundary Conditions | 73 |
| Table 4-1: Specification..... | 79 |
| Table 4-2: The layer-by-layer outcome Ultimate Tensile Stress (UTS), strain and yield stress | 83 |
| Table 4-3: Pressure Sheath layer experimental analysis result for the entire length | 84 |
| Table 4-4: External Sheath layer experimental analysis result for the entire length | 84 |
| Table 4-5: HST Observation result..... | 85 |
| Table 4-6: Elongation and tensile strength sample result | 88 |
| Table 4-7: Zeta Tensile Result..... | 89 |
| Table 4-8: Carcass layer experimental analysis..... | 92 |
| Table 4-9: Results of the investigated Layers..... | 92 |
| Table 4-10: Sample A and B Layers as it were | 93 |
| Table 4-11: Material Specifications..... | 94 |
| Table 4-12: Values of average measurements | 95 |
| Table 5-1: The working properties of the flexible pipe | 110 |
| Table 5-2: 7-Layers 6” Non-bonded flexible Pipe Properties | 110 |
| Table 5-3: Carcass and Pressure Armour Equivalent Properties | 110 |
| Table 5-4: Computation of the equivalent Materials for Carcass and Pressure Armour | 111 |
| Table 5-5: Loading values | 112 |
| Table 5-6: Stress for Sample A and Sample B layers..... | 113 |

| | |
|--|-----|
| Table 5-7: Hoop stress, Displacement and Reaction force for Sample A and Sample B layers | 115 |
| Table 5-8: Hoop stress, Displacement and Reaction force for Sample-A and Sample-B layers..... | 117 |
| Table 5-9: Simulated Blockage (Plug) Sizes | 118 |
| Table 5-10: Numerical stress values under various load conditions-Designed and Experimental..... | 120 |
| Table 6-1: Hoop stress and the Reaction force | 127 |
| Table 6-2: Mises's stress, Hoop stress and Displacement for Sample-A and Sample-B layers..... | 128 |
| Table 6-3: Hoop stress, Displacement and Reaction force for Sample A and Sample B layers | 135 |
| Table 6-4: Hoop stress, Displacement and Reaction force for Samples A & B layers..... | 138 |
| Table 6-5: The layer-by-layer stress and strain outcome..... | 141 |
| Table 6-6: Numerical stress values under various load conditions..... | 141 |
| Table 6-7: Computation Results of Hoop Stress using (a) Lame's (b) Normal Equations..... | 146 |
| Table 6-8: Comparison of Hoop Stress in Table 6-7 A and B..... | 147 |
| Table 6-9: Axial Stiffness for the Carcass and Pressure Armour | 147 |
| Table 6-10: Tension in the Tensile Wire | 149 |

LIST OF EQUATIONS

| | |
|--------------------|-----|
| Equation 2-1..... | 24 |
| Equation 2-2..... | 34 |
| Equation 2-3..... | 34 |
| Equation 2-4..... | 35 |
| Equation 2-5..... | 35 |
| Equation 2-6..... | 38 |
| Equation 2-7..... | 38 |
| Equation 2-8..... | 38 |
| Equation 2-9..... | 38 |
| Equation 2-10..... | 38 |
| Equation 2-11..... | 38 |
| Equation 3-1..... | 73 |
| Equation 3-2..... | 73 |
| Equation 3-3..... | 73 |
| Equation 3-4..... | 74 |
| Equation 3-5..... | 74 |
| Equation 3-6..... | 74 |
| Equation 3-7..... | 74 |
| Equation 3-8..... | 74 |
| Equation 3-9..... | 75 |
| Equation 3-10..... | 75 |
| Equation 5-1..... | 132 |
| Equation 6-1..... | 164 |
| Equation 6-2..... | 165 |
| Equation 6-3..... | 165 |
| Equation 6-4..... | 165 |
| Equation 6-5..... | 165 |
| Equation 6-6..... | 165 |
| Equation 6-7..... | 167 |
| Equation 6-8..... | 167 |
| Equation 6-9..... | 169 |
| Equation 6-10..... | 176 |

NOTATIONS

| | |
|---------------------------------------|---|
| COPPE | Alberto Luiz Coimbra Institute for Graduate Studies and Research in Engineering |
| AISI | American Iron and Steel Institute |
| API | American Petroleum Institute |
| F | Applied force (N) |
| AUV | Autonomous Underwater Vehicle |
| σ_a | Axial Stress (MPa) |
| P_z | Axial tension (kN) |
| M | Bending Moment (N.m) |
| M_x , and M_y | Bending moment components |
| Φ' and Θ' | Bending curvatures about the pipe x and y axes |
| BC | Boundary Condition |
| A & B | Constants in Lamé's equation |
| mu or μ | Coefficient of friction |
| CF + CS | Coefficient of Friction + Contact stiffness |
| CA | Comparative Assessment |
| CF | Compressive Force |
| CFD | Computational Fluid Dynamics |
| P_{cj} | Contact pressure between the j.th and the (j+1)-th layers |
| C3D8R | Continuum 3D 8 nodes Reduced elements |
| XLPE | Cross-Linked Polyethylene |
| A, J and L_p | Cross-sectional area, torsion constant and pitch length |
| k | Curvature |
| Sample A | Damaged Flexible Pipe sample |
| DECC | Decommissioning of Offshore Oil and Gas Installations |
| DoF | Degree of Freedom |
| ° | Degrees (Angle) |
| °C | Degrees Celsius |
| C_d | Discharge coefficient (0.82) |
| DP | Dynamic Positioning |
| τ | Effective tension (N) |
| E | Elastic material Stiffness (N/M ²) |
| D and L | Elongation or Compression and Original Length |
| EIA | Environmental Impact Assessment |
| $P_{(s)}, P_{(t)}, M_{(s)}$ and m_s | Equilibrium equation derived by Love (Power Law) |
| γ | Expansion coefficient (1) |
| EP | External Pressure (Pascal) |
| Exp | Experiment |
| p_{extj} | External pressure applied on the internal cylinder surface |
| UFRJ | Federal University of Rio de Janeiro |
| FDP | Field Development Program |
| FE | Finite Element |
| FEA | Finite Element Analysis |
| FPSO | Floating Production Storage Offloading |

| | |
|----------------------------------|--|
| Q | Flowrate (m ³ /s) |
| FL | Flowline Sections |
| ρ | Fluid density (kg/m ³) |
| FEED | Front End Engineering Design |
| GE | General Electric |
| GPa | Giga Pascal |
| HSE | Health and Safety Executive UK |
| HST | High Strength Tape |
| HST | High Strength Tapes |
| HDPE | High-Density Polyethylene |
| σ _h or H _s | Hoop Stress (MPa) |
| d _z | Incremental length (mm) |
| d _i | inner diameter (mm) |
| ID | Internal Diameter (m) |
| IP | Internal Pressure (bar or Pascal) |
| IP+CF | Internal Pressure + Compressive Force |
| p _{intj} | Internal pressure applied on the internal cylinder surface |
| r _i | Internal Radius (mm) |
| ISO | International Standard Organization |
| kN | Kilo Newton |
| H | Kinetic Hardening Modulus |
| α | Lay angle |
| r or R | Mean Radius (mm) |
| MDPE | Medium-Density Polyethylene |
| MN | Mega Newton |
| MPa | Mega Pascal |
| MPa | Mega-Pascals |
| EA, EI and G _j | membrane, torsional stiffness and bending |
| m | Meters |
| m/s | Meters per second |
| μm | Micron metre |
| mm | Millimeters |
| N.m | Newton Meter |
| N/mm ³ | Newtons per Millimeter Cubed |
| Num | Numerical |
| A_o | Orifice area (m ²) |
| OEMs | original equipment manufacturers |
| OSPAR | Oslo and Paris Convention for the Protection of the Marine Environment of the Northeast Atlantic |
| r _o | Outer Radius |
| OD | Overall Diameter |
| P _i | Pipe internal pressure |
| PA11 | Polyamide (Grade 11) |
| PE | Polyethylene |
| PVDF | Polyvinylidene Fluoride |

| | |
|----------------------------------|---|
| P_2 | Pressure (Pa) just downstream of the hydrate |
| P_1 | Pressure (Pa) just upstream of the hydrate |
| ΔP | The pressure difference between the upstream and downstream face of the hydrate |
| P_i | Pressure intensity at an internal radius of thick cylinder |
| P_o | Pressure intensity at an external radius of thick cylinder |
| σ_r | Radial Stress (MPa) |
| β | The ratio of Orifice to Pipe diameter (m) |
| RP-1 and RP-2 | Reference Points |
| ROV | Remote Operated Vehicle |
| RCA | Root Cause Analysis |
| RG | Riser Guide |
| I | Second Moment of area of the pipe |
| I_{eq} | The second moment of inertia |
| γ_x and γ_y | X-Z and Y-Z planes represented by the shear angles |
| P_x and P_y | Shear force components |
| S4R | Shell 4-noded Reduced elements |
| SD | Standard Diameter |
| nk | Stiffness Constant |
| F_{ipj} and F_{opj} | stress-resultants (per unit of pipe length) |
| I_r | Strip Thickness |
| I_t | Strip Width |
| SCMs | Subsea Control Modules |
| SEMs | Subsea Electronic Modules |
| surf 1 and surf 2 | Surface |
| T | Tensile Load |
| δ | Tensile Stress (MPa) |
| THI | Thermodynamic Inhibitor |
| h | Thickness |
| 3D | Three Dimensional |
| M_z | torque |
| F_j | Traction force supported by the layer |
| M_{tj} | Twisting moment supported by the layer |
| 2D | Two Dimensional |
| UTS | Ultimate Tensile Stress |
| Sample B | Undamaged Flexible Pipe sample |
| UCL | University College, London |
| UKCS | United Kingdom Continental Shelf |
| MMS | United State Mineral Management Services |
| V_2 | Velocity (m/s) just downstream of the hydrate |
| V_1 | Velocity (m/s) just upstream of the hydrate |
| VIV | Vortex Induce Vibration |
| σ | Yield strength |
| E_s , G_s and ν or ν | Young's modulus, Shear modulus and Poisson's ratio |

CHAPTER 1: INTRODUCTION

1.1 Background

A typical non-bonded flexible pipe comprises multiple layers made up of metallic and non-metallic materials, assembled as a unit structure that is commonly used in transporting or extracting oil, gas and water due to their mechanical and chemical properties [2]. The layers are free to interact with each other, either in static or dynamic positions when in operation.

The layered systems (flexible pipes) have existed for decades due to excellent performances and flexibility in their usage and application. At present, longer flexible flowlines are installed with fewer intermediate joints to minimize the danger or associated leakage issues at flange connections. Flexible pipes exist as bonded and non-bonded systems with the principal difference in the vulcanization process. The bonded layers are joined and do not slip over one another while the layers are contacted and interact with friction in a non-bonded flexible pipe [3]. The ideal system would enable flexibility of the structure against wear and tear due to ocean conditions, such as Vortex-Induced Vibration (VIV), Ocean current, waves, and blockages. However, many problems affect the pipes during operations in which this present research work attempts to investigate.

This chapter presents an overview of the design and composition of layered pipes and their usage within the oil and gas industry and highlights the need for research to address hydrate blockage issues.

1.2 Flexible pipe and its layers

Flexible pipes are made up of key layers, each of which has a specific function or functions and are designed explicitly for a given application. Moreover, there is an extensive range of possible layer combinations dependent on the exact nature of the application.

Typical flexible pipe layers comprise of the following elements: the tensile armours, external sheath, pressure sheath, interlocked steel carcass and pressure armour, as shown in Figure 1-1. The arrangement and composition (number, type, and sequence) of the layers are dependent on the composition of the fluid and the requirements of the process application. The following section describes the rationale of the design approach for each layer and any relevant issues on the material and design approach for that sub-component.

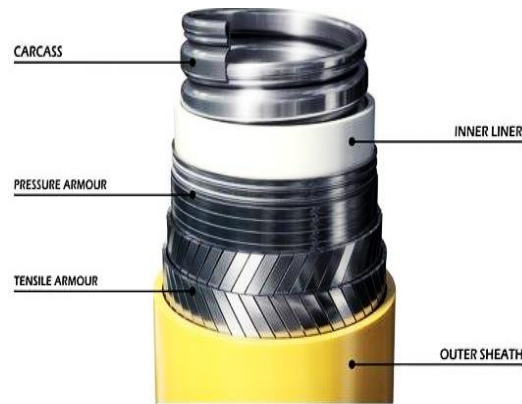


Figure 1-1: Non-bonded flexible pipe [2]

1.2.1 Carcass Layer

This layer is designed to guide against external hydrostatic pressure and perhaps the axial load, if present, being the innermost layer. Also, it gives the pipe radial support to resist external loads, which can lead to crushing. The carcass layer is not a leak-proof layer but provides some protection to the inner liner against erosion by solid particles and pigging (cleaning) of the pipe [4]. The collapse capacity of the carcass is determined by assuming that the external hydrostatic pressure is being applied directly to the inner liner to account that the pipe may be flooded because of a damaged outer sheath which could be determined through an annulus test. Generally, it is made from American Iron and Steel Institute (AISI) 304-grade stainless-steel by cold forming a flat stainless-steel strip to form an interlocked structure, as shown in Figure 1-2.

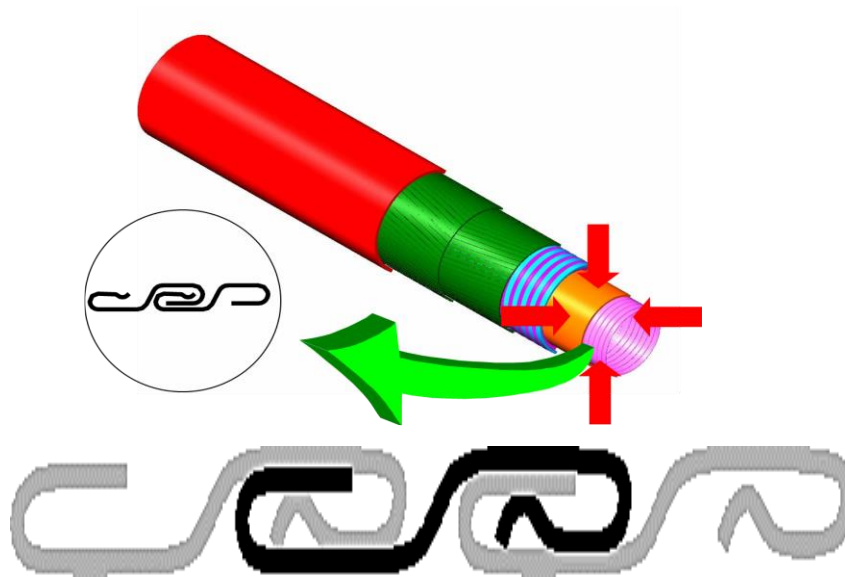


Figure 1-2: Conventional carcass structure for a non-bonded flexible pipe [5]

1.2.2 Pressure Sheath

The pressure sheath is made of either High-Density Polyethylene (HDPE) or Cross-Linked Polyethylene (XLPE), Polyamide (PA11), or Polyvinylidene fluoride (PVDF), which is based on a solid extrusion hence, making it serve as leak-proof.

Depending on design requirements, a sizeable number of pressure sheath layers can act as leakproof for the flowing liquid or gas and give further protection to both the carcass and pressure armour layers. It is essential to consider the pressure build-up between the layers of a multi-layered inner liner caused by gas seeping through the carcass layer since it is not leak-proof. This could cause the carcass layer to collapse if the pipe bore is de-pressurised. As shown in Figure 1-3, the pressure sheath determines the maximum allowable temperature of the flowing content, which is often between 60 and 140 °C. It is noted that the pipe under consideration for this research programme is made from polyamide and has a maximum allowable temperature of 80°C.

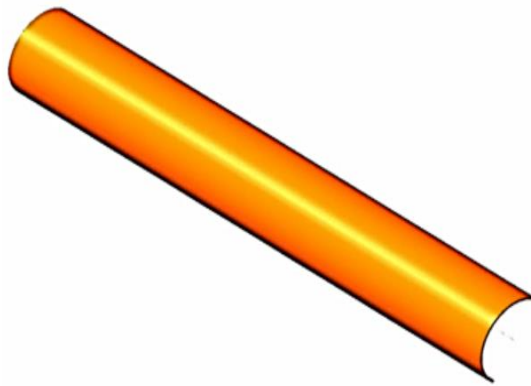


Figure 1-3: Showing the Pressure Sheath layer [5]

1.2.3 Pressure Armour

This layer protects the flexible pipe against internal pressure due to hoop and radial stresses and protects against external hydrostatic. The pressure armour can also be designed to give the carcass layer additional support and increase the overall collapse capacity of the pipe. Figure 1-4 shows the interlocking wire profiles typically used, which is the wires that make up the pressure armour fabricated from low-alloyed carbon steels with a high yield strength between 850 and 1000 MPa.

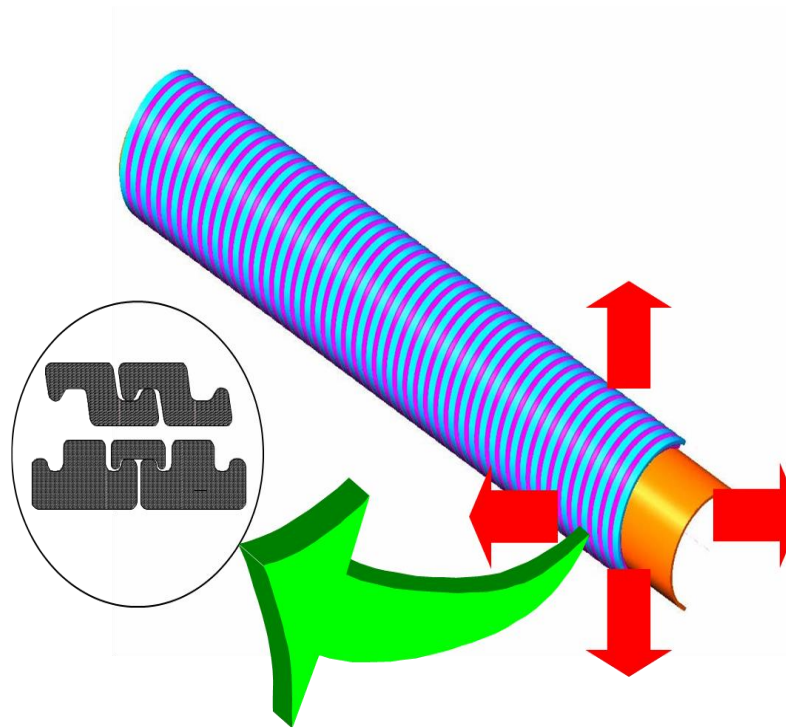


Figure 1-4: Typical pressure armour layer-interlocking wire profiles [5]

1.2.4 Tensile Armour

Otherwise known as the tensile wires, this layer often consists of two (2) strips wound in opposite directions, first and second tensile wires. However, this depends on the required configuration and customer demand. They provide strength in the axial direction of the pipe. The armour offers tensile strength capacity to help support the pipe weight and resist external tension and end cap loads. Like the pressure armour, it is made up of helically wound metallic wires, but with a relatively low lay angle, between 25 and 35°. The wires have a rectangular cross-section; however, round profiles may also be used depending on the application. Typical sizes can be 2 x 7 mm, as applicable in the present research, and 2.5 x 8 mm, 4 x 8 mm, 3 x 6 mm etc. and so on. The wires are cross-wound in pairs to ensure the best possible torsional balanced design for the pipe. This means that axial tension or compression loads do not cause significant twisting or torsion on the pipe. They are made of low-alloyed carbon steel, with very high yield strength, typically between 700 and 1500 MPa, as shown in Figure 1-5.

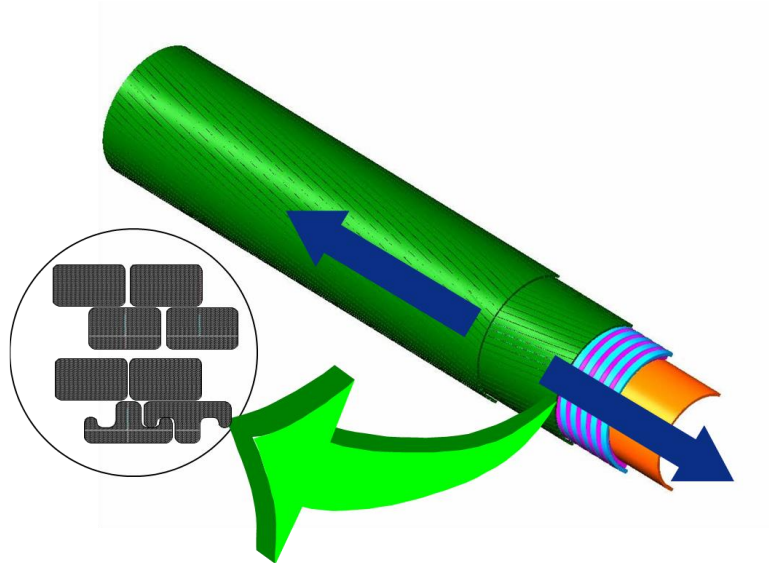


Figure 1-5: Tensile Armour layer [5]

1.2.5 High Strength Tape (HST)

It is often placed around the tensile armour layer(s) to limit the radial displacement of the tensile wires. This tape is a must-have for pipelines designed for marine applications. The external hydrostatic pressure is so high that it can cause sizeable axial compression loads in the pipe. The hydrostatic pressure difference between the pipe bore and the seawater determines the magnitude of this compression load. This compression load can cause a ‘bird cage’ failure, which is where the tensile wires relieve their compression stresses through radial buckling, causing the outer sheath to rupture. The tape is generally from a fibre-reinforced polymer material- Kevlar wound around the outermost tensile armour with a lay angle of 35°.

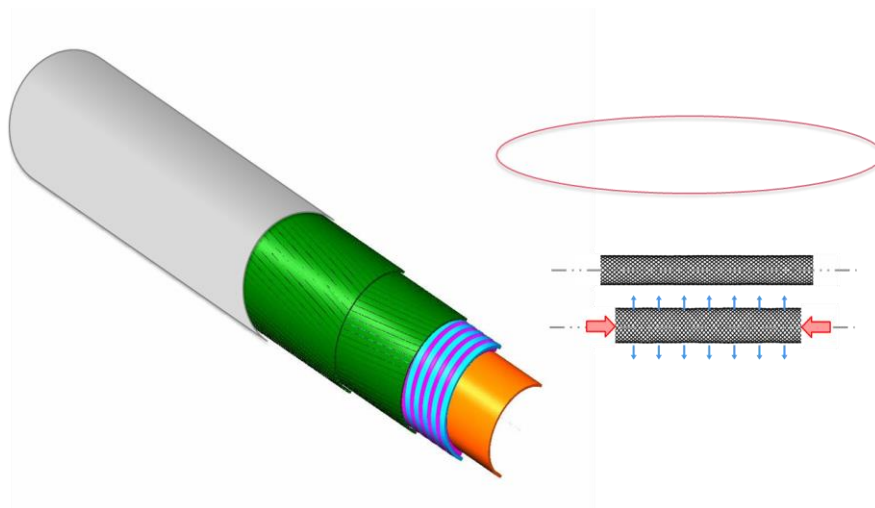


Figure 1-6: High Strength Tape [5]

1.2.6 External Sheath

This layer protects the other layers, especially the armour steel, as it is in contact with the seawater, reducing the risk of corrosion and providing mechanical protection to the outermost tensile armour layer. It is similar to the inner liner, made from a solid extrusion of either polyethylene (MDPE) or polyamide (PA11) material. MDPE is typically used in static applications, such as flowlines and jumpers, whereas PA11 is for dynamic applications, such as found in flexible pipes, due to its superior mechanical strength, as shown in Figure 1-7.

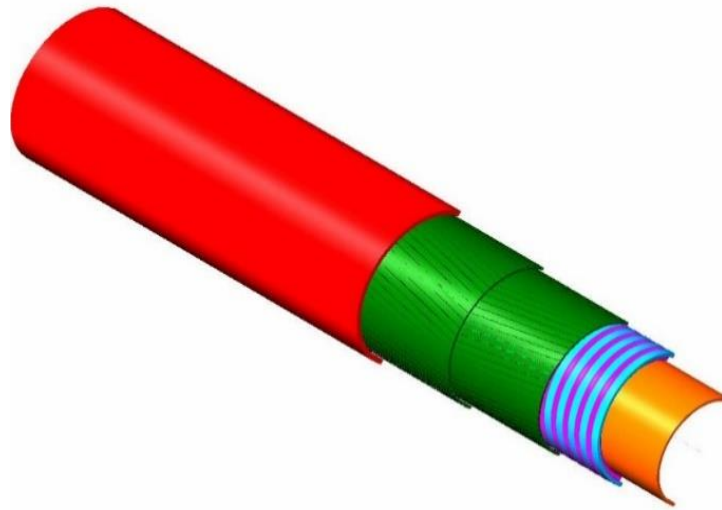


Figure 1-7: External Sheath layer [5]

In the oil and gas industry, flexible pipes are specifically to transport oil, gas, and water in offshore deep or shallow waters, common between wells and floating production units or, in some cases, as an export line for offloading [6]. They have low bending stiffness and high axial stiffness, the reason for their flexibility in nature.

Consequently, the combination of flexibility and strength make the flexible pipes suitable for the highly dynamic conditions on the seabed with both metallic and non-metallic parts.

The metallic armour layers provide the pipes with their strength and are structured in such a way to retain flexibility. There are also non-metallic polymer layers with low stiffness that seal the pipeline from the outside or inside environment. In the non-bonded flexible pipes, the layers are free to move within each other when subject to external loads. Figure 1-8 shows a 2D diagram of a typical non-bonded flexible pipe and the profiles of the various layers relative to Figure 1-1, which shows the 3D diagram.

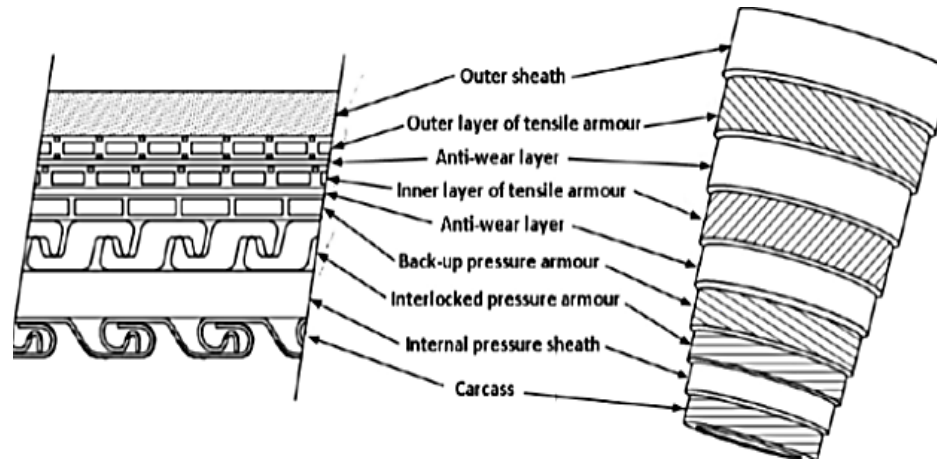


Figure 1-8: Typical non-bonded flexible pipe structure [7]

Industrial standards such as those produced by the American Petroleum Institute (API) are considered and applied to aid flexible pipe systems design. API Specification 17J [8] provides the safe design of non-bonded flexible pipes by considering the load conditions to determine the minimum thickness of the layers and materials. API Recommended Practice 17B [1] provides supplementary guidelines for designing and analysing flexible pipes [9]. There are many mechanical failure modes considered when designing or analysing a flexible pipe. These include but are not limited to the following:

1. The collapse of the carcass layer is due to excessive external pressure.
2. It was rupturing/Bursting of pressure or tensile armour layers due to excessive internal pressure.
3. Tensile failure unlocks wires in armour layers or ruptures polymer layers caused by excessive tensile loads or over bending.
4. The compressive failure of tensile armour layer, also known as ‘bird caging’.
5. Fatigue Failure.

Proper design of a flexible pipe should ensure that none of these failure modes occurs, however in practice, some factors primarily contribute to the failure of the layers. Examples are the corrosion of metallic layers and erosion of the carcass by the bore fluid. Another mechanism that can increase the risk of failure is the blockage of the pipe bore by gas hydrates.

Whilst flexible pipes have been extensively used for many years, and several design codes address the main failure modes. These documents do not address all failure modes, and as such, the present work aims to examine the effect of failure by the formation of gas hydrates, which can eventually lead to rupture and catastrophic failure.

1.3 Flexible Pipe Applications and Hydrate Formation

The applications of non-bonded flexible pipes in deepwater oil and gas production have witnessed tremendous growth since the 1990s because of their insulation properties, compatibility with chemicals, and flexibility against other available pipes [10]. They are commonly found in a water depth of around 2000 m; however, as the search for oil and gas goes deeper, there is an increase in the application of flexible pipes leading to changes in the technology to suit the requirements. Subsequently, General Electric (GE) has been working tirelessly on better technology as demand increases. This includes adopting composite material layers to enhance the tension capacity and reduce the structure's weights [11]. The approach will enable the possibility of producing a multi-section pipe assembly to suit any client requirements. Figure 1-9 shows the design currently proposed, alongside the current conventional flexible pipe technology.

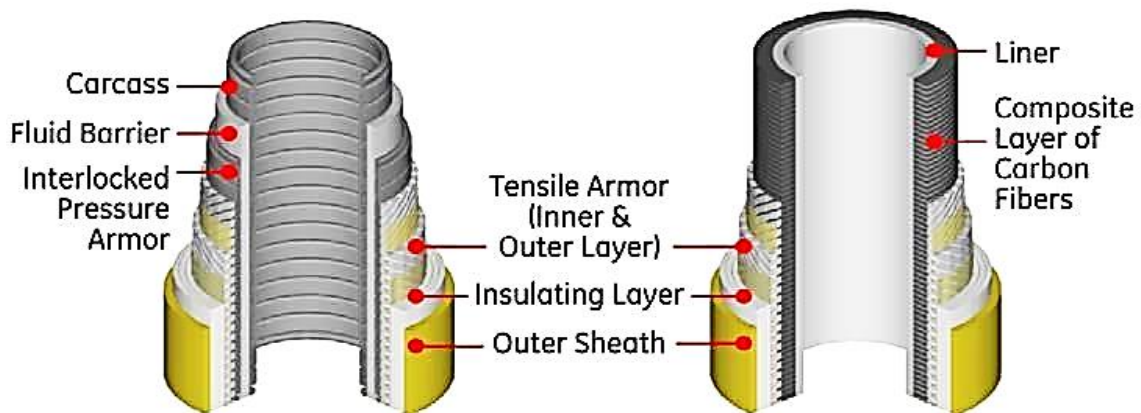


Figure 1-9: Conventional and new proposed technology, L-R [11]

In furtherance, studies have shown that flow assurance in flexible pipes has become an issue in offshore applications which requires proper attention. The flow is hindered by gas hydrates build-up that sometimes becomes enormous, complicated and impacts production operations. Hydrates are crystalline compounds like ice, composed of gas molecules trapped inside water molecules. And there are three (3) main types depending on the formation viz: Structure I (forms naturally), Structure II (forms in pipelines), and Structure H (forms in condensate) [12] [13]. The longer the flexible pipes, the probable the hydrated state is due to pressure drops along the length of the pipe. Chemical injection such as Thermodynamic Inhibitors (THI) prevents hydrate formation, as presented in Figure 1-10. Application of chemicals, though costly, can shift the equilibrium curve to more severe pressure and temperature conditions by allowing the pipeline to operate outside the hydrate forming region [14].

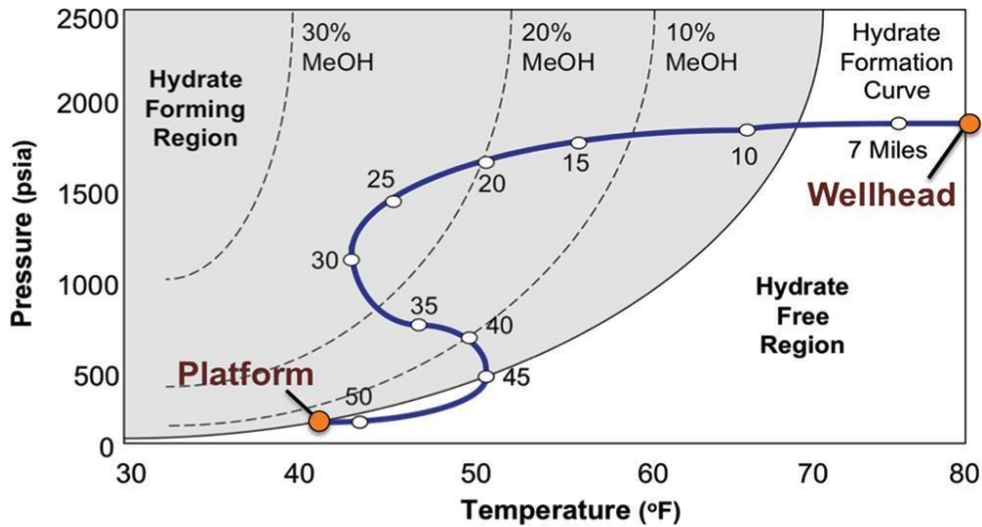


Figure 1-10: Model of Hydrate in Multiphase Flow [14]

1.4 International outlook of the flexible pipe

More than 6000 flexible pipes have existed and deployed globally since 1974. Available records show that Brazil uses flexible pipes with over 2600, followed by the UK with over 800 and Norway with over 600 flexible pipelines fabricated and installed. Globally, Petrobras has 2570 units of pipes while BP is above 400 units in their fields [10].

In Africa, Angola is leading the usage of flexible pipes with almost 400 in operation and the reason a flexible pipe plant was established in the country by Technip. At the same time, Nigeria has over 200 confirmed flexible pipes of various lengths (see Appendix A).

South America accounted for over 40% of the total flexible pipes manufactured and installed around the world. The pipelines have a pressure rating ranging from 0.7 to 103 MPa, with most non-bonded flexible pipes between 20.7 and 34.5 MPa. Although the pressure range has not changed significantly, the pressure rating for a given diameter was adjusted as required. The increase in diameter is due to larger extruders, and 1" pipes are almost extinct. So the range now is 2" to 18" (ID), though the more significant part is within the range of 4" to 12" while 6" flexible pipe is the most demanded. The operating temperatures are in the range of -10 and 130°C, with over 40% of the flexible pipes operating at 80 and 90°C, although about 5% work above 100 to 130°C.

There is an increase in the flexible pipes demand annually, with the maximum demand between 2007 - 2015 compared to 1974 -1993 [15]. It shows the importance of the usage and the cost and maintenance advantages over rigid pipes.

It is noted that much has changed over the years in the production of flexible pipes in terms of usage, application, operational requirement, configuration, types, pressure ratings, internal diameters, and materials. The most significant change in flexible pipe applications is the operating water depth with

50% of currently deployed systems in less than 500 m while the remaining 50% are in greater depths, and it is increasing. About 15% of pipes are now in more significant than 2000 m water depth. An increase in water depths raises concerns about overflow assurance challenges. It has necessitated the development of insulation and heating systems to prevent the flow challenges with new initiatives of replacing steel tensile armours with similar rods carbon fibres.

Subsequently, more failures are recorded globally because of the increase in the number of flexible pipes. The data used for this research was sourced from Technip, a renowned manufacturer of flexible pipes with over 80% supplying of global non-bonded flexible pipes. The outlook of flexible pipes usage globally can be found in appendix A [15].

1.5 Statement of the problems

The Gulf of Guinea, in recent times, has experienced different types of flexible pipes failure amongst other things hence, the need for research into the root causes and challenges posed by such failures. Much time, effort, and money have been spent on repairing and replacing the failed subsea equipment and structures without end; thus, regrettably, the problems persist. Therefore, the present research focuses on the failure's main causes, which was not explicitly covered by the international standard. Solutions to prevent future occurrences are recommended at the end of this research work focusing on the location of the Gulf of Guinea, Nigeria's deepwater operations. This present work covers a specific facility issue that happened in recent years. In the end, the findings could apply to all Oil and Gas flexible pipes and their applications globally.

Flexible pipes experienced the first unexpected blockage at the start of the twentieth century, precisely in 1934. The blockages which appeared to be ice were gas hydrates [16]. The formation of gas hydrates is undesirable, mainly when they stick to the inner surface of the walls and eventually decrease the inner diameter of the pipe. The blockage ultimately formed may not be present at the site of the hydrate formation due to the possibility of hydrates being released from the pipe wall and accumulating at sagging sections of the pipe [17].

As demand for oil and gas increases globally, more exploration and exploitation go deeper offshore, leading to the rise in the subsea production system structures on the seabed. It is, therefore, essential to enhance the smooth transportation of oil to the surface facilities, such as the FPSO. These activities have led to many original equipment manufacturers (OEMs) producing various marine structures and equipment. As a result, several marine structures are exposed to cyclic operations, leading to fatigue failure upon long exposure. Subsequently, a critical review of the subsea production systems is required to reduce the consequences of these failures and their effects.

Many papers are available in the literature where numerous identified problems are documented [10]. Yet, there is still much research required in deepwater situations in various oil and gas fields globally. Consequently, subsea problems vary from one field to another; thus, collating the issues has not been easy because of non-transparency amongst the operators in reporting and documenting the problems encountered.

Some of the challenges include but are not limited to:

1. Flexible pipe rupture/blockage; this occurs because of changes in characteristics of crude oil, operational and environmental factors such as pressure, temperature, and flow. The pipe may rupture in the process of removing the blockage during pigging operations.
2. Subsea Control Module (SCMs) leakages/Faulty Subsea Electronics Modules (SEMs) and obsolesce; often occurs because of material deterioration and weakened structures due to usages. A lot of SCMs/SEMs have been replaced over the years.
3. Flexible pipe/Pipe Integrity challenges (Water Ingress, Corrosion, and Fatigue); water ingress is caused by damages during installation or accidental fall of objects on the structures during operation and due to corrosion of the facilities, which often happens naturally because of the environment.
4. Pipe Flex Joint leakage and corrosion; material deterioration is a significant cause of flex joint leakages, and it has been a substantial issue in the subsea world.
5. Umbilical (Hydraulic line blockage); inappropriate hydraulic fluids and chemicals have been the primary source of the umbilical.
6. Flexible pipe & Spools/Jumpers lateral movement on the seabed; trenching of the spools due to inappropriate meteorological data and seabed texture is a common phenomenon that is currently improving.

Generally, due to constant occurrences, much has been spent on the problems such as root cause analysis (RCA) to determine their trigger factors and repair or replace the structures. However, many of the challenges often occur more than the others. Experience has shown flexible pipe integrity challenges such as blockage, rupture, etc. Flex joint leakages and corrosion are also prominent, while umbilical, SCMs/SEMs, and Spools movement have less occurred due to tremendous improvements in their configurations.

Due to obsolescence, oil and gas producing companies have reported related issues with subsea control modules, subsea electronics modules, and other software.

In addition, there are other unmentioned activities in other parts of the world pending resolutions. Therefore, this present work is not limited to the Gulf of Guinea but also reflects worldwide challenges.

There is concern over the number of subsea structures failures at an alarming rate and, as such, have impacted oil and gas production.

This present work is confined to a non-bonded flexible pipe with hydrate blockage. It is investigated and analysed in detail under different load conditions, including pressure, compression, and axial loads and their combinations. Recommendations are made to prevent the failures and associated consequences concerning recommended practice [1].

1.6 Research Aim and Objectives

The research aims to consider and analyse a methane hydrate blocked multi-layer non-bonded flexible pipe under different load conditions (internal and external pressure and compressive and tensile longitudinal forces). This determines the root causes of its failure and remedial measures in deepwater operations in the Gulf of Guinea.

This is achieved through the following specific objectives:

1. To build a thorough understanding of the subject and available research by undertaking a literature review
2. To establish and review experimental investigation of a 6", 7-layers blocked and unblocked pipe; determine the stress values and analyse according to the failure modes in [1] standard.
3. To develop a robust and comprehensive nonlinear finite element model for the investigated flexible pipe samples.
4. To undertake a comparison analysis with experimental results and numerical results.
5. To combine the model and undertake a parametric study to analyse the effects of hydrate blockage and predict the impact on the flexible pipe, including but not limited to pipe under the influence of internal pressure, compression force, and combined loads.
6. To compare the results of both the experimental and numerical investigations of the hydrate blocked flexible pipe in line with API standards
7. To analyse results, combine, develop, and present for industrial guide against hydrate formation removal and manage industrial challenges associated with hydrate formation, focusing on the critical information on flexible pipes failure modes during operation and life extension.

1.7 Research Scope and its Significance

The primary scope is to develop, analyse and validate finite element models of a flexible pipe subjected to different load conditions and investigate the effects of dynamic stress. The focus is to examine the models under various load conditions and use the same models to evaluate the responses of a hydrate blocked flexible pipe as a case study.

The effects of the hydrate plug on individual layers are assessed and compared with both the finite element analysis (FEA) and experimental results.

The parameters considered for developing the Finite Element models are:

- Size (Diameter),
- Operating pressure,
- Temperature,
- Layer composition
- Materials and their interactions

Despite numerous available literatures on flexible pipes, none specifically considered the hydrate blocked pipeline, and similarly not explicitly covered in the international standard recommended practice. It makes the research work so significant; as a result, it confirms blocked flexible pipes result from several factors sometimes overlooked during the life of the structures. They include but are not limited to overpressure during pigging operation, environmental factors, and axial forces exerted by the crude flowing inside the pipe. Another significant advance understands the effects of a hydrate blockage in the non-bonded flexible pipe, its impact, and proper ways of managing the formation. The process of removing the blockage through pigging operation, which involves pressurizing and depressurizing the pipe, is better understood.

1.8 Thesis outline

This thesis consists of seven chapters as follow:

- Chapter 1 Introduction shows the aim, objectives, and general presentation of the research.
- Chapter 2 Literature Review describes the previous research on the subject
- Chapter 3 Flexible Pipe Numerical Modelling presents the methodology and applicable international standards and codes.
- Chapter 4 Experimental Investigation presents the experimental investigation, the root cause, and failure studies on a ruptured hydrate blocked flexible pipe: a case study.
- Chapter 5 Numerical Investigation presents the FEA of the flexible pipe under investigation.
- Chapter 6 Result and Discussion presents the analysis of the results of the modelled flexible pipes and a comparison of experimental, numerical, and computational results.
- Chapter 7 Conclusion and Recommendation presents the brief notes of the thesis and provides the conclusions, recommendations, and future research work.

CHAPTER 2: LITERATURE REVIEW

2.1 Introductory Remarks

A literature review on the non-bonded flexible pipe and associated failure modes are presented in this chapter. It is noted that there has been little research on the flexible pipe with hydrate formation and its consequences. This chapter is based on the outcome of numerous reviews on several available works of literature on numerical, experimental, and analytical models/analyses, hydrate formations, and specifically on the problem in this work. It is split into three sections; analytical models of flexible pipes, experimental tests conducted on physical specimens of flexible pipes, and Finite Element Analysis (FEA) models.

The review focused on summarising the findings, assumptions, and problems associated with flexible pipes and failures. Additionally, the kinds of literature on hydrate formation were reviewed and assisted in determining the mode of hydrate formations in flexible pipes and their consequences. It gives insight into the present study of non-bonded flexible pipe with hydrate blockage, investigating the implications and most appropriate operational data to apply in removing the hydrates.

This chapter presents the literature review on flexible pipes, hydrate formation, finite element analysis of non-bonded flexible pipes, experimental analysis of damaged and undamaged flexible pipes, including the study on flexible pipe with hydrate blockage under different load conditions such as compressive force, pressures, and effect of stiffness and coefficient of friction.

2.2 Research Review on Non-bonded Flexible Pipe and State of the Art

Numerous papers were reviewed on finite element analysis of flexible pipe and the blockage formation to get a deeper understanding of the area of the study. The work focuses more on the hydrate blockage flexible pipes under different load conditions such as pressures, forces, the effects of coefficient of friction, and stiffness constant on the layers and associated failure modes.

Flexible pipes are designed with different layers to accommodate high tensile, compressive, and other environmental loads experienced during installation. They are subjected to various load conditions such as pressure (design, burst, operating, and carcass collapse pressure), pull (damaging), stiffness (bending, axial, torsional), and compressive forces in the process to determine their suitability and abilities to withstand the mentioned loads. Nevertheless, little or no research has been carried out on hydrate blocked non-bonded flexible pipes, their secondary effects on the life span and associated failure modes. Pipe blockage can result from wax and hydrate formation, which causes flow assurance amongst other significant challenges in the petroleum industry. The unconsolidated sand formations is also a dominant

material in oil and gas reservoirs, which has hindered the free flow of the crude from their respective wells [18]. Failures due to sand and hydrate from different sources that have caused blockages in flexible pipes are the principal reasons for various simulations.

Therefore, the literature on flexible pipe analysis is divided into three general sections: numerical, analytical, and experimental methods. Numerical models are categorised by computer-based modelling, commonly using high volume numerical computations to simulate model behaviour. Analytical models work using simple mathematical equations developed to give accurate approximations of specific models. Many analytical models used for multilayer, non-bonded flexible pipes are based on Euler beam theory as beam elements have been the most used approach. Experimental models consist of observational analysis performed on small scale representations undergoing various loadings, displacements, and setups. The literature review on hydrate formation its effects on flow assurance are also reviewed accordingly.

2.2.1 Numerical Analysis

Many modern engineering industries rely heavily on computational models for many purposes, primarily used for multiple types of complex failure analysis; additionally, it is used heavily for optimisation regarding design. Simulating, fluid dynamics, thermodynamics, and combustion are also critical applications. This gives insight into the behaviour of high-speed energy transfer that would otherwise be very difficult to understand and record. Flexible pipes are no different, with computational analysis being the widely used and most important method in the field. This is because of efficiency in computational models regarding time and cost and primarily due to the considerable advancements in modern-day computational speed. The Finite Element Method (FEM) is the most used, optimised and powerful method found in almost all modern-day computational software. Nowadays, FEM is widely known as 3D Finite Element Analysis (FEA). FEM is one of the most flexible and valuable for handling complex 3D geometry, non-linear deformation and how two or more specific components work or “couple” together to share loads simultaneously and behave in unique ways. Additionally, different boundary conditions could be applied to FEM models allowing for a broader range of simulations.

2.2.1.1 Ben Edmans, Dinh Chi Pham, Zhiqian Zhang, Tianfu Guo, Sridhar Narayanaswamy (2014)

Edmans et al. introduced a new multiscale approach for the analysis of FE flexible pipes. The primary focus is on the prediction of failure modes and increases in design life against hydrostatic loading. Dynamic research was conducted to find the displacements at specific points in the pipe, which was then emulated on more detailed local models. The author used a local model to help in predicting failure mechanisms, fatigue damage and buckling. The models were designed by first looking at flexible pipes analytically as homogenized composite cylinders. Interlayer slip can be thought of as plastic flow

through the homogenous material. A non-linear constitutive model (in structural mechanics, describe the relationship between strain or strain-like measures and stress or stress-like measures) can accurately mimic the behaviour of hysteresis bending in flexible pipes and shows the impact of internal pressure and hydrostatic loading as illustrated in Figure 2-1. This paper conclusively shows ordered multiscale designs for flexible pipe model, with evidence of hybrid beam FE implementation in a two-dimensional (2D) system. Accordingly, further works should be focused on “implementing a three-dimensional hybrid beam element and creating a fully nested computational procedure”, with considerations of global and local systems.

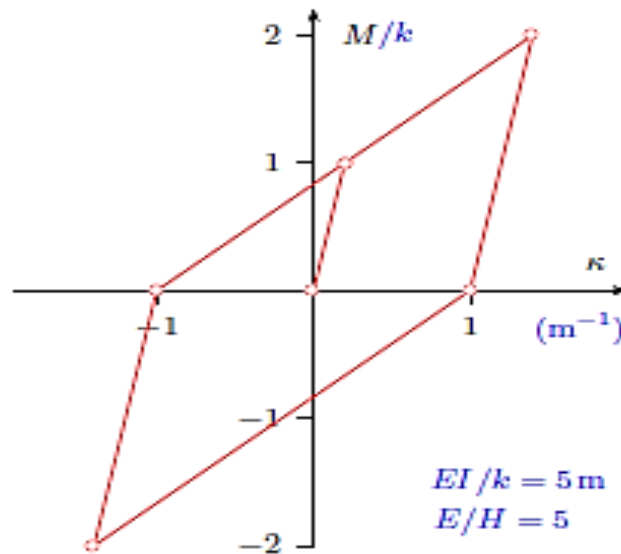


Figure 2-1: Bending Hysteresis loop obtained from Constitutive model [19]

The governing tangential bending stiffness under non-elastic loading/unloading is given in the following equation:

$$\frac{dM}{dk} = \frac{EH}{E+H} I \tag{Equation 2-1}$$

where M is the bending moment, k is the curvature, E is the elastic material stiffness, H is the kinetic hardening modulus, and I is the second moment of area of the pipe [20]. However, the work is limited to 2D, which did not consider certain conditions.

2.2.1.2 Li, Qiu and Ju (2015)

Li, Qiu and Ju published a research article in 2015, which involved a 10-layer ABAQUS model that represented a non-bonded flexible riser. The analysis involved three different load conditions: tension, internal pressure, and external pressure. The model generation is well noted, with ten layers modelled

individually considering friction, contact interaction, geometric non-linearity, and metallic (steel wires) interaction at specific layers. Presented is a typical section and model of carcass layers in Figure 2-2. This model's assumptions and attention to detail were impressive and a good benchmark for future ABAQUS work. The model used a mesh of 55000 elements and was solved using a modern-day eight (8) core CPU, with 24 Gb of memory. The model was limited to tension and pressure but did not consider the variation of other variables such as coefficient of friction, normal contact stiffness, and perhaps compressive force. If considered, the result would have been a good confirmation of flexible pipe-risers behaviour under different loads and boundary conditions.

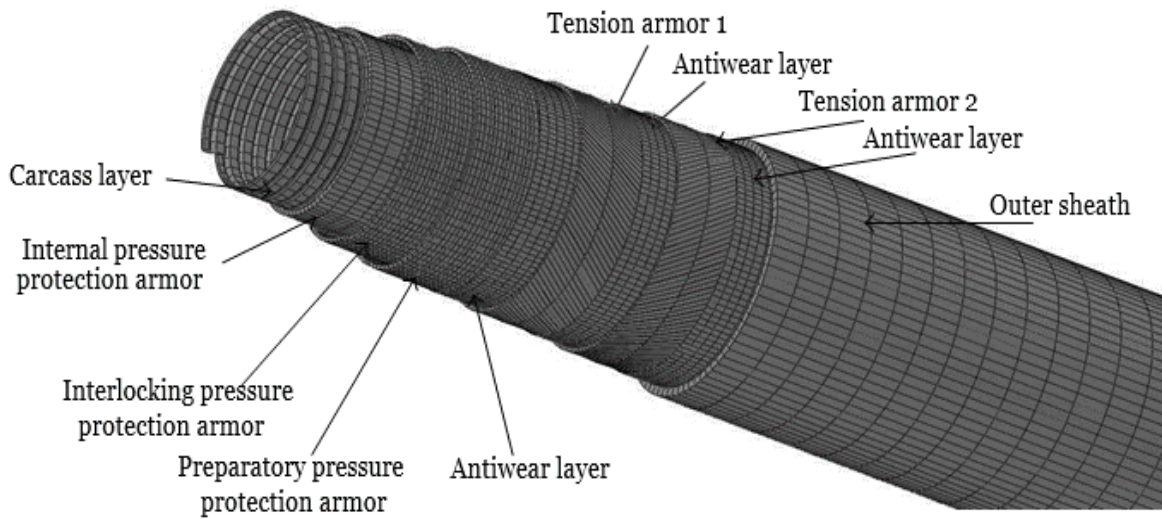


Figure 2-2: Ten layer's Riser [21]

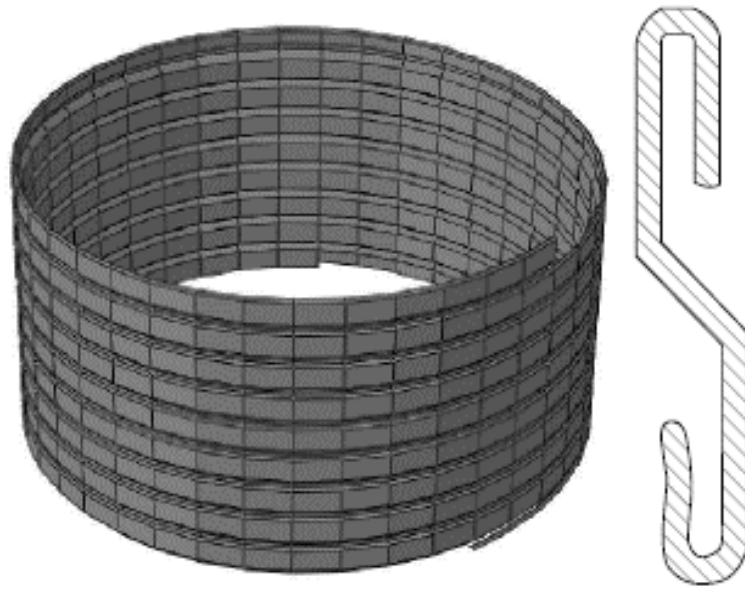


Figure 2-3: Section and model of carcass layer [21]

An FEA model was created, and all the layers were modelled separately, as shown in Figures 2-3 for the carcass layer. Appropriate contact interfaces were introduced between the layers to recreate a scenario like the flexible pipes. The specification of the riser layers is as detailed in Table 2-1.

Table 2-1: The specification of the riser layers used by J.Y Li and others [21]

| Layer | Inner diameter (mm) | Thickness (mm) | Modulus (Pa) | Poisson's ratio (ν) | Density (ρ) |
|---------------------------|---------------------|----------------|--------------|---------------------------|--------------------|
| Inner carcass | 178 | 3.5 | 207E9 | 0.30 | 7800 |
| Internal Pressure armour | 185 | 3.0 | 0.18E9 | 0.38 | 920 |
| Interlock pressure armour | 191 | 3.0 | 207E9 | 0.30 | 7800 |
| Pre pressure armour | 197 | 3.0 | 207E9 | 0.30 | 7800 |
| Anti-wear tape 1 | 203 | 1.5 | 0.18E9 | 0.38 | 920 |
| Tension armour1 | 206 | 2.0 | 207E9 | 0.30 | 7800 |
| Anti-wear tape 2 | 210 | 1.5 | 0.18E9 | 0.38 | 920 |
| Tension armour 2 | 213 | 2.0 | 207E9 | 0.30 | 7800 |
| Anti-wear tape 2 | 217 | 1.5 | 0.18E9 | 0.38 | 920 |
| Outer sheath | 220 | 4.5 | 0.18E9 | 0.38 | 920 |

Length of pipe: 1.17m

The mechanical behaviour of the model was evaluated under other loads and the three loading conditions: tension force, internal and external pressure. This paper is evidence that modern computational methods are continually improving and showing strongly correlated data for static loading or singular dynamic loading when compared to benchmarked experimental or analytical

analysis. This shows a clear trend in this field of computational study of the non-bonded flexible riser, with the possibility of the problem being fully solved computationally in the future [22]

The results of the study shown in Table 2-2: based on load case-Tension of 150 kN were compared to analytical research showing a strong correlation, with enough data to validate the model.

Table 2-2: 10-layers flexible pipe model stress results

| Stress | Layers | | | | | | |
|-------------------------------|---------------|-------------------------------------|---|---------------------------------|------------------|------------------|--------------|
| | Carcass Layer | Internal Pressure protection Armour | Interlocking pressure protection armour | Preparatory pressure protection | Tension armour 1 | Tension armour 2 | Outer sheath |
| Von Mises Stress (MPa) | 6.140 | 0.1104 | 14.32 | 19.61 | 98.48 | 91.51 | 0.1241 |

The analytical result obtained value of 87.01MPa is 11.7% and 4.9% smaller than the tension armour 1 and 2 simulation results 98.48MPa and 91.51MPa, respectively. This shows a good agreement between the analytical and numerical results. Other load conditions such as load case 2- Internal Pressure; load case 3-External Pressure also showed good understanding.

The model was revalidated, and the concept was considered in the actual work scenario due to its relationship with the loading conditions experienced by flexible pipes under blockage.

Conclusively, the model is relevant to this work as introducing hydrate into the model has significant differences in the stress values for the three load conditions.

The improvement is on introducing the Hydrate blockage and variation of coefficient of friction and stiffness constant, including the application of compressive force and longitudinal force already used.

2.2.1.3 Gabriel Gonzalez, Jose Renato Mendes des Sousa, and Luis Sagrilo (2015)

Gonzalez et al. presented a finite element model, entirely developed in ABAQUS® environment, fully capable of calculating stresses and strains in those several layers when subjected to different types of loads. The finite element model employs four nodes reduced integration shell elements. The inner layers, located below the first tensile armour, are condensed into a unique cylinder with its distinct properties well assured. The same assumption applied to the layers placed above the second tensile armour. Moreover, rebar elements were considered for the carcass and pressure armour modelling. As for the tensile armours, each steel tendon is modelled individually by shell elements. The interactions between tensile armours tendons and the tensile armours and the adjacent layers are handled with tangential and normal contact formulations. As a case study, a 9-layers 2.5" non bonded flexible pipe is considered under pure tension. The results are compared to an existing analytical model developed on six

simplifying hypotheses and from previously published experimental data. All results agreed quite well but without hydrate blockage, which was studied in this work.

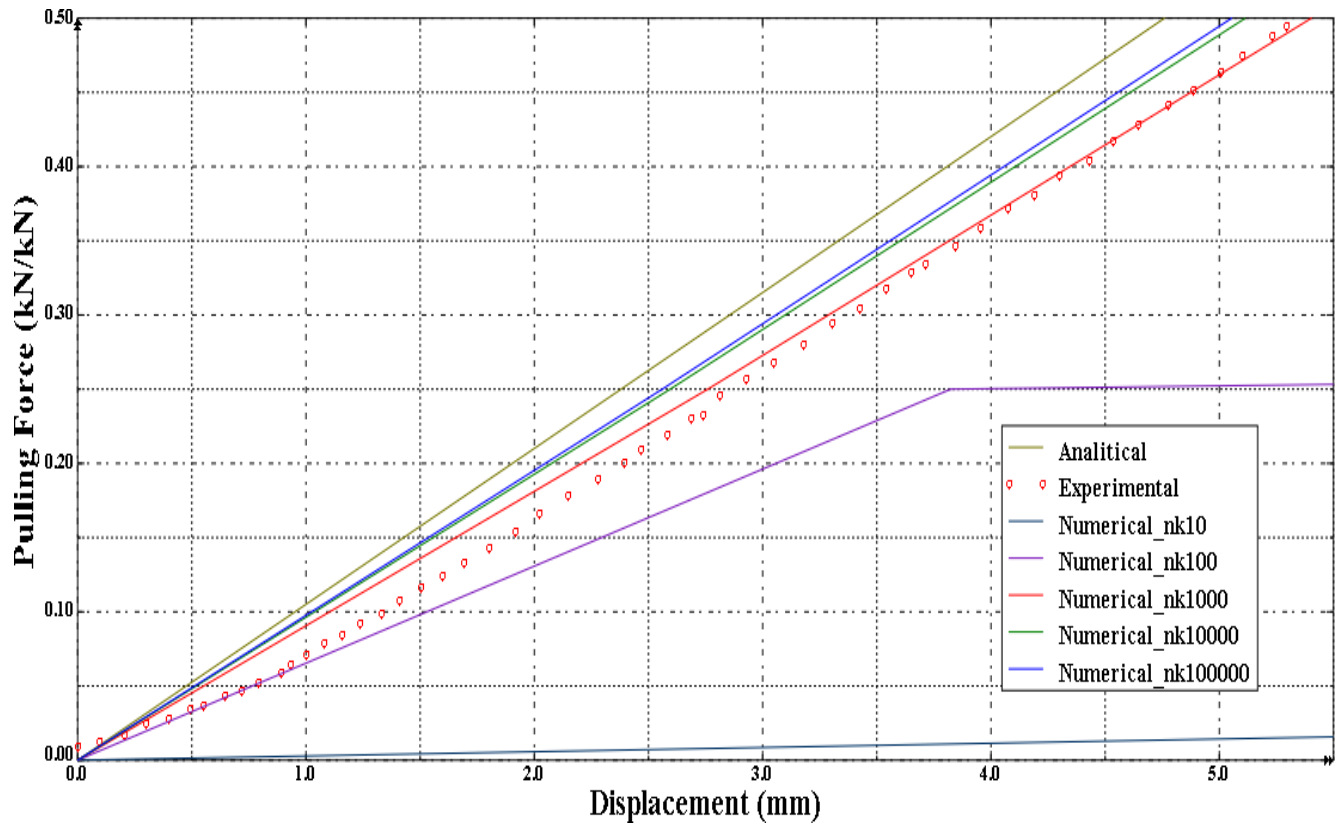


Figure 2-4: Displacement vs Pulling load for **normal contact stiffness variation** [2]

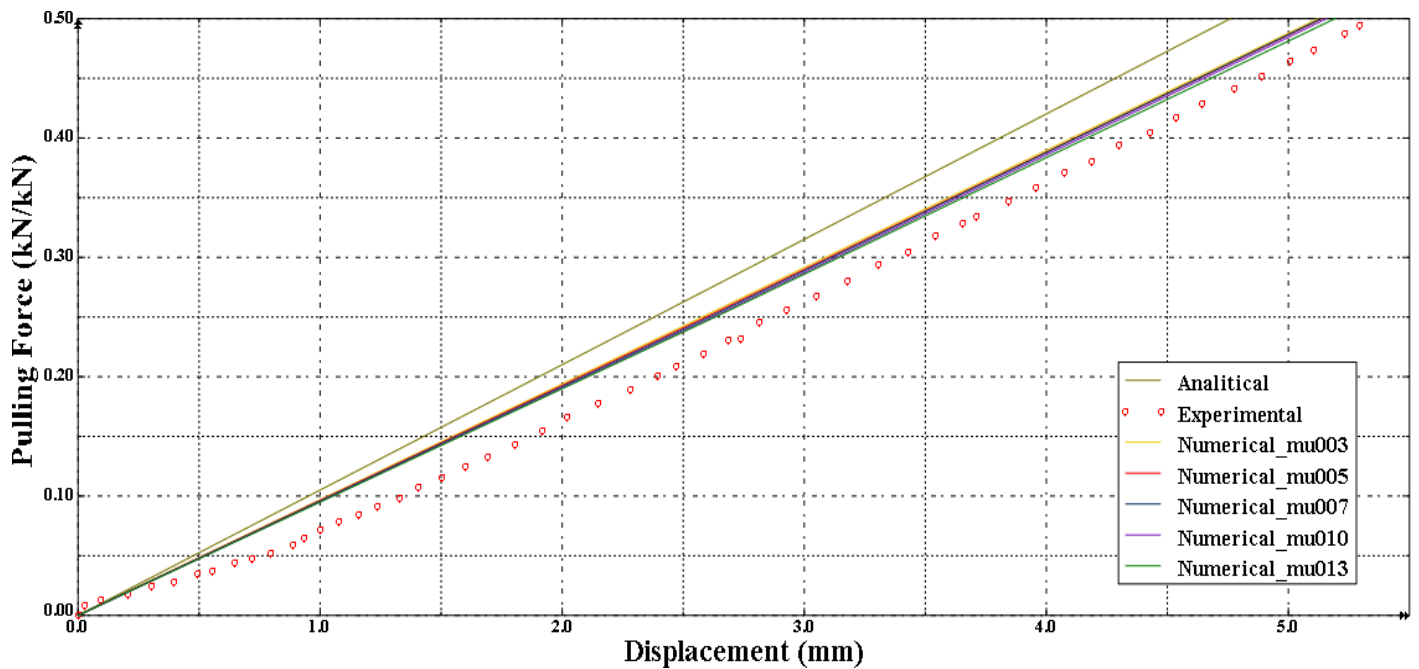


Figure 2-5: Displacement vs Pulling load for **frictional coefficient variation** [2]

The analyses considered the variation of normal contact stiffness (nk) and coefficient of friction (μ) which were chosen from $10-10^5$ ($\mu = 0.10$) and $0.03-0.13$ ($nk = 5000$) for Normal stiffness and coefficient of friction as illustrated in Figures 2-4 and 2-5 respectively. The same model was verified and served as the basis for the developed models for this present work, including hydrate layer and other boundary conditions. In conclusion, the obtained results in numerical analyses varied with the analytical result. The numerical model depends on contact stiffness. This generates a model without physical correspondences if the value of stiffness is not well chosen. The best parameters that give the desired result are when the friction coefficient is 0.10 and contact stiffness is 1000 N/mm^3 .

2.2.1.4 J. de Sousa, Paulo F. Viero, Carlos Magluta N. Roitman and R. Motta. (June 2010)

De Sousa et al. dealt with a nonlinear three-dimensional finite element (FE) model capable of predicting the mechanical response of flexible pipes subjected to axisymmetric loads focusing on their axial compression response. Moreover, to validate the model required experimental tests, which were carried out at COPPE/UFRJ. In these tests, a typical 4" flexible pipe was subjected to axial compression until it failed with radial and axial displacements measured and compared to the model predictions. The excellent agreement between all obtained results indicates that the proposed FE model efficiently estimates flexible pipes' response to axial compression. Furthermore, it can potentially be employed in identifying the failure modes related to excessive axial compression and the mechanical analysis of flexible pipes under other types of loads.

De Sousa conducted axial compression experiments on a 4" flexible pipe, measuring the displacement under varying loads. The pipe is similar to the one analysed in this project but of a different diameter. The experiment results could therefore be helpful in the verification of an FEA model; however, this project does not concern axial loading conditions. The axial shortening of the pipe specimen under varying load is shown in Figure 2-6:

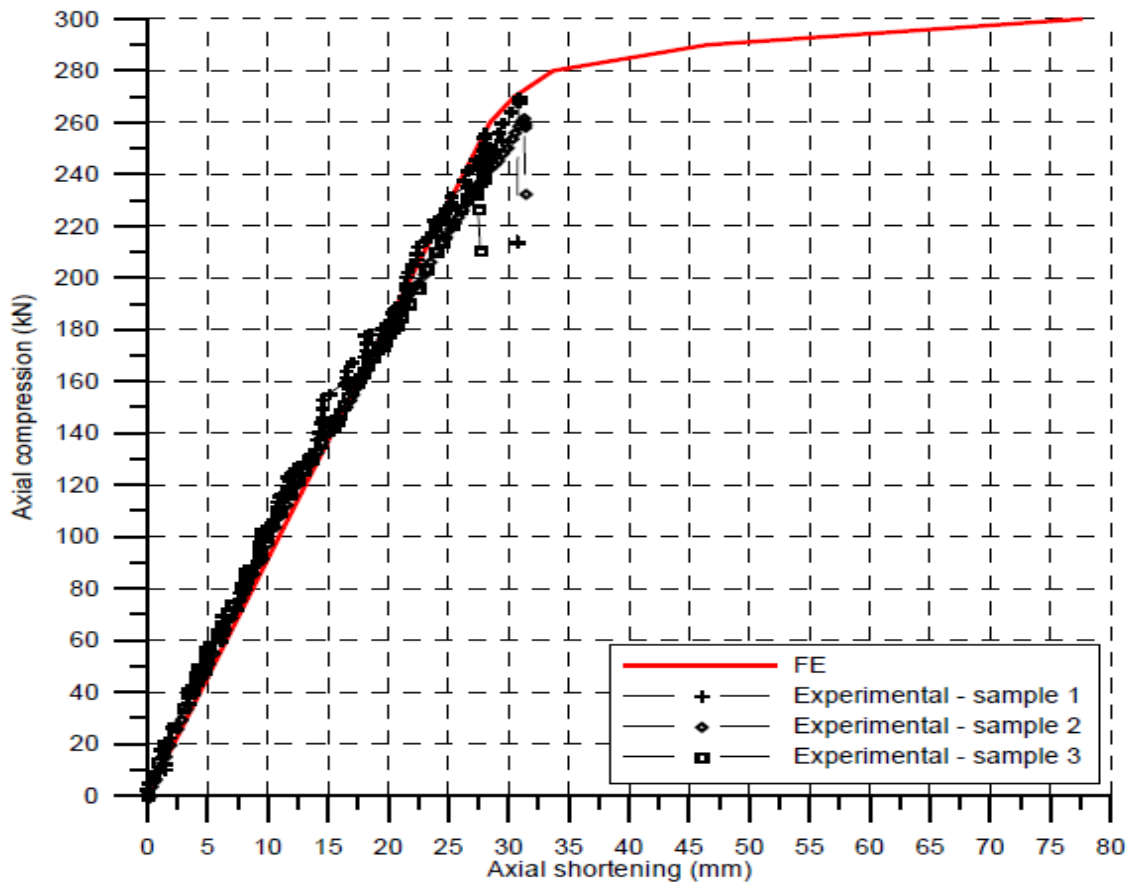


Figure 2-6: Axial Shortening of Flexible Pipe Under Axial Compression [23]

The results may not be accurate based on certain assumptions in the model, which includes but are not limited to:

1. The internal friction in the layers is negligible
2. No interaction between the laying direction of the tendons and their usual direction.
3. The thickness of the inner carcass and pressure armour is small compared to the internal diameter of the layers

Though the approach hypothesis as claimed may not have a significant effect on the results but was taken into consideration in the model of this present work.

2.2.1.5 Xu Yang, Svein Sarvik and Liping Sun (2015)

Yang et al. stated that the flexible pipes might be exposed to high axial compression and bending during deepwater installation. The compression force is mainly sustained by the tensile armour layers, resulting in localized lateral or radial buckling failure in these layers. This paper created a finite element model to evaluate the critical instability load of tensile armour wires under external pressure and compression using different software such as Abaqus, Bflex, Bflex2, and M.A. Vaz. The tensile armour wires are modelled by curved beam elements under loxodromic (rhumb line) assumptions. Spring elements and equivalent beams simplified other layers' contributions. The buckling load capacity and associated

failure modes are obtained. The results are also compared with the results based on 3D Euler beam elements and results published in the literature. Parametric analyses were further included with the external pressure, friction modelling and the influence of initial imperfections. The simulation results for different software are presented in Figures 2-7, 2-8 and 2-9.

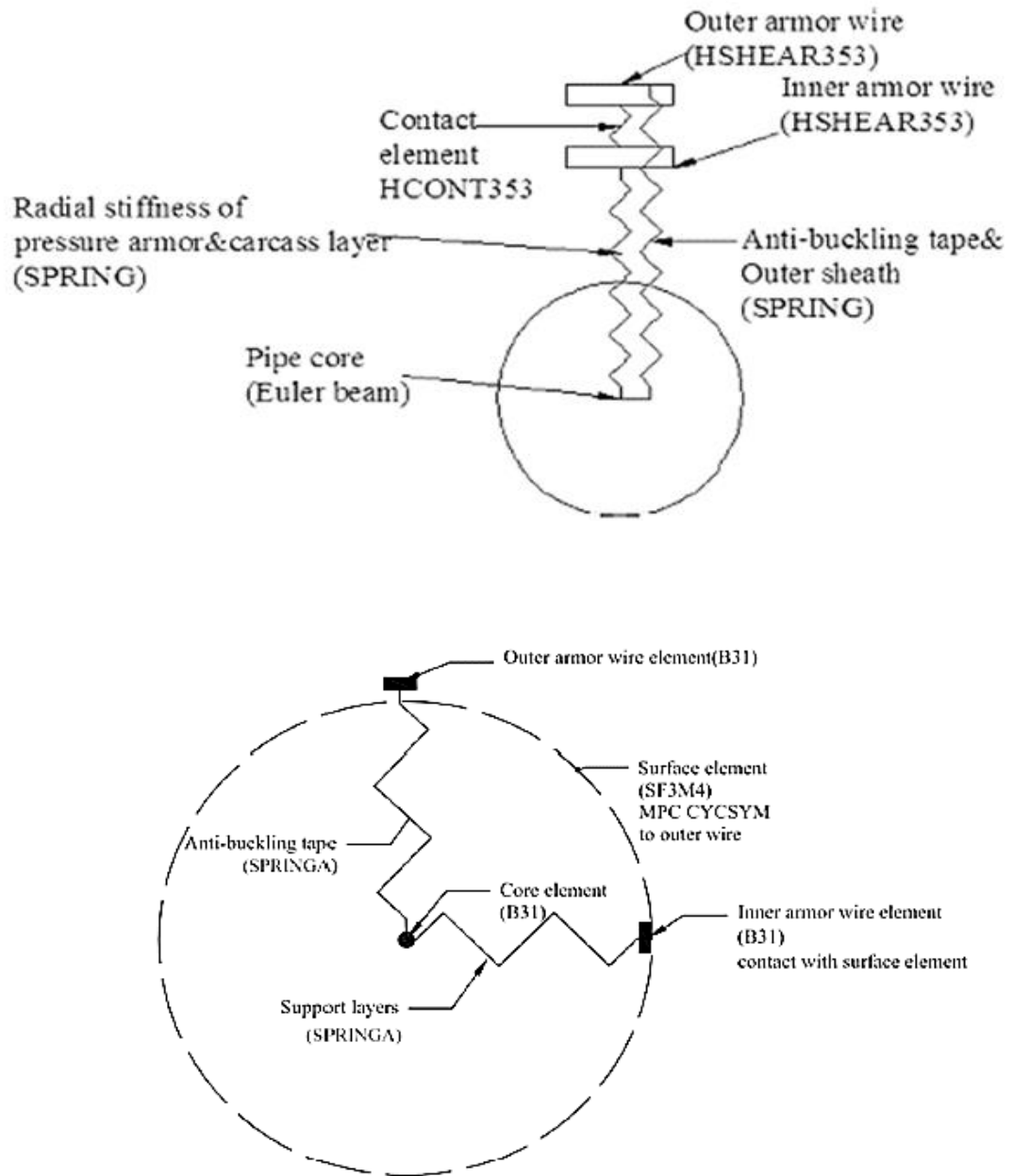


Figure 2-7: Schematic diagram of curved and straight beams models [24]

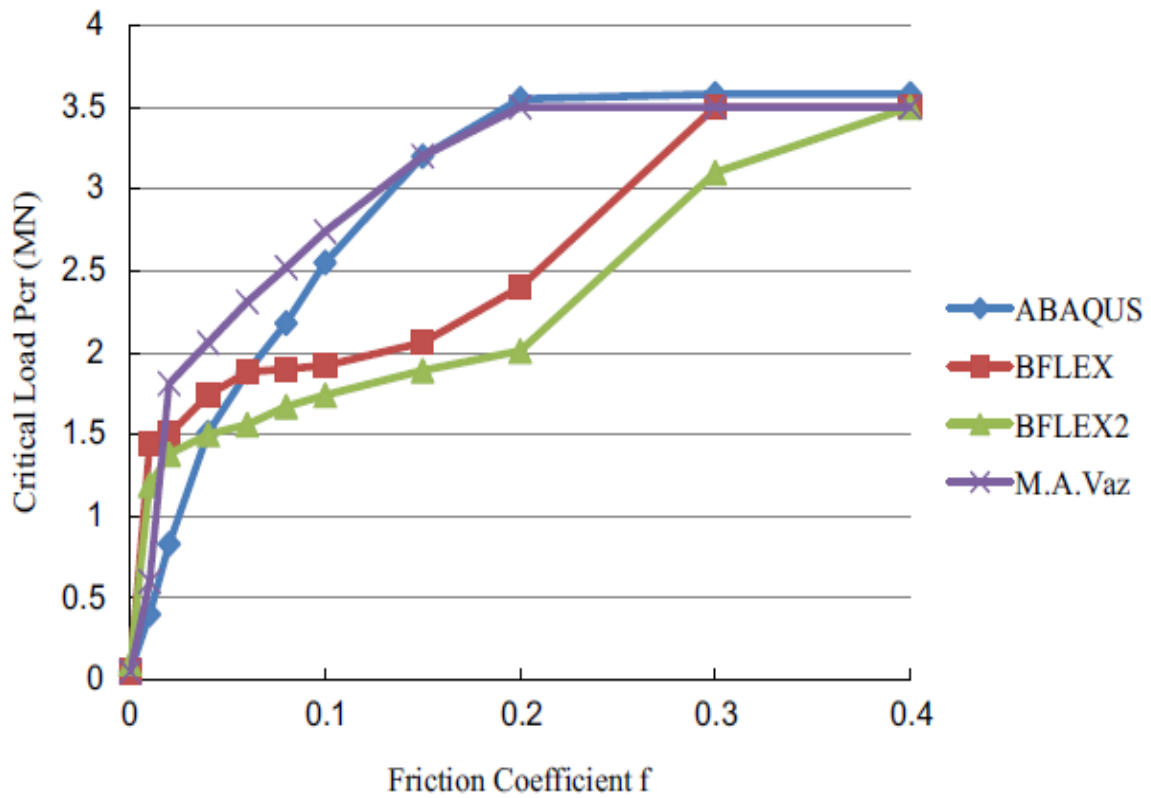


Figure 2-8: Critical load in different coefficient of friction at a pressure of 2MPa [24]

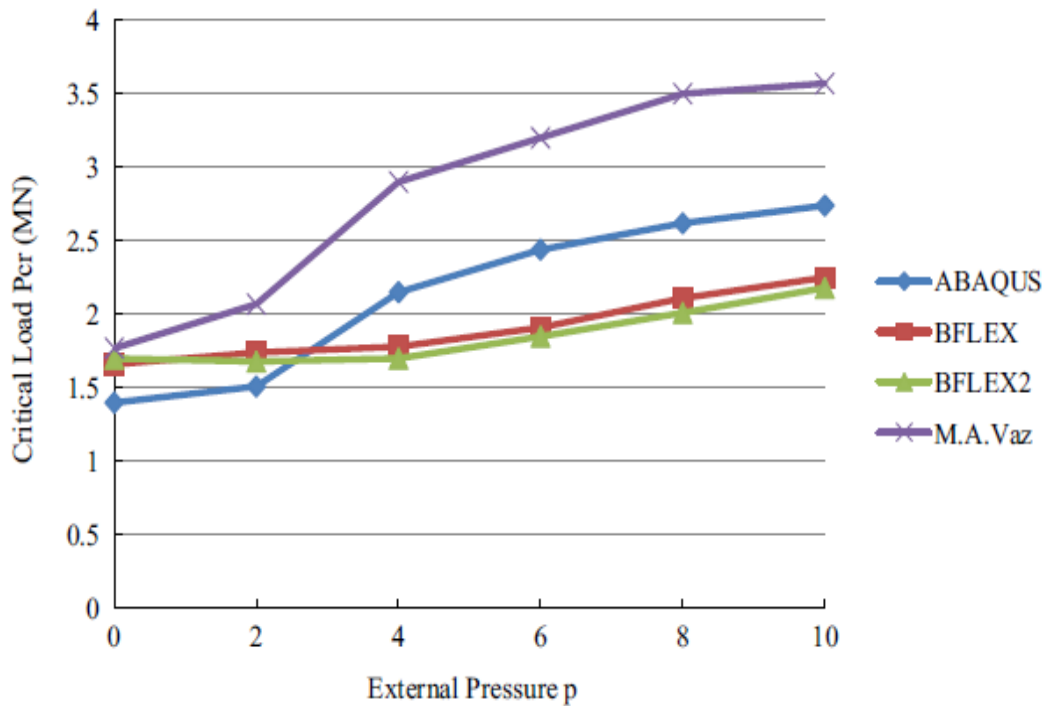


Figure 2-9: Critical load in different pressure at the coefficient of friction of 0.04 [24]

2.2.2 Analytical Analysis

Analytical models are the foundations of all engineering, as mathematics has been around for thousands of years with uses in engineering throughout history. Analytical modelling of flexible pipes is the oldest and most widely used method before modern computational advancements and accurate FE models. However, the basis of many FE models is a solid analytical model. The most common form of analytical modelling is to treat flexible pipes as cross-sectional models or composites. This method assumes that the pipe is not homogenous and is made of many different unique parts. The model can then predict the behaviour of the pipe by summing the values of the “composite”. This method simplifies the problem significantly; however, the ability to analyse individual components or the effects acting between layers. This simplified analysis gives only the overall macro properties of the pipe.

In contrast, more complex multi-layer analysis is often done with different properties and degrees of freedom assigned to each layer. This gives a more detailed, physically representative look into the micromechanics of flexible pipes. This section discusses analytical models and their pros and cons.

2.2.2.1 McIver (1995)

The paper presented the analytical basis used to model the complex behaviour of the individual components of the flexible pipe, which was employed to model the intricate details and structural behaviour of both non-bonded and bonded flexible pipes. Homogenous layers were represented as thick-walled cylinders while multiple loads were considered; “tension, torque, shear forces, bending moments, wall pressure.

Temperature pressure differentials, friction effects were monitored, and curvatures were noted. The model represented helical wires with beam elements, using Love’s equations for equilibrium balancing and kinematic analysis. Serret-Frenet Formulae was used to transpose geometric data, to relate data to the flexural axis. Slippage is considered through material stresses and wire loading. The program “FLEX-ABLE” was developed based on the analytical findings, which reasonably predict axial loading. There were vital signs of coupling between most of the Degree of Freedom (DoF). Until this point (1995), programs available and made were not accurate enough to simulate this complex interactivity between multiple DoF, so there was a basis for future work. The Coulomb friction model should also be considered for future models to predict fatigue; however, this would require more detail for individual components in each layer of the analytical model [25].

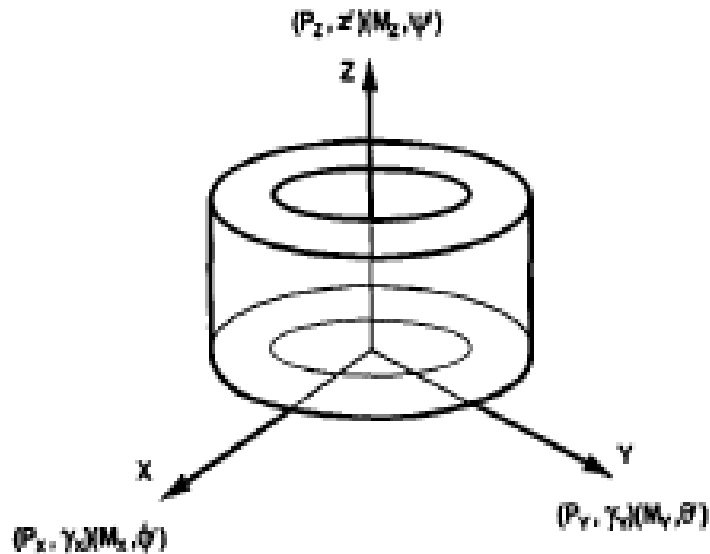


Figure 2-10: Pipe section load and deformation convention [25]

The pipe model applies to a total length, dZ , subjected to an axial tension P_z , torque M_z , shear force components P_x and P_y , bending moment components M_x , and M_y , pressure and temperature differentials through the pipe wall. The coordinate axis Z is directed along the pipe axis, as shown in Figure 2.10. The pipe section, and therefore each layer in the area, undergoes uniform axial strain z' , shear deformations in the X - Z and Y - Z planes. They are represented by the shear angles x and y , bending curvatures about the pipe X and Y axes, respectively.

2.2.2.2 Roberto Ramos Jr. and Alexandre Kawano (2015)

This paper analysed numerically a 2.5" flexible pipe subjected to traction and internal pressure. The effect of internal and external pressures on the displacement of flexible pipe, when subjected to axisymmetric loads, was discussed. A typical example is presented in Figure 2-11. The paper went further to derive the linear operators, which established the relationship among the stress resultants, displacements, or deformations in the individual layer of the flexible pipe, along with the process of deriving an analogous linear operator to represent the response of the entire flexible pipe. These are presented, highlighting interest, measured aspects, and their related meaning.

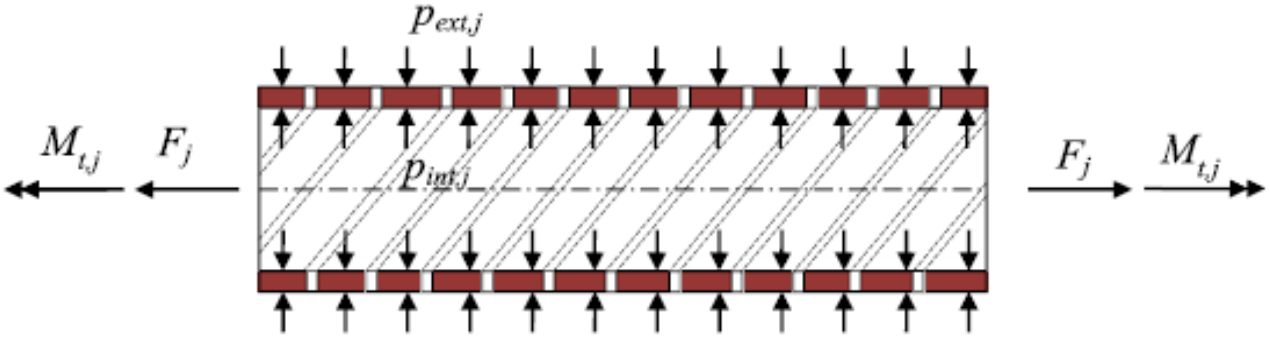


Figure 2-11: Load applied to the boundaries of a generic plastic layer [26]

- Traction force supported by the layer (F_j)
- Twisting moment supported by the layer (M_{tj})
- Internal pressure applied on the internal cylinder surface (p_{intj})
- External pressure applied on the internal cylinder surface (p_{extj})

The internal and external pressures applied to the respective cylindrical surfaces of the j -th layer can be related to stress-resultants F_{ipj} and F_{opj} (per unit of pipe length) defined respectively by:

$$F_{ipj} = 2\pi R_{ij} \cdot P_{intj} \quad \text{Equation 2-2}$$

and

$$F_{opj} = 2\pi R_{ij} \cdot P_{intj} \quad \text{Equation 2-3}$$

It is also important to stress that the internal and external pressures applied to the respective surfaces of the cylindrical layer are related to the contact pressures by:

$$P_{intj} = P_{cj} - 1 + n_{j,int} \cdot P_i \quad \text{Equation 2-4}$$

$$P_{extj} = P_{cj} - 1 + n_{j,ext} \cdot P_o \quad \text{Equation 2-5}$$

where P_{cj} is the contact pressure between the j .th and the $(j+1)$ -th layers and is a flag that returns “1” if the layer is the minimum innermost waterproof layer of the pipe internal pressure P_i . This was applied in this work in terms of subjected loads [26]. The research is only limited to pressure, while other load conditions were not considered.

2.2.2.3 R. Cuamatzi-Melender, O. Castillo-Hernandez, A.O. Vazquez-Hernandez et. al (2017)

This work presents analytical and finite elements modelling strategies to study both types of collapse risers fabricated with an “S” carcass profile to predict collapse failure, as presented in Figure 2-12. The

developed methodologies were applied to a 50.8 mm (2 in.) non-bonded flexible riser. The results showed the importance to perform 3D finite element modelling for a proper carcass design and collapse assessment, calibration of the length of the finite element models, and boundary conditions defined to obtain reliable results and computer time optimization. It also finds a difference in collapse loads for each type of collapse; ovality type collapse, and the development of a finite element of the carcass only is sufficient. But for the other types of failure, it is necessary to develop a finite element model including carcass, internal polymer sheath and pressure armour. Furthermore, it was found that the analytical formulations developed to date can only evaluate the collapse properties of the carcass. Still, they are limited to being used to design carcass for flexible risers [27].

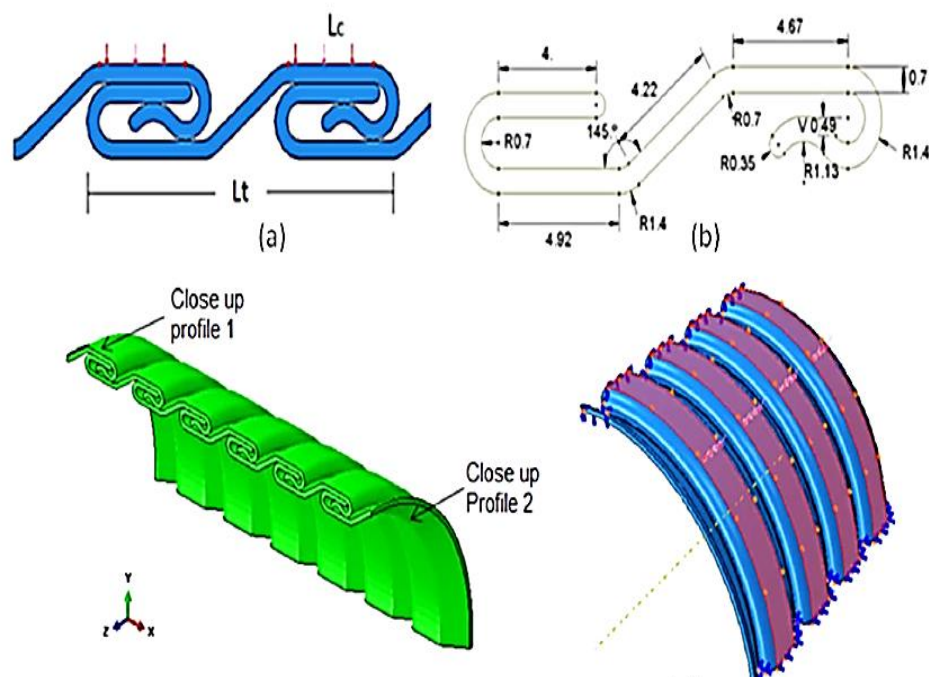


Figure 2-12: Typical Design of Carcass Layers [27]

The paper focused and limited the simulation to only the carcass layer, while the limited study was on other layers. The stress-strain carcass and sensitivity analysis are presented in Figures 2-13 and 2-14.

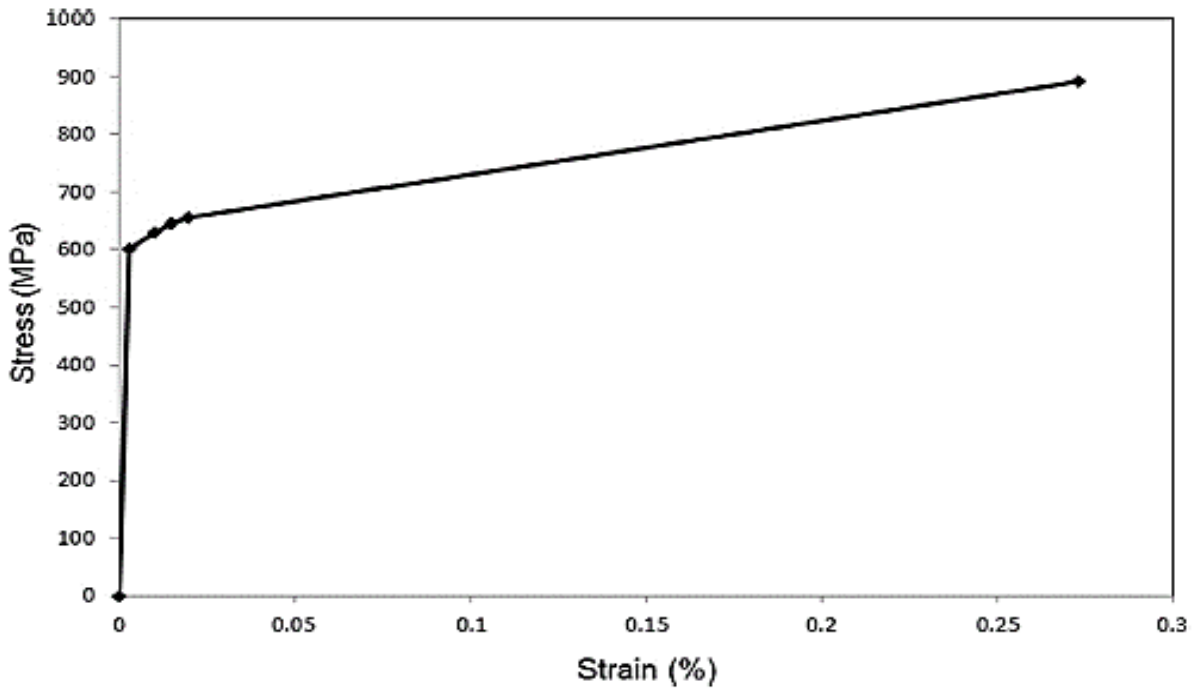


Figure 2-13: Stress-Strain curve of the carcass (R. Cuamatzi-Melendez, O. Castillo-Hernández, A.O. Vázquez-Hernández, M.A. Vaz, 2017)

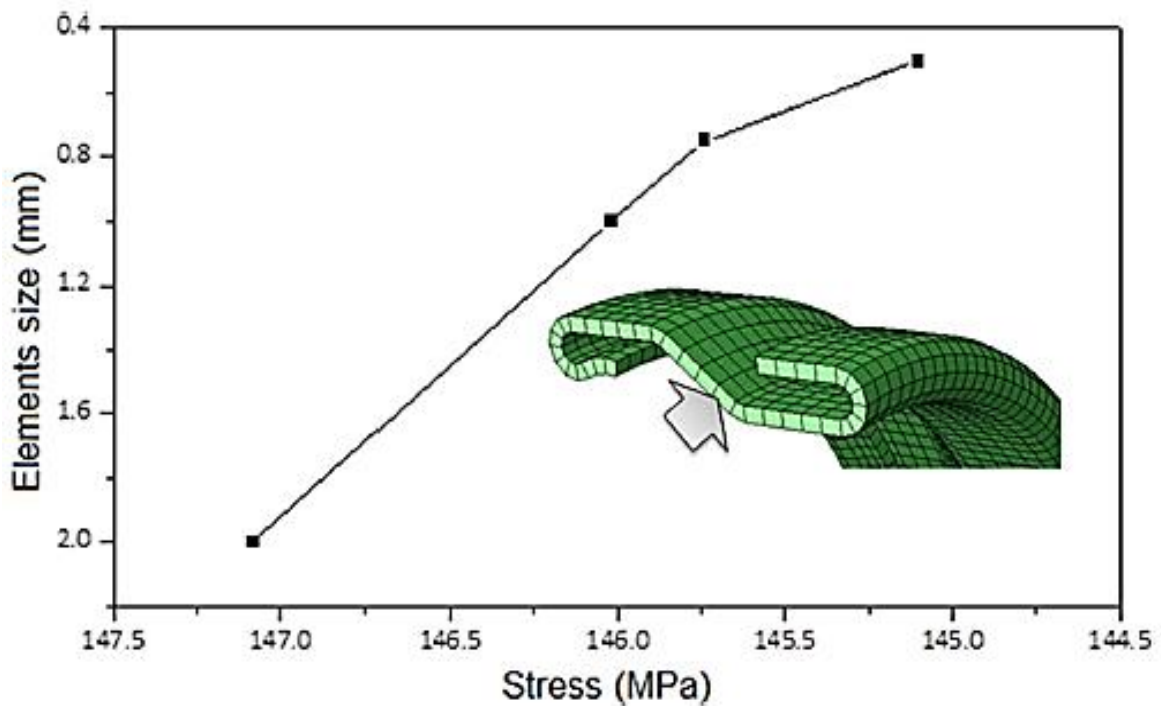


Figure 2-14: Sensitivity analysis maximum Von Mises Stress [27]

In conclusion, the study only considered the carcass layer, which limited understanding of the behaviour of other layers with the same load conditions.

2.2.2.4 Niels Højen Østergaard, Anders Lyckegaard, Jens H. Andreasen

The paper analysed lateral wire buckling in helical tensile armour layers. The study looked at understanding the effects of extreme deep-sea conditions. At these depths' pipes can undergo cyclic bending forces from tidal currents and experience axial compression. Flexible pipes are better for tensile forces; the tendons pull tightly together under tension, becoming slightly straighter and sitting in a more axial orientation. This increases their tensile axial load capacity; however, in compression, the tendons are pushed together, lowering the lay angle and causing their orientation to move more in the hoop direction than the resting state. This makes their ability to handle compression worse, and in extremes, can cause bird caging and structural failure. A spiral model was developed using thin curved beams (Figure 2-15), with a frictionless surrounding layer, using these single helical wires could be studied. The model's equations used curved beam equilibrium and compared different beam model sizes, validating results through multiplicative use through computational comparison, from these force-displacement graphs were obtained.

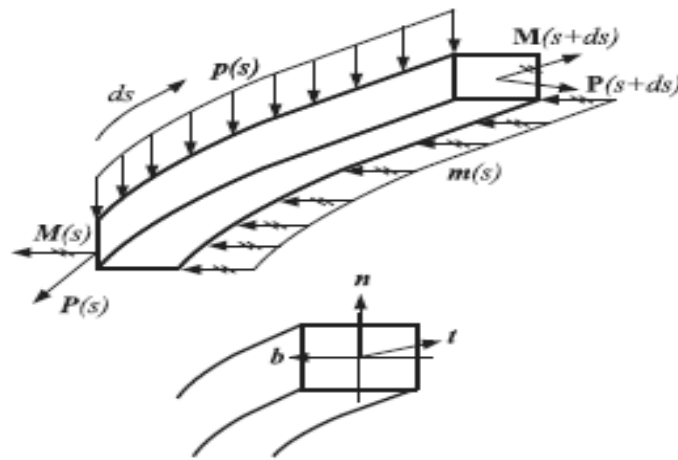


Figure 2-15: Curved beam equilibrium [28]

Component wise equations of equilibrium as derived by Love; the expressions (a power law) as shown below:

$$\left(\frac{dPt}{ds}\right) - KnPn + KgPb + pt = 0 \tag{Equation 2-6}$$

$$\left(\frac{dPn}{ds}\right) + KnPt - \tau Pb + pn = 0 \tag{Equation 2-7}$$

$$\left(\frac{dPb}{ds}\right) - KgPt + \tau Pn + Pb = 0 \quad \text{Equation 2-8}$$

$$\left(\frac{dMt}{ds}\right) - KnMn + KgMb + mt = 0 \quad \text{Equation 2-9}$$

$$\left(\frac{dMn}{ds}\right) + KnMt - \tau Mb - Pb + mn = 0 \quad \text{Equation 2-10}$$

$$\left(\frac{dMb}{ds}\right) - KgMt + \tau Mn + Pn + mb = 0 \quad \text{Equation 2-11}$$

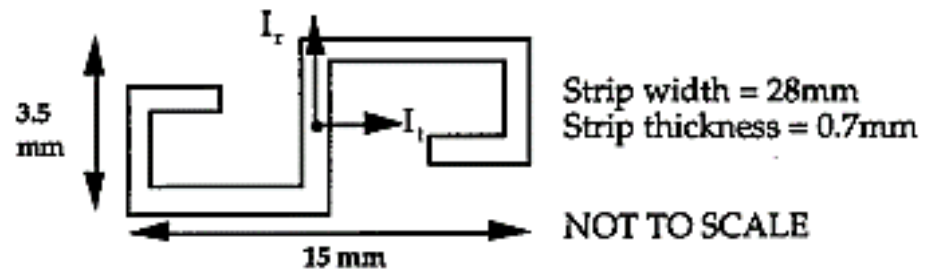
The results showed that the pitch of the helical layers was the most crucial parameter for axial loading. As the pitch increases, the axial loading lowers significantly. There is not much research into slip mechanics, and future work should focus on lateral wire buckling with slip considered [28]

2.2.2.5 J.A Witz

Witz conducted a study into the response of flexible pipelines under various loading conditions. He then compared his results with the analytical solutions provided by ten (10) well-known institutions, including Lloyds Register, Statoil, and University College London (UCL). Some institutions chose to use purely mathematical models, while others used computer simulation software. The pipe used in the study was a 2.5” version of the pipe, and the participants were required to calculate the following curves for deformations within elastic limits:

1. Tension-axial elongation curve and twisting angle-axial elongation curve with ends free to rotate
2. Tension-axial elongation curve and twisting moment-axial elongation curve with ends prevented from rotating
3. Clockwise and anti-clockwise twisting moment-twisting angle curve and axial force-twisting angle curve with ends free to elongate
4. Clockwise and anti-clockwise twisting moment-twisting angle curve and axial force-twisting angle curve with ends prevented from moving axially
5. Bending moment-curvature curve for two internal gauge pressures of zero and 300 bar.

CARCASS



PRESSURE REINFORCEMENT

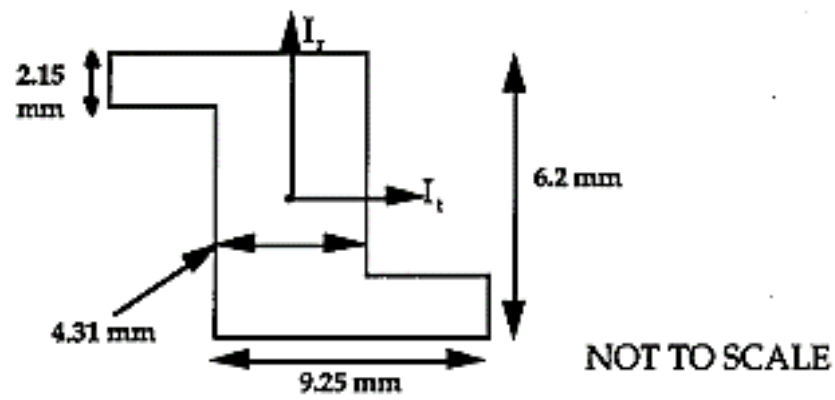


Figure 2-16: Carcass and Pressure reinforcement layers [29]

Figure 2-16 presents the mean axial force-elongation curve and the curves associated with stiffnesses one standard deviation on either side of the mean stiffness. Also shown in Figure 2-17 is the measured axial force-elongation curve for the first three load cycles. The measured curve shows noticeable non-linearity with hysteresis in the loading cycle. Also evident is the difference between the first and subsequent load cycles. This is observed with non-bonded flexible structures and is commonly attributed to the bedding of the component layers. All models used in this case study, apart from the Coflexip model, predict axial stiffnesses larger than the measured axial stiffness.

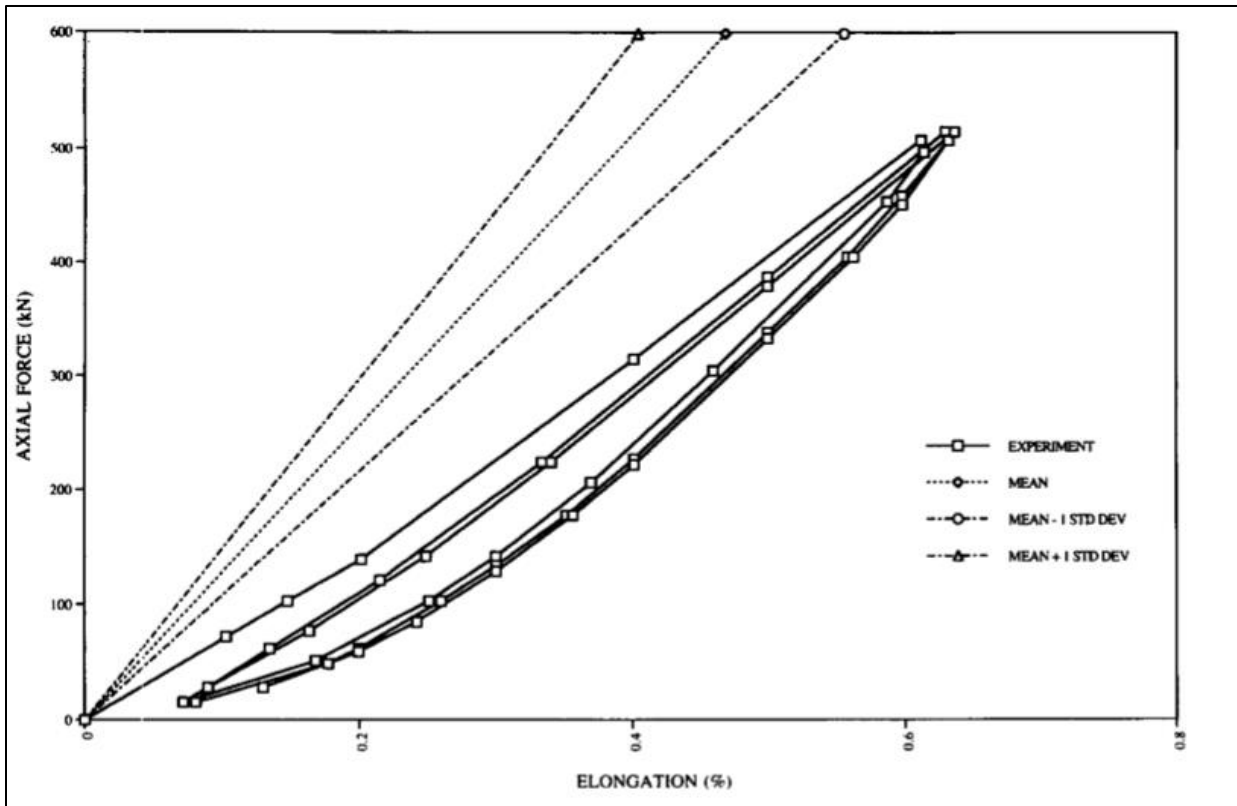


Figure 2-17: Cross-section analysis: Axial force/Elongation curve [29]

Additionally, the pipeline displayed a non-linear deformation with a degree of hysteresis after the initial loading. The mean value for stiffness provided by the ten institutions was significantly higher than was measured during the tests. The force divided by the strain of the pipeline was approximately 80MN. Coflexip, who used the Eflex software, were closest to the experimental result and calculated a value of 89MN. The mean value provided by the institutions was 128 MN, with UCL calculating a value more than double the value measured was the closest experiment. This shows that accurately modelling the behaviour of a non-bonded, layered, flexible pipe is a complex process. The study recommended further research to establish the structural behaviour of the flexible pipes under combined load, which is being investigated in this work. The loads recommended were applied to the model, which includes axial load. Figure 2-17 is a typical plot for the cross-section analysis of flexible risers.

2.2.3 Experimental analysis

The numbers of experimental published studies are relatively low compared to Analytical and Numerical studies. This might be due to the challenges and expenses required to set up the facilities necessary to carry out tests and analysis. Few reviews associated with the experimental study are presented below:

2.2.3.1 M. T. Rahmati, S. Norouzi H. Bahai and G. Alfano (2017)

This paper investigated a 4-layer flexible pipe which was examined through both experimental and numerical methods. The practical test was carried out on an adjustable riser to determine its responses when subjected to specific load conditions, and FEA was used to validate the results. The composition of the layer is two cylindrical polycarbonate tubes and two steel helical wires, and the helical is the carcass and tendon armour layers. Investigation with a bending load was carried out on the model, and provided helpful information on the behaviour of flexible pipe and its structures and subsequently performed the finite element models with all layers modelled separately and applied a surface-to-surface frictional contact interaction. The results comparison were finally made and predicted the responses of the investigated flexible pipe.

Experimental tests were to predict the flexible pipe nonlinear structural response. The riser consists of four layers which include two cylindrical polycarbonate tubes and two steel helical layers. One helical layer represents the carcass layer in a flexible riser, while the other represents the tendon armour layer.

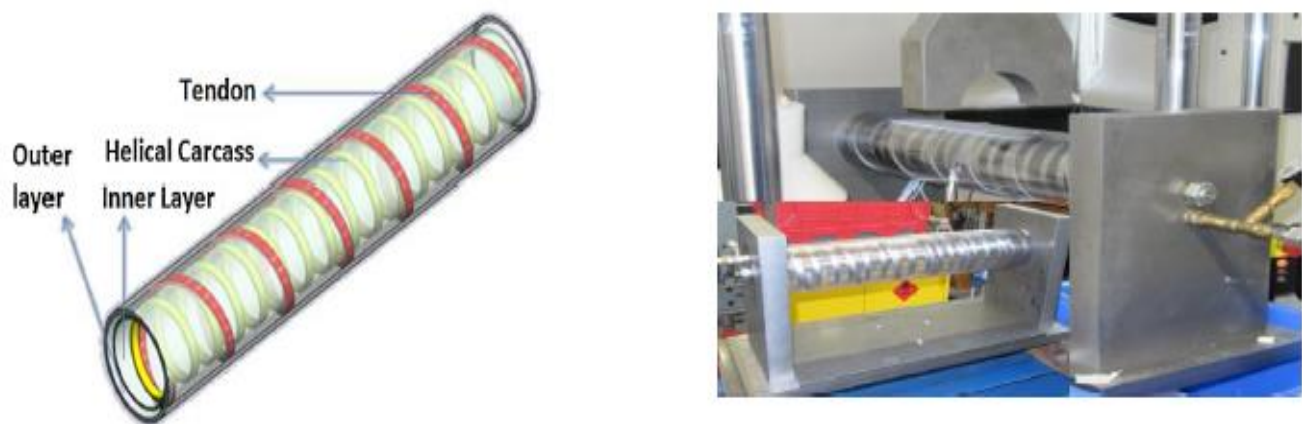


Figure 2-18: Assembly of prototype layers and specimen for bending test [30]

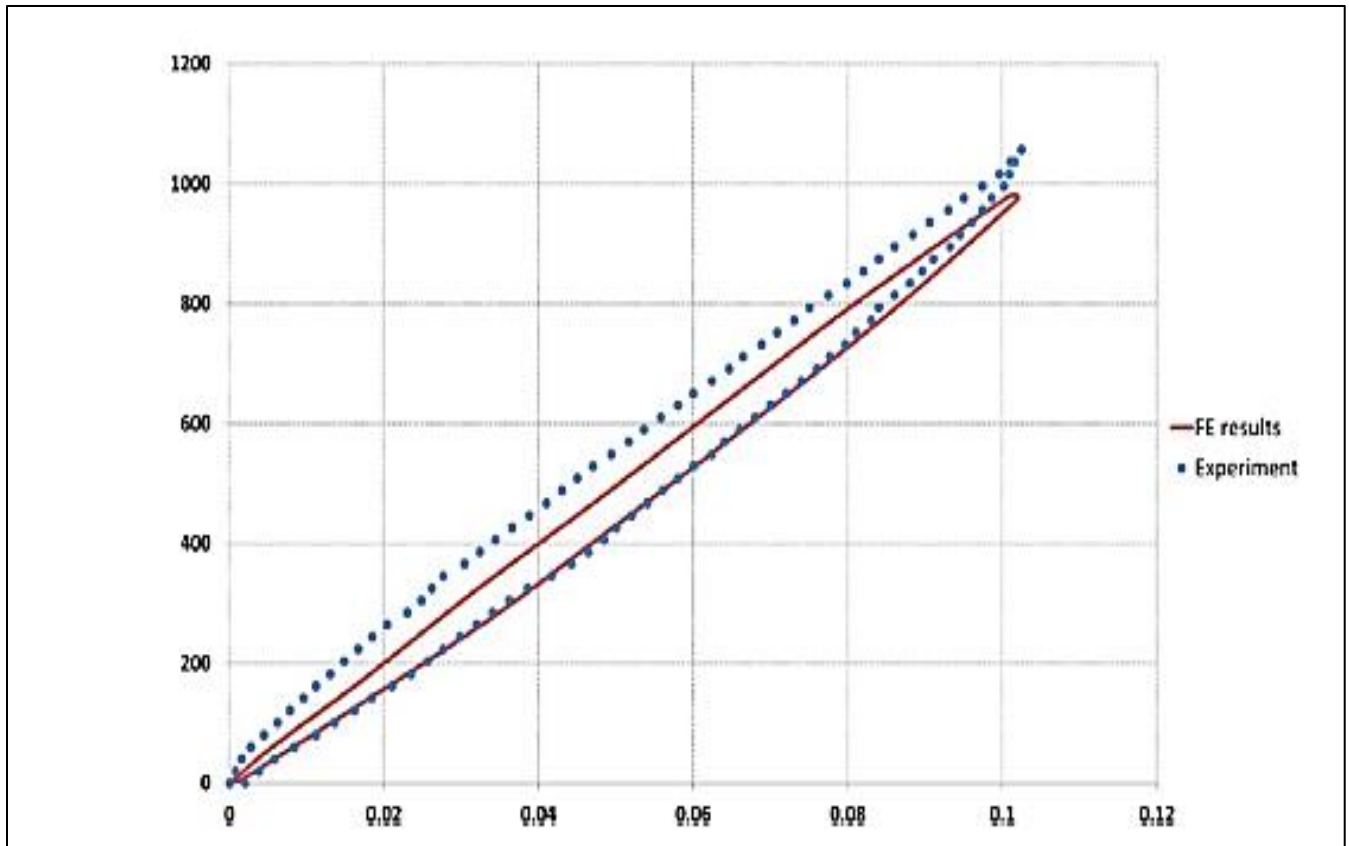


Figure 2-19: Predicted bending moment (N.m)-curvature (1/m) [30]

First, bending load experiments on the model are described, which provide some insight regarding the fundamental behaviour of flexible pipe structures (Figure 2-19). The description of the FE models follows this. All layer components are individually modelled, and a surface-to-surface frictional contact model is used to simulate their interaction. Finally, the FE numerical results were compared with the test data to outline the capacity of the numerical method to predict the response of flexible riser structures. Still, not all the results agreed both experimentally and numerically. This makes the authors suggest further investigation in the evaluation of various contact modelling approaches.

2.2.3.2 S. Péronne, Cecile Izarn, Pascal Estrier, Olivier Caro, Jean-Narc Leroy et al. (2015)

Péronne et al. performed research on hysteric bending behaviour in flexible pipes, with experimental characterization and FE analysis. Over 50 tests were run on a full-scale flexible pipe, with a focus of the studying being on how internal pressure affects bending behaviour. The inclusion of tension, external pressure, and temperature were considered in the setups. The setup is as presented in Figures 2-20 and 2-21.

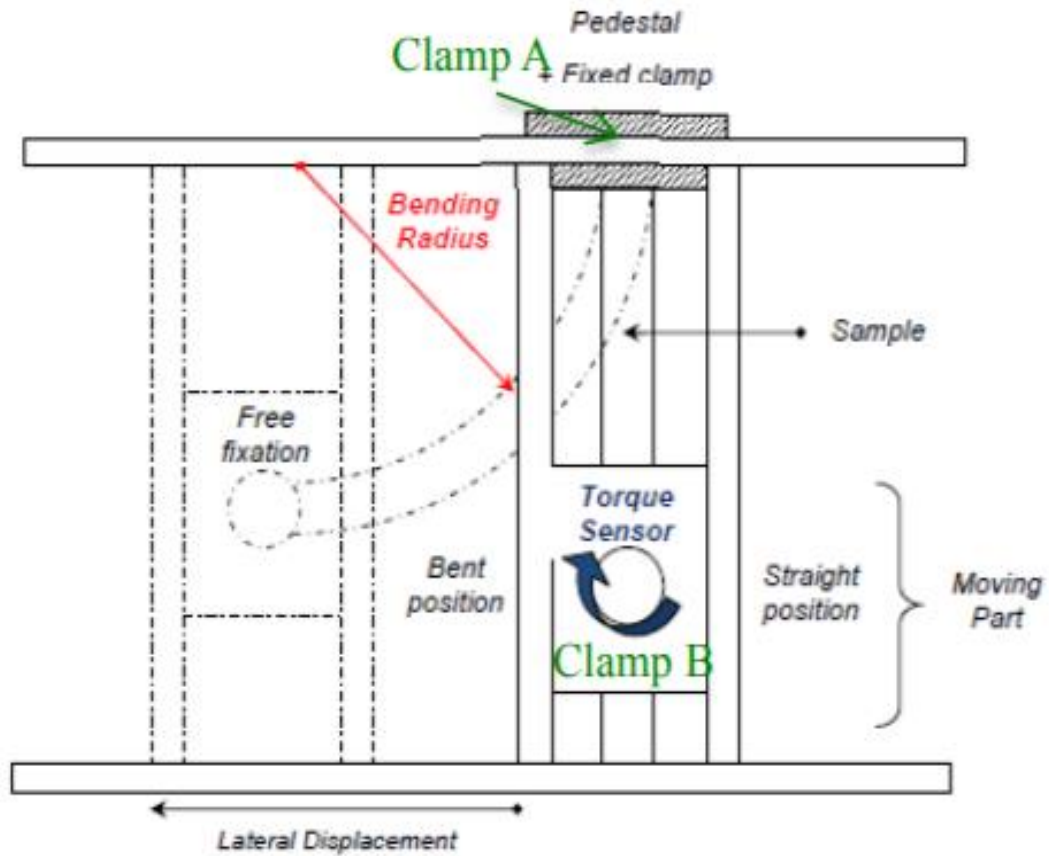


Figure 2-20: Bending characterization test-Sketch instrumentation [31]

Potentiometers were placed evenly along the pipe to record curvature time evolution, with strain gauges and torque sensors used at each end of the test specimen. The conditions used attempted to simulate a deep-sea condition with a water depth of 2000 m, as this is where most flexible pipes are used in practicality. The results showed “the bending stiffness is much lower than its torsional and axial stiffnesses and therefore has a larger influence on its static and dynamic behaviour.”, additionally the experiment showed linear bending stiffness is only affected by thermal loading. An FE design program, “STIFFNESS” based on IFPEN Life6, was presented, explicitly considering the tensile armour’s layers effects on bending. The static outcomes were compared with the experimental results to show a strong correlation. Some slight differences were found when comparing uncertainties in global stress results, and dynamic tests do not show promising results. As the model generated is shown to be a reasonable overall predictive model, it should be helpful for future fatigue and high-stress failure analysis studies [31].

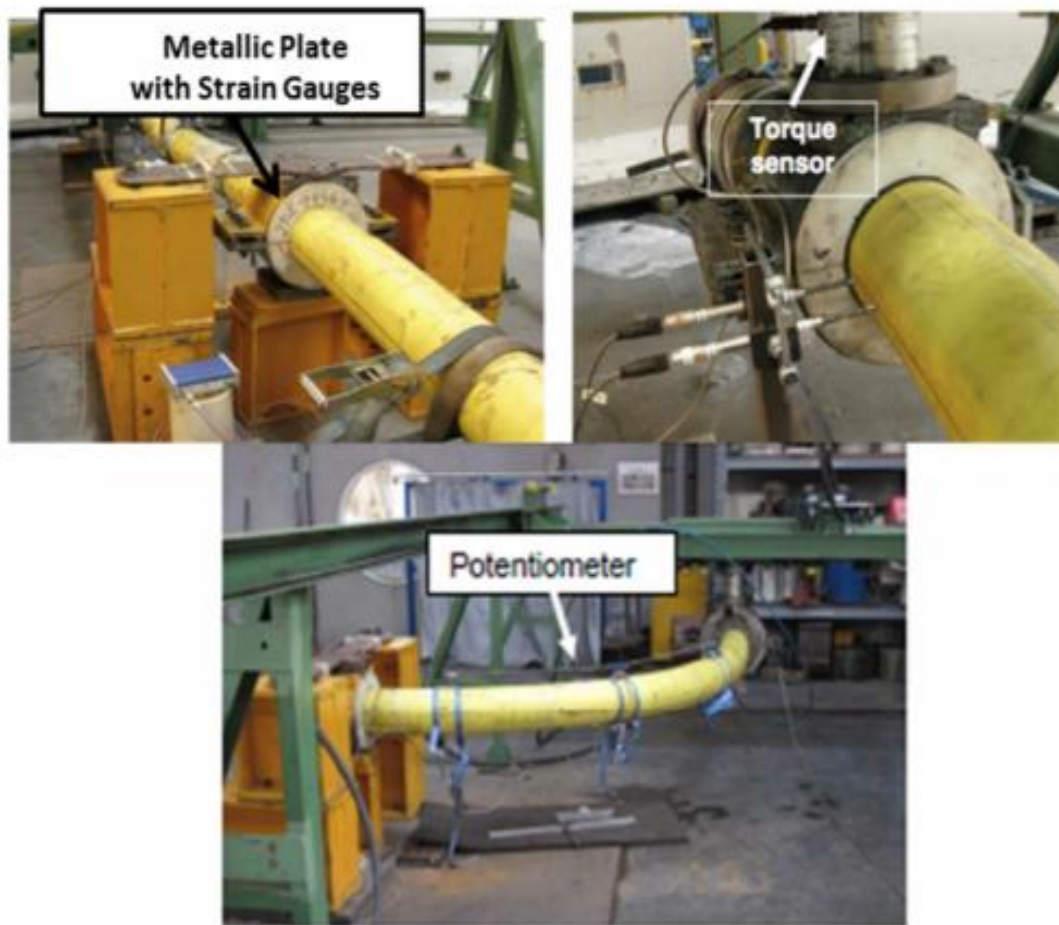


Figure 2-21: Characterization Test-Instrumentation [31]

2.3 Research Review on Hydrate Formation

Gas hydrates are solid crystalline compounds resembling ice in appearance, consisting of the main water lattice, the host, and individual gas molecules, the guests. The structure of these gas hydrates is determined by the size and composition of the gas molecule captured by the water lattice. The most common types of “guest” gas molecules are methane, ethane, propane, carbon dioxide, and hydrogen sulphide, as illustrated in Figure 2-22. Gas hydrates form when water and these gases become mixed in conditions with low temperature, generally below 25°C, and high pressures, usually greater than 1.5 MPa for natural gas hydrate formation. The two most common types of naturally occurring gas hydrates are structure I and structure II, as shown in Figure 2-22.

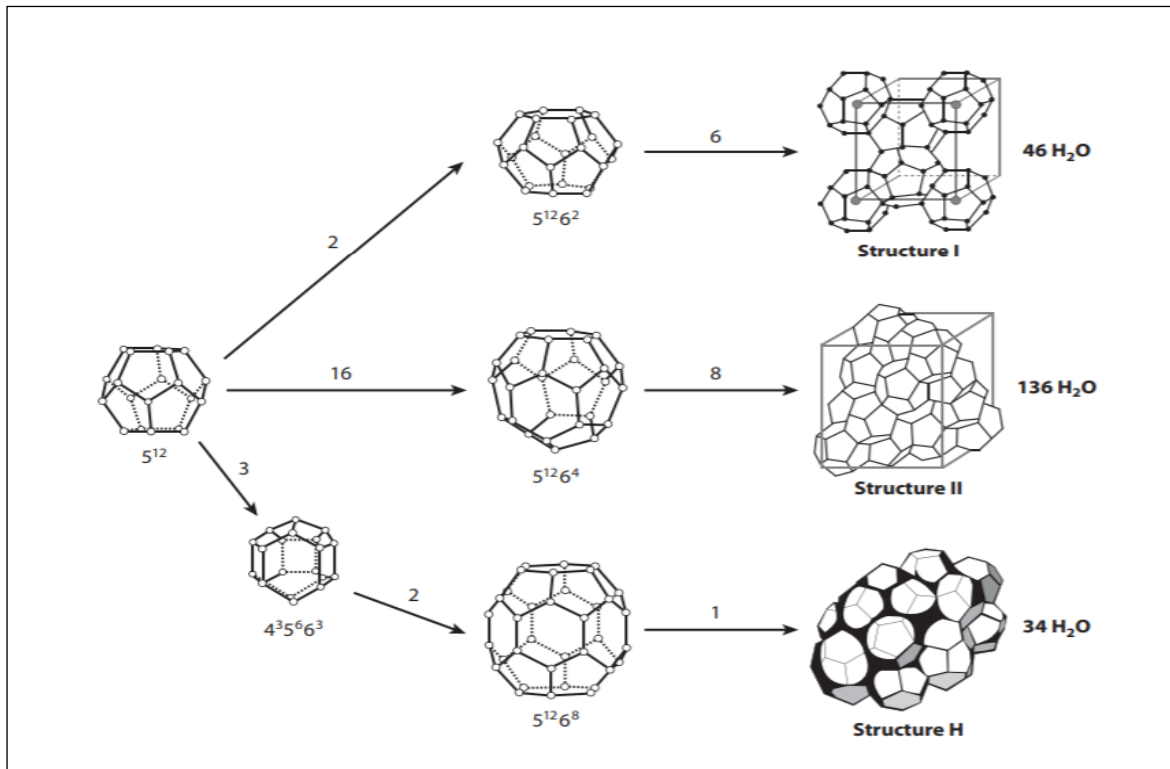


Figure 2-22: Three common hydrate unit crystal structures [32]

Gas hydrate formation becomes an issue in gas pipelines, particularly in subsea pipelines where the temperature and pressure conditions are ideal. The gas hydrate formation depends upon the needs of low temperature, high pressure, and the composition of the water-vapour mixture. Once these conditions are met, the gas hydrate formation can be accelerated through high-velocity flow streams and pressure pulsations. The hydrate formation can be considered a problem for oil and gas pipelines. Due to their solid crystalline form, they are non-flowing and build up in the pipeline until the pipe becomes plugged. This can be seen in Figure 2-23.

Removal of these hydrate blockages. Once they have occurred, it can take time, sometimes several months, leading to costly production stoppages. Several options are available to achieve this; one is a pigging operation, which can only be undertaken if the flow is possible in the pipe. A ‘pig’ is a device inserted into the pipeline and can sweep away any blockages. Another method is depressurisation of the pipeline, which aims to dissociate the hydrate from the pipe wall. However, this takes time and can be dangerous as a dislodged hydrate plug can cause damage to the pipeline. And finally, the hydrate can also be heated to dissociate the hydrate, but this can lead to rupture of the pipe if the gas hydrate expands. Therefore, rather than shutting down a pipeline to remove a hydrate plug, it has generally been preferred to find ways of preventing the formation of gas hydrates within pipelines. Four techniques that have been used to avoid the appearance of hydrates are as follows.

1. Remove the free and dissolved water from the system with separators, glycol dehydrators, molecular sieves, or other methods.
2. Maintaining temperatures above the range in which hydrates can form.
3. Maintaining low pressures to keep all phases fluid.
4. Injecting an inhibitor to prevent the formation of hydrate. An inhibitor is a substance that slows down or stops a chemical reaction or a process or reduces the activity of a reactant, catalyst, or enzyme.

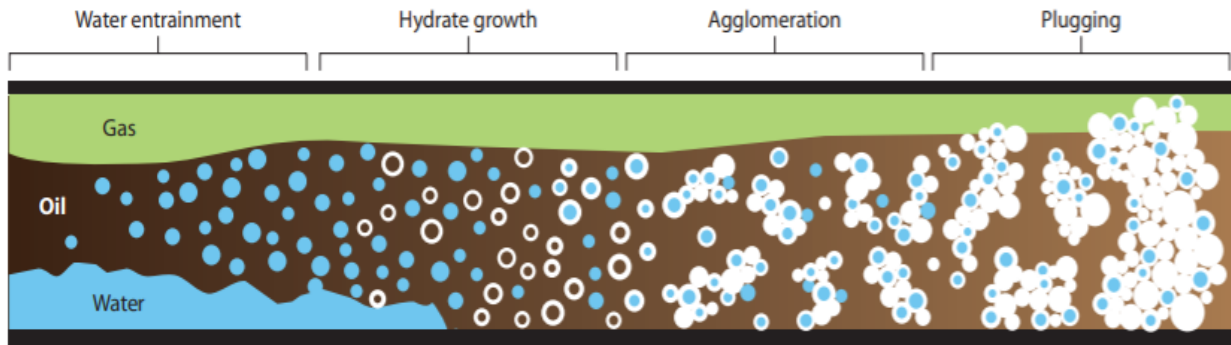


Figure 2-23: Gas Hydrate Build-up in Pipeline and Eclipse pipes (E Dendy Sloan, Carolyn Ann Koh et al., 2011)

The first of these methods is the most reliable; however, it may not be viable for all applications, particularly pipelines located in remote or submerged locations. Flow channels could be operated with inhibitor injection at the well, with dehydration of the flow occurring further downstream to solve. Compared with the flexible pipe analysis described above, the research of hydrate formation in flexible pipes is an area that has not seen the same amount of study. As such, no papers could be found looking specifically at the effect hydrates have on flexible pipes. Most of the current research is based on how hydrates form in multi-phase flow. Some experimental work has been undertaken on this topic but has proved relatively unsuccessful, primarily due to the complexity and unpredictability of hydrate formation. Key elements of the practical work, which informed assumptions made for this paper, are discussed below.

2.3.1 Samim, Soroush Zarinabadi and Amir

The paper discussed the problems gas hydrate cause in the oil and gas industry which may increase pipeline explosion if not prevented, using Iran as an example. One of the issues discussed is flow assurance; when oil is transported from the wellhead to the production site, if the temperature and pressure fall within the hydrate forming region, hydrate particles could start to form. They could eventually plug the pipeline, as shown in Figure 2-24.



Figure 2-24: Hydrate formation in the natural gas pipeline [33]

Hydrate blockages can cause production stoppages for months at a time, so it is advisable not to let them reach this stage. Hydrate propagation forms a plug that splits the pipe into two pressure sections: a high pressure, upstream section, between the wellhead and the plug, and low pressure, downstream section, between the plug and the production vessel. In this high-pressure section, a blast can occur in the pipe due to pressure growth. The plug, therefore, has the potential to destroy the pipe if the pressure difference between the high and low-pressure sections becomes too large, endangering personal safety and expensive production. A typical burst pipe on hydrate formation and eliminating clogging pipes with time is presented in Figures 2-25 and 2-26, respectively.



Figure 2-25: (a) Burst pipes on hydrate formation (b) Eliminating clogging in pipes [33]

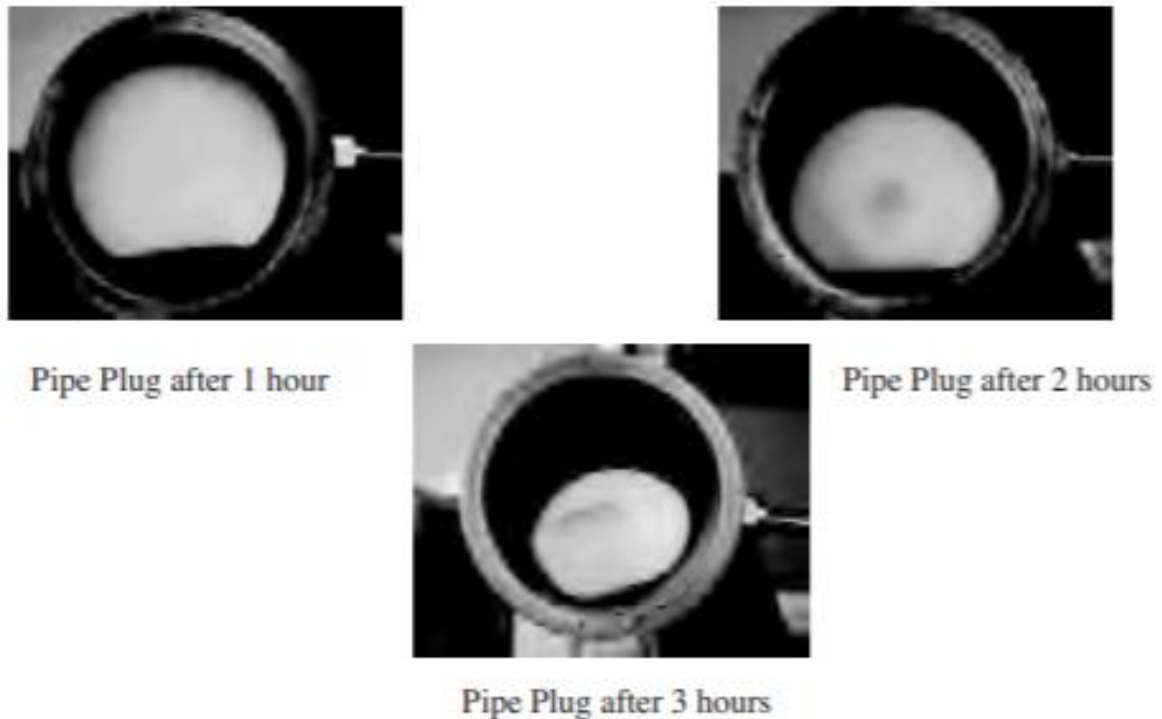


Figure 2-26: Eliminating clogging pipes with time [34]

2.4 Subsea system configuration and technology

The operator's requirements largely determine different configurations of subsea systems. Moreover, an individual company determines the design and the structure of the subsea layout at the concept selection stage when designing the field development program (FDP). After that, improvement is carried out during Pre-FEED, Front End Engineering Design (FEED) and Detail Engineering phases. The configurations are dependent on the reservoir, production facilities, well arrangements, drill centre, seabed structure, ocean properties and forces. The complexity of different configurations is shown in Figures 2-27 to 2-30.

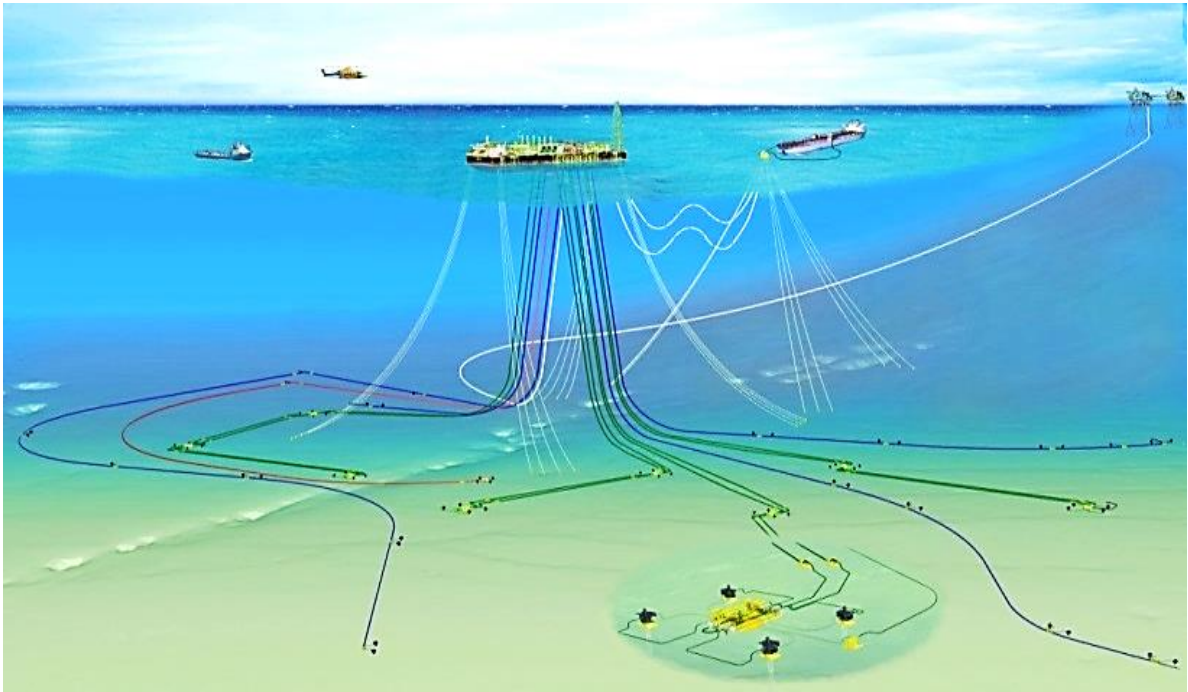


Figure 2-27: Typical Subsea layout [35]

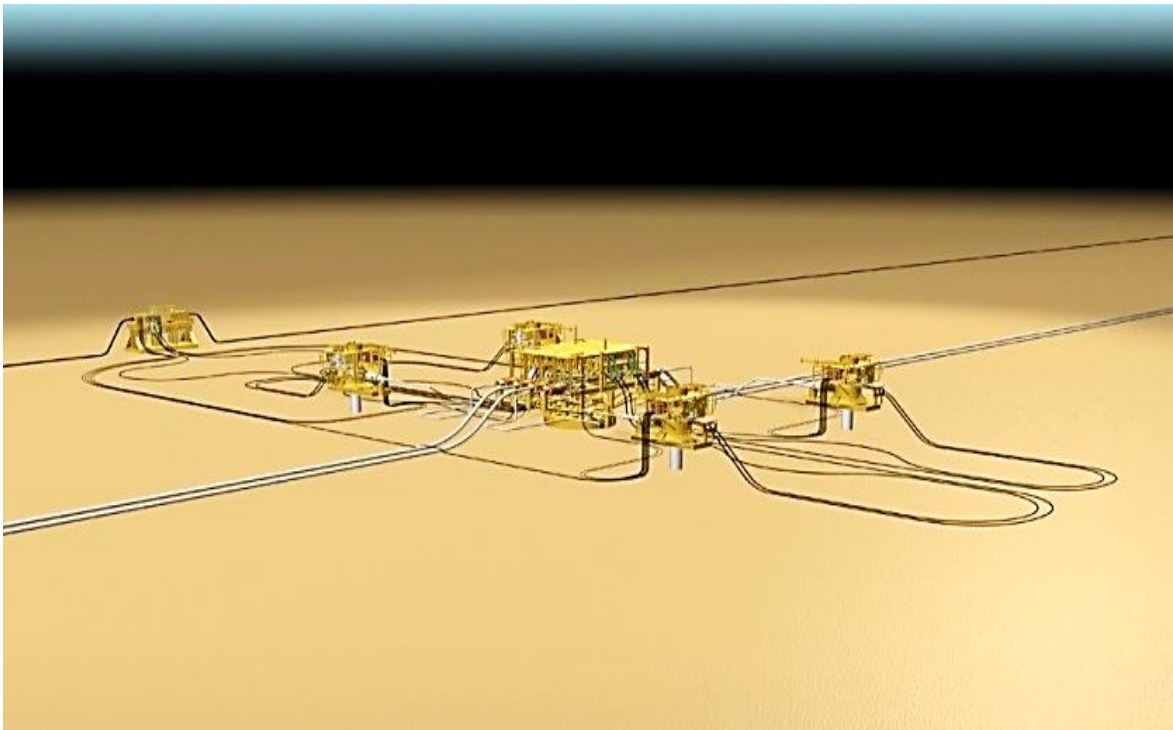


Figure 2-28: Manifold and the Subsea trees [35]

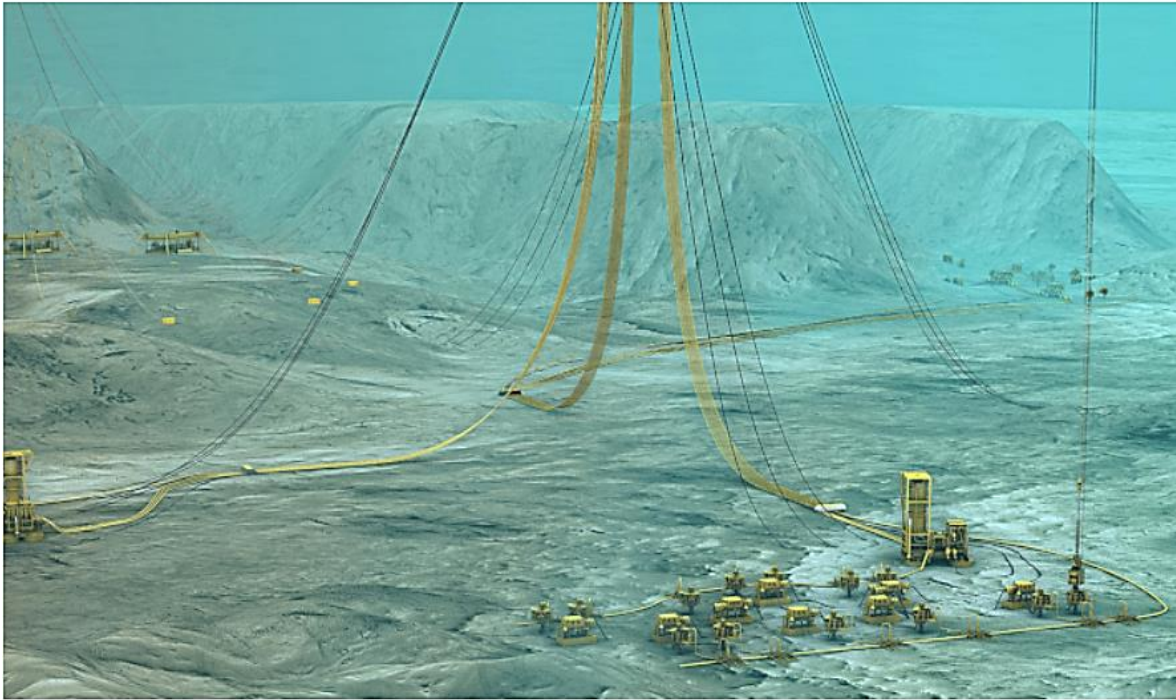


Figure 2-29: Subsea production manifolds, flow lines and risers on the seabed [35]

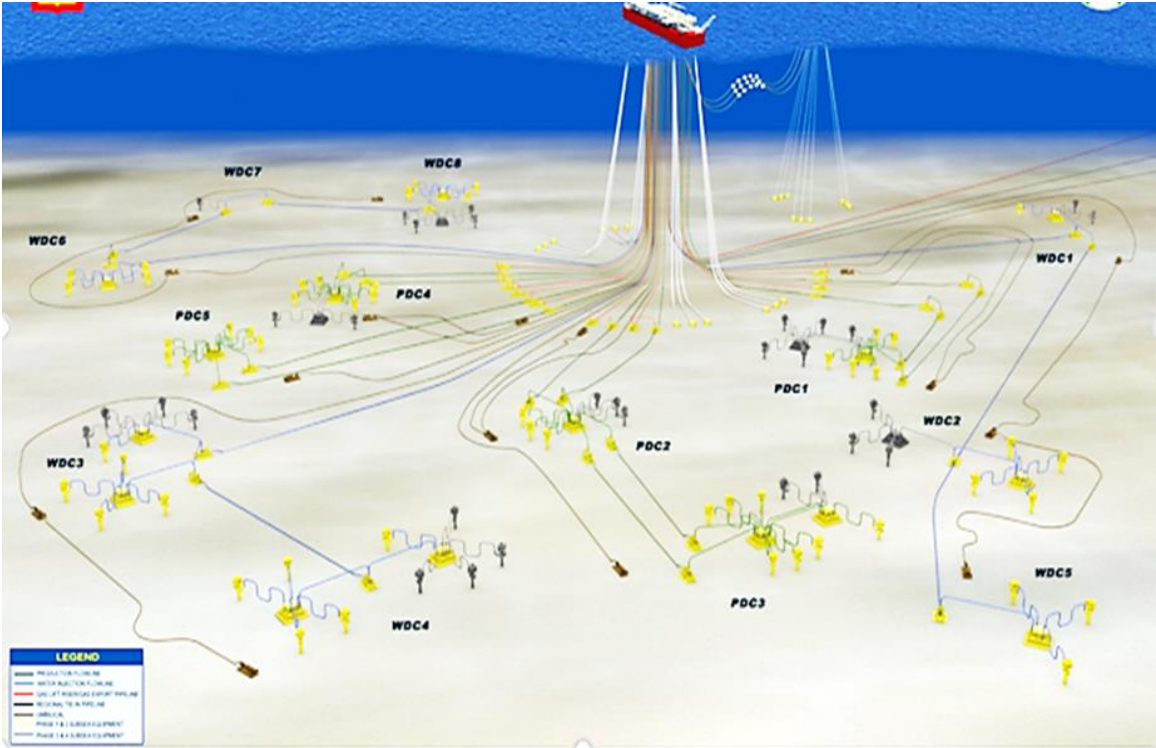


Figure 2-30: Configuration of a deep-water subsea system [36]

The technology in the exploitation of oil and gas is continually advancing; thus, recent improvements have led to cost-saving in the operation and production of oil and gas industries. These new technologies are available in offshore markets across the globe. However, the technology is facilities dependent,

mainly on the size of the field, small or large. Thus, to develop a small or large size field, subsea tree and wellhead requirements vary greatly. A large field with many Drill centres can have two (2) or more wells tied together through a centralized manifold or other structures. This requires a specialized technology adopted during the concept selection process.

The wells are connected from the seabed through subsea trees, jumper, manifold, flowline to riser then to surface facility as shown in Figure 2-31.

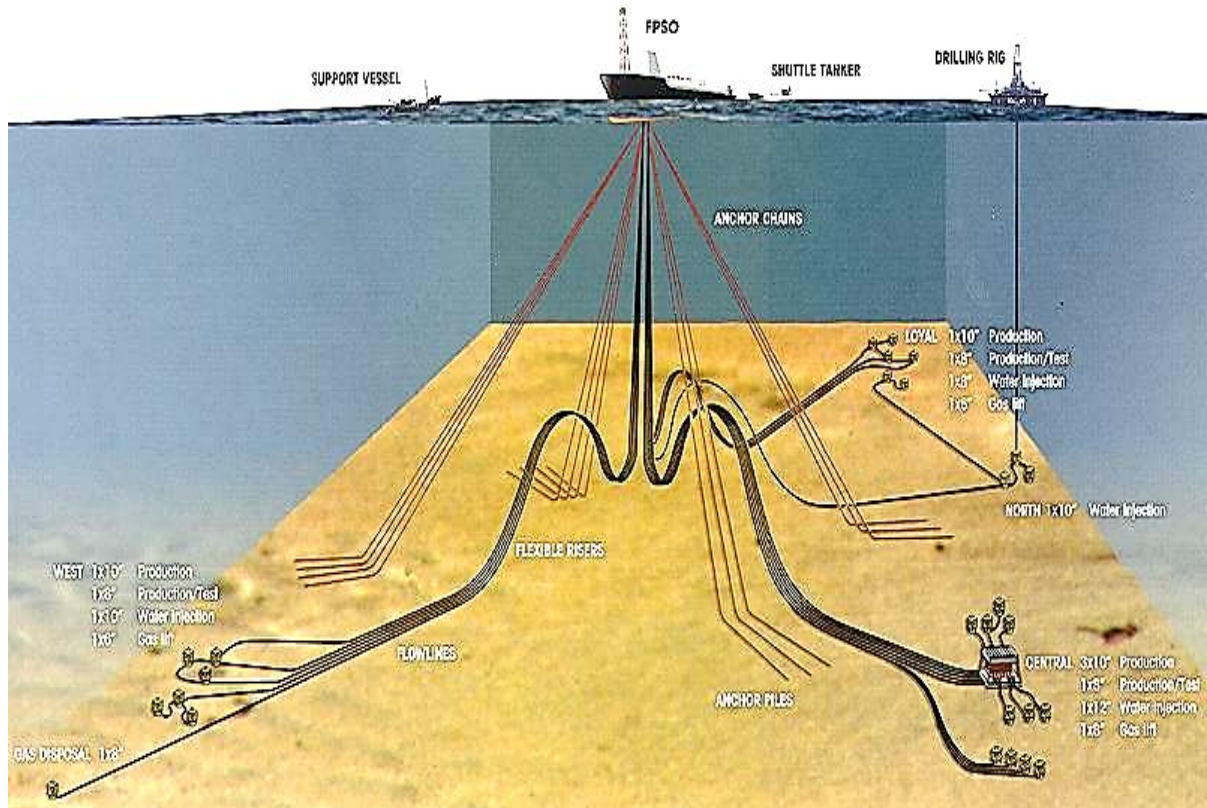


Figure 2-31: Typical Subsea Connection-Exxon Mobil, Nigeria [37]

2.4.1 Installation and maintenance of the structures

Diverse specialized equipment, vessels and methods are employed in the installation and operation of the subsea equipment. These include Dynamic Positioning (DP) vessels, Remote Operated Vehicle (ROV), Autonomous Underwater Vehicle (AUV), etc. are designed and dedicated for deep-water operations. The vessel can be DP1, DP2 and DP3, and their deployment depends on the installation requirements. These can be drillship, semi-submersible rigs, jack-up rigs, crane barge etc. They are all used for the installation of subsea structures.

2.4.1.1 Conventional maintenance programs

In subsea development, all the structures are connected to take As mentioned, the more technological advancements, the more complex the maintenance of such facilities is becoming. Shown in Table 2-3 are the required maintenance program designs basically for marine structures.

Table 2-3: Subsea structure maintenance [1]

| Structure | Maintenance Program |
|------------------|--|
| Flowline | Annulus test, Integrity Test, Thermal Management, Pigging, Corrosion Management, External scanning, General Visual Inspection (GVI) |
| Flexible pipes | Annulus test, Integrity Test, Thermal Management, Pigging, Corrosion Management, External scanning, GVI |
| Pipeline | Integrity Test, Thermal Management, Pigging, Corrosion Management, External scanning, Pipeline walking mitigation |
| Manifold | Thermal Management, Corrosion Management, External scanning, GVI |
| Spool | Annulus test, Integrity Test, Thermal Management, Pigging, Corrosion Management, External scanning |
| Jumper | Annulus test, Integrity Test, Thermal Management, Pigging, Corrosion Management, External scanning, GVI |
| Umbilical | GVI, Integrity Test, Preservation |
| Subsea Trees | Integrity Test, Thermal Management, Corrosion Management, GVI |

2.4.2 General Subsea Challenges

Most major offshore fields worldwide have experienced mild and fatal subsea structures failures at a time in the life of a field [10]. Accordingly, there are existing issues such as flexible pipe ruptures, failure, and blockage; subsea control modules/subsea electronics modules (SCM/SEM) leakages, umbilical failure, and fatigue of mechanical structures that new further studies to overcome the challenges. However, the deeper the offshore exploration, the higher offshore liabilities in terms of failures and associated impact on productions and the environment.

Globally, the repair and replacement of damaged structures often cost millions of US Dollars which sometimes lead to facilities shut down and production loss for a longer period. The present deepwater challenges are particularly relevant to the following subsea structures:

1. Flexible pipe
2. Christmas Trees
3. Pipelines/Jumpers
4. Umbilical
5. SCMs /SEMs

The Gulf of Guinea that covers production areas in deep-water Africa is not exempted from these challenges; thus, most companies have explored risk transfer through insurance because of the enormous liabilities involved in subsea structures.

Experts are reviewing the solution to the hydrate blockage in these components on an ongoing basis by carrying out root cause analysis to determine the formations and reduce the problem if not controlled. The remedial measure is adopted but cautioned not to allow the occurrence of the blockage. Preventing the formation reduce costs and the usage of harmful chemicals in pipeline operations.

Presented in Figures 2-32 to 2-34 are clear examples of pipeline blockages and riser, jumper or spool trenching, amongst other subsea problems. As shown in Figure 2-34, there is a global problem with trenching of subsea structures lying on the seabed due to many factors ranging from poor soil texture resulting from an inaccurate geotechnical survey, poor design dynamic motion, and to mention but a few.

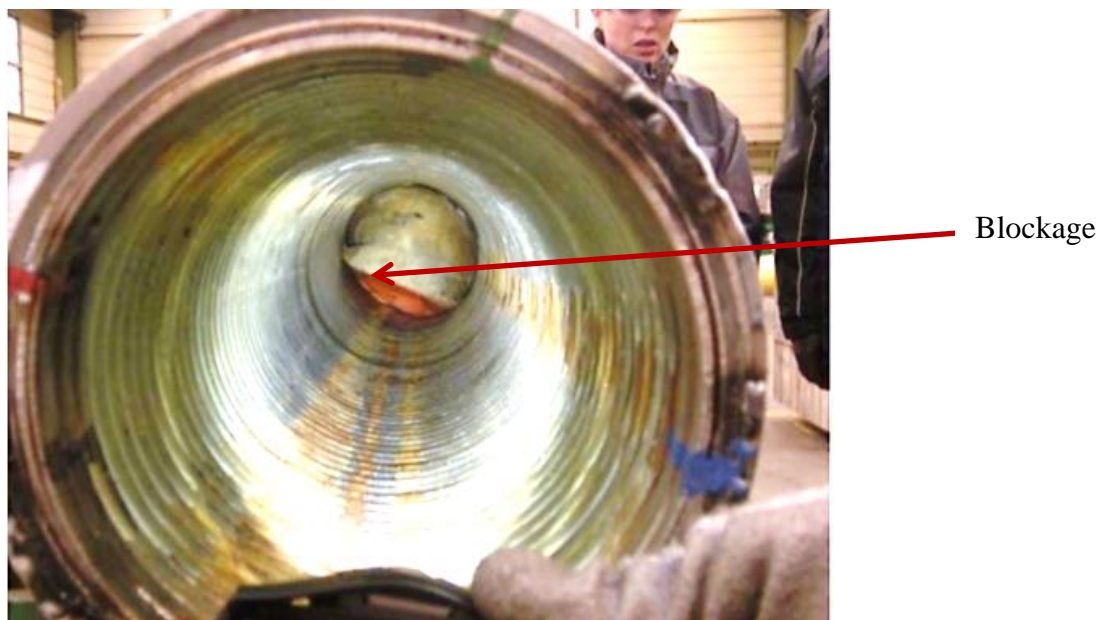


Figure 2-32: Blockage inside a flexible pipe suspected to be a pig [5]

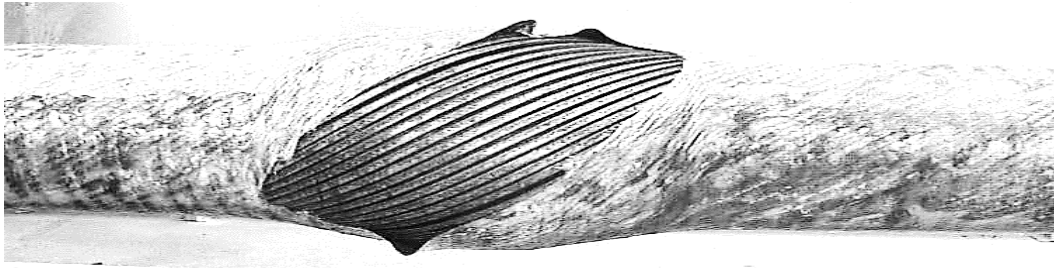


Figure 2-33: Bird cage' failure caused by excessive axial compression load [38]

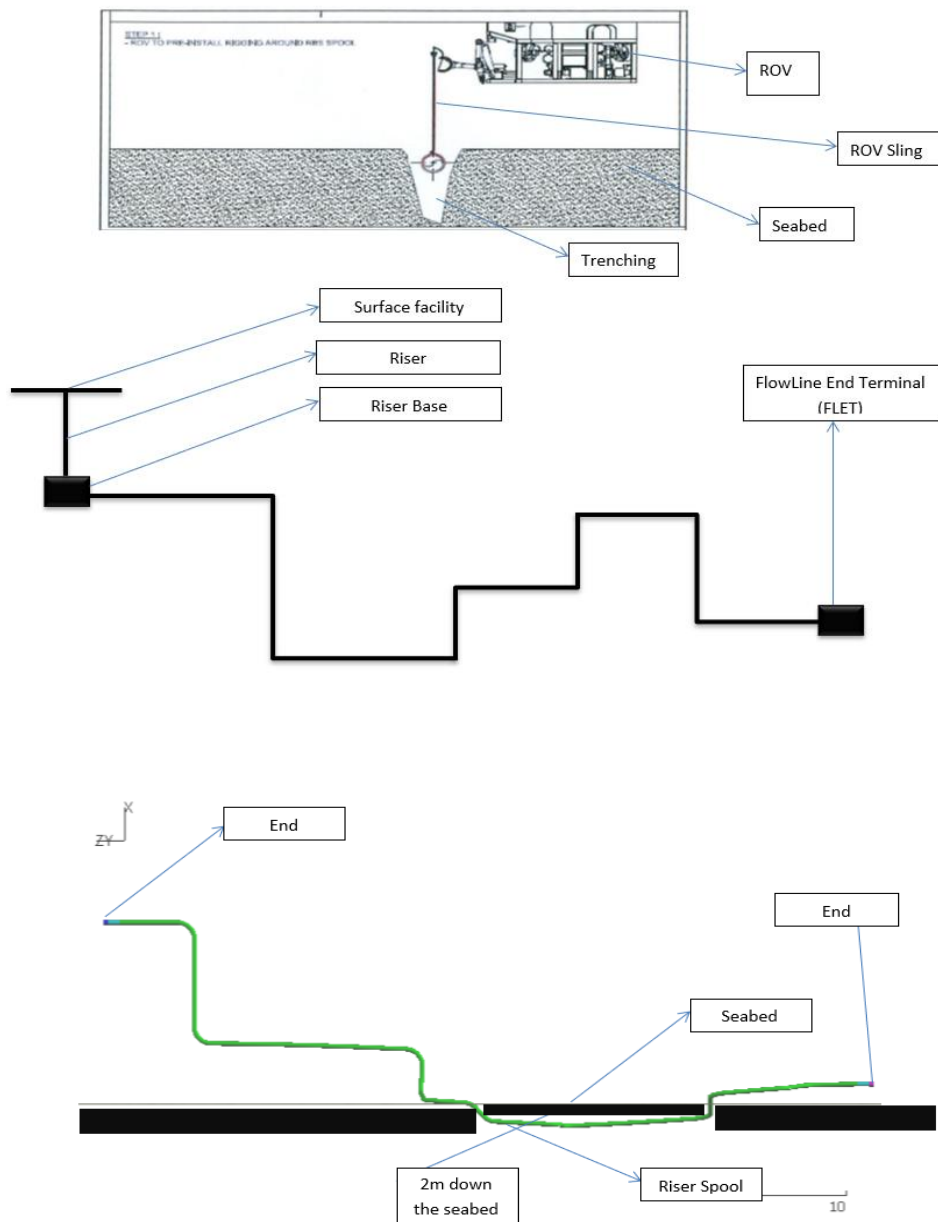


Figure 2-34: Riser base jumper-spool trenching and diagrammatic representation

2.5 Concluding Remarks

The above literature review on non-bonded flexible pipes shows no research study focussed on the hydrate blockage in flexible pipes and their consequent failures. Several research publications on non-bonded flexible pipes and their applications in oil and gas considered various configurations layers and material compositions up to 10-layers even above and subjected to multiple load conditions such as pressure, forces, moments, and other variables (coefficient of friction and constant stiffness). In addition, the literature also considered various boundary conditions and surface contacts depending on the models. These, amongst others, have provided a good understanding of the different loads and resulted in failure modes, including those limiting the recommended practices. Consequently, the reviewed literature on FEA of non-bonded flexible pipes clearly explained flexible pipes' behaviour and structural responses under different loads such as torsion, axial, compressive, internal, and external pressures. It was built on and guided the approach used to model the flexible pipe in the present research. This guidance is not limited to the materials but also pipe specifying loads, clarity on surface contact, interactions, penetration, boundary conditions, coefficient of friction, and constant stiffness applications on ABAQUS. The experimental research also guided invalidating the practical tests and outcomes, while the analytical aided invalidating some numerical results. The current research models are derived based on the methodologies and experiences from the literature. They are to examine the flexible pipe under hydrate blockage to determine the effects on the layers, failure mode, and the hydrate's consequences on the entire system.

CHAPTER 3: FLEXIBLE PIPE NUMERICAL MODELLING

3.1 Introduction

The work outlined in this chapter focused on different types of flexible pipes family, the guiding international codes, and standards that described the failure modes and detailed finite element model methodology of non-bonded flexible pipe investigated in this research work. Two general numerical schemes were considered, which includes explicit and implicit time integration algorithms. While implicit algorithm entails iterative solutions for each time increment, precisely time step, an explicit algorithm is used for nonlinear problems with many degrees of freedom for which iterations are costly with significant convergence problems and no iteration. Explicit algorithm lacks global tangent stiffness matrix, which ordinarily goes with implicit algorithm but used in this research work methodology due to time primarily determined by the number of elements. The most diminutive dimensions require a small-time incremental size that relies on the model's highest natural frequencies, independent of the type and loading period.

3.2 Types of flexible pipe

Flexible pipes are composed of a fixed number of distinctive and essential layers, each of which has a specific function or function. They are uniquely designed for a given application and are not seen as standard ‘off-the-shelf’ products. As such, there is an extensive range of possible layer combinations and configurations depending on the nature of the exact application. From an industry perspective, flexible pipe families are clearly defined and presented in American Petroleum Institute (API)-Recommended Practice (RP) and Specification codes [1] and [8] standard, respectively, and they are:

1. Smoothbore pipe (family I)
2. Rough bore pipe (family II)
3. Rough bore reinforced pipe (family III)

However, this research focused on smooth bore pipe family (family I type), which comprises pressure sheath, pressure armour, pressure sheath, intermediate sheath, tensile armour 1, tensile armour 2 and outer sheath. Others, such as the rough bore pipe family, contains internal carcass, pressure sheath, tensile armour, and outer or external sheath. While the rough bore reinforced pipe family has an internal carcass, inner liner, pressure armour, tensile armour, and an outer sheath [38].

Concerning the present research, extra layers such as high strength tapes, thermal insulation, and anti-wear layers are included in the family I type flexible pipe and are incorporated in the pipe model.

3.3 Codes and Standard Practices

Industrial standards such as the American Petroleum Institute (API) aid the design of different flexible pipe families described above. API Specification 17J [8] provides the safe design of non-bonded

flexible pipes by considering the load conditions to determine the minimum thickness of the layers and materials used. API Recommended Practice (RP) 17B provides supplementary guidelines for designing and analysing flexible pipes [1].

The API describes various failure modes that must be considered when designing or analysing a flexible pipe, and these include but are not limited to the following:

1. The collapse of the carcass layer is due to excessive external pressure.
2. Rupture/Bursting of pressure or tensile armour layers due to excessive internal pressure.
3. Tensile failure unlocks wires in armour layers or ruptures polymer layers caused by excessive tensile loads or over bending.
4. Compressive failure of tensile armour layer, also known as bird-caging.
5. Fatigue Failure.

Proper design of a flexible pipe should ensure that none of these failure modes occurs, however in practice, some factors primarily contribute to the failure of the layers. Examples can be found in the corrosion of metallic layers and erosion of the carcass by the bore fluid. Another mechanism that can increase the risk of failure is the blockage of the pipe bore by gas hydrates and not explicitly covered in API RP. Primary factors considered in the flexible pipes design process, amongst others, include structural integrity and the detailed requirements such as size (length and diameter), pressure rating and internal coatings and are dependent upon the service conditions and installation processes.

For this research work, only American Petroleum Institute standards (API): [1] and [8] are considered out of various international standards (DnV [39], ASME [40], etc.) and focussed mainly on relevant failure modes.

Flexible pipe (flowline or riser) failure during service indicates loss of ability to transport fluids efficiently, minor uncontrolled loss of pipe integrity or blockage in the pipe, which can be disastrous. The flexible pipe failure modes and critical features and their applicability are summarised in Table 3-1.

Consequently, the problem for this research is not explicitly covered as earlier mentioned, and this form the main reason for the current research work.

3.3.1 Failure mode and recommended practices API RP

Due to the complexity of the flexible pipe layers, understanding the failure mode and behaviour is paramount; hence, the need to provide a relative failure mechanism and appropriate design strategies/solutions. These protocols meet the design criteria specified in ISO 13628-2 [41] and are provided for in API 17B displayed in Table 3-1 checklist.

Table 3-1: Checklist of failure modes for non-bonded flexible pipe; [1]

| Pipe global failure mode to design against | Potential failure mechanism | Design solution or variable (ISO 13628-2) |
|--|--|---|
| Collapse | <ol style="list-style-type: none"> 1. The collapse of carcass and pressure armour due to excessive tension. 2. The collapse of carcass and pressure armours due to excess external pressure 3. The collapse of carcass and pressure armour due to installation loads or ovalization due to installation loads 4. The collapse of internal pressure sheath in the smooth-bore pipe. | <ol style="list-style-type: none"> 1. Increase the thickness of carcass strip, pressure armour or internal pressure sheath (smooth-bore collapse) 2. Modify configuration or installation design to reduce loads 3. Add intermediate leak-proof sheath (smooth-bore pipes) 4. Increase the area moment of inertia of carcass or pressure armour |
| Burst | <ol style="list-style-type: none"> 1. Rupture of pressure armours because of excess internal pressure. 2. Rupture of tensile armour due to excess internal pressure. | <ol style="list-style-type: none"> 1. Modify design, e.g., change the lay angle, wire shape etc 2. Increase wire thickness or select higher strength material if feasible 3. Add additional pressure or tensile armour |
| Tensile Failure | <ol style="list-style-type: none"> 1. Rupture of tensile armours because of excess tension 2. The collapse of carcass and pressure armour and internal pressure 3. Snagging by fishing trawl board or anchor, causing over bending or tensile failure | <ol style="list-style-type: none"> 1. Increase wire thickness or select higher strength material if feasible. 2. Modify configuration design to reduce loads 3. Add two or more armour layers 4. Bury pipe |
| Compressive failure | <ol style="list-style-type: none"> 1. Bird-caging of tensile armours due to excess tension. 2. Compression leading to upheaval buckling and excess bending | <ol style="list-style-type: none"> 1. Avoid riser configurations that cause excessive pipe compression 2. Provide additional support/restraint for tensile armours such as tape and additional or thicker outer sheath. |
| Overbending | <ol style="list-style-type: none"> 1. The collapse of carcass and pressure armour or internal pressure sheath. 2. Rupture of internal pressure sheath 3. Unlocking of interlocked pressure or tensile armour layer 4. Crack in the outer sheath | <ol style="list-style-type: none"> 1. Modify configuration design to reduce load |
| Torsional failure | <ol style="list-style-type: none"> 1. Failure of tensile armour wires 2. The collapse of carcass and internal pressure sheath 3. Bird-caging of tensile armour wires | <ol style="list-style-type: none"> 1. Modify system design to reduce torsional loads 2. To increase torsional capacity, modify cross-section design (e.g., change the lay angle of wires, add extra layer outside armour wires). |
| Fatigue failure | <ol style="list-style-type: none"> 1. Tensile armour wire fatigue 2. Pressure armour wire fatigue | <ol style="list-style-type: none"> 1. Increase wire thickness or select alternative material so that fatigue stresses are compatible with service-life requirements 2. Modify design to reduce fatigue load. |
| Erosion | <ol style="list-style-type: none"> 1. Erosion of internal carcass | <ol style="list-style-type: none"> 1. Modify material selection, increase the thickness of carcass, Reduce sand content & Increase MBR |
| Corrosion | <ol style="list-style-type: none"> 1. Of internal carcass 2. Of pressure or tensile armour exposed to seawater. 3. Of pressure or tensile armour exposed to diffused products | <ol style="list-style-type: none"> 1. Modify material selection 2. Cathodic protection system design 3. Increase layer thickness 4. Add coatings or lubricants. |

3.3.2 Failure mode and recommended allowable degradation

Apart from the failure modes, ISO and API identified some critical degradations in non-bonded flexible pipes but to the extent of tolerance that cannot result in a breakdown. This is summarized in Table 3-2.

Table 3-2: Recommended allowable degradation for non-bonded flexible pipes; API 17B

| Component | Degradation mode | Recommendation |
|--|--|--|
| Carcass | <ol style="list-style-type: none"> Corrosion Erosion | <ol style="list-style-type: none"> Limited corrosion is acceptable provided structural capacity and functional requirements are maintained. Same as for corrosion |
| Internal Pressure Sheath | <ol style="list-style-type: none"> Creep Thermal/chemical degradation Cracking | <ol style="list-style-type: none"> Limited creep acceptable provided <ol style="list-style-type: none"> Structural capacity to bridge gaps maintained No cracks No leakage. No locking of the carcass or pressure armour Sealing maintained at end fittings Capacity at design life remains within specified usage factors with maximum gaps between layers. No leakage allowed. Increased permeation is allowed if the system has been designed for an increased level of permeation. Essential considerations are increased damage rates (corrosion, HIC, SSC) for armours and limited gas venting system capacity. Strain capacity enough to meet design requirements of ISO 13628-2 No cracking because of dynamic service. |
| Pressure and tensile armours | <ol style="list-style-type: none"> Corrosion Disorganization or locking of armouring wires Fatigue and wear | <ol style="list-style-type: none"> Only general corrosion accepted; no crack initiated acceptably. No disorganization of armouring wires when bending to a minimum radius Modify design to reduce fatigue load is enough |
| Anti-wear | <ol style="list-style-type: none"> Wear | <ol style="list-style-type: none"> No, wear through the thickness of the layer over its service life. |
| Intermediate Sheath | <ol style="list-style-type: none"> Thermal degradation | <ol style="list-style-type: none"> Functional requirements are maintained |
| Thermal insulation | <ol style="list-style-type: none"> Thermal degradation | <ol style="list-style-type: none"> Insulation capacity is maintained equal to or above a minimum specified value |
| Outer sheath | <ol style="list-style-type: none"> General degradation Radial deformation (loosening) Breaching | <ol style="list-style-type: none"> Strain capacity is enough to meet the design requirements of ISO 13628-2 No loosening causes the disorganization of armour wires or strain failure of the outer sheath material. No breaching is allowed unless the pipe design under flooded annulus conditions can be shown to meet the design requirements and remaining service life requirements. |
| End fitting and carcass sheath interference | <ol style="list-style-type: none"> corrosion | <ol style="list-style-type: none"> no corrosion that reduces capacity, the possibility for leakages, or damage to any sealing or locking mechanism is acceptable. |

3.4 Finite element analysis suitability

Finite element analysis (FEA) software is designed for complex analyses that are tasked and cumbersome and meant to analyse stress and respective strain. Nowadays, it is utilized for other processes requiring numerical solutions like magnetic fields, lubrication, fluid flow, electric, heat transfer, and many others. It is relatively straightforward to design and optimise structures and

components within this engineering environment. The current approach to undertaking research of the layered pipe with hydrate blockage required the use of FE as the principal analysis tool, which helped determine the magnitude of stresses and interaction on the entire surface of a flexible pipe and between the layers where they are analysed individually.

Consequently, it is hoped this approach showed that the investigated flexible pipe failure modes and mechanism are predicted with limited available physical test results reviewed and compared with finite element computational results. Again, for better security, Abaqus FEA and ANSYS software are used to conduct analyses in this research out of many globally available finite element software packages with open source. Other finite element software is also available to study complex problems involving contact interaction in flexible pipes. It is meant for general-purpose, and a nonlinear finite element analysis software is used to analyse the nonlinear static and dynamic response of inelastic structures, mainly three-dimensional. Its fully automated contact analysis capability and error-checking features have successfully enabled users worldwide to solve many complex problems. The manufacturer develops sophisticated tools for modelling and simulating the significant deformation behaviour of structures. These tools include LS-DYNA for analysis, LS-POST for post-processing which is interfaced with leading CAD, FEA, and FEM systems. However Abaqus explicit is used to carry out the modelling and studies [42].

ABAQUS software was selected to perform the analyses despite the variety of software packages. It was chosen based on its versatility and simulation capabilities besides from its more comprehensive range of material modelling features used extensively to predict how different layers interact with each other when subjected to loads. The key focus was on the fidelity of the mesh and the element's choice due to the layered pipe's complexity. It is essential to understand how elements behave mathematically within an FEA code and correctly choose suitable varieties, sizes, and shapes of features and how they can be used. Also, it is crucial to fully understand the mathematical assumptions and limitations of the theory within the program to determine the physical behaviour of the design. A responsible user must consider the physical nature of any problem and the conduct of FEA well enough to prepare a suitable model and evaluate the quality of the results. Abaqus is a general-purpose analysis program applied to many research fields due to its extensive material modelling capability. The Abaqus modelling processes involved in this research work are shown in Figure 3-1.

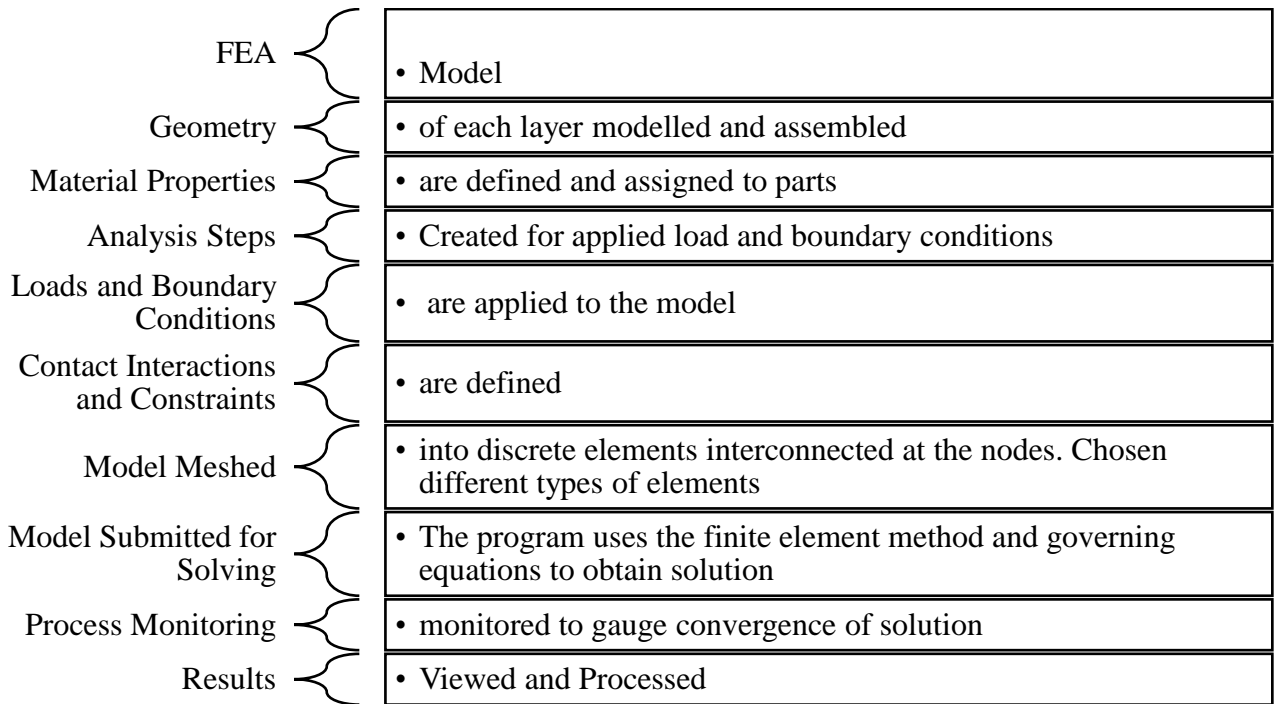


Figure 3-1: Process flow chart

Understandably, Abaqus has no built-in system of units; thus, all input data are specified in consistent units of measure without any deviation.

Based on the above, smooth bore family 1 type of flexible pipe and codes, including the standard practices, were all considered in the finite element model and simulation of the flexible pipe, taking cognisance of the failure modes as contained in the API RP for this research work. The materials, sizing, pressure, the temperature were selected accordingly. And, as stated by the manufacturer of the flexible pipe under investigation, this was explained in detail below.

In conclusion, having reviewed many papers on the subject research, it indicates that most papers either carried out an experimental, analytical, or numerical analysis on a particular area of flexible pipe. They failed to consider a specific problem that might lead to multiple issues in practice, which was not explicitly explained in the recommended practice stipulated in API 17B. This research, therefore, sees this as a knowledge gap that must be addressed hence, the investigation of hydrate formation in the pipe that led to blockage and eventual rupture.

The flexible pipe under question is modelled and analysed according to the recommended practice described later in this work.

3.5 Geometry and element

A typical 6” (152.4 mm) flexible pipe was developed to analyse primary layers' geometric properties, including the pipe layer specification and material properties, as shown in Figure 3-2 and detailed in Table 3-3.

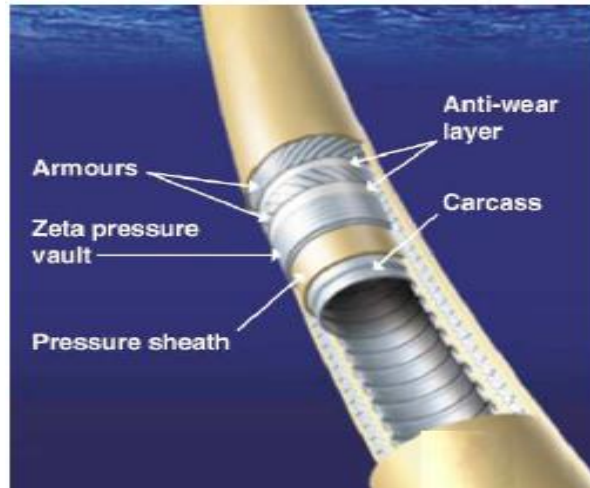


Figure 3-2: Schematic of a typical seven-layer flexible flowline [43]

For this research work, all layers were modelled in both 8-noded SOLID C3D8R and 4-noded shell element SHELL S4R as represented in Figures 3-3 and 3-4, respectively, with both elements showing consistency in their results. The standard solid element is a solid model where the material is represented throughout the component or structure. At the same time, a shell is hollow on the inside and models the outer “shell” and are the mathematical simplification of solids of a particular shape. More focus is on a solid element as far as this present work is concerned due to its simplicity in modelling the parts and easier to place the load on the surfaces.

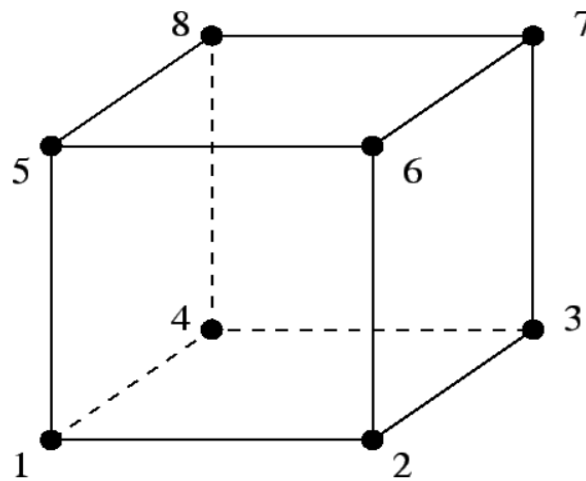


Figure 3-3: 8-Nodes linear brick Element (C3D8R) [44]

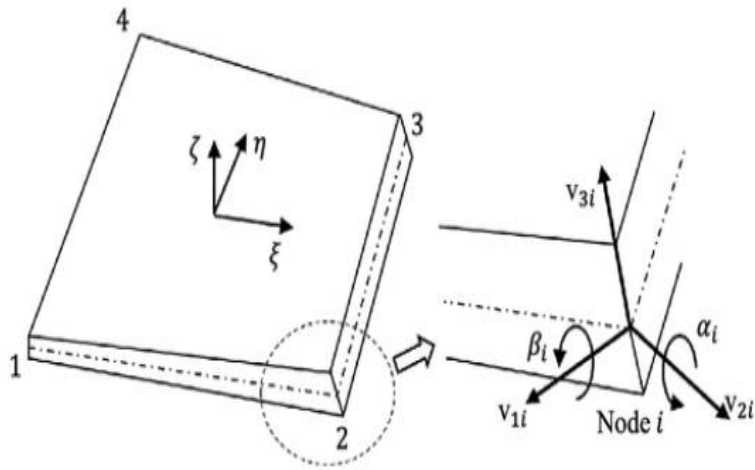


Figure 3-4: 4-Nodes Shell Element (S4R) [45]

Table 3-3: Non-bonded Flexible Parts, Model 1-C3D8R

| Layer | Type | Material | Element Type |
|-------|--------------------------------|--------------|--------------|
| 1. | Carcass | Metallic | Solid |
| 2. | Pressure Sheath | Non-Metallic | Solid |
| 3. | Zeta/Pressure Armour | Metallic | Solid |
| 4. | 1 st Tensile Armour | Metallic | Solid |
| 5. | 2 nd Tensile Armour | Metallic | Solid |
| 6. | High Strength Tape | Non-Metallic | Solid |
| 7. | Outer Sheath | Non-Metallic | Solid |
| 8. | Methane Hydrate | Hydrate | Solid |

Table 3-4: Non-bonded Flexible Parts, Model 2- S4R

| Layer | Type | Material | Element Type |
|-------|--------------------------------|--------------|--------------|
| 1. | Carcass | Metallic | Shell |
| 2. | Pressure Sheath | Non-Metallic | Shell |
| 3. | Zeta/Pressure Armour | Metallic | Shell |
| 4. | 1 st Tensile Armour | Metallic | Shell |
| 5. | 2 nd Tensile Armour | Metallic | Shell |
| 6. | High Strength Tape | Non-Metallic | Shell |
| 7. | Outer Sheath | Non-Metallic | Shell |
| 8. | Methane Hydrate | Hydrate | Solid |

The manufacturer supplied the geometry of the flexible pipe under consideration as presented in Table 3-4, and a further detailed view of the flexible pipelayers is shown in Figure 3-5.

Table 3-5: Flexible Layers geometry Properties

| Layer | No. Layer description | h (mm) | r _i (mm) | r _o (mm) | r (mm) | Lay angle (α°) |
|-------|--|-----------|------------------------|------------------------|-----------|-------------------|
| 1 | Interlocked carcass, 48.0 x 1.0 AISI 304 (FE) 20 | 5 | 80.03 | 85.03 | 82.53 | 87.6 |
| 2 | Internal plastic sheath RILSAN P4 0TL TP01 | 4 | 85.03 | 89.03 | 87.03 | |
| 3 | Zeta-clip, 2 tendons th 6.2 FM 35 (FI 11) | 6.2 | 89.03 | 95.23 | 92.13 | 85.6 |
| 4 | First Armour Lay 35.0 deg FI41 2x7mm, 40 wires | 2 | 95.23 | 97.23 | 96.23 | 35 |
| 5 | Second Armour Lay -35.0 deg FI41 2x7mm, 44 wires | 2 | 97.23 | 99.23 | 98.23 | -35 |
| 6 | High Strength Tape 1 Tape-BA09 KV 400daN130mm | 1.25 | 99.23 | 100.48 | 99.855 | |
| 7 | External Sheath FINATHENE (TP 04) | 4.8 | 100.48 | 105.28 | 102.88 | |

r_i Internal Radius
r_o Outer Radius
r Mean Radius

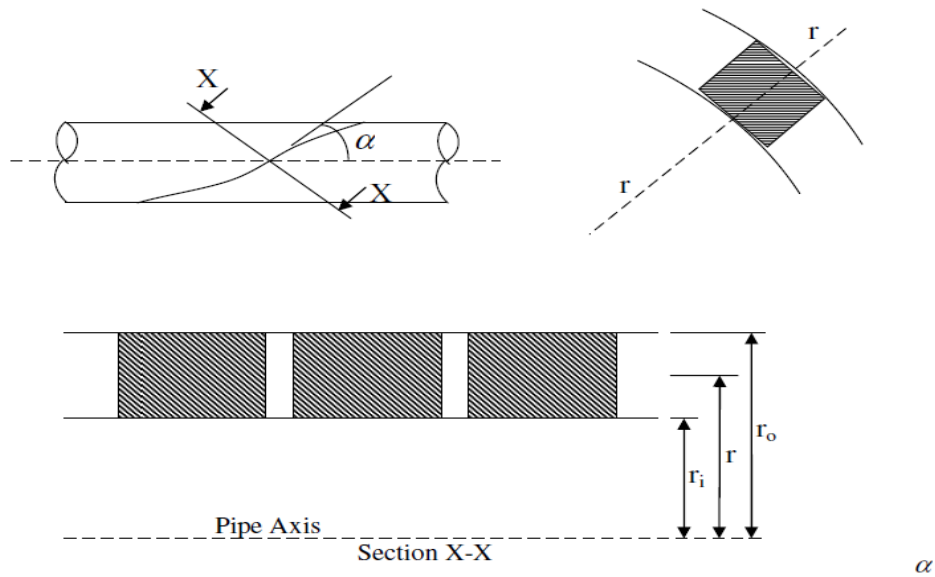


Figure 3-5: Geometry of the Flexible Pipe [42]

3.6 Material properties

Table 3-6: Flexible Pipe material data based on the equivalent orthotropic materials

| Layer | Layer description | UTS (MPa) | SDP (MPa) | Mass (kg/m) | I.D. (mm) | h (mm) | Area (mm ²) | E (MPa) |
|-------|--|-----------|-----------|-------------|-----------|--------|-------------------------|---------|
| 1 | Interlocked carcass, 48.0 x 1.0 AISI 304 (FE) 20 | 550 | - | 11.70 | 160.05 | 1.17 | 19.6 | 16507 |
| 2 | Internal plastic sheath RILSAN P4 0TL TP01 | 48 | - | 2.31 | 162.40 | 6.42 | - | 345 |
| 3 | Zeta-clip, 2 tendons th 6.2 FM 35 (FI 11) | 1000 | 380 | 22.73 | 175.23 | 3.78 | 54.1 | 13692 |
| 4 | First Armour Lay 35.0 deg FI41 2x7mm, 40 wires | 1400 | 403 | 8.27 | 182.80 | 2.00 | - | 345 |
| 5 | Second Armour Lay -35.0 deg FI41 2x7mm, 44 wires | 1400 | 461 | 8.39 | 186.80 | 2.00 | - | 20500 |
| 6 | High Strength Tape 1 Tape-BA09 KV 400daN130mm | 3400 | - | 0.40 | 190.80 | 1.25 | - | 345 |
| 7 | External Sheath FINATHENE (TP 04) | 34 | - | 2.81 | 202.90 | 4.80 | - | 20500 |

For this research work, the layers were modelled in isotropic geometric except for the carcass and the pressure armours modelled as orthotropic properties type. The flexible pipe data for the analysis is presented in Table 3-6 with new equivalent material thickness. The carcass and the pressure armour layers are replaced by an equivalent material and geometric orthotropic layers because of the computational solution time of modelling the three-dimensional layers. However, the overall flexible pipe thickness remains the same.

The exact material property of the equivalent orthotropic layers for the carcass and pressure armour, including the results from the embedded orthotropic sheath layer, are all considered in the present work.

3.7 Developing the Metallic Parts

3.7.1 Tensile armours

The tensile wires were modelled as solid, deformable, and revolution, and it revolves from a sketch of the tendon of a large cross-section. In the wires model, the part was created using the cross-sectional dimensions of a 2 x 7 mm tendon sketched with the mid-point taken from the distance equal to the mean radius of the pipe layer and half the pitch of other layers. Solid Continuum 3D represented the tensile wires nodes reduced elements (C3D8R) and in Shell (S4R) [13].

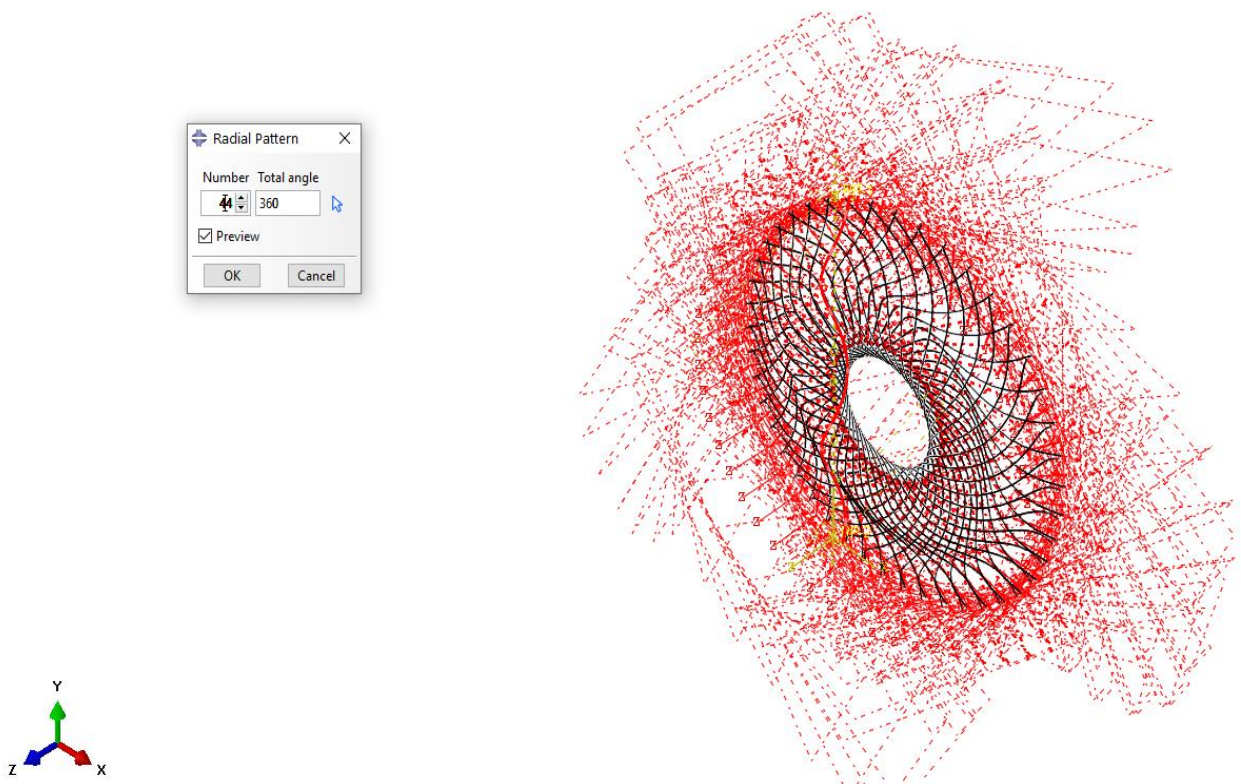
It starts with creating parts with 3D, deformable, and revolution options, were selected under modelling space, part type and base feature point, respectively.

The wires were then made from coordinates using rectangular shapes with the dimension 2 x 7 mm and material properties of carbon steel assigned tendons. The material orientation is given with discrete

options to get accurate stress and displacement sizes. On the primary axis, direction one is used, and direction three was chosen for the normal axis and defined as normal to the wire surfaces, as shown in Figure 3-11.

However, in the revolve dialogue window, the move sketch normal to path option is selected, and the cross-section of the wires is revolved based on an angle and pitch. The pitch is half the length of other parts as considered for both inner and outer tensile wires. Though, the length of the external tensile wires may be deviated slightly from the internal tensile wires to coincide with the size of the other parts in the model.

Instances are created in the assembly module with radial patterns based on the number of the strand of wires which in this model is 44 wires, as presented in Figures 3-7 to 3-10. The angle is set to 360° and the tensile wires are created along the longitudinal pipe axis.



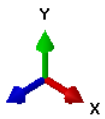
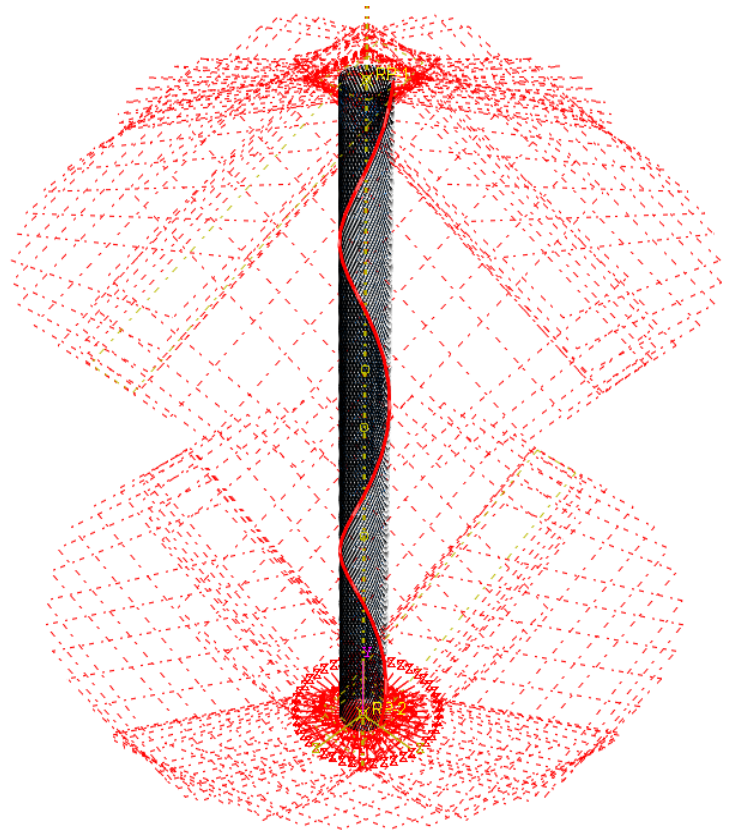
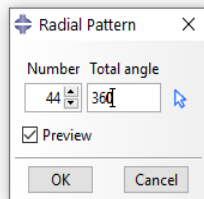
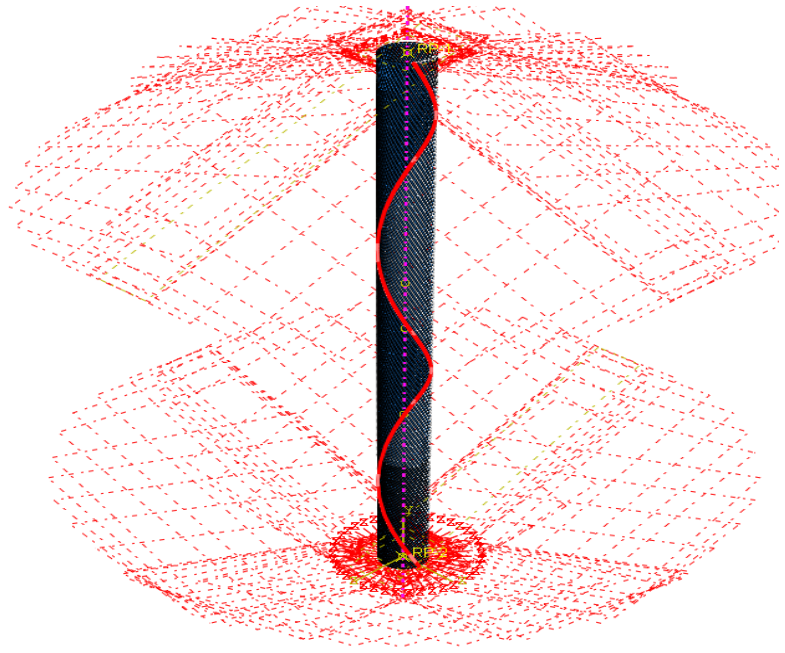
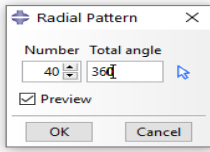
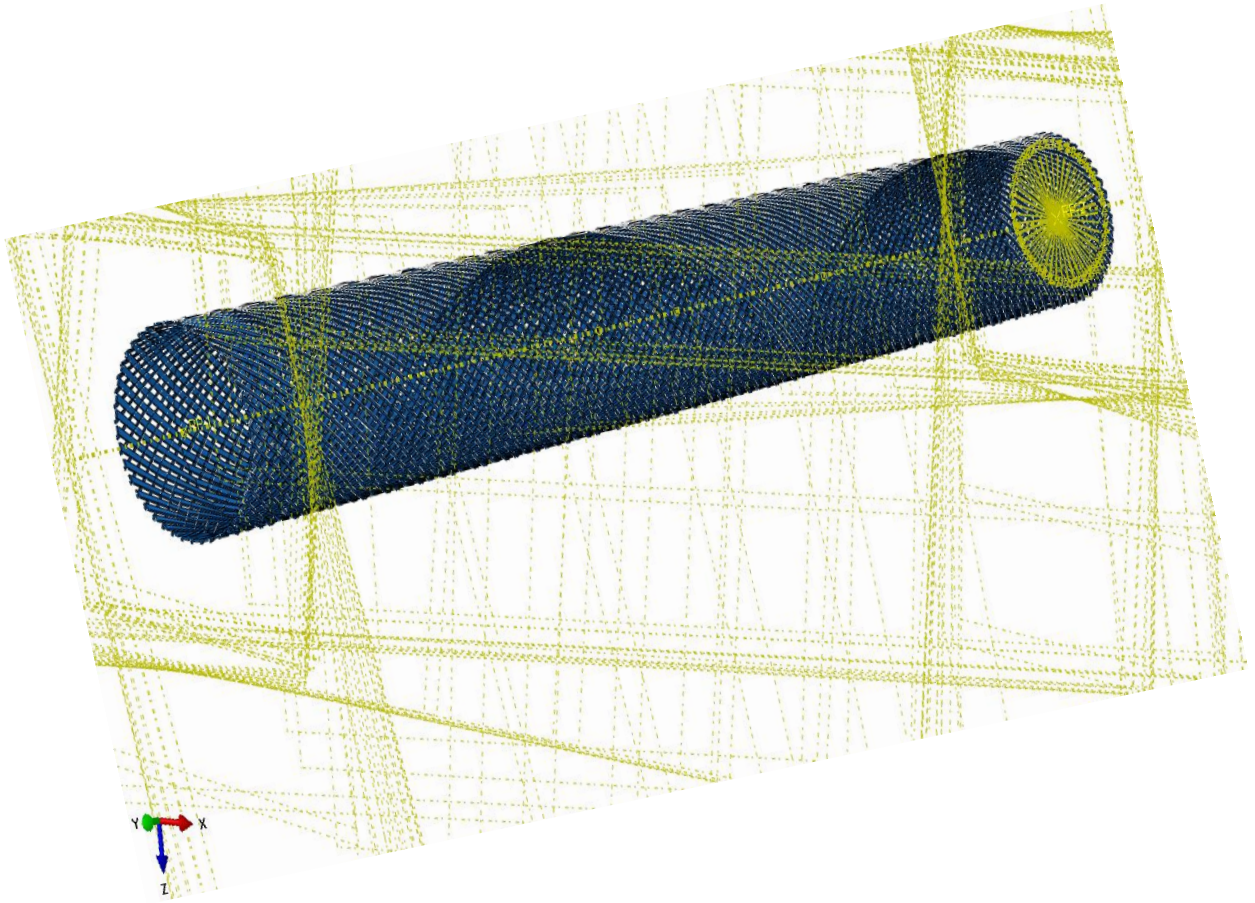
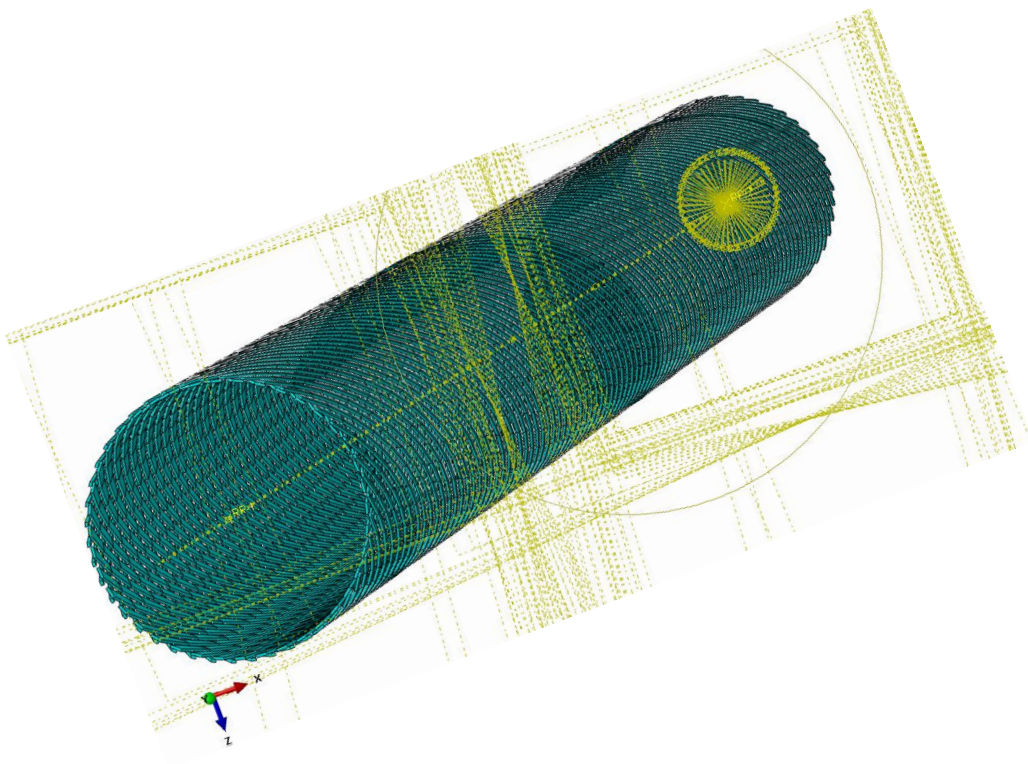


Figure 3-6: 40 tendons of first tensile and 44 tendons of second tensile wire



(a) First tensile wire



(b) Second tensile wire

Figure 3-7: Tensile wires

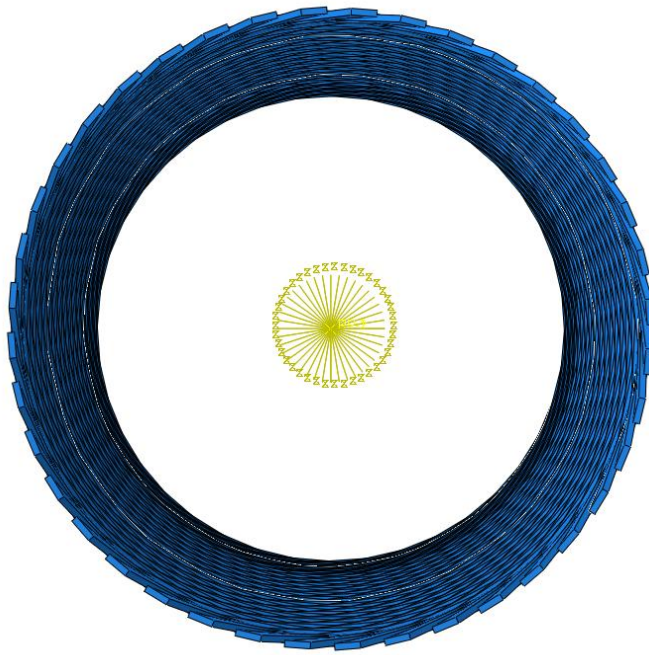


Figure 3-8: Complete tensile wire armour

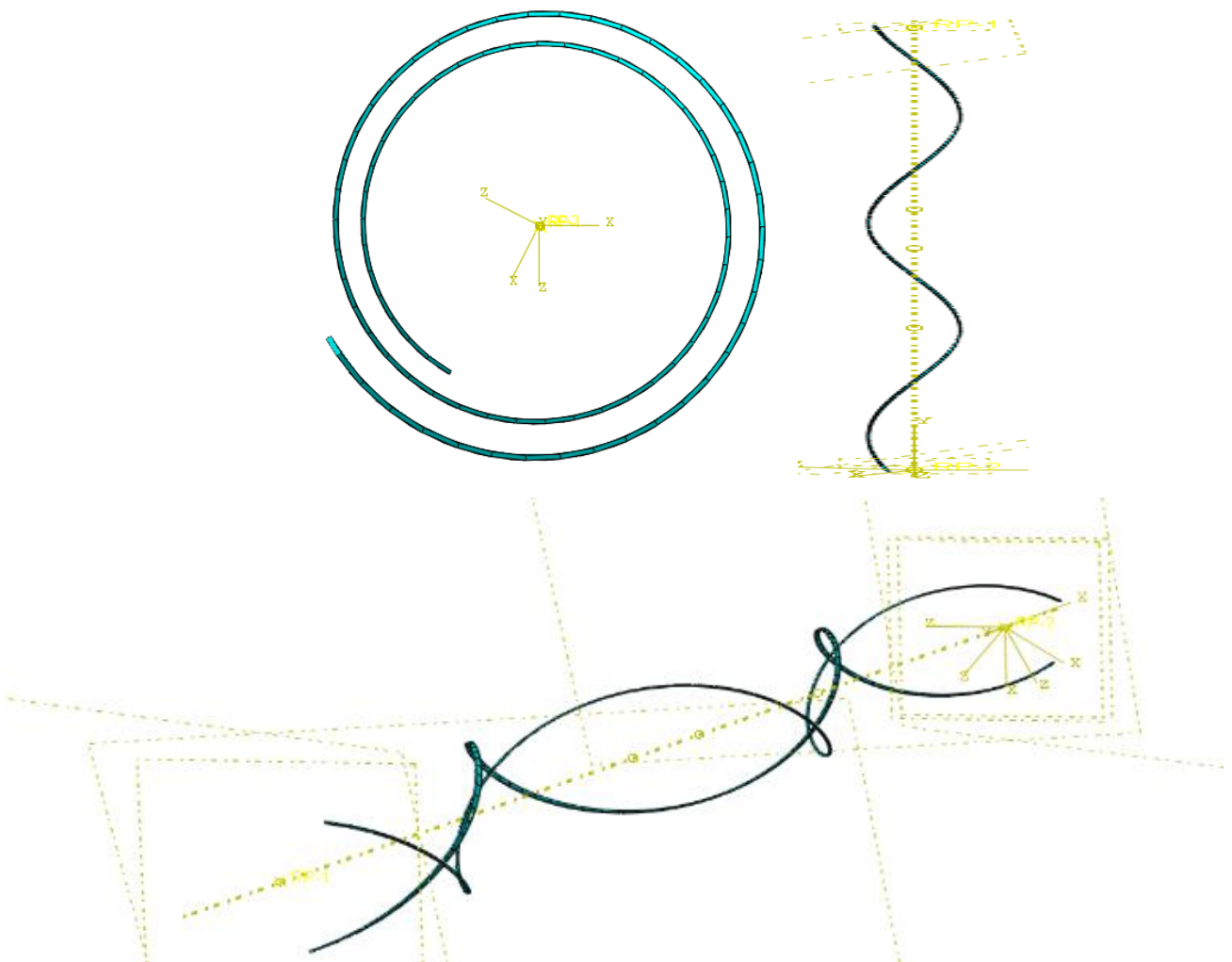


Figure 3-9: Tensile Wire Pitch

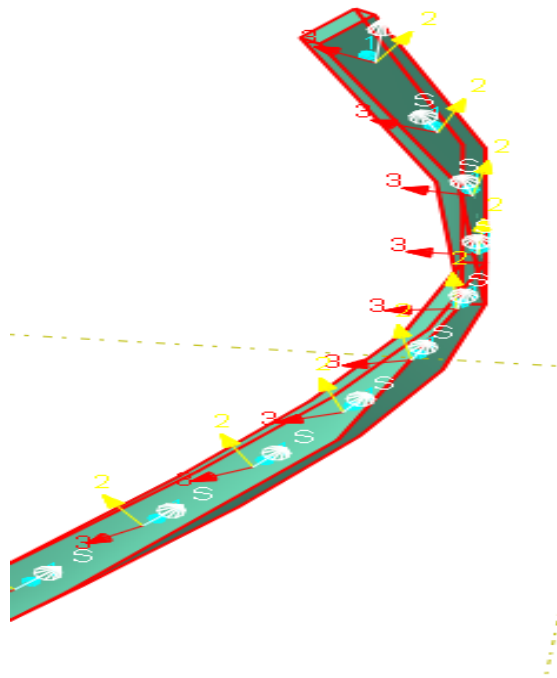


Figure 3-10: Tensile Wire with Orientation

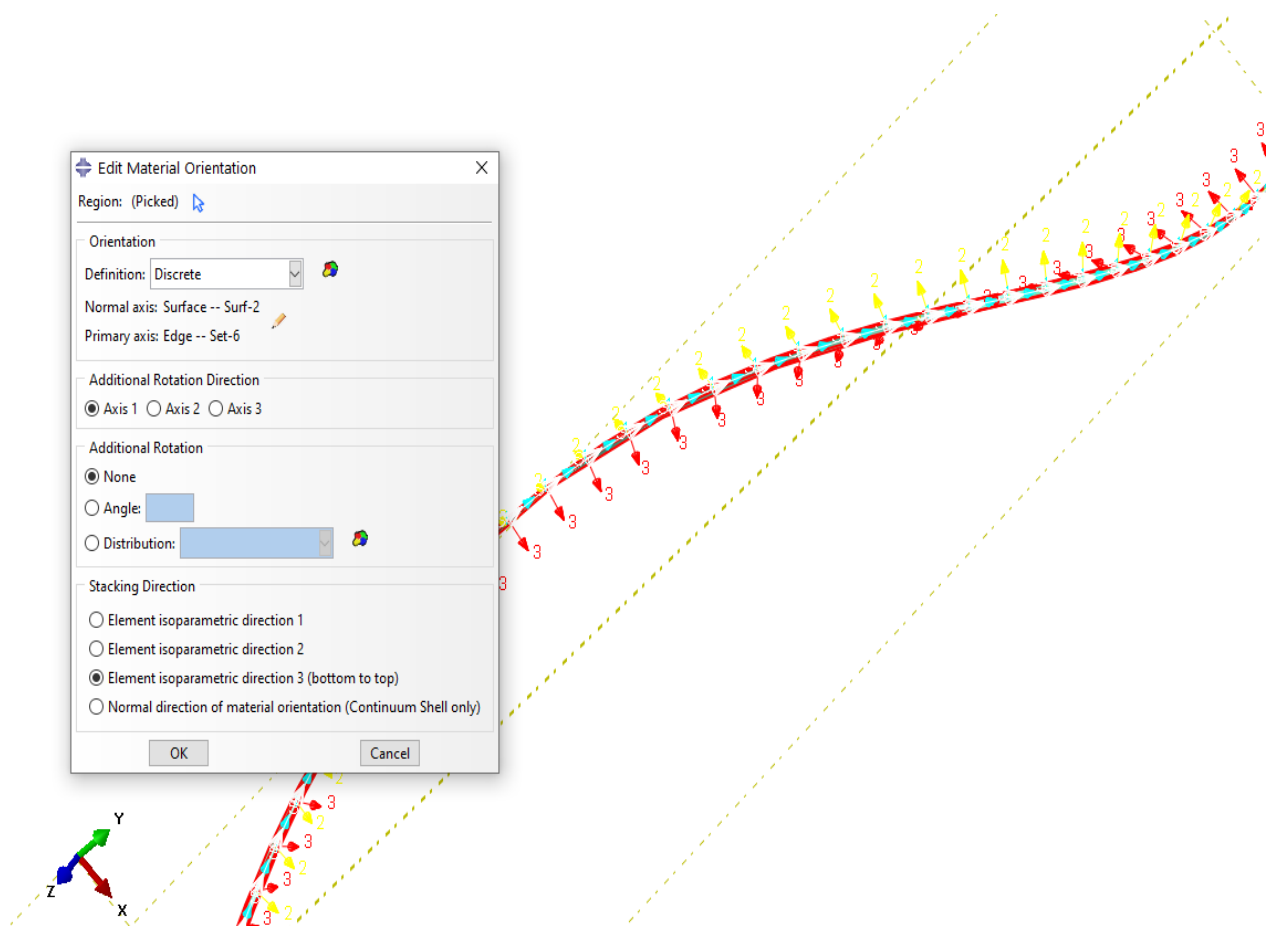


Figure 3-11: The pitch and orientation of the tensile wire

3.7.2 Carcass and Pressure Armour

Carcass and Pressure armour layers are helically wrapped with small angles (long pitch) to support axial loads for the amours. The layers are helically wrapped with high angles (short pitch); they tend to resist hoop stress due to internal and external pressure, and this is mainly concentrated on the carcass and pressure armour. An equivalent material property was developed to simulate an exact or near layer behaviour of the two layers. The postulations used in this development were based on established standard procedure and theory [14]. The layers are represented by C3D8R, similar to the non-metallic parts (Pressure Sheath, High Strength Tape and External Sheath). Orthotropic materials and engineering constants were used for the carcass/pressure armour, while isotropic materials properties were used for the tape and sheath layers.

The equivalent material properties were developed by considering the lay angle for both carcass and pressure armour layers. The study provides a background understanding of lay angle application and its features in orthotropic materials (engineering constant) within the Abaqus CAE environment.

3.7.2.1 Application of lay angles as applicable to Carcass and Pressure Armour

The lay angle application in this study was established from a combination of postulations that has exhibited a near-perfect result with flexible pipe behaviour under loading conditions. De Sousa, J. R. M., proposed a method to evaluate the analogy between helical tendons and orthotropic shells under the following assumptions [23].

1. The internal friction between the layers under the influence of lay angles is assumed to be negligible.
2. There are no relationships and interactions between the lay direction of the tendons and their normal behaviour.
3. The thicknesses of the layers are small compared to the internal diameter of the pipe.
4. Shear effects are assumed to be negligible; thus, the linear elements perpendicular to the middle plane of the structure remain straight and normal to the deflection surface of the structure after bending.

Generally, lay angles are made close to 90 degrees with the internal gaps; hence, the thickness to diameter ratio is small enough. De Sousa argues that this validates the four hypotheses. The tendons can be considered and modelled as a 3D-beam instead of representing the carcass and pressure armour as traditional orthotropic shell elements.

3.7.2.2 Process of arriving at appropriate computational values using a known lay angle, Young's modulus, and Poisson's ratio.

The stress-strain relationship is given in the equations (3-1) to (3-3) as presented in Figures 3-12.

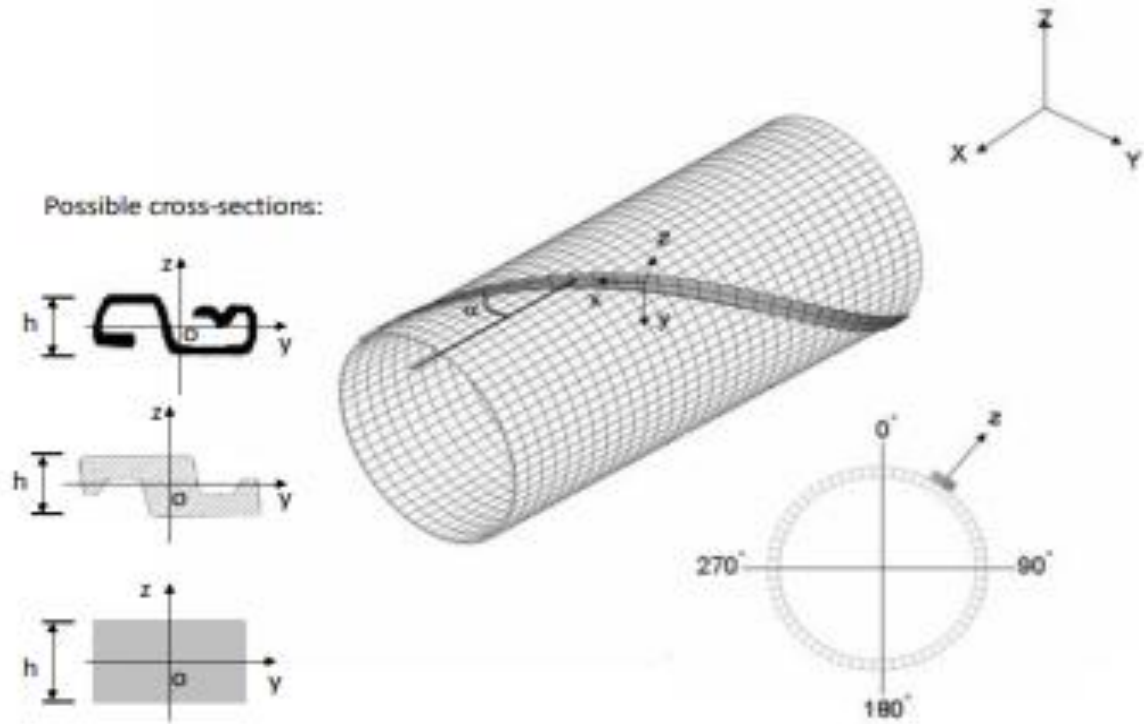


Figure 3-12: Stress-Strain relationship [23]

$$\alpha_{sx} = \frac{E_{sx}}{1-\nu_{sxy}\nu_{syx}} \epsilon_{sx} + \frac{E_{sx}\nu_{syx}}{1-\nu_{sxy}\nu_{syx}} \epsilon_{sy} \quad \text{Equation 3-1}$$

$$\alpha_{sy} = \frac{E_{sy}\nu_{syx}}{1-\nu_{sxy}\nu_{syx}} \epsilon_{sx} + \frac{E_{sy}}{1-\nu_{sxy}\nu_{syx}} \epsilon_{sy} \quad \text{Equation 3-2}$$

Consequently,

$$\tau_{syx} = G_{syx} \gamma_{syx} \quad \text{Equation 3-3}$$

Where α and τ are the normal and shear stress at the shell surface, elongation, and angular distortion, respectively. E_s , G_s and ν_s are represented as the young's modulus, Shear modulus and Poisson's ratio of the shell material, respectively. Since the tendons do not resist loads normal to lay direction according to hypotheses 1 and 2, it is assumed that $E_{sx}=0$ and $\nu_{syx}=\nu_{sxy}=0$. Thus; $\alpha_{sx} = E_{sx}\epsilon_{sx}$
 $\alpha_{sy} = 0$ $\tau_{sxy} = G_{sxy}\gamma_{sxy}$

The membrane, torsional stiffness and bending of an orthotropic shell element are given in the equation below:

$$(EA)_s = h_s E s_x \quad (EI)_s = \left(\frac{H^3 s}{12}\right) E \quad (GJ)_s = \left(\frac{h^3 s}{3}\right) G s_{xy} \quad \text{Equation 3-4}$$

where h_s is the shell thickness of the plate theory (Woinowsky-Krieger, 1959). The axial, bending and torsional stiffness of a helical tendon is further given by;

$$(EA)_t = \left(\frac{A * nt}{L_p}\right) E \quad (EI)_t = \left(\frac{I_{eq} * nt}{L_p}\right) E \quad (GJ)_t = \left(\frac{J * nt}{L_p}\right) G \quad \text{Equation 3-5}$$

E and G are used to represent the young's modulus and the Shear modulus of the tendon material, "nt" is the number of tendons defined in the layer. In contrast, A , J and L_p represent the cross-sectional area, torsion constant and pitch length, respectively. The pitch length can then be expressed as;

$$L_p = \frac{2 * \pi * R}{\tan \alpha} \quad \text{Equation 3-6}$$

Where α is the lay angle of the tendons in degrees and R is the mean radius of the layer. Furthermore, the mean radius can be calculated as follows.

$$R = \frac{d_i}{2} + \frac{h}{2} \quad \text{Equation 3-7}$$

Where d_i represents the inner diameter of the layer and h represents the thickness of the layer. The second moment of inertia is then given as

$$I_{eq} = 12 * nt * \frac{L_y^2}{L_p} * \frac{1 - \nu^2}{h^3} \quad \text{Equation 3-8}$$

I_{eq} represents the second moment of inertia, ν represents the Poisson's ratio. The carcass's equivalent material properties, geometry, and pressure armour (orthotropic layer materials) are given below.

$$h_s = \frac{\sqrt{12 * I_{eq}}}{A} \quad E_{sx} = \left(\frac{nt * A}{L_p * h_s}\right) * E \quad G_{sxy} = \left(\frac{3 * nt * J}{L_p * h_s^3}\right) * G \quad \text{Equation 3-9}$$

Note that E represents the given young's modulus. To calculate the young's modulus in the circumferential direction, the young's modulus inlay direction is multiplied by the sin of the given lay angle as follows;

$$E \text{ (in circumferential direction)} = E_{sx} * \sin(\alpha) \quad \text{Equation 3-10}$$

A calculated sample of carcass and pressure armour by following the highlighted steps above has been detailed as attached. Contrary to my initial application of lay angles in place of the orientation

angle of the carcass and pressure armour materials, the lay angle is designed to resist hoops stress due to internal and external pressures [46].

The carcass layer and pressure armour layer were modelled as hollow pipes putting into consideration their orthotropic nature. Thus, engineering constant was used in their material properties and composition, finding their equivalent shear modulus, Poisson's ratio, and Young's Modulus in all three directions of x, y and z. Identical materials as proposed by De Sousa were employed by considering: Lay angles, shear modulus, Young's modulus, and equivalent Poisson's ratios.

The carcass and pressure armour layers modelling was followed by assigning the orientation angles

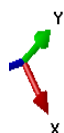
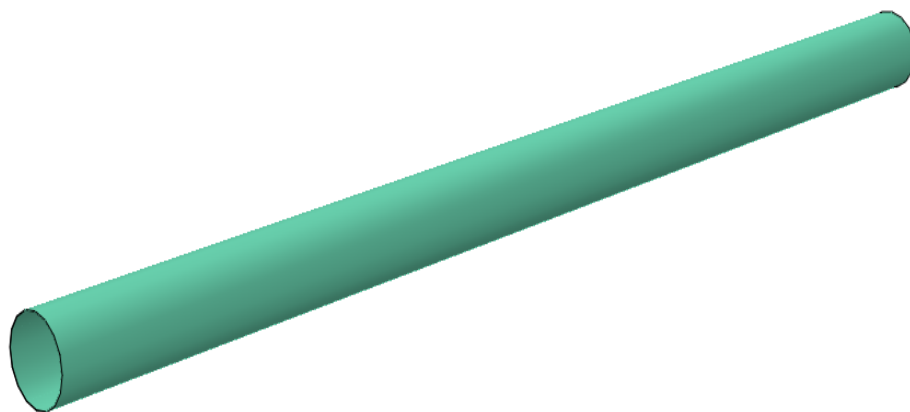


Figure 3-13: Modelling of Carcass Layer

3.8 Developing the Non-Metallic Parts

3.8.1 Pressure sheath, High Strength Tape, and Outer sheath layers

The Pressure sheath, High strength tape and external sheath layers are modelled individually as a cylindrical hollow pipe.

The basic geometric properties of non-metallic layers, including specification and material properties, are detailed in Figure 3-14, while Figure 3-15 depicts the isotropic of non-metallic materials

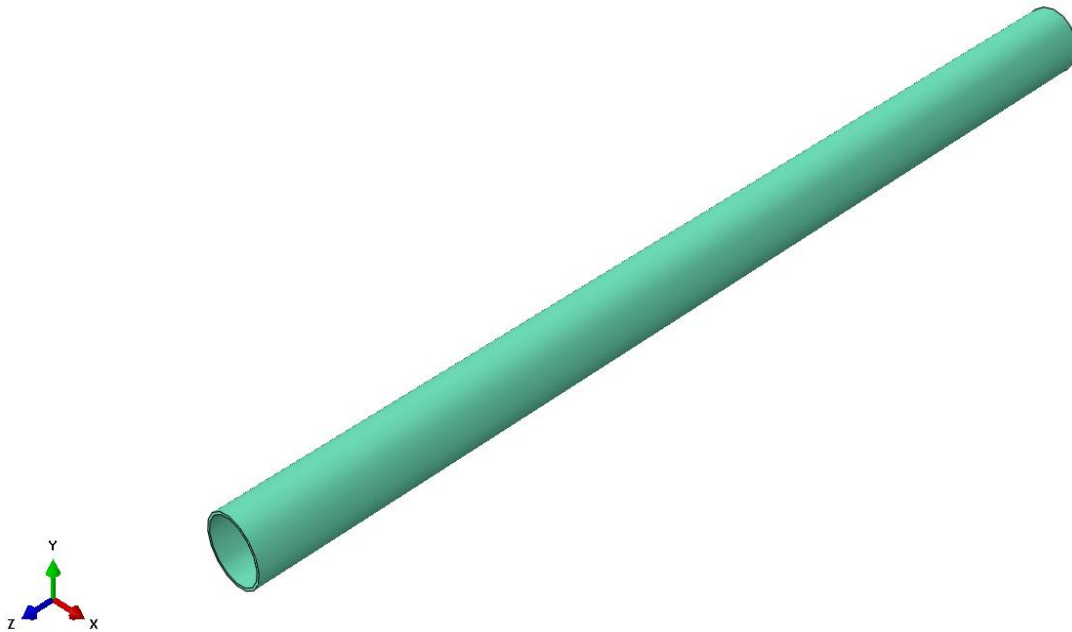


Figure 3-14: The non-metallic part

3.9 Developing the Hydrate Blockage

3.9.1 Hydrate Plug Properties and Dimension

A complete blockage model of methane hydrate materials is used, as presented in tables 3-7. The hydrate was modelled in different sizes ranging from length 0.5 to 1.0 m at the interval of 0.1 m. The results obtained, which are detailed in the subsequent chapters, showed the effects of the hydrated size.

Table 3-7: Blockage (plug) properties

| Length (m) | Inner diameter (mm) | Modulus (GPa) | Poisson's ratio (ν) | Density (ρ) (Kg/m³) |
|-----------------------|--------------------------------|--------------------------|---|---|
| 1.0 | 0.0762 | 8.52 | 0.38 | 2,500 |

3.10 General Mesh

The typical finite element mesh of the individual flexible pipelayers is shown in Figures 3-15 and 3-16 with global seeds of approximately global size curvature control of maximum deviation factor of 0.1 and minimum size control by a fraction of global size 0.1 applied. This was applied to all seven (7) layers, including the plug/blockage. The effect of different element sizes in the cross-section of the pipe layers was examined to provide accurate results at a reduced computation time.

The layers were finely meshed and observed for better results. The number of the element was carefully chosen so that the aspect ratio of the elements was as close to one as possible. Therefore,

mesh sensitivity analyses were performed to verify the number of elements in each of the parts. Abaqus/Explicit is used to determine which slave nodes in the predicted configuration penetrate the master surfaces to prevent penetration of layers in the radial direction.

Table 3-8 shows the mesh sensitivity analysis with the problem size, which includes the total number of elements, nodes and variables in the assembly that is large enough to provide better results.

Table 3-8: Mesh sensitivity analyses- Problem Size

| Parts | No of Elements | No of Nodes | Total No of Variables |
|-------|----------------|-------------|-----------------------|
| Solid | 53,599 | 118,039 | 267,033 |
| Shell | 60,343 | 99,165 | 273,117 |

The total number of solid and shell parts elements is 53,599 and 60,343, respectively, while the node is 118,039 and 99,165 for both solid and shell elements.

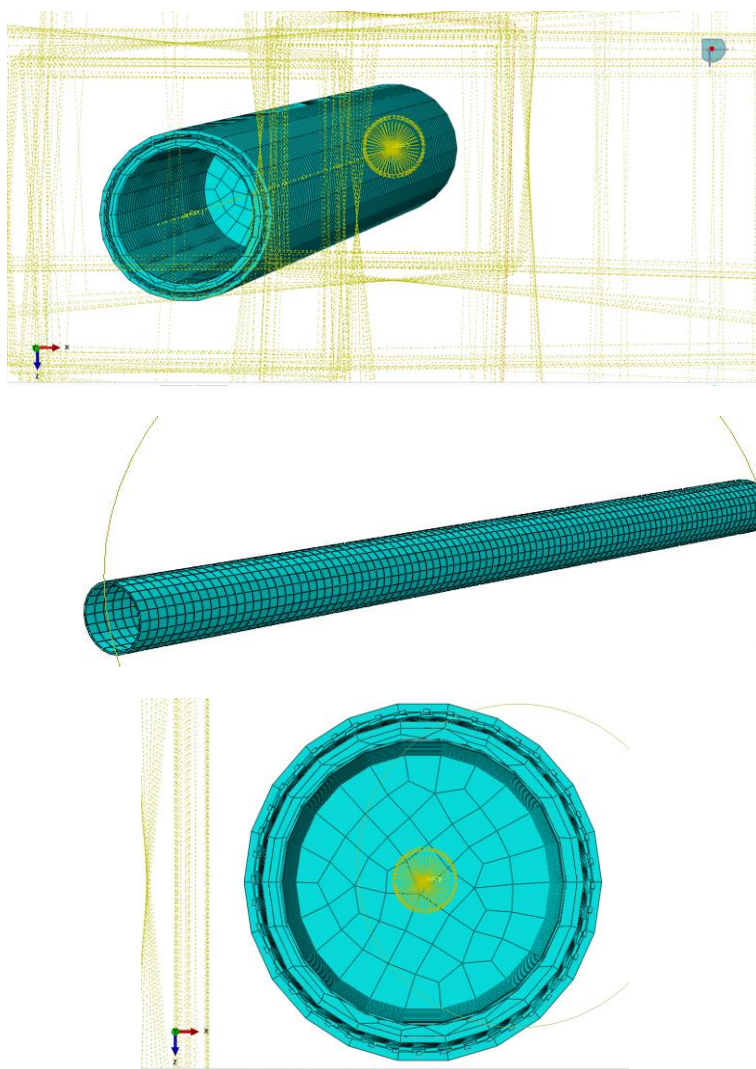


Figure 3-15: Meshed Solid Elements

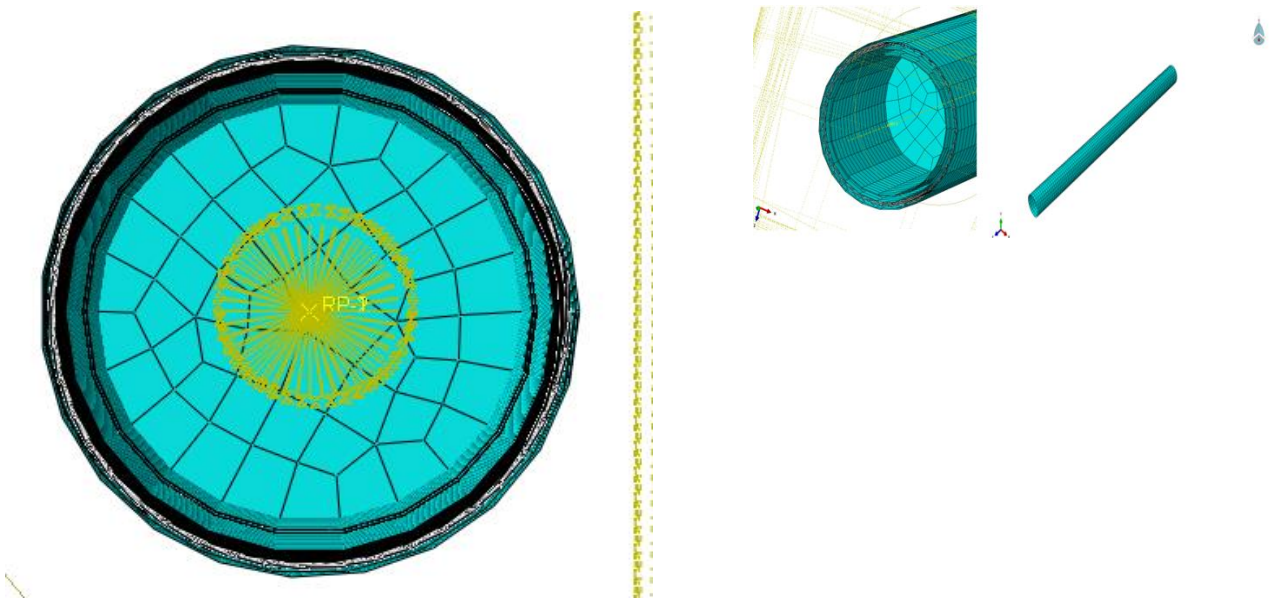


Figure 3-16: Meshed Shell Elements

3.11 Assembly of Non-bonded Flexible Part Layers

The layers are assembled along the normal axis, and the tensile wires were initially arranged with coaxial constrained of the tendons to form a complete spiral pipe. The process is shown in Figure 3-18 with the first tensile 40 tendons and the second tensile with 44 tendons/wires, while Figure 3-19 shows the entire parts assembly.

3.11.1 Assembled Layers

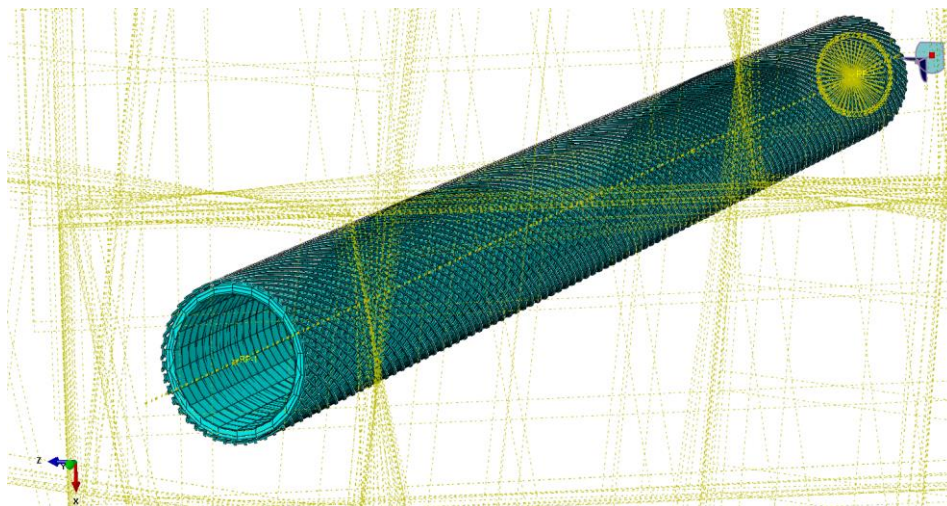


Figure 3-17: Assembled meshed parts

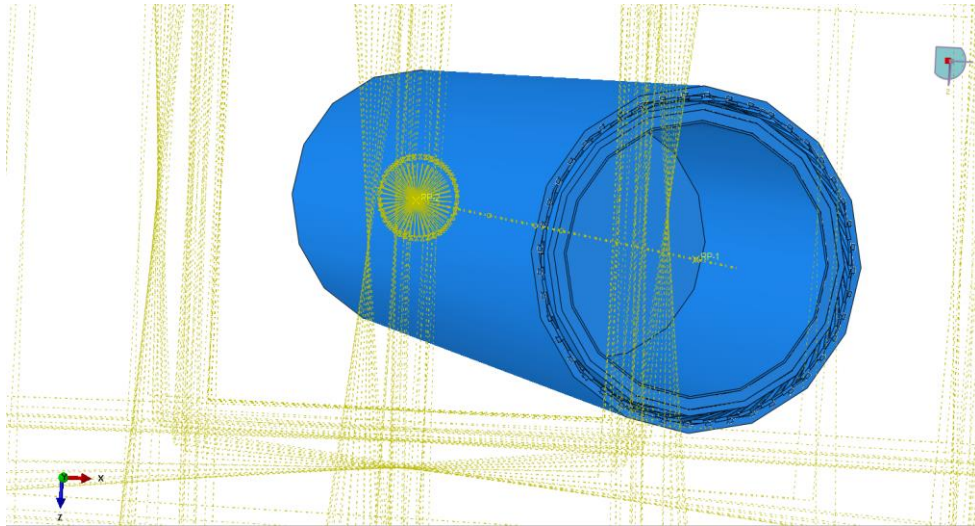


Figure 3-18: Assembled parts

3.12 Interactions and Constraints

General contact algorithm in Abaqus/Standard explicit, which is surface to surface contact formulation, was used for all layers. Two surfaces, surf 1 and surf 2, were created each for the parts, and the contact domain contains surface pairs of a master and a slave, as presented in Figure 3-20. It is therefore important to note that the metallic parts were all made masters while the non-metallic are slaves; this is to protect unnecessary absorption and separation after contact has been established. For the numerical simulations, it is normal behaviour, pressure overclosure: hard contact, constraint enforcement method by default, and allow separation after contact was adopted. Otherwise, pressure overclosure: Linear, constraint enforcement method by default with contact stiffness of 10^{-5} was adopted while in tangential behaviour, friction formulation: frictionless was used.

The penalty algorithm was used for both normal and tangential directions in which the contact stiffness factor is calculated (i.e., in the normal direction) based on penetration of the master surface into the slave surface. Two contact properties models were used to define the initial step for the first interaction and step 1 for the second interaction. In the initial step, the normal behaviour is recorded with hard contact by default. While in step 1 with type static, generally has the time of 1, at the maximum number of increments 100 with increment sizes initial, minimum, and maximum values 10, 0.00001, and 10 respectively. The tangential behaviour now includes friction, and the penalty method selected for the friction formulation with isotropic directional though 0 friction coefficient was used that is frictionless.

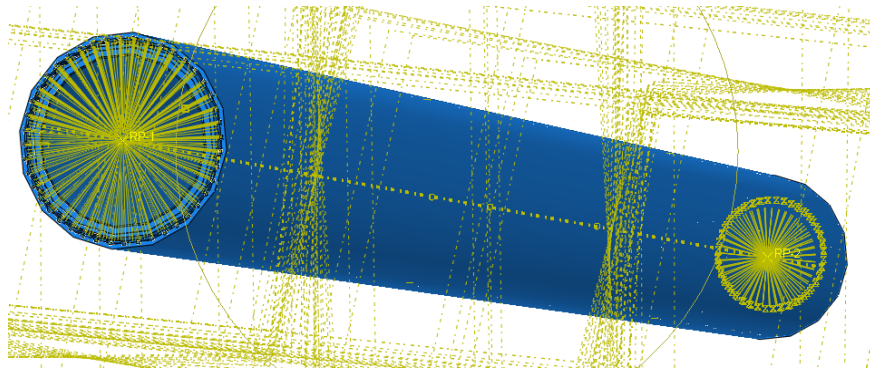


Figure 3-19: Application of constrained points RP-1 and RP-2

3.13 Load and Boundary Conditions

The ends boundary conditions were imposed through reference points RP-1 and RP-2 located at both ends of the pipe segment. One end RP-2 is constrained at all points while RP-1 is free. Coupling the end nodes of the elements in six degrees of freedom with the reference node simulated the axial and radial constraint of the end fitting. At the end 1, the layers were constrained in all directions using Encastre, while at End 2, the layers are constrained to a reference point RP-1.

3.13.1 Load Cases and Boundary Conditions

The simulation investigates the influence of the following loads' case 1 to 5 for samples A and B as shown in Table 3-9:

Table 3-9: Load Cases and Boundary Conditions

| Load Case | Load Type | Boundary Conditions |
|-----------|---|--|
| 1. | Internal Pressure (IP) | One end (RP-1) is constrained in all directions using encastre, while end 2 (RP-1) is free |
| 2. | Compressive Force (CF) | |
| 3. | External Pressure (EP) | |
| 4. | Internal Pressure + Compressive Force (IP+CF) | |
| 5. | Coefficient of Friction (CF) + Contact stiffness (CS) | Varied CF+ constant CS |

Subsequently, for all the load cases, the essential boundary conditions were defined one end fixed while the other pipe end was free.

3.14 Simulation and Effect of Blockage

A geometrically non-linear problem was analysed, and the non-linearity resulting from the contact surfaces presence, including the rigid body that produces large displacement in the tensile layer. Elements are distorted from their original shapes as the deformation increase along the pipe axis. All elements are of acceptable shape concerning aspect ratio and others by carefully monitoring the hourglass energy to internal energy around 5%. A complete blockage of tangential behaviour, penalty, and normal behaviour of stiffness constant 10^{-5} shows a significant decrease in the displacement and high-stress concentration in all directions in the flexible pipe.

It is clearly shown that the plugin of the flexible pipe imparts more von mises stress, reacting force and hoop stress on the entire structure, especially the carcass and the tensile wires. There is no significant movement of the plug because the two ends were fixed and constrained to RP-1; the relocation started with increased internal pressure. Figure 3-20 shows the meshed and unmeshed hydrate formation.

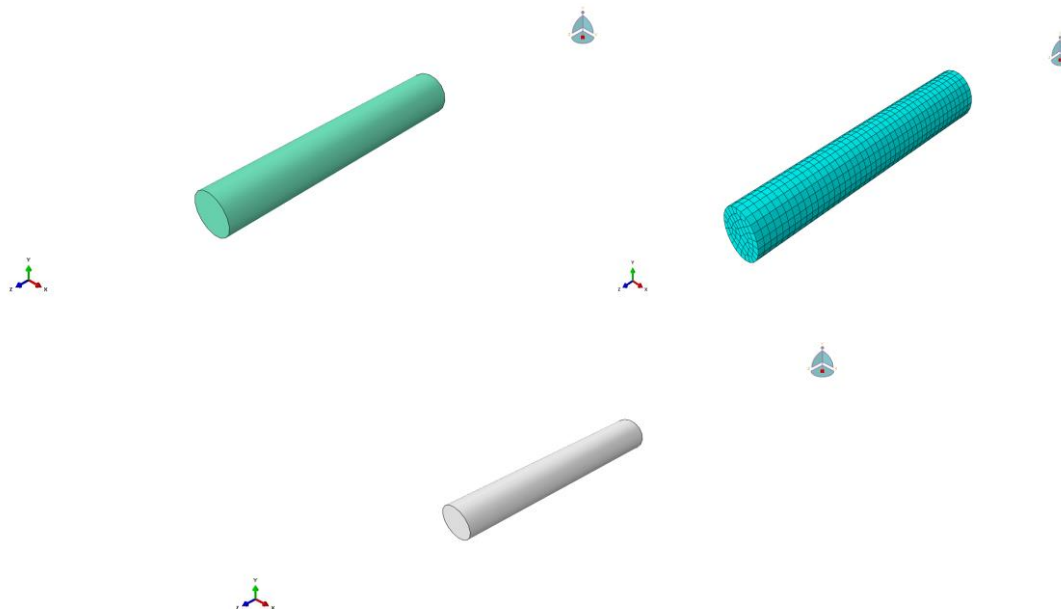


Figure 3-20: Meshed and unmeshed blockage/plug

The analysis considers the effects of large deformations and rotations. These non-linear effects are ignored when validating the results, as presented in chapter 5 for the numerical analysis. However, chapter 4 data may not be sufficient due to limited equipment during the experimental study. Consequently, the magnitude of loads in all cases was kept practicably within the allowable values to ensure that the resulting strains were kept within elastic limits.

3.15 Model Results Validation

The numerical FEM analysis results for pressure distribution, axial and compressive loads and the resulting stresses, including the displacement, were compared against that of existing research work conducted by [2] to ensure validation of the finite element models using Abaqus.

This comparison was carried out to verify and validate the accuracy of the finite element model. The FEA results were compared for the pressure concentration, radial displacement, axial displacement, axial stress, pulling force, hoop stress, Von-mises stress, and the entire flexible pipe prototype. The pulling forces and displacement values at various stiffness constants are recorded from 10-100,000 based on the research conducted by [2] and that of the present work using ABAQUS/CAE 6.14 Software. The comparison of the results obtained from Gonzalez's paper shows the excellent result as detailed in Table 3-10 with above 96% plot accuracy as shown in Figure 3-21 [2] and 63% average deviation in the values shown in Table 3-10.

Table 3-10: Comparison between Numerical and Abaqus pulling force and displacement

| Displacement (mm) | | 0 | 1 | 2 | 3 | 4 | 5 | Average Deviation | |
|---------------------|-----------------|-----------------|-----------|------------|-------------|-------------|-------------|-------------------|-----------------|
| Pulling Forces (kN) | nk10 | Gonzalez et. al | 0 | 0 | 0.01 | 0.01 | 0.01 | 0.02 | |
| | | Abaqus | 0 | 0.02 | 0.03 | 0.03 | 0.04 | 0.03 | |
| | Comparison (%) | | 0% | 0% | (2%) | (2%) | (3%) | (1%) | 2% more |
| | nk100 | Gonzalez et. al | 0 | 0.06 | 0.13 | 0.20 | 0.25 | 0.25 | |
| | | Abaqus | 0 | 0.02 | 0.05 | 0.07 | 0.09 | 0.11 | |
| | Comparison (%) | | 0% | 67% | 62% | 65% | 64% | 56% | 63% less |
| | nk1000 | Gonzalez et. al | 0 | 0.09 | 0.18 | 0.27 | 0.37 | 0.46 | |
| | | Abaqus | 0 | 0.09 | 0.18 | 0.28 | 0.37 | 0.47 | |
| | Comparison (%) | | 0% | 0% | 0% | (4%) | 0% | (2%) | 1% more |
| | nk10000 | Gonzalez et. al | 0 | 0.09 | 0.19 | 0.29 | 0.39 | 0.49 | |
| | | Abaqus | 0 | 0.06 | 0.12 | 0.18 | 0.25 | 0.31 | |
| | Comparison (%) | | 0% | 33% | 37% | 38% | 36% | 37% | 36% less |
| | nk100000 | Gonzalez et. al | 0 | 0.10 | 0.20 | 0.29 | 0.39 | 0.50 | |
| | | Abaqus | 0 | 0.04 | 0.07 | 0.11 | 0.14 | 0.18 | |
| | Comparison (%) | | 0% | 60% | 65% | 62% | 64% | 64% | 63% less |
| Experimental | Gonzalez et. al | 0 | 0.07 | 0.16 | 0.27 | 0.36 | 0.46 | | |
| Analysis | Gonzalez et. al | 0 | 0.10 | 0.21 | 0.32 | 0.42 | 0.50 | | |

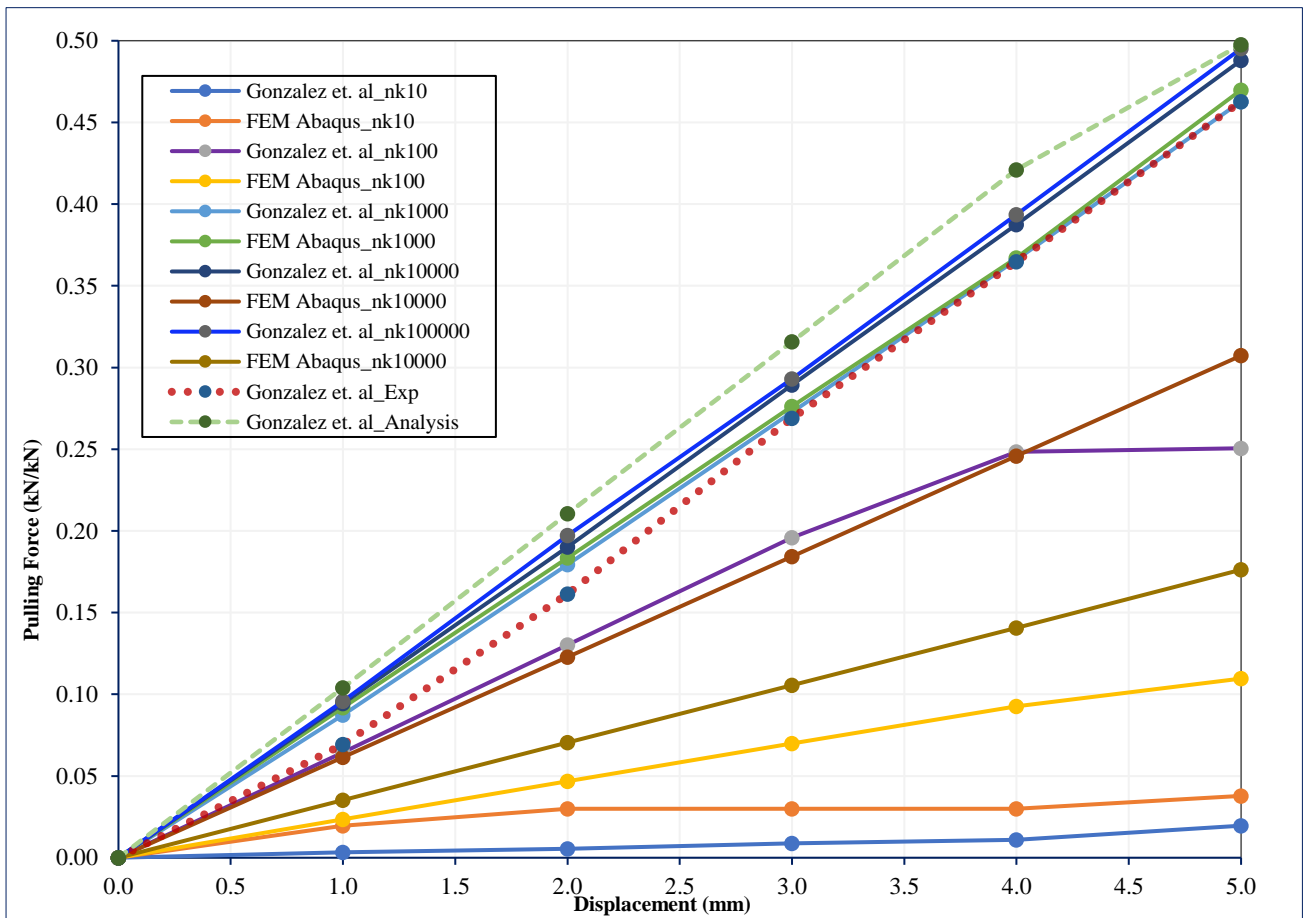


Figure 3-21: Displacement vs Pulling load for normal contact stiffness variation

Additionally, the model showed the best correspondence for a normal contact stiffness value between 1,000 and 100,000 N/mm² and 0.10 for the friction coefficient with stress distribution shown in Figure

3-22. The flexible pipe significantly reduces pulling forces and displacement in X, Y and Z directions when the blockage is introduced into the model. It is indicated that the plugin of the flexible pipe imparted more axial load on the entire structure with maximum von mises stress of 185 MPa and the pulling forces with lateral displacement of 0.0036 mm as presented in Figure 3-23. The mechanical behaviour of this model has been evaluated under three conditions; tension force, pressure and a complete hydrate blockage modelled with methane material. The developed finite element model predicts the behaviour of the flexible pipe subjected to both mechanical loading. Studies were carried out on the model to understand the effect of blockage on flexible pipe behaviour.

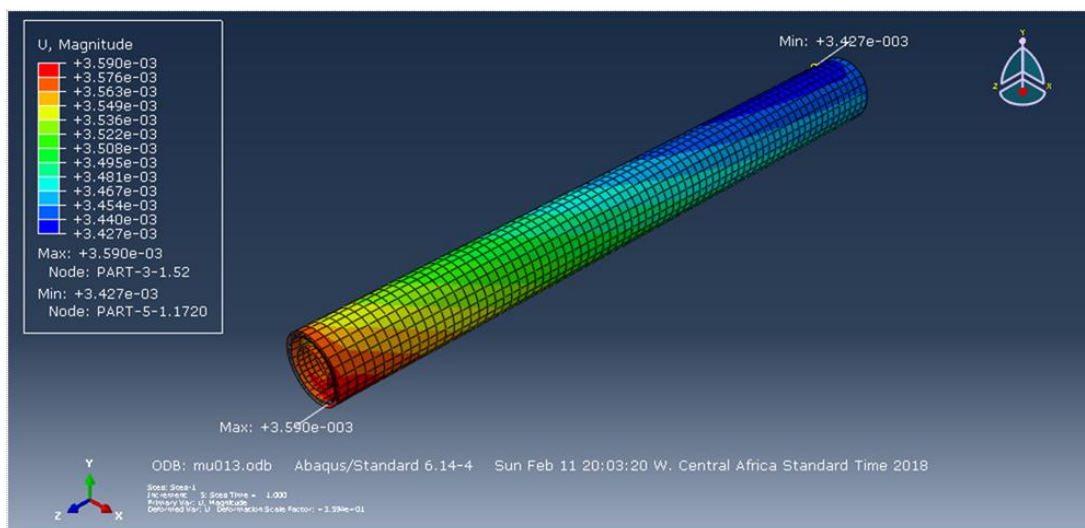


Figure 3-22: Stress distribution on 9-layer's pipe

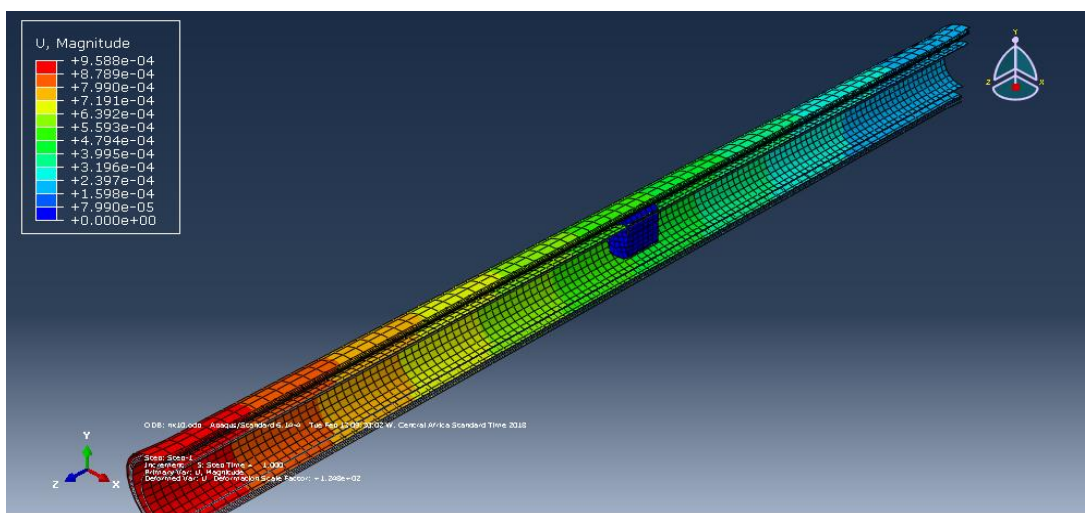


Figure 3-23: Stress distribution on 9-layer's pipe with blockage

There was a deviation when introducing the blockage into the existing model, and this shows that the effect of blockage in a flexible pipe cannot be completely neglected. The pulling force and lateral displacement increase with the increase in the contact stiffness and vis-à-vis. This indicated that the contact stiffness and coefficient of friction should be chosen when designing the flexible pipe. With the results obtained thus far, the two variables were carefully selected for the numerical analyses in

this present work. Better results were obtained for the contact stiffness of 1000 and above and the coefficient of friction of 0.1 and above. These are dimensionless magnitude, including the pulling force.

3.16 Conclusion

The numerical models detailed in this chapter was validated with Gonzalez et al. paper that the results were compared when the blockage was introduced and presented. In some cases, the result showed 96% plot accuracy and a maximum average value deviation of 63%. The simulation was subsequently used to model the non-bonded flexible pipe in this present work. The 7- layers 6" flexible pipe specimen was divided into two Samples A and B; Sample A is a blocked section, while Sample B is intact and unblocked. The flexible pipe has an inner and outer diameter of 152.4 mm and 193.3 mm, respectively and was simulated considering the contacts interfaces, interaction, and constriction. In this paper, the coefficient of friction is assumed to be frictionless and, in some cases, varied. The normal contact behaviour is set at linear with a stiffness value of 0.00001. The detailed experimental and numerical analyses are explicitly carried out in Chapter 4 and Chapter 5, respectively, using the developed model and applying the international codes and standards. The total result is discussed in Chapter 6, with further work in Chapter 7.

CHAPTER 4: EXPERIMENTAL INVESTIGATIONS

4.1. Introductory remarks

This chapter presents the outcome of the experimental analysis on a 6” diameter seven layers non-bonded flexible pipe under different conditions. To have a better conclusion, a further experiment on a 6” diameter 9-layer flexible pipe was considered. The tests carried out on the sampled specimen include but are not limited to the following: pressure test, compression, and tensile tests, to determine the failure modes by verification and validation with numerical analysis. The flexible reference pipe was divided into the riser and flowline, both in the one-line pipe to inject gas into the oil reservoir. It is well-known in the industry how often the gas injection line is blocked due to environmental conditions or human errors in managing hydrate formation in the pipe.

Most pipelines are designed with the inclusion of thermal management and often injecting methanol whenever the pipe is not in use; all these are necessary to avoid hydrate or wax formation in the pipe. The damage occurred on the pipe under investigation due to internal blockage by hydrate; however, because of flushing out or dissolving the methane hydrate through pigging operation and unfortunately due to a significant pressure differential in the flexible pipe, having pressurized and depressurized several times, ultimately resulting in the pipe failure. This, of course, has been a source of concern the experts around the world as there is no clear way to access the internal section of the pipe. This frequently arises due to internal pressures and forces generated on the seabed, bringing tidal and hydrostatic forces. More so, the initial pressure required to pump the oil up to sea level is significantly high, resulting in a combination of stresses through many sections of these flexible pipes. These high stresses mean that the pipe design must withstand significant internal, external, and tensile loadings. Afterwards, lead to the extreme difficulty of getting access internally during the pipe use, which gives a limited range of solutions to blockages that can frequently occur depending on what geographical location is being minded. The experimental procedure focused on testing combined stresses as its goal. However, only a tensile test was carried out on the specimen due to experimental limitations but supported with numerical analysis for validation and verification of the causes of the failure modes to the investigated pipe.

4.2. Test specimens

4.2.1 Description of non-bonded flexible pipe makeup and flexible pipe design basis

The flexible pipe specimen used for the experiment in this project has been in operation since 2003. As shown in Figure 4-1, the layers consist of the external sheath, the white outer thermoplastic layer, with the primary job of preventing seawater from getting into any layer, usually known as annulus flooding and avoiding any damage or corrosion that seawater could cause. The Outer Sheath is followed by Fabric/High strength tape to help with interlayer friction. The tensile armour layers (2),

otherwise known as helical tendons, serve as dynamic stress redistributors for the entire pipe. They are set at a -35 and 35-degree angle, meaning they cross over and go over each other. The slight angle differences ensure the geometry matches up, having a slightly larger internal diameter than the other. In addition, these are often constructed with an additional backup pressure armour layer.

However, the sample which was used did have this layer.

Additionally, the anti-wear tape is applied on the inside of the inner tensile armour layer. This separates the inner tensile armour layer from the pressure armour clip layers, though it depends on the design as some do not have. The pressure armour or zeta layer allows for bending and better geometrical redistribution of the tensile armour layers. Its name, 'Pressure Armour', also states its primary purpose is to resist pressure loading or hoop stresses applied internally or externally. The second plastic sheath layer is positioned after this, with its purpose being to make sure none of the internal fluid or oil makes its way into neighbouring layers. It also serves to protect against thermal loadings coming from the internal fluid. The most inner layer is the interlocked carcass; this layer is designed to resist external pressure and axial loadings. The internal fluid is in contact with this layer, so it is made of highly corrosive material. The schematic diagram of a 7-layer pipe is depicted in Figure 4-1.

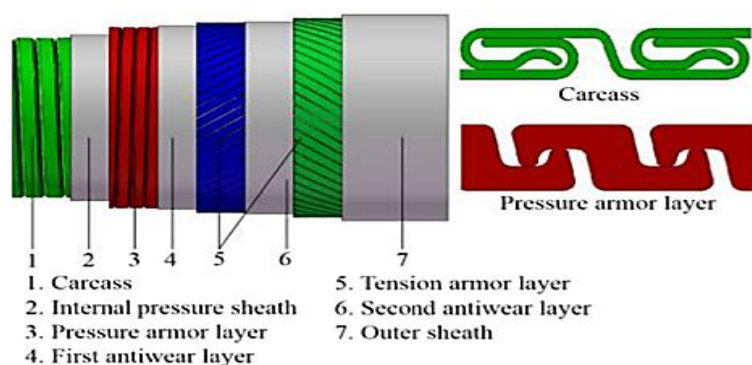


Figure 4-1: 7-Layers non-bonded flexible pipes [47]

4.3 Analysis of the test specimens

The specimen originated from an active oil pipeline in a field located 60 km away from the Nigerian coast installed in 2003 for oil and gas production in the Gulf of Guinea at a water depth of 350-780 m. The non-bonded flexible pipe was severely damaged during a pigging operation to clear its sample specifications blockage by applying internal pressure to flush it out or dissolve it. The schematic of the gas injection line segmentation process and the dissection is shown in Figure 4-2, while Table 4-1 presents the original specifications of the specimen.

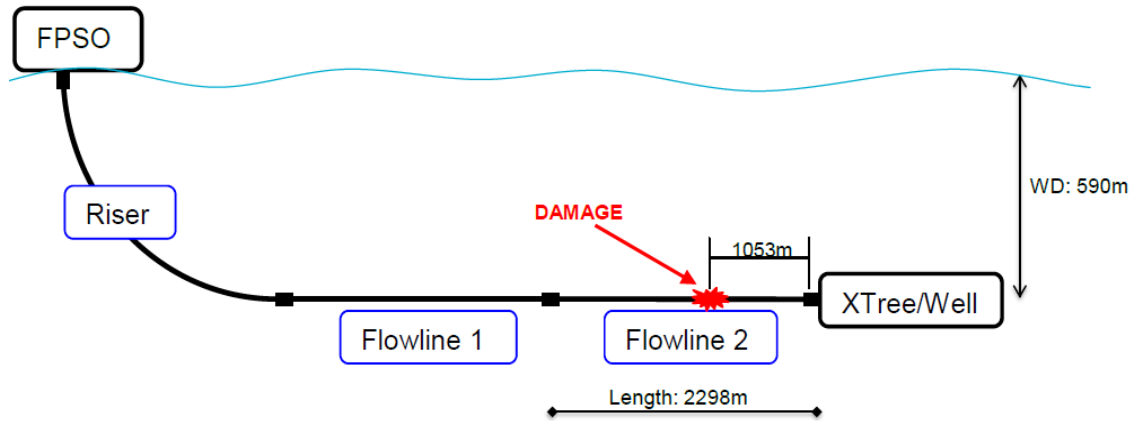


Figure 4-2: Gas injection line segmentation and Schematic of the dissection [5]

Table 4-1: Specification

| S/N | No. Layer description | I.D. (mm) | h (mm) | Lay angle (°) | Area (mm ²) | E (MPa) |
|-----|---|-----------|--------|---------------|-------------------------|---------|
| 1 | Interlocked carcass, 48.0 x 1.0 AISI 304 | 152.4 | 5.0 | 87.6 | 19.6 | 207000 |
| 2 | Internal plastic sheath RILSAN P40 TP01 | 162.4 | 4.0 | | | 800 |
| 3 | Zeta-clip, 2 tendons th 6.2 FM 35 (FI 11) | 170.4 | 6.2 | 85.6 | 54.1 | 207000 |
| 4 | First Armour Lay 35.0 deg High FI41 | 182.8 | 2.0 | 35 | | 207000 |
| 5 | Second Armour Lay -35.0 deg High FI41 | 186.8 | 2.0 | -35 | | 207000 |
| 6 | High Strength Tape 1 Tape (BA09 KV) | 190.8 | 1.25 | | | 112000 |
| 7 | External Sheath FINATHENE (TP 04) | 193.3 | 4.8 | | | 800 |

4.3.1 Operating History of the Sample

The flexible pipe under investigation operates at a pressure of 227 bar and temperature of 78°C at the riser inlet, while the suitable borehole temperature is 30°C. It was installed in 2003 and has been in operation for seven years, from 2003 till 2010 and no incident was reported until May 2010 when the flexible pipe experienced the first hydrate blockage.

The first hydrate plug was removed by depressurization in May 2010, and the same year the second hydrate plug was pulled by several depressurizations with methanol injection (June - August 2010). The third hydrate plug was also removed by several depressurizations using the same process as the second plug, methanol injection, within August - September 2010. In October 2010, it was noticed that the pressure on the pipe wasn't going above 58 bars, which resulted from the gas bubbles observed [5].

In February 2011, an ROV inspection was carried out, and the leak on the flow line was detected, and the line was recovered in September 2011.

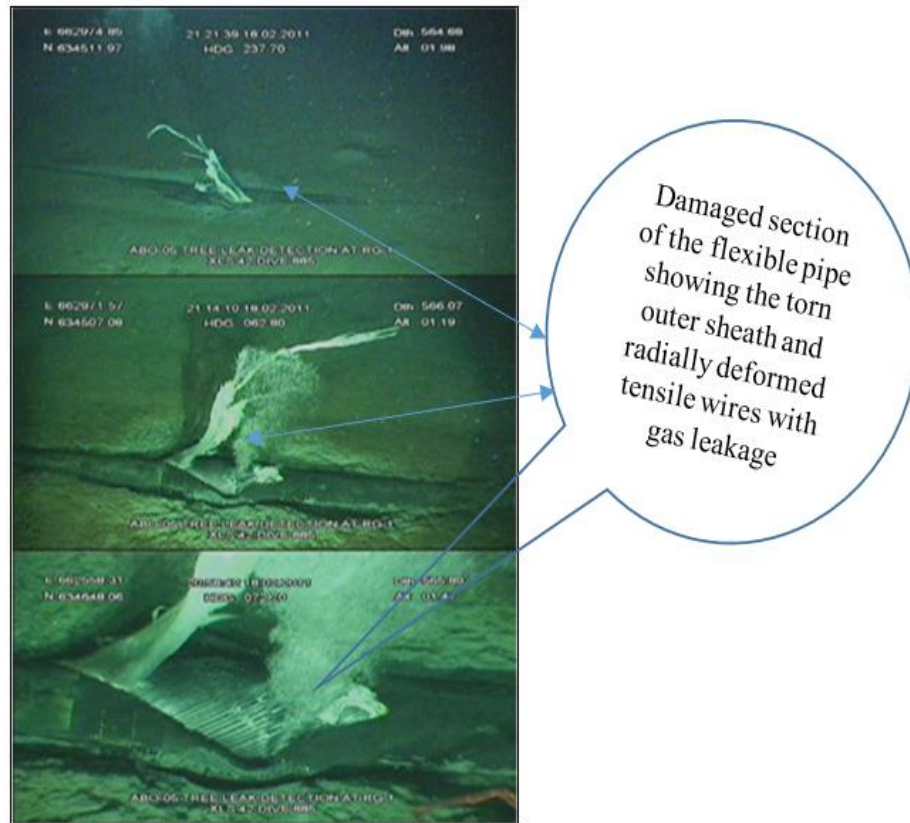


Figure 4-3: Subsea structural overview with ROV of flexible pipe failure [48]

Following API 17 J requirements and Technip internal design rules, the flexible pipe under observation was designed to have a service life of 15 years. With a design pressure of 27.6 MPa, operating pressure between 22.7 to 25.1 MPa, design temperature around 80°C and the flow line with a length of 590 m. Fluid flowing through the pipe is described as dehydrated gas without H₂S, but no fluid composition was specified at the design stage.

Subsequently, to determine the failure scenario of the flexible pipe being studied, different tests were carried out separately. The results obtained were analysed, followed by numerical analysis to validate and verify the conclusion of the experimental results.

The primary objectives of the tests were set on the following:

- Compare all materials of the damaged sample to the undamaged sample through tensile tests
- Detect failures and find their origin
- Find evidence of any event suspected during dissection or operation
- Compare the experimental values of stress with the numerical results

4.4 Materials properties

The flexible pipe specimen was carefully examined to determine the root cause of the failure. The specimen was divided into three (3) samples A, B, and C. Sample A is the damaged section, while Samples B and C are intact and have the same form and similar materials make up. However, the investigation studies were carried out on only samples A and B. The longitudinal strain was determined

using strain gauges and a calibrated extensometer of the required gauge length. Sample A is between 1051.5 m and 1054.3 m which includes the birdcage area at 1053 m towards the wellhead site, and it is approximately 2.8 m in length, while Sample B dimension is 3 m long between (1063.4 and 1060.4) close to the FPSO. Sample C is a 1.3 m (1060.4 m and 1059.1 m) long part of the flow line, following directly after sample B. Regarding this experiment, samples B & C are considered one since they are both intact and remain undamaged. Initial visual inspection was carried out on a layer-by-layer basis to confirm that the flexible pipe was designed and built from the multi-layering of different materials that gave its properties.

The materials were subjected to several tests, though the tensile test was the focus. Figure 4-4 shows the dissection of the specimen, and Figure 4-5 shows the tensile test configuration and setup.

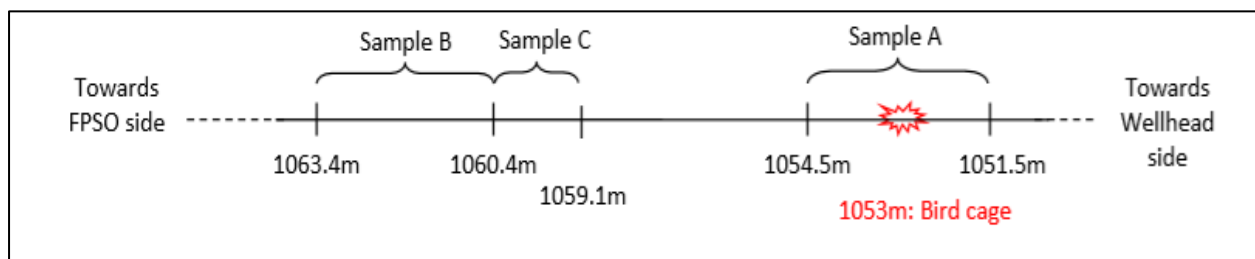


Figure 4-4: Dissection of the flexible pipe specimen [5]

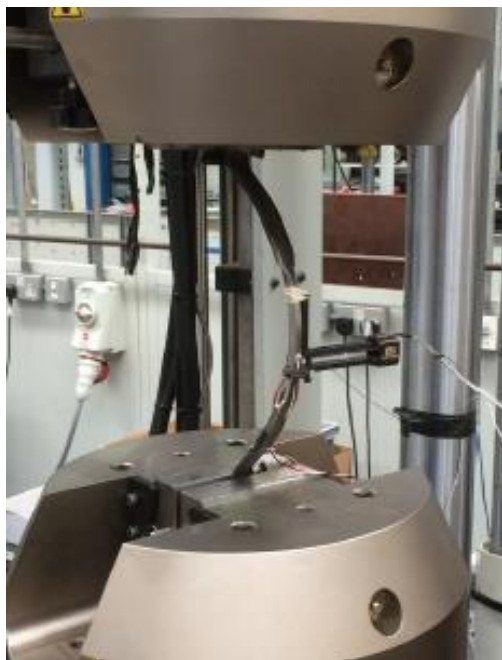


Figure 4-5: Tensile test Configuration and Setup

4.5 General Test procedure

The samples were tested under the same boundary conditions as both ends fixed, and the loads were applied directly. The test was carried out under two different scenarios: dry and wet. This is in addition to a visual inspection carried out on some of the layers, and the findings were recorded. The samples were divided into specimens of various lengths and thicknesses. The test Sample A is measured as 2.8

m which represents the length of the failed section, while Sample B is 1.3 m long represents the intact or undamaged length.

The samples are set up in the workshop for testing, with both pipes (Samples A and B clearly shown in Figures 4-6 and 4-7. Visual inspection shows the pipe near the damage is deformed, and the fracture of the external sheath and the second armours were corroded in the same section of the pipe.

Moreover, the object inside the pipe is visible and was confirmed to be a pig launched inside the pipe to remove the hydrate blockage/plug. Figure 4-6 shows the pig stuck at the middle of the pipe when trying to remove the blockage and the sectional views of the pipe layer during analysis.

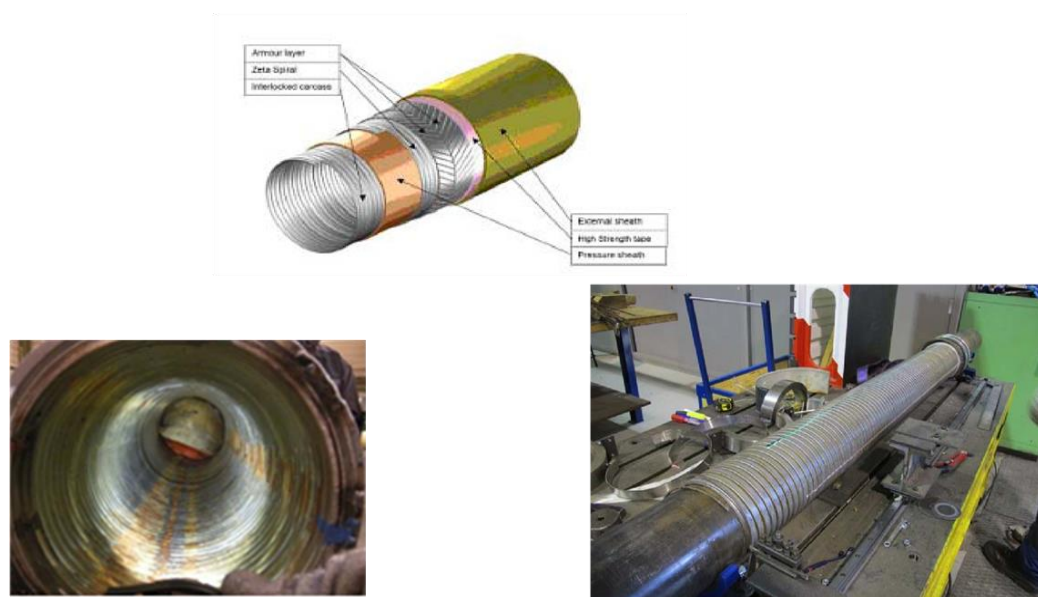


Figure 4-6: Flexible pipe sectional view of layers during analysis



Figure 4-7: Sample description of the investigated flexible pipe

The laboratory investigation on the dissected flexible pipe on samples A and B showed the possible individual layers that conform to the API 17B & 17 J. The overall experimental results as measured using the set up in Figure 4-5 and the designed data for the stress and strain are in Table 4-2.

Table 4-2: The layer-by-layer outcome Ultimate Tensile Stress (UTS), strain and yield stress

| Layers | UTS as Designed (MPa) | SAMPLE A | | | SAMPLE B | | |
|-----------------------|-----------------------|-----------|------------|--------------------|-----------|------------|--------------------|
| | | UTS (MPa) | Strain (%) | Yield Stress (MPa) | UTS (MPa) | Strain (%) | Yield Stress (MPa) |
| Carcass | 550 | 860.7 | 31.4 | 294.3 | 853.7 | 30.6 | 290.5 |
| Pressure Sheath | 48 | 56.3 | 312.3 | 27.5 | 52.7 | 308.2 | 26.4 |
| Zeta-Pressure Armour | 1000 | 1036.5 | 8.7 | 536.5 | 1032.0 | 8.2 | 545.0 |
| First Tensile Armour | 1400 | 1537.3 | 3.9 | 1286.3 | 1541.5 | 5.8 | 1285.0 |
| Second Tensile Armour | 1400 | 1545.8 | 4.8 | 1297.5 | 1534.8 | 5.5 | 1265.6 |
| High Tensile Strength | 3400 | 476.3 | | | 510.3 | | |
| External Sheath | 34 | 32.7 | 709.7 | 19.3 | 32.9 | 700.3 | 18.9 |

4.6 Tensile tests of non-metallic layers

4.6.1 Test specimen-pressure sheath

The same specimen length was used for all the layers without any deviation, while the diameter of both samples remained intact. Figures 4-8 and 4-9 show the pressure sheath assessment and the specimen location and orientation on the sheath, respectively. The actual value of tensile stress of the layer was determined, with the pressure sheath sample further divided into sub specimens and measured (when dry and wet) with the results shown in Table 4-3.



Figure 4-8: Pressure Sheath assessment



Figure 4-9: Specimen location and orientation on the sheath

The stress result in Table 4-3 was obtained by conducting a tensile test on the entire length of sample A and sample B of the pressure sheath.

Table 4-3: Pressure Sheath layer experimental analysis result for the entire length

| | Stress at Yield (MPa) | Strain at Yield (%) | Stress at break (MPa) | Strain at break (%) |
|-----------------|----------------------------------|--------------------------------|----------------------------------|--------------------------------|
| Sample A | 27.5 | 39.7 | 56.3 | 312.3 |
| Sample B | 26.4 | 43.4 | 52.7 | 308.2 |

4.6.2 Test specimen-external sheath

As regards the layer-by-layer measurement, the diameter of samples A and B for the external sheath remained the same except at the mark 1053m, the birdcage. The change in diameter resulted from the tear of the flow line. This can be visible in figure 4.8; The External sheath is made of polyethene (FINATHENE® 3802), and the effects of the failure are because of tear; the sleeves are thinner with the end in yielded areas.

The direction of failure was noticed at the angle of the first armours layer, no ageing was detected at the point of damage and maximum temperature was seen by the sheath: 50-55°C (line buried). It was concluded that the external sheath failed due to a mechanical load underneath. Table 4-4 shows the result of the external sheath layer experimental analysis for the entire length.



Figure 4-10: External Sheath stress

The stress result in Figure 4-10 was obtained by conducting a tensile test on the entire length of sample A and sample B.

Table 4-4: External Sheath layer experimental analysis result for the entire length

| | Stress at Yield (MPa) | Strain at Yield (%) | Stress at break (MPa) | Strain at break (%) |
|-----------------|----------------------------------|--------------------------------|----------------------------------|--------------------------------|
| Sample A | 19.3 | 10.7 | 32.7 | 709.7 |
| Sample B | 18.9 | 11.0 | 32.9 | 700.3 |

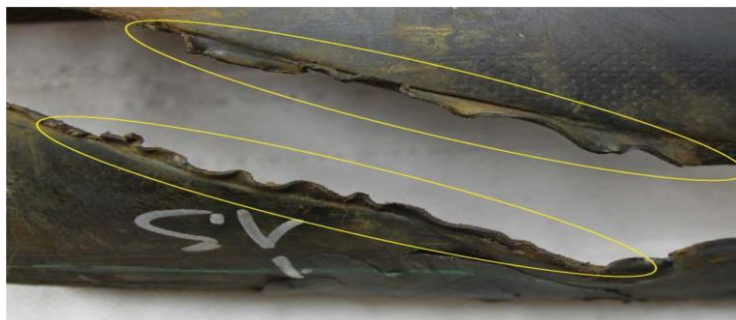


Figure 4-11: Shown the torn External Sheath

4.6.3 Test specimen-high strength tapes (HST)

The High Strength Tapes (HST) diameter remained OK for both samples, but for sample A, HST got damaged at mark 1053 m, as shown in Figure 4-12. HST is made of Polyaramid (Kevlar®), and when it was observed in the laboratory, there was a slight strength at break decrease due to light hydrolysis, which means that there was water in the flexible pipe annulus.



Figure 4-12: Overview of external layers damage

4.6.3.1 Test Procedure

The specimens were tested when dry and wet under the API loading condition as specified in API 17J (2004); the specimens of various lengths and thicknesses were tested. Though, slight hydrolysis (typical of the flooded annulus) is within the acceptable design criteria.

Table 4-5: HST Observation result

| | UTS (MPa) |
|-----------------|------------------|
| Sample A | 476.3 |
| Sample B | 510.3 |



Figure 4-13: High Strength Tape assessment

4.7 Tensile tests of metallic layers

The tensile test was carried out on the metallic layers- namely the Carcass, Pressure armour and tensile wires. Therefore, presented in Figures 4-14 to 4-16 are the layer-by-layer tensile test results:

1.7.1 Test specimen-armour layers

The armour layers are made of steel; there was no rust visible at the failure detection, so high corrosion took place at the failure location (storage) at a moderate corrosion rate of 1–2 $\mu\text{m}/\text{year}$, which does not affect the Tensile properties.

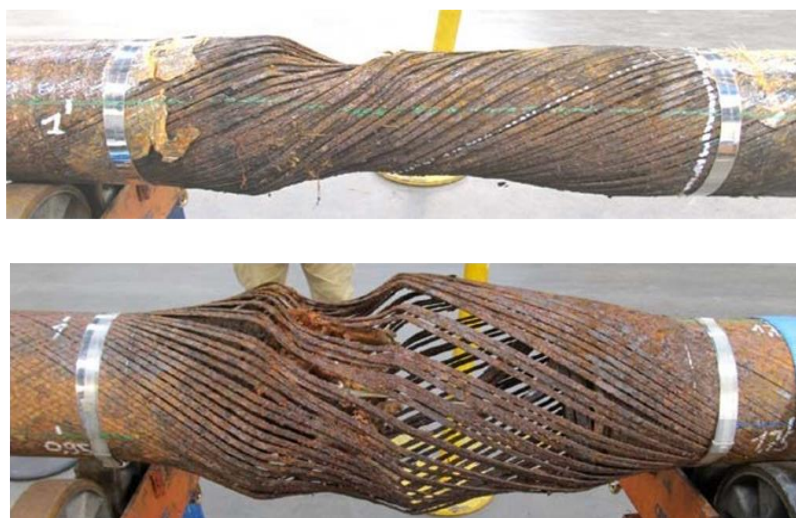


Figure 4-14: Overview of Armour layer damage, birdcage and torsion

It is observed that the birdcage formed in armour wires is due to axial compression because of excess load by the hydrate.

4.7.1.1 Test Procedure

The specimens were tested when dry and wet under the API loading condition as specified in API 17J (2004); the specimens of various lengths and thicknesses were tested.

4.7.2 First armour layer

From Figure 4-15, it is evident that there is a drastic change in the diameter of sample A while that of sample B experienced no change.



Figure 4-15: First armour layer assessment

4.7.2.1 Results – Layer 4 (First Armour)

Min. thickness: 1.4 mm

Min. thickness: 1.86 mm

No thickness reduction

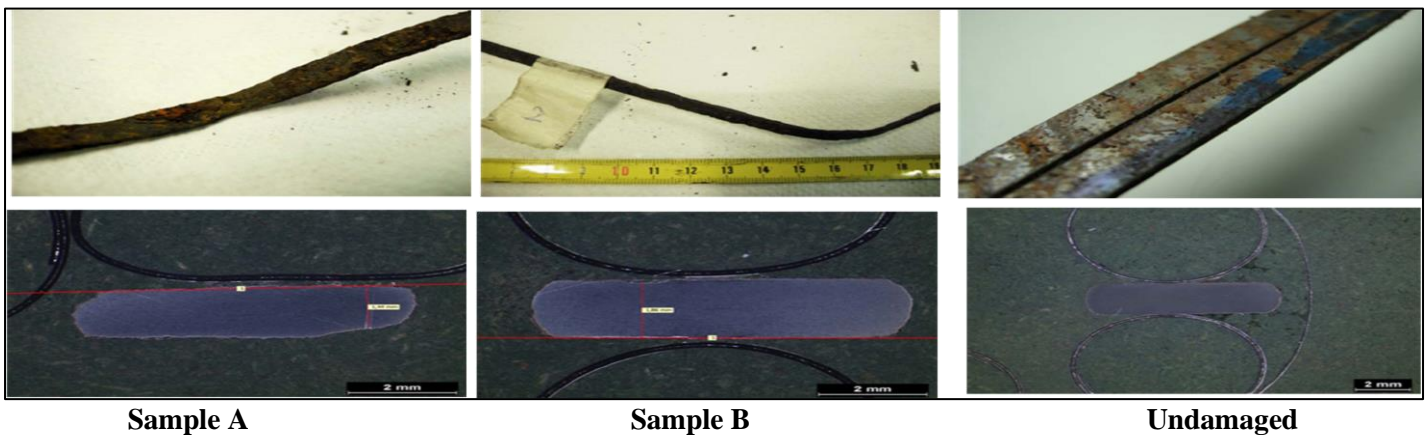


Figure 4-16: First Armour Thickness Comparison

4.7.2.2 Second Armour Layer

Observation of the second armour layer shows that the diameter of sample B remained the same as built while sample A was distorted.



Figure 4-17: Second armour layer analysis

4.7.2.3 Results – Layer 5 (Second Armour)

Min. thickness: 0.7 mm

Min. thickness: 1.77 mm

No thickness reduction

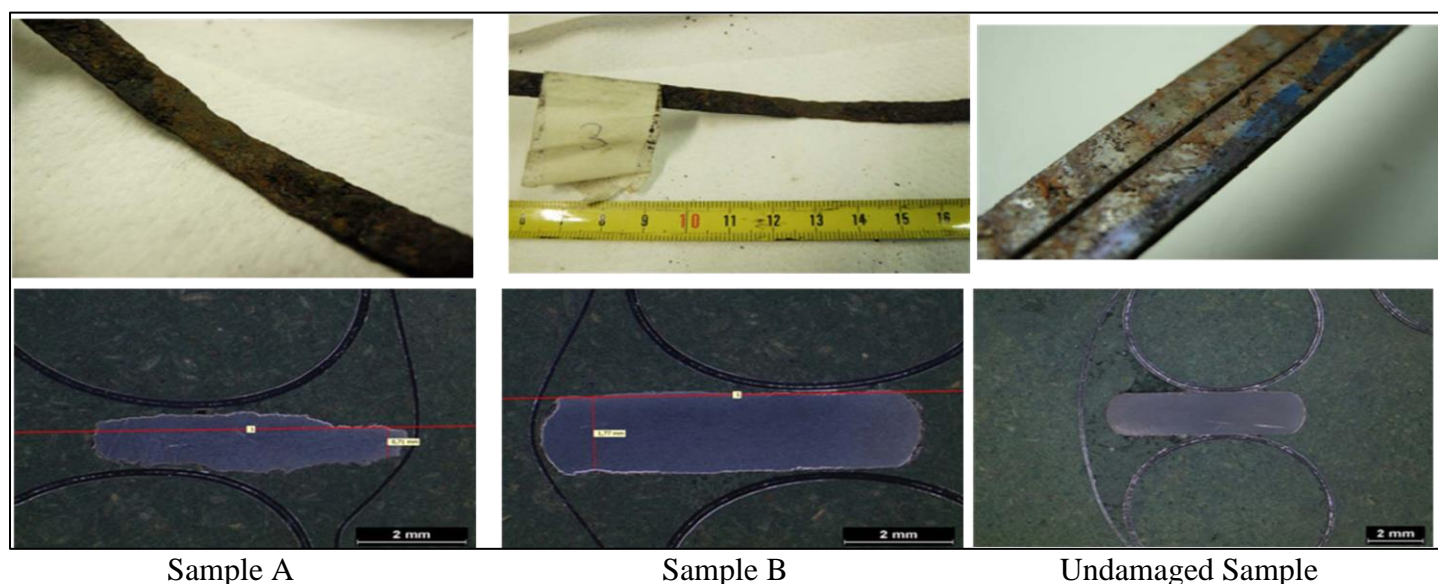


Figure 4-18: First Armour Thickness Comparison

Table 4-6: Elongation and tensile strength sample result

| | | Yield strength (MPa) | Ultimate tensile strength (MPa) | Elongation at break (%) |
|-----------------|----------------------|----------------------|---------------------------------|-------------------------|
| Sample A | First Armours layer | 1286.3 | 1537.3 | 3.9 |
| | Second Armours layer | 1297.5 | 1545.8 | 4.8 |
| Sample B | First Armours layer | 1285.0 | 1541.5 | 5.8 |
| | Second Armours layer | 1265.8 | 1534.8 | 5.5 |

4.7.3 Test Specimen-Zeta layer (Pressure Armour)

The Zeta layer is made of unlocked carbon steel, and high corrosion was noticed at the failure location. Like the armours, it also has moderate corrosion, 2 µm/year and no significant change in the properties.

4.7.3.1 Test Procedure

The specimens were tested when dry and wet under the API loading condition as specified in API 17J (2004); the specimens of various lengths and thicknesses were tested.

4.7.3.2 Results – Material Properties – Layer 3 Zeta (Pressure Armour)

The microstructure (ferritic pearlitic) is compatible with steel type (F111 carbon steel with UTS 1000 MPa). In the central zone (damaged), the specimens are deformed and show a layer of corrosion products made by iron oxides and hydroxides. These compounds are typical of natural environments (i.e., atmospheric or marine exposure).

There is no evidence of significant reduction of the cross-section. There is no evidence of stress corrosion cracking or corrosion fatigue for all the observed specimens, and there is no thickness

reduction. The Zeta thicknesses comparison is presented in Figures 4-19, while the results are presented in Table 4-7.

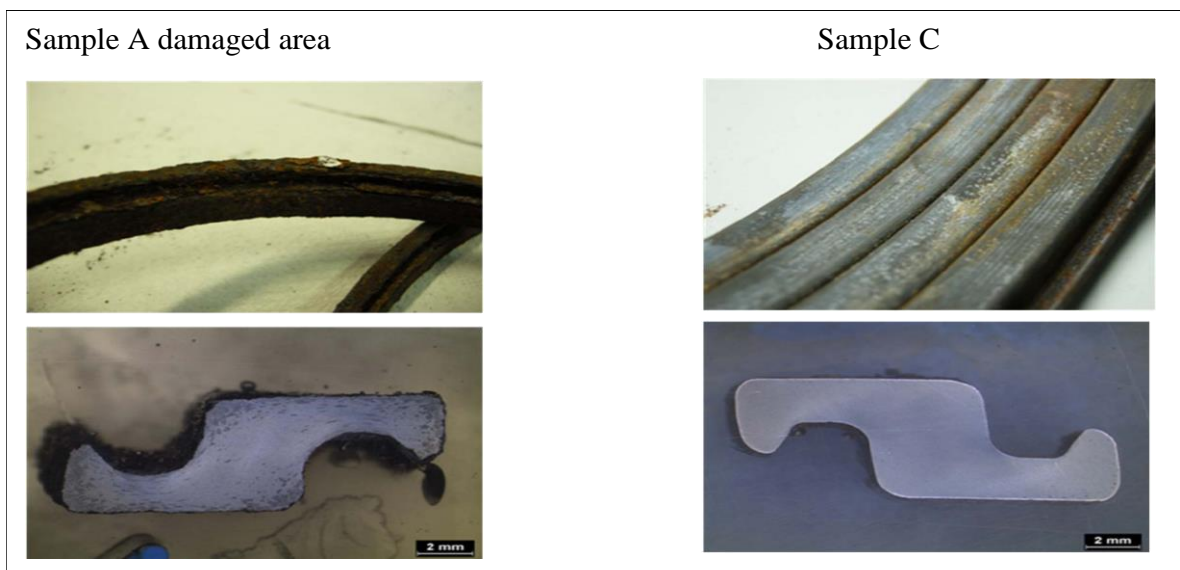


Figure 4-19: Zeta Thickness Comparison

Table 4-7: Zeta Tensile Result

| | Yield strength (MPa) | Ultimate tensile strength (MPa) | Elongation at break (%) |
|-----------------|-----------------------------|--|--------------------------------|
| Sample A | 536.5 | 1036.5 | 8.7 |
| Sample B | 545.0 | 1032.0 | 8.2 |



Figure 4-20: Pressure armour layer analysis

Samples' diameter is acceptable; however, sample A corroded while sample B corrosion happened at just one extreme.

It was also detected that the layer of sample A was unlocked and unrolled at the mark 1053 m, and sample B remained the same as presented in Figure 4-21.



Figure 4-21: Zeta layer assessment

4.7.4 Test Specimen-Carcass

Stainless steel (AISI 304) is the significant component that makes up the carcass; thus, the reason for its circumferential ductile break, perpendicular to the pipe axis, ductile failure at birdcage location and shape distorted though does not affect the mechanical properties. The deformation and rupture of the carcass were due to axial load. The diameter for both samples remained the same as the initial model. As seen in Figures 4-22 to 4-24, the carcass of sample A was broken and unwound while sample B remained intact.

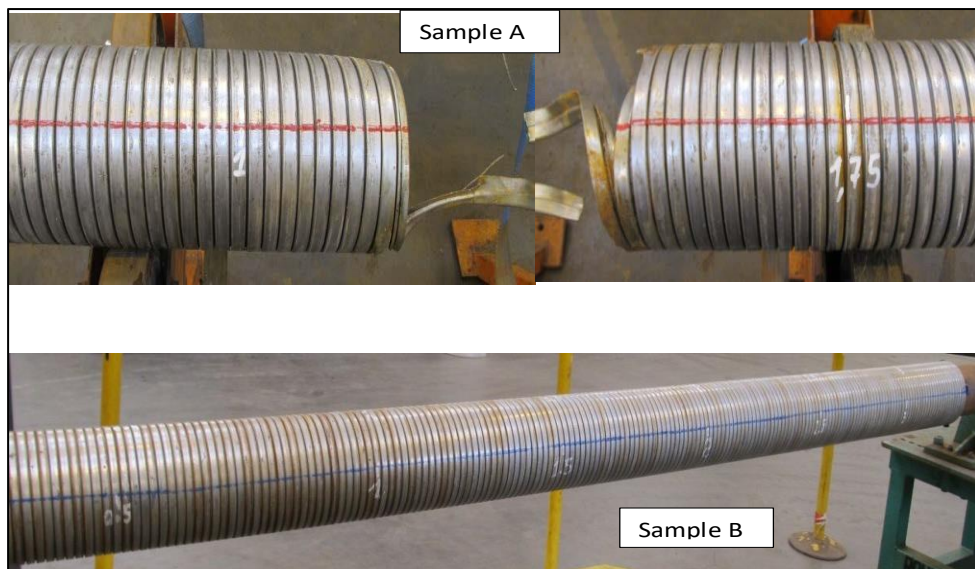


Figure 4-22: Carcass layer assessment

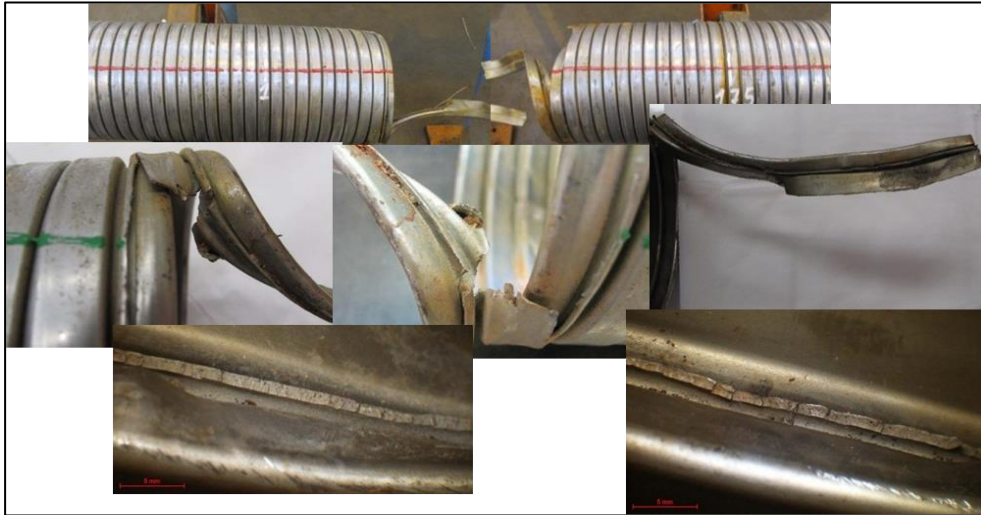


Figure 4-23: Damaged and Twisted Carcass

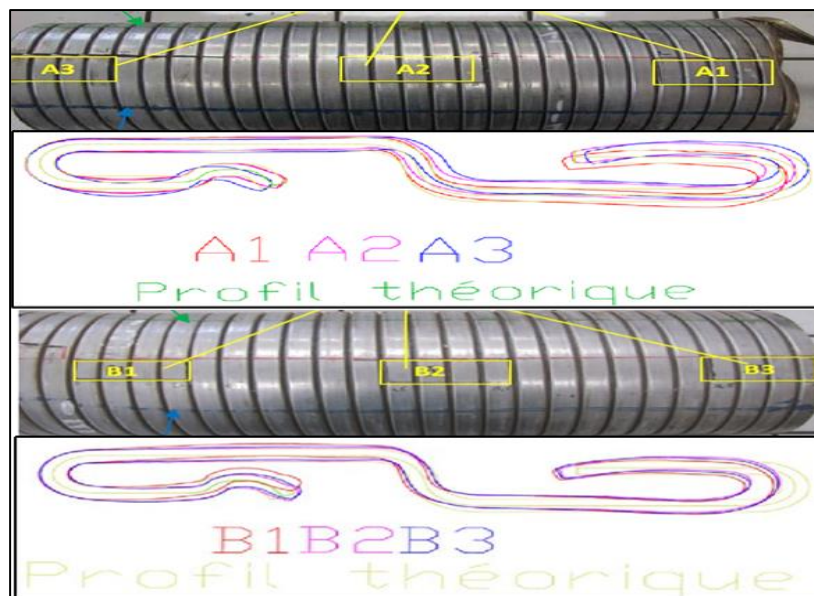


Figure 4-24: New Carcass Configuration

4.7.4.1 Test Procedure

The specimens were tested when dry and wet under the API loading condition as specified in API 17J (2004). The specimens of various lengths and thicknesses were tested.

4.7.4.2 Results – Material properties – layer 1: Carcass

The microstructure and the presence of main alloying elements (both from samples A and C) agree with AISI 304.

Slight corrosion phenomena have been observed on the carcass of sample A (mainly in the central zone), very probably related to the exposure of the material after the failure to seawater and marine atmosphere.

The cross-section was not reduced. There was no sign of stress corrosion cracking, pitting, or crevice corrosion was observed.






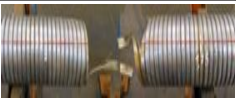
Table 4-8: Carcass layer experimental analysis

| | Yield strength (MPa) | Ultimate tensile strength (MPa) | Elongation at break (%) |
|-----------------|---------------------------------|--|------------------------------------|
| Sample A | 294.8 | 860.7 | 31.4 |
| Sample B | 290.5 | 853.7 | 30.6 |

4.8 Conclusion

The tensile test was conducted on all seven (7) layers that made up the non-bonded flexible pipe under investigation. They were all subjected to the same loading conditions as specified in the API 17 J. The results showed a spread of stress from layer to layer based on the properties and the function of the layers in the pipe. Table 4-9 summarises the findings and conclusion of the experimental investigation of the non-bonded flexible pipe specimen.















Table 4-9: Results of the investigated Layers

| S/N | Layers | Dissection | Laboratory | Sample |
|------------|--------------------|-------------------------------------|--|---|
| 1. | External sheath | Torn and swollen at 1053m | Not aged, Max T°≈ 50-55°C |  |
| 2. | High Strength Tape | Torn at 1053m | Moderate level of ageing (hydrolysis) presence of water in the annulus |  |
| 3. | Armours layers | Birdcage at 1053m | Undamaged area: slight corrosion rate presence of water in the annulus Mechanical properties unchanged |  |
| 4. | | Corrosion (due to offshore storage) | | |
| 5. | Zeta layer | Unlocked and elongated | Corrosion (offshore storage) Mechanical properties unchanged |  |
| 6. | Pressure sheath | Torn at 1053m | Ductile failure by axial overloading Not aged Max T°≈ 50-55°C |  |
| 7. | Carcass | Elongated and broken at 1053m | Shape distorted Ductile failure by axial overloading Mechanical properties unchanged |  |

The same specimen properties are used in Chapter 5 for the numerical model, simulation, analysis, and results verified using Abaqus software, a globally utilized finite element simulator.

Table 4-10 presents the investigated Samples A and B with the layers represented as they were original.

Table 4-10: Sample A and B Layers as they were

| Layers | Sample A | Sample B |
|---------------------|--|---|
| External Sheath |  |  |
| High Strength Tapes |  |  |
| Second Armour |  |  |
| First Armour |  |  |
| Zeta |  |  |
| Pressure Sheath |  |  |
| Carcass |  |  |

4.10 Further Experimental Investigation on a 9-Layer Flexible Pipe

A further experiment was conducted on a similar 6'' diameter 9-layers non-bonded flexible pipe at the University of Strathclyde laboratory workshop. The investigation was based on the available equipment that enabled load tests on the sample, including compressive and tensile loading tests. This is an additional verification and validation of the behaviour of flexible pipe subjecting to different loads.

4.10.1 Sample Specifications

The samples data values were formulated based on the case study data, being differently where the data was unavailable and looked partially damaged with some vocalisation and buckling occurring in different sections.

The measurements of the dimension were taken the same way it was done on the previous samples. Table 4-11 presents the material specification of the layers.

Table 4-11: Material Specifications

| Layer # | No. Layer description | No. of wires | Poisson's Ratio | E (MPa) |
|---------|---|--------------|-----------------|---------------|
| 1 | Interlocked carcass, 48.0 x 1.0 AISI 304 (FE) 20 | 1 | 0.3 | 207000 |
| 2 | Internal plastic sheath RILSAN P4 0TL TP01 | - | 0.38 | 800 |
| 3 | Zeta-clip, 2 tendons th 6.2 FM 35 (FI 11) | 2 | 0.3 | 207000 |
| 4 | Anti-wear (polyamide (BF 01) | - | 0.3 | Not Available |
| 5 | First Armour Lay 35.0 deg. FI41 2x7mm, 40 wires | 35 | 0.3 | 207000 |
| 6 | Anti-wear (polyamide (BF 01) | - | 0.3 | Not Available |
| 7 | Second Armour Lay -35.0 deg. FI41 2x7mm, 44 wires | -35 | 0.3 | 207000 |
| 8 | Fabric Tape 1 Tape (BA09 KV 400daN; 130mm) | - | 0.3 | 112000 |
| 9 | External Sheath FINATHENE (TP 04) | - | 0.3 | 800 |

The pipe had experienced slight minor vocalisation; nevertheless, it was measured at 8 points around the cross-sectional circumference to get a better average thickness. The values were taken with a digital calliper at 8 circumferential points A-H, as shown in Figure 4-25.

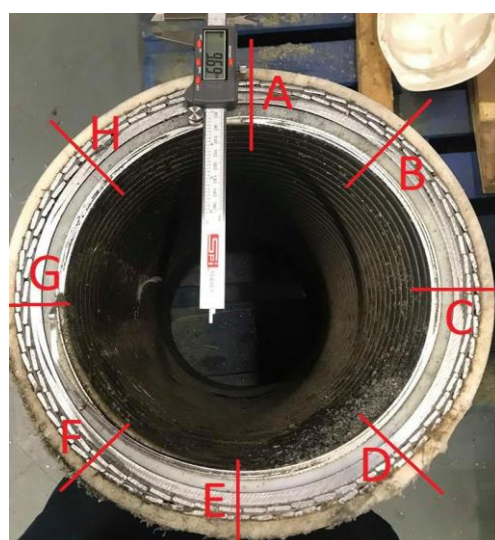


Figure 4-25: The flexible pipe with calliper

Table 4-12 shows the values found from these average measurements, and there is an error margin of 1% in the dimension resulting from the slight buckling and ovality of the specimen pipe.

Table 4-12: Values of average measurements

| Layers # | ID (mm) | H (mm) | Lay angle | Area (mm ²) |
|-----------------------|---------|--------|------------|-------------------------|
| 1.0 | 246.10 | 6.11 | N/A | 4841.20 |
| 2.0 | 258.32 | 8.14 | N/A | 6811.91 |
| 3.0 | 274.60 | 7.96 | N/A | 7061.31 |
| 4.0 | 290.51 | 1.98 | N/A | 1817.05 |
| 5.0 | 294.46 | 1.80 | N/A | 1672.97 |
| 6.0 | 298.06 | 3.10 | N/A | 2928.15 |
| 7.0 | 304.25 | 1.74 | N/A | 1672.63 |
| 8.0 | 307.73 | 3.07 | N/A | 2993.82 |
| 9.0 | 313.86 | 9.61 | N/A | 9768.33 |
| Outer Diameter | 333.08 | | Total Area | 39567.37 |

4.11 Experimental Investigation

4.11.1 Test equipment

Due to the limitation, only a functional tensile machine rated 250 kN was used for the experiment against the initial plan of a 1000 kN rated machine. Due to the constraint, only compressive and tensile tests could be performed. The internal pressure would have been achievable; however, keeping the pressure inside the pipe while putting a tensile load seemed highly challenging.

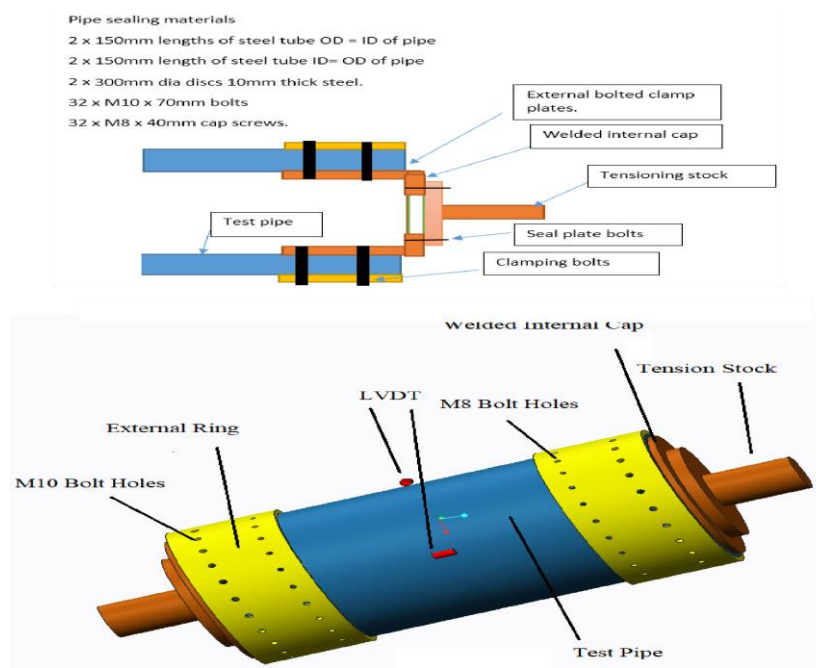


Figure 4-26: Original Pipe Seal Solution

A combined stress loading of tension and internal pressure could not be performed, despite the design of an end cap which the sketch was made into a 3D CAD model by the author, using Creo Parametric 2.0. An annotated version of this model is shown in Figure 4-26, and Figure 4-28 show the drawing sheet for this alternative solution, which contains the dimensions for that design.

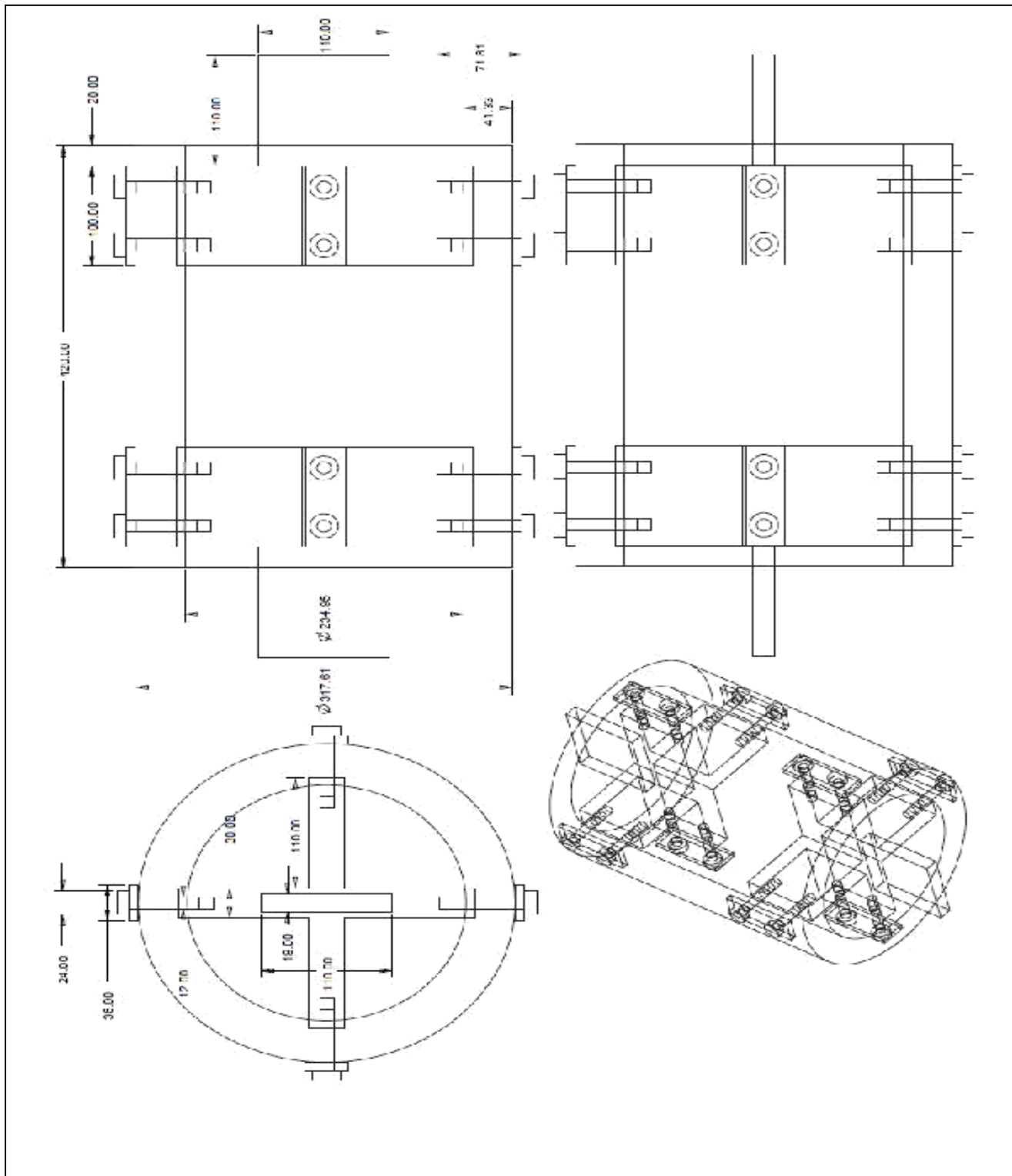


Figure 4-27: Annotated Original 3D Solution

A new design was made with Creo parametric 2.0 for better visibility. Screen capture of the final tension design assembled is shown in Figure 4-28. The Tensile testing design consisted of 2 cross-sectional bars made of 30 mm steel welded together.

4.11.2 Tensile test bar

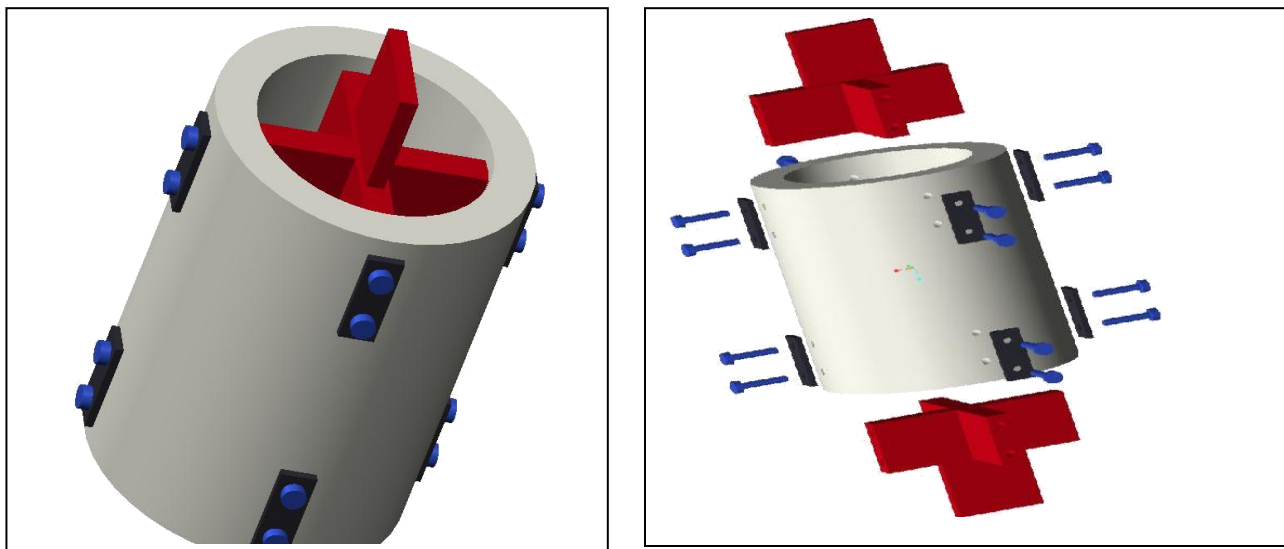


Figure 4-28: Tensile test bar

4.11.3 Tensile Testing Machine - Instron 8802 (250 kN) Fatigue Testing System

The Primary Testing equipment used was the Tensile testing machine, the Instron 8802 (250 kN) Fatigue Testing System. This was used for both the compression and tension test. It has a maximum loading of 250 kN and can plot force, displacement, and time simultaneously. The results can be plotted to the 4th decimal place of an mm, meaning it's accurate to the 0.1 micrometres. A picture of the Instron 8802 (250 kN) Fatigue Testing System is shown in Figures 4-29.



Figure 4-29: Tensile Testing Machine - Instron 8802 (250 kN) Fatigue Test System

4.11.4 Instron – Fast Track 8800

The recording device was an INSTRON Fast Track 8800, a control system linked to the Instron 8802 (250 kN) fatigue testing system. This is the intermediate between the computer used to input and record data to and from the tensile machine. The Instron-Fast track machine is as presented in Figure 4-30.



Figure 4-30: INSTRON - Fast Track 8800

4.11.5 RDP Electronics Spring Transducer

An RDP Electronics Spring Transducer used for the compressive test takes measurements by applying a voltage and measuring the charge over the output using a LabVIEW data acquisition module and program with the hoop expansion taken during the compression test. An illustration of the RDP Electronics Spring Transducer is presented in Figures 4-31.



Figure 4-31: RDP Electronic Spring Transducer

4.12 Methodology and Observations

4.12.1 Procedure for Compression Test

The compression test with tensile load was carried out by directly applying the tensile load to the pipe. The 300 mm pipe section was placed between two thick steel plates inside the tensile machine, and an axial compression loading was applied; the first load set was from 0 to 100 kN. The compression loading was done at 300 N/s; the load speed was chosen based on a similar experiment by De Sousa et al. [14]. After the load had been taken up to 100 kN, the force was taken back down to 0 kN. A transducer was set up against the outside layers central point to monitor any expansion in the outside polyamide 11 plastic layers. However, this only recorded results at that specific point.

Afterwards, the loading was performed from 0 kN-250 kN-0 kN, which caused some slight deformation of the outer plastic layer, where there was already some cracked damage. The results for both the 100 kN test and 250 kN test were recorded and plotted, with the transducer data being plotted separately but simultaneously.

Compressive loading was applied after the 250 kN, and the compression was unloaded back down to 1 kN. The load cycle was repeated once more to see if there was any change in results. After the second load cycle, the tensile machine loading was entirely removed from the steel plate and pipe. At this

point, the pipe only has a small loading of 450 N, acting over the whole axial cross-section because of gravity and the weight of the steel plate.

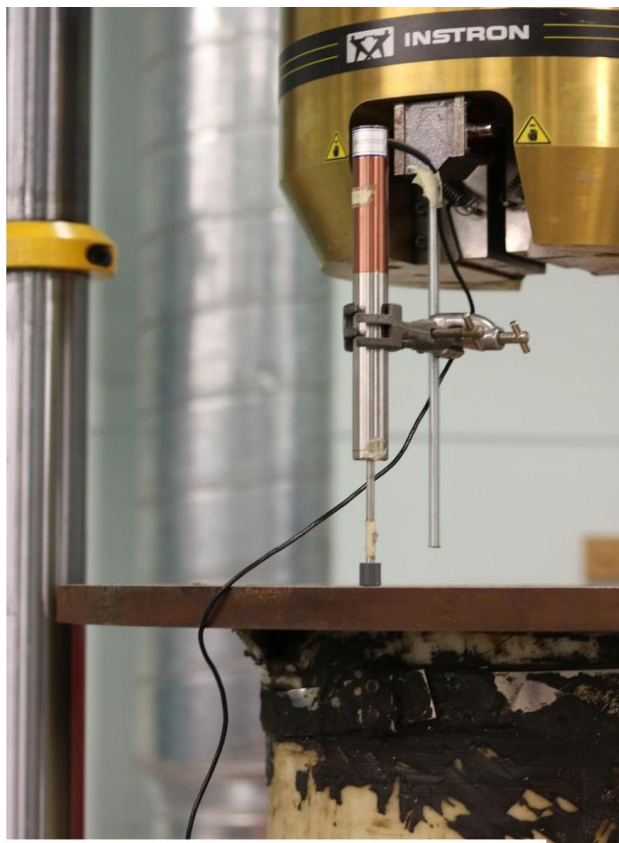


Figure 4-32: Transducer Setup for Recovery Strain

4.13 Results

The results for both the compression and tension experiments are analysed as recorded.

4.13.1 Compression Test Results

The compression results for the applied loads 100 kN, 250 kN and unloaded recovery strain were processed as shown in Figures 4-33 to 4-37. Figure 4-35 shows the applied force against axial displacement with hysteresis, which indicates the loading cycle (loading and unloading) of the 250 kN load. This likely indicates that the overall force value has moved over the static resistive friction of a specific layer. After this point, the layers slide easily between each other until the void is filled, limited by the interlayer spacing geometry. At a point, another layer will start to take the majority of additional loading.

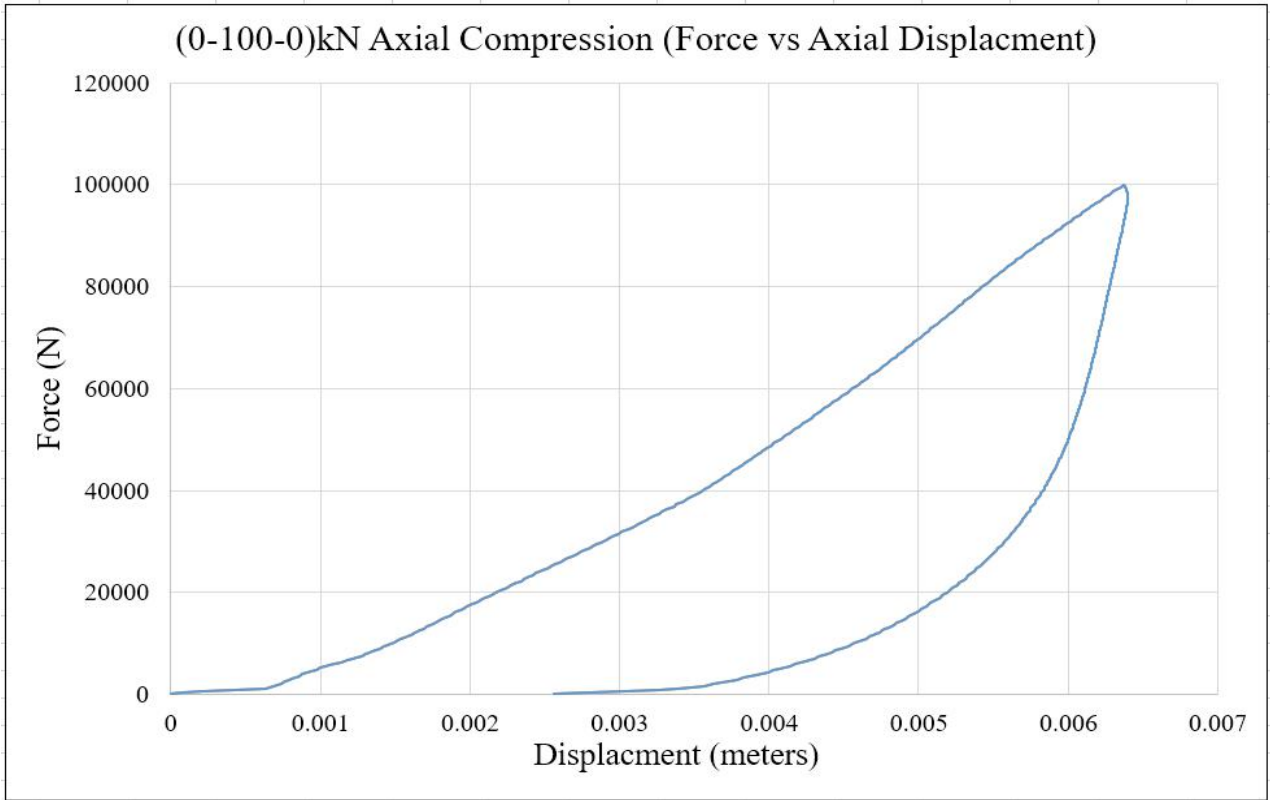


Figure 4-33: 100 kN Compression Test- Axial Compression Displacement

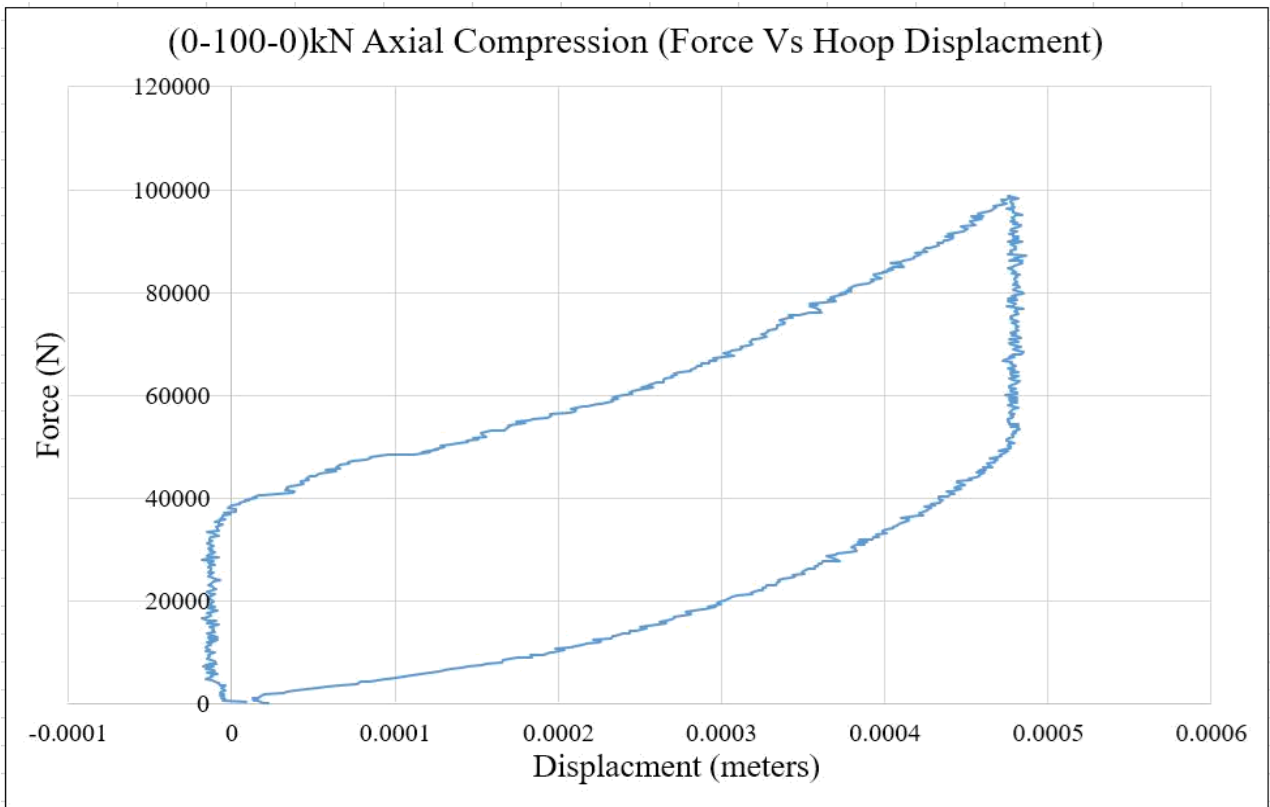


Figure 4-34: 100 kN Compression Test - Hoop Expansion Displacement

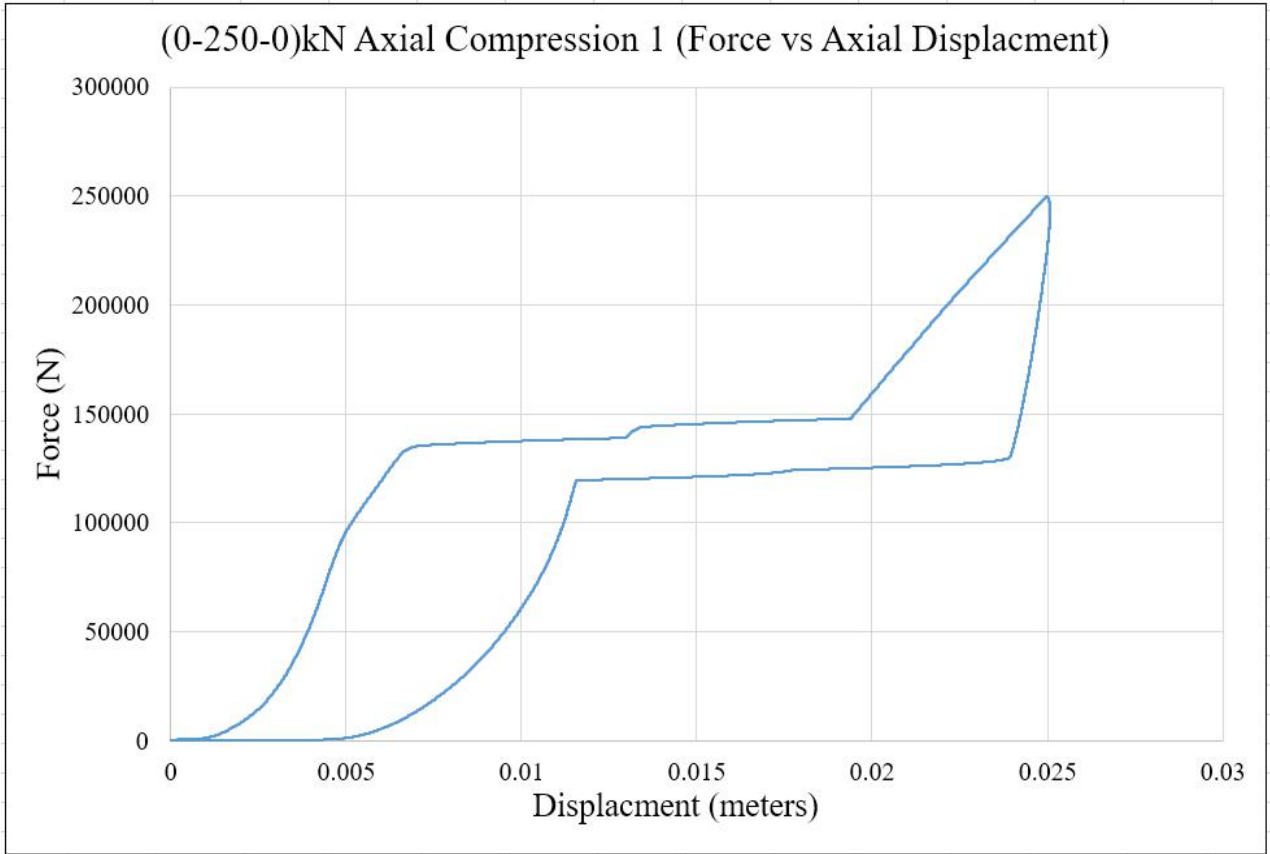


Figure 4-35: 250 kN Compression Test 1 - Axial Compression Displacement

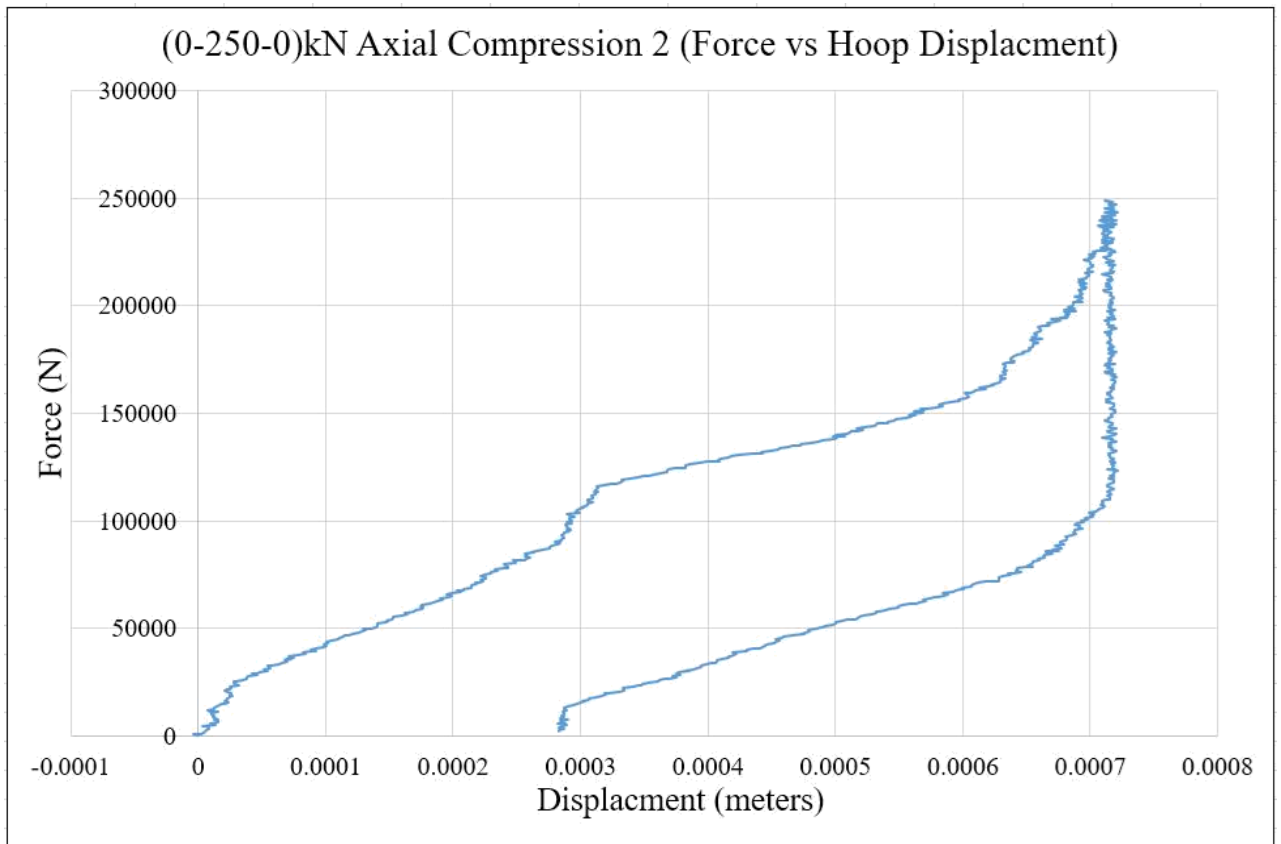


Figure 4-36: 250 kN Compression Test 2 - Hoop Expansion Displacement

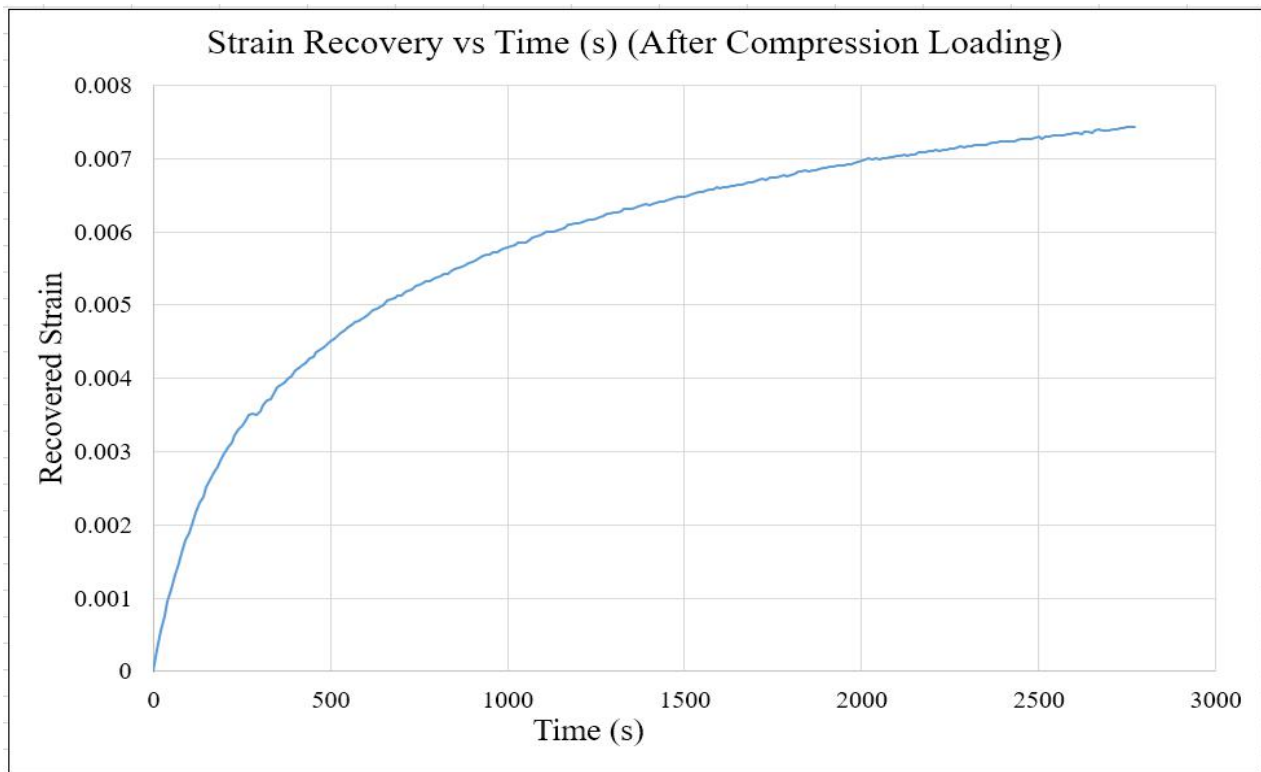


Figure 4-37: Unloaded Compression Strain Recovery

4.14.2 Tensile

The tensile data monitored axial elongation displacement against force. The experiments went well up until 233.5 kN.

4.12.2 Tensile Test

An axial tension loading was applied, the first load was set from 0 to 100 kN to straighten a 300 mm pipe out and shift the internal layers into a more load-bearing condition. This initial 100 kN load had a slight effect on the arrangement. This axial loading was done at a rate of 300 N/s like the compression test to keep the values the same; this was based on experiments loading speed [49]. After the loading sequence of 100 kN, the force was taken back down to 0 kN.

While the tensile loading was approaching 250 kN, some deformation started occurring around the base of the test specimen 105 kN.

In terms of tensile loading, it appeared that the interlocked carcass was taking most of the tensile loading. It is observed that a 105 kN load is large enough to overcome the resistive friction in the interlocked carcass layer, causing the interlocked carcass layer to slide into a more elongated position. This resulted in part of the carcass protruding slightly out the bottom of the pipe while under 105 kN tension or higher. The loading process could not get to 250 k as the tensile loading hit a maximum at 233.5 kN and was repeated several times to confirm the results.



Figure 4-38: Tensile testing arrangement before loading

4.13.2 Tensile Test Results

The tensile test recorded from 100 to 233 kN as against the compressive test that reached 250 kN. Nonetheless, the results show a kind of similarity despite the abruptness experienced.

Figure 4-39 shows the 100 kN tensile test loading, while Figure 4-40 shows the attempt at hitting the 250 kN tensile loading, which ends up peaking at 233.5 kN and Figure 4-41 shows the test data for the loading from 0-160-110-150-50kN.

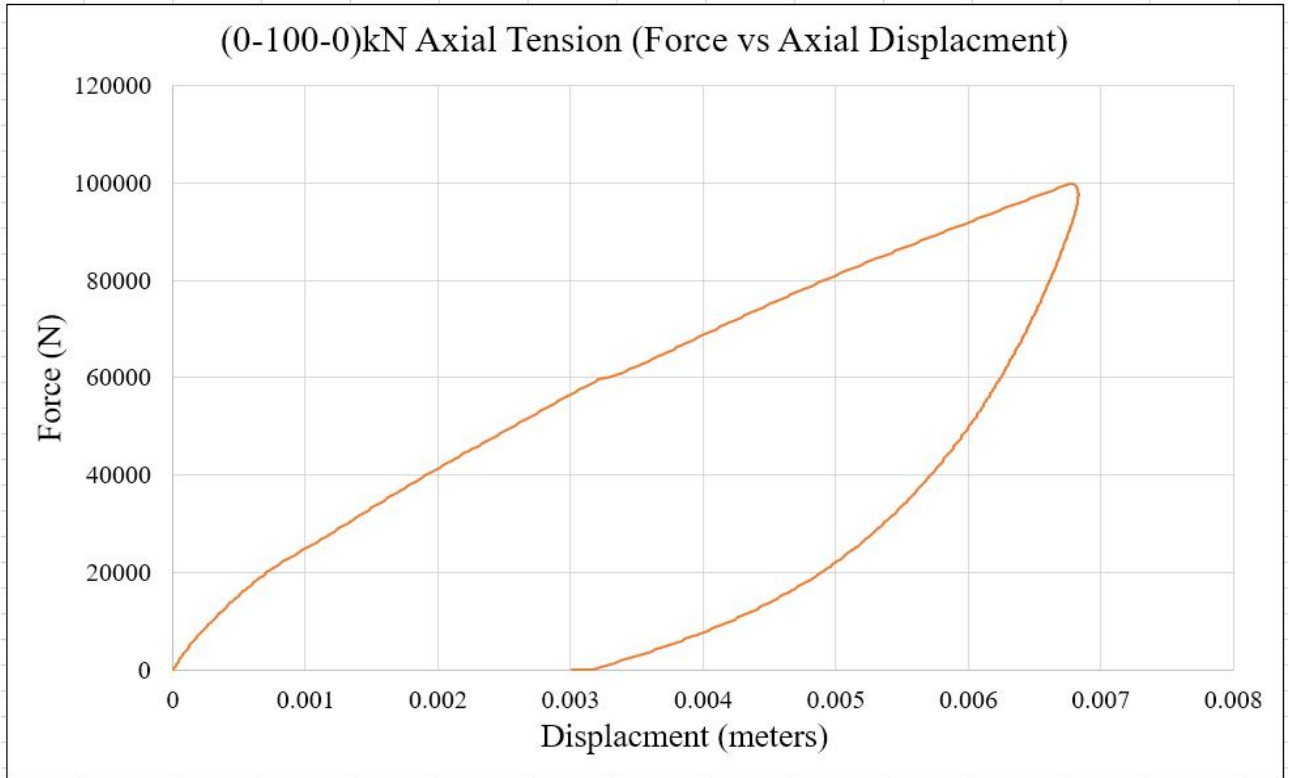


Figure 4-39: 100 kN Tension Test - Axial Tension Displacement

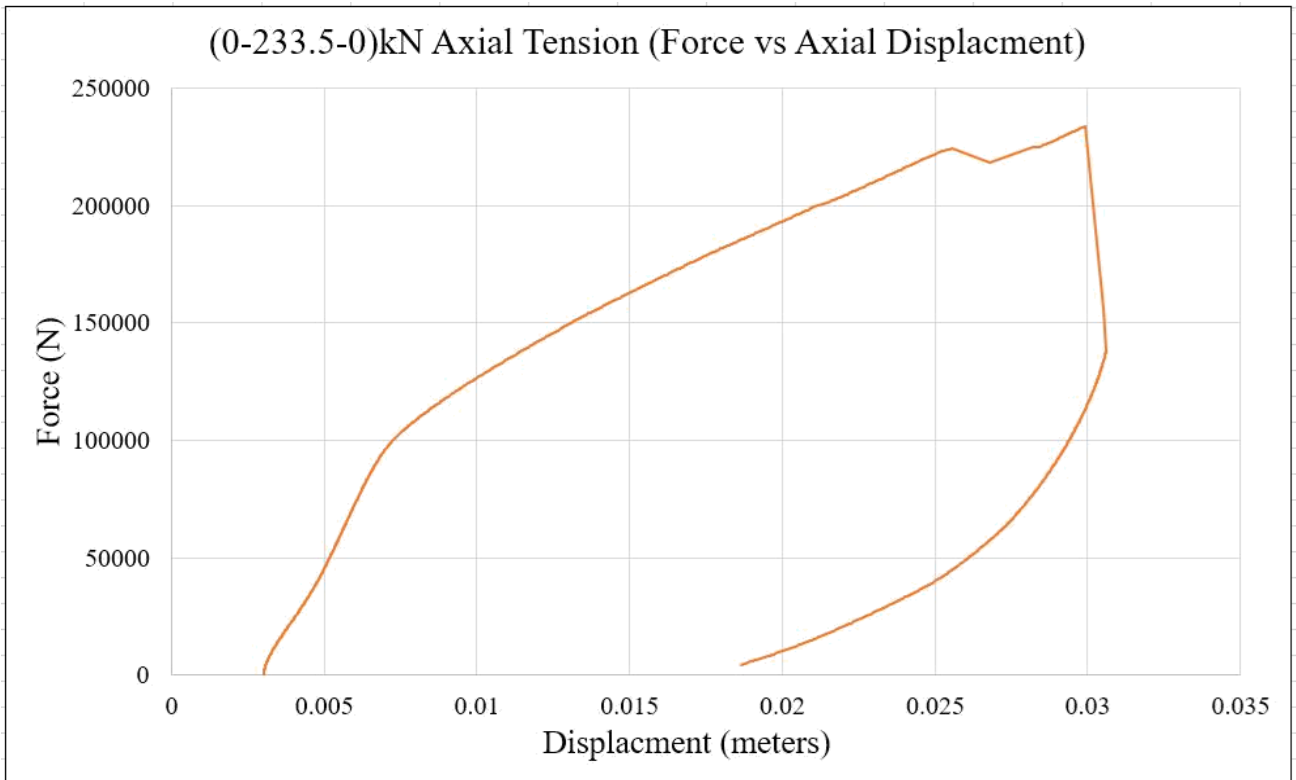


Figure 4-40: Attempt at 250 kN Tensile Loading – Axial Tension Displacement

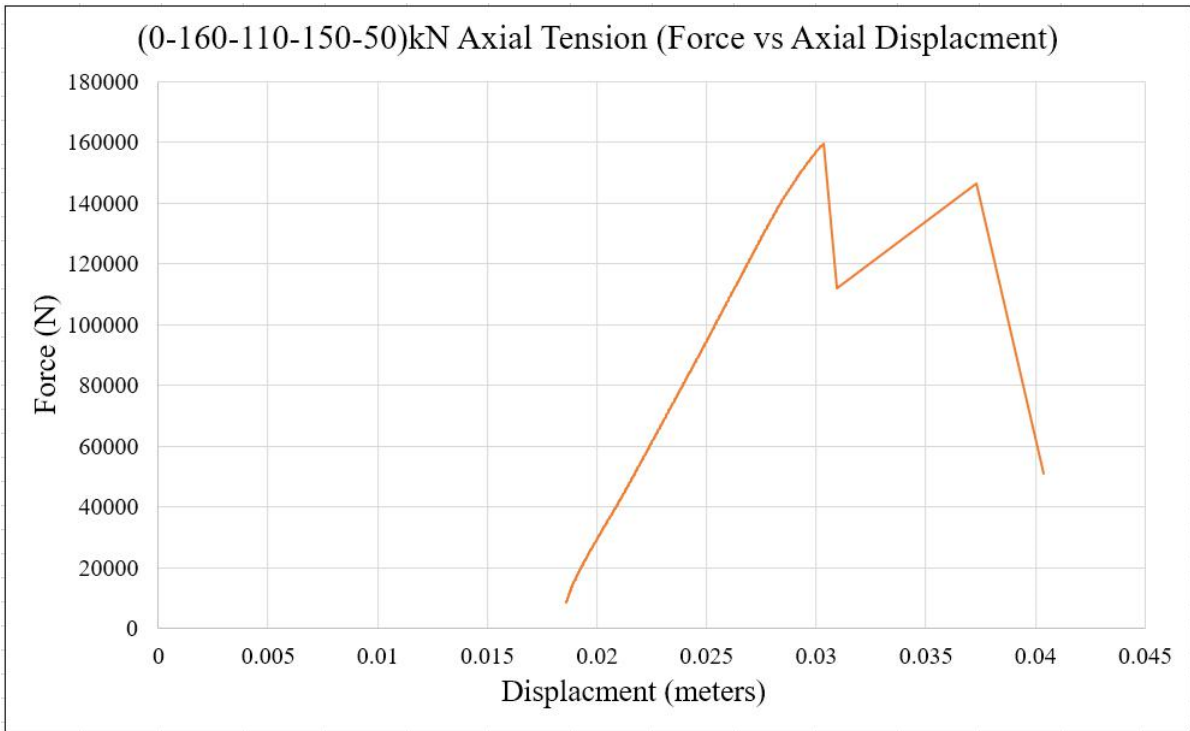


Figure 4-41: Reloading up until failure after one set of bolts sheared

4.13 Conclusion

The tensile and compressive tests were conducted on the nine (9) layers of the non-bonded flexible pipe. They were all subjected to the same loading conditions as specified in the [8] with tensile load (0-110 KN) while the compressive load is (0-250 KN). The results showed similar values with the other experimental results carried out on the 7-layers. Still, there is a limitation to the load applied due to the unavailability of some essential equipment when the tests were carried out.

CHAPTER 5: NUMERICAL INVESTIGATIONS

5.1 Introductory Remarks

This chapter presents the simulation of a methane hydrate blocked non-bonded flexible pipe using a non-linear general-purpose finite element program Abaqus 6.14-4 [13]. The configuration of the non-bonded flexible pipe used in this thesis is a typical multiple layer's types found in many deep and shallow water globally. Thus, with the availability of various literature on the flexible pipe and its analysis, none has focussed on the hydrate blocked pipe. This, therefore, makes the configuration different from other existing researcher works on non-bonded flexible pipes.

The numerical investigations are based on the flexible pipes used in the experimental test programme presented in Chapter 4. Two (2) flexible pipe specimen samples, A and B, whereas simulated using finite element models developed in Chapter 3 and compared with the limited experimental results in Chapter 4. The 7-layers flexible pipe was modelled based on 2.8m sample lengths, and results were compared with the available data. In the finite element model, the measured cross-section dimensions and the material properties provided by the manufacturer are shown in Tables 5-1 and 5-2.

The Finite Element Method (FEM) is a numerical approach that gives an approximation to the exact solution based on the mechanic of a solid element. The physical component is discretized into smaller and discrete parts referred to as finite elements. The elements approximate the object's geometry by mathematical functions, with each element comprising several nodes depending on the element type. Therefore, instead of solving equilibrium equations for the whole object as one, the displacement in each node is found. The equations describing each element are combined to form a global system of equations that can then solve for the entire displacement field. The number of elements and how well the object geometry is approximated will determine the accuracy of the analysis for the actual stress gradient distribution. While it is important to have accurate results, it is important to consider the refinement of the mesh as higher numbers of elements and nodes in the mesh leads to significant computational time.

The analysis considered herein is a non-linear simulation which is necessary for the flexible pipe-cases under consideration. This is required as the physical movement of the flexible pipe can include large displacements, contact, and material nonlinearities. In addition, other factors are varied, including the external conditions, such as internal and external pressure, which can govern the friction moment, and by extent, the pipe behaviour in bending. In addition to material nonlinearities that may be applicable, there are geometric nonlinearities that, for flexible pipes, arise when tensile wires enter the slip phase.

5.2 Case Study

The present work has considered the finite element analysis of the behaviour of a 6" gas injection flexible pipe, made up of seven (7) layers; 3 of the layers are non-metallic, polyester, and the remaining four layers are metallic steel.

The affected flexible pipe was discovered after a comprehensive Remote Operated Vehicle (ROV) survey, and the damaged section is shown in Figure 5-1.

It is envisaged that the failure of the flexible pipe might have been a result of continuous pressurization and depressurization process without considering the design and burst pressure values.

The schematic of the flexible pipe and the damaged sections are shown in Figures 5-1 and 5-2 as identified, while Figure 5-3 shows the applied pressure during pigging operation that led to the failure. The functional properties of the flexible pipe are presented in Table 5-1.

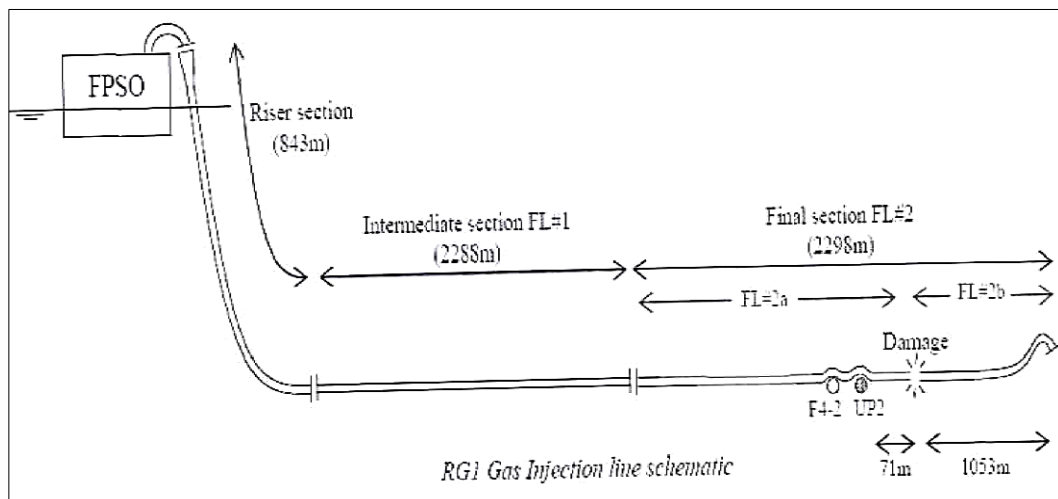


Figure 5-1: Case Study sketched flexible pipe sample

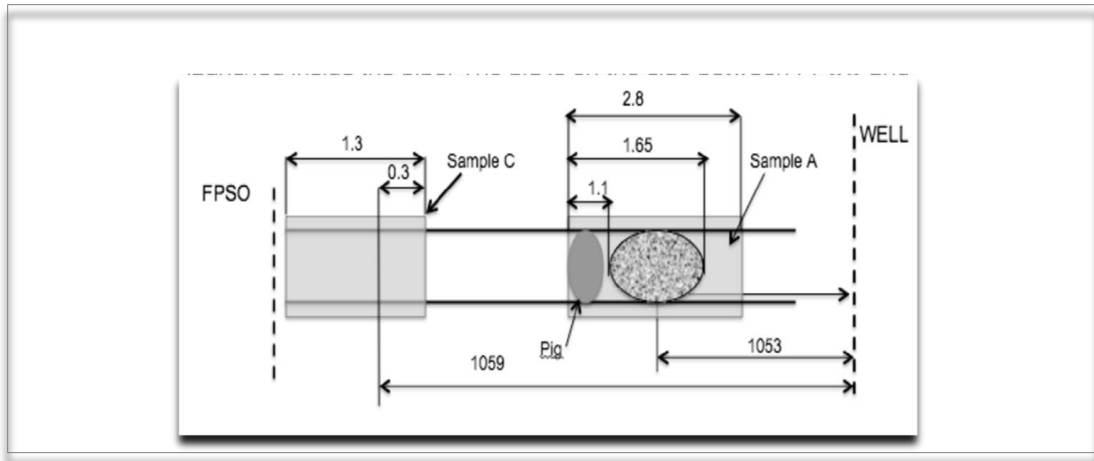


Figure 5-2: Schematic diagram of the flexible pipe under investigation

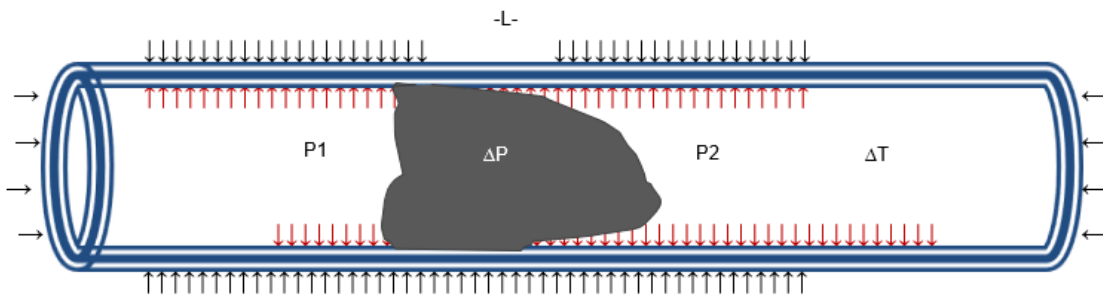


Figure 5-3: Applied pressure during pigging

Table 5-1: The working properties of the flexible pipe [15]

| Properties | Value/Remark |
|------------------------|-----------------------------------|
| Design type | Gas Injection Flexible pipe (FL2) |
| Service | Sweet (no H ₂ S) |
| Design Pressure | 276 bar |
| Max Operating Pressure | 251 bar (227bar) |
| Design Temperature | 80 deg C |
| Inner Diameter | 152.40 mm |
| Outer Diameter | 202.90 mm |
| Design Life | 15 Years |
| Well water Depth | 530 m |
| Line Length | 2298 m |
| Collapse Resistance | 117 bar |

A typical 6" flexible pipe was developed for the analysis. The basic geometric properties for all the layers, including the pipe layer specification and material properties, are shown in Table 5-2, with the full detail in Table 5-4. As given by the manufacturer in Table 5-2, the values of the equivalent materials for carcass and pressure armour in the young modulus E and shear modulus G are calculated with the values shown in Table 5-3.

Table 5-2: 7-Layers 6” Non-bonded flexible Pipe Properties

| No. Layer description | I.D. (mm) | h (mm) | E (MPa) | v | I.R (m) | O.R (m) |
|--|--------------|-----------|------------|------|------------|------------|
| Interlocked Carcass 48.0 X 1.0 AISI 304 (Fe 02) | 160.05 | 1.17 | 165065 | 0 | 0.08003 | 0.0812 |
| RILSAN P40tl Tp01 Pressure Sh. | 162.40 | 6.42 | 800 | 0.4 | 0.0812 | 0.08762 |
| Zeta Wire Th. 6.0 FM 35 (Fi 11) | 175.23 | 3.78 | 136919 | 0 | 0.08762 | 0.0914 |
| First Armour Lay 35.0 Deg. High Character. Fi41 (2x7) 44 wires | 182.80 | 2.00 | 207000 | 0.3 | 0.0914 | 0.0934 |
| Second Armour Lay -35.0 Deg. High Character. Fi41 (2x7) 44 wires | 186.80 | 2.00 | 207000 | 0.3 | 0.0934 | 0.0954 |
| High Strength Tape 1 Tape (BA09 KV 400dab,130 Mm) | 190.80 | 1.25 | 112000 | 0.35 | 0.0954 | 0.09665 |
| External Sheath FINATHENE (TP 04) | 193.30 | 4.80 | 800 | 0.4 | 0.09665 | 0.10145 |

Table 5-3: Carcass and Pressure Armour Equivalent Properties

| Carcass | | | | Pressure Armour | | | | Poisson's Ratio |
|-----------|--------|----|-------|-----------------|--------|----|-------|-----------------|
| | MPa | | MPa | | MPa | | MPa | nu |
| E1 | 100000 | G1 | 22940 | E1 | 100000 | G1 | 84605 | 0 |
| E2 | 165065 | G2 | 22940 | E2 | 136919 | G2 | 84605 | 0 |
| E3 | 165065 | G3 | 22940 | E3 | 136919 | G3 | 84605 | 0 |

The De Sousa principle was used for the Carcass and Pressure armour [23]. These were calculated using the equations expressed in Chapter 3 and gave rise to the new diameter and thickness of carcass and pressure armour as shown in the property Table 5-3 and detailed in Table 5-4.

Table 5-4: Computation of the equivalent Materials for Carcass and Pressure Armour

| S/N | No. Layer description | UTS (MPa) | SDP (MPa) | Mass (kg/m) | I.D. (mm) | h (mm) | Lay angle | Area mm ² | E (MPa) | E (Pa) | G (Pa) | ly (mm ⁴) | V | nt-no of wires/Tendon | | | | | | | | | |
|-----|--|-----------|-----------|-------------|-----------|--------|-------------------|---------------------------------------|---------|-----------------|----------------|------------------------|-----------------|------------------------------|------------------|---------------|----------------|----------|--------------|--------------|------------------------|--|--|
| 1 | Interlocked carcass, 48.0 x 1.0 AISI 304 (FE) 20 | 550 | - | 11.7 | 152.4 | 5 | 87.6 | 19.6 | | 2.07E+11 | 8.00E+10 | 23.1 | 0.3 | 1 | | | | | | | | | |
| 2 | Internal plastic sheath RILSAN P4 0TL TP01 | - | - | 2.31 | 162.4 | 4 | | | 301 | | | | 0.4 | | | | | | | | | | |
| 3 | Zeta-clip, 2 tendons th 6.2 FM 35 (FI 11) | 1000 | 380 | 22.73 | 170.4 | 6.2 | 85.6 | 54.1 | | 2.07E+11 | 8.00E+10 | 173.4 | 0.3 | 2 | | | | | | | | | |
| 4 | First Armour Lay 35.0 deg High charact.FI41 (2x7mm) 40 | 1400 | 403 | 8.27 | 182.8 | 2 | 35 | | 207000 | | | | 0.3 | | | | | | | | | | |
| 5 | Second Armour Lay -35.0 deg High charact.FI41 (2x7mm) 44 | 1400 | 461 | 8.39 | 186.8 | 2 | -35 | | 207000 | | Carcass | Pressure Armour | 0.3 | 40 | | | | | | | | | |
| 6 | High Strength Tape 1 Tape (BA09 KV 400daN; 130mm) | | | 0.4 | 190.8 | 1.25 | | | 112000 | w | | 8.7258 | mm | 0.35 | | | | | | | | | |
| 7 | External Sheath FINATHENE (TP 04) | | | 2.81 | 193.3 | 4.8 | | | 800 | r | 4.4565 | | mm | 0.4 | 44 | | | | | | | | |
| | | | | | | 25.25 | | | | J | 3.2013 | 407.6024 | mm ⁴ | EQUIVALENT DIMENSION | | | | | | | | | |
| | | | | | | | | | | R | 78.7000 | 88.3000 | mm | No. Layer description | I.D. (mm) | h (mm) | E (MPa) | v | I.R m | O.R m | Shell Thickness | | |
| | | | | | | | | | | Lp | 20.7245 | 42.6887 | mm | Interlocked carcass | 160.05 | 1.17 | 166676 | 0 | 0.0800 | 0.0812 | 0.0012 | | |
| | Young Modulus | | | | | | | | | Ieq | 2.2493 | 64.5451 | mm ⁴ | Internal plastic sheath | 162.40 | 6.42 | 800 | 0.4 | 0.0812 | 0.0876 | 0.0064 | | |
| | Material | | | | | | | Density | | hs | 1.1735 | 3.7838 | mm | Zeta-clip, 2 tendons | 175.23 | 3.78 | 138255 | 0 | 0.0876 | 0.0914 | 0.0038 | | |
| | Steel | | | | | 7850 | kg/m ³ | | | Esx | 166822 | 138663 | MPa | First Tensile Armour | 182.80 | 2.00 | 207000 | 0.3 | 0.0914 | 0.0934 | 0.0020 | | |
| | Polyamide 11 | | | | | 1040 | kg/m ³ | | | Ecir | 166676 | 138255 | MPa | Second Tensile Armour | 186.80 | 2.00 | 207000 | 0.3 | 0.0934 | 0.0954 | 0.0020 | | |
| | Axial stiffness (testing in [13]) | | | | | 153 | | | | Gsxy | 22940 | 84605 | MPa | High Strength Tape | 190.80 | 1.25 | 112000 | 0.35 | 0.0954 | 0.0967 | 0.0013 | | |
| | Carcass | | | | | | | Local cross-section dimensions | | E-longit | 100000 | 100000 | MPa | External Sheath | 193.30 | 4.80 | 800 | 0.4 | 0.0967 | 0.1015 | 0.0048 | | |
| | Strip length | | | | | 28 | mm | | | E-Circ | 166676 | 138255 | MPa | Hydrate Plug | | | | | | | 0.0812 | | |
| | β | | | | | 0.196 | | | | E-radial | 166676 | 138255 | MPa | | | | | | | | | | |
| | π | | | | | 3.1415 | | | | V12 | 0 | 0 | | | | | | | | | | | |
| | Strip thickness | | | | | 0.7 | mm | | | V13 | 0 | 0 | | | | | | | | | | | |
| | Second Moment of Inertia Carcass | | | | | 20 | | | | V23 | 0 | 0 | | | | | | | | | | | |
| | Second Moment of Inertia Pressure Arm | | | | | 100000 | MPa | | | Gs12 | 22940 | 84605 | MPa | | | | | | | | | | |
| | | | | | | | | | | Gs13 | 22940 | 84605 | MPa | | | | | | | | | | |
| | | | | | | | | | | Gs23 | 22940 | 84605 | MPa | | | | | | | | | | |
| | | | | | | Length | 2.8m | | | | | | | | | | | | | | | | |

5.3 Applied boundary factors and load values

5.3.1 Applied boundary factors

The ends boundary conditions were imposed through reference points RP-1 and RP-2 located at both ends of the pipe segment. One end RP-2 is constrained at all points while RP-1 is free. Coupling the end nodes of the elements in six degrees of freedom with the reference node simulated the axial and radial constraint of the end fitting. At the end 1, the layers were constrained in all directions using Encastre, while at End 2, the layers are constrained to a reference point RP-1. Figure 5-4 shows the applied boundary condition (BC) as described.

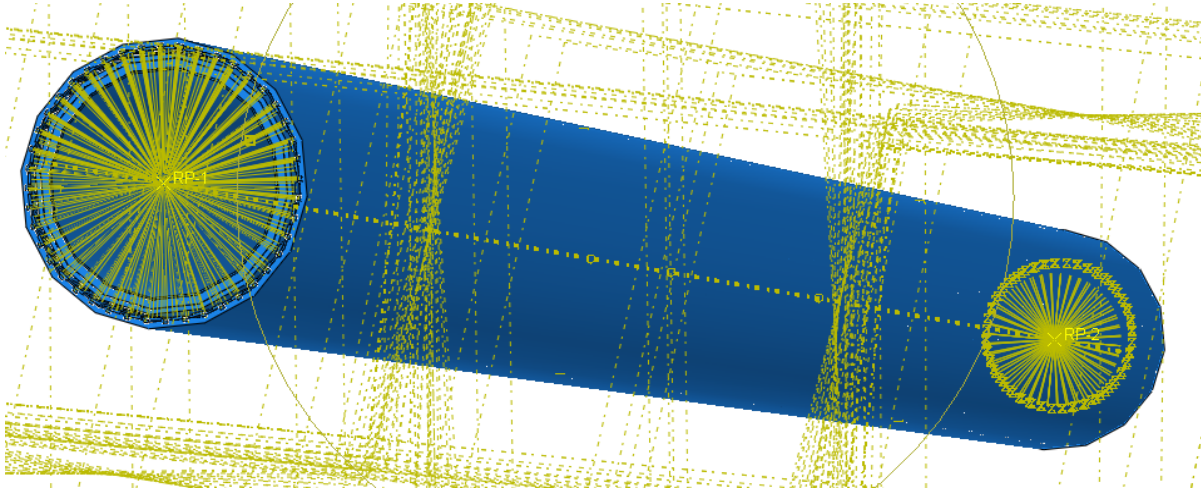


Figure 5-4: Application of constrained at points RP-1 and RP-2

5.3.2 Applied load values

The simulation investigates the influence of the following loads for samples A and B, as shown in Table 5-5:

Table 5-5: Loading values

| Load Case | Load Type | Load Value |
|-----------|---|-----------------------|
| 1. | Internal Pressure (IP) | 22.7 MPa |
| 2. | Compressive Force (CF) | 1747.79 kN |
| 3. | External Pressure (EP) | 11.7 MPa |
| 4. | Internal Pressure + Compressive Force (IP+CF) | 22.7 MPa + 1747.79 kN |
| 5. | Coefficient of Friction (CF) + Contact stiffness (CS) | 0.1 to 0.5 + 0.00001 |

5.3.2.1 Flexible Pipe Internal Pressure

The stress analyses were performed for Sample A blocked, and Sample B unblocked flexible pipe specimen under different pressure as detailed by the manufacturer include:

- Operating Pressure 22.7 MPa
- Design Pressure 27.6 MPa
- Factory Test Pressure 41.4 MPa
- Pressure Nominal Bursting 65.4 MPa

In each pressure case, the flexible pipe experienced an internal pressure as stated, without an external pressure in the models, which is assumed to be negligible since the pipe is in a static position. However, if it is dynamic, the hydrostatic pressure would have been considered along with the internal pressure.

The internal pressure condition is applied to the internal surface of the carcass layer, and the results under various internal pressures from 22.7 MPa to the Maximum 65.4 MPa while the two (2) ends and the blockage/plug was constrained in all directions. Therefore, the stresses on each layer show that the internal pressure transits from layer to layer, from internal to external layers through interaction contact. The pressure armour or zeta usually resists the load under internal pressure; however, the stress concentration is more in the carcass, followed by zeta and high strength tape. The concentration in the tensile wires and the external sheath are in the same range. The concentration of stress is much more in Sample A compared to Sample B. This implies that blockage/plug in the flexible pipe creates more stress in the layers. The stress distribution is at the maximum value on the carcass layer for both samples, as shown in Table 5-6, with 1926 MPa and 1844 MPa for Sample A and Sample B, respectively.

Table 5-6: Stress for Sample A and Sample B layers

| Internal Pressure | Frictionless, stiffness constant=0.00001 | |
|--------------------------|---|-----------------|
| | Sample A | Sample B |
| Load type | S (MPa) | S (MPa) |
| Carcass | 1926 | 1844 |
| Pressure Sheath | 0.889 | 0 |
| Zeta Pressure Armour | 128.8 | 0 |
| First Tensile | 0.682 | 0 |
| Second Tensile | 1.815 | 0 |
| High Strength Tape | 109.0 | 0 |
| External Sheath | 0.790 | 0 |

The stress and reaction force increase with the increase in the value of internal pressure from operating pressure to burst pressure. In this research, the operating pressure is considered the normal pipe behaviour that could only be experienced, verified, and validated under pressure ranges from 22.4-25.4 MPa, as shown in Figures 5-5 and 5-6.

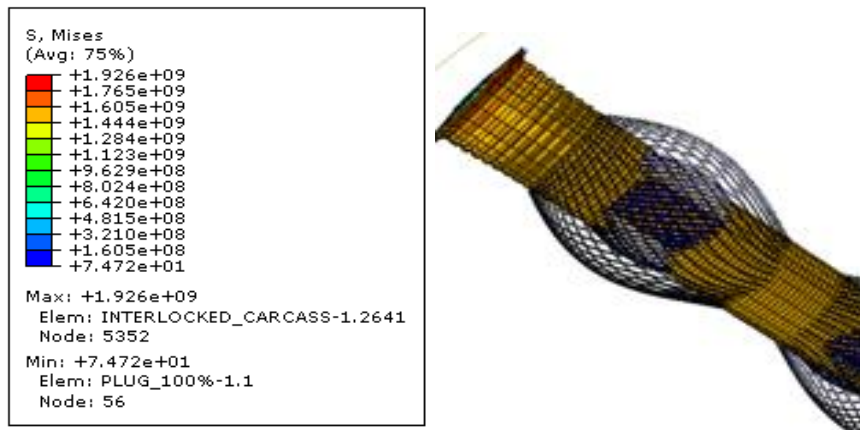


Figure 5-5: Stress Contours under Operating Conditions - 3D Model



Figure 5-6: Stress Contours under Factory Test Pressure from the end - 3D Model

The plug imparts more on the carcass of Sample A than Sample B. Hence, the analyses for both Samples A and B when modelled in solid (C3D8R) and shell (S4R) under the operating, design, and factory test conditions showed higher values of mises stress, reacting force, and hoop stress on the entire Sample A layers most especially the carcass and the tensile wires compared to Sample B layers. Importantly, there is no significant movement of the plug because the two ends were fixed and constrained to RP-1, but the relocation started with increased internal pressure.

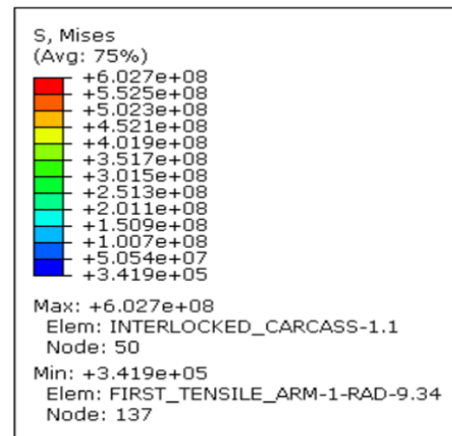
5.3.2.2 Damaging pull/Compressive in a straight line: ± 1747.79 kN

The load was applied to a reference point RF-1 at a free end of the flexible pipe while the other end was constrained in all directions. It is, however, observed that both Sample A and Sample B experienced the same

stress concentration and displacement except the reaction force that varied. It is higher in sample-A, as depicted in Table 5-7. The tensile wires are susceptible to both compressive and pulling forces. Still, it seems the blockage has no significant effect under compressive and pulling loads because the flexible pipe deformation and damages were similar when the force approaches the damaging pulling force of ± 1747.79 kN applied longitudinally along Y-axis inwardly and outwardly for compressive and pulling loads, respectively. The stress contours under damage pull and comprehensive forces are presented in Figures 5-7. The tension is mainly concentrated on the tensile wires being the layer to resist tension load. The deformation of the tensile wires looks like a birdcage that was formed in sample A.

Table 5-7: Hoop stress, Displacement and Reaction force for Sample A and Sample B layers

| Damaging pull/Compressive force (kN) | Frictionless, stiffness constant=0.00001 | | | | | |
|--------------------------------------|--|-----------------------|--------|--------------------------|-----------------------|--------|
| Reacting Force (kN) | 2198 | | | 1748 | | |
| | Sample-A | | | Sample-B | | |
| Load type | S _{mises} (MPa) | S ₂₂ (MPa) | U (mm) | S _{mises} (MPa) | S ₂₂ (MPa) | U (mm) |
| Carcass | 2315 | 1574 | 0.129 | 2206 | 1574 | 0.1035 |
| Pressure Sheath | 4.341 | 0.1435 | 0.127 | 3.452 | 0.114 | 0.1013 |
| Zeta Pressure Armour | 628.8 | *0.00271 | 0.1274 | 50 | *0.00215 | 0.1013 |
| First Tensile | 3.328 | 1.484 | 0.1275 | 2.647 | 1.180 | 0.1014 |
| Second Tensile | 8.861 | 0.410 | 0.1854 | 7.046 | 0.326 | 0.1474 |
| High Strength Tape | 532 | 27.89 | 0.1274 | 423.1 | 22.18 | 0.1013 |
| External Sheath | 3.857 | 0.288 | 0.1274 | 3.067 | 0.229 | 0.1013 |



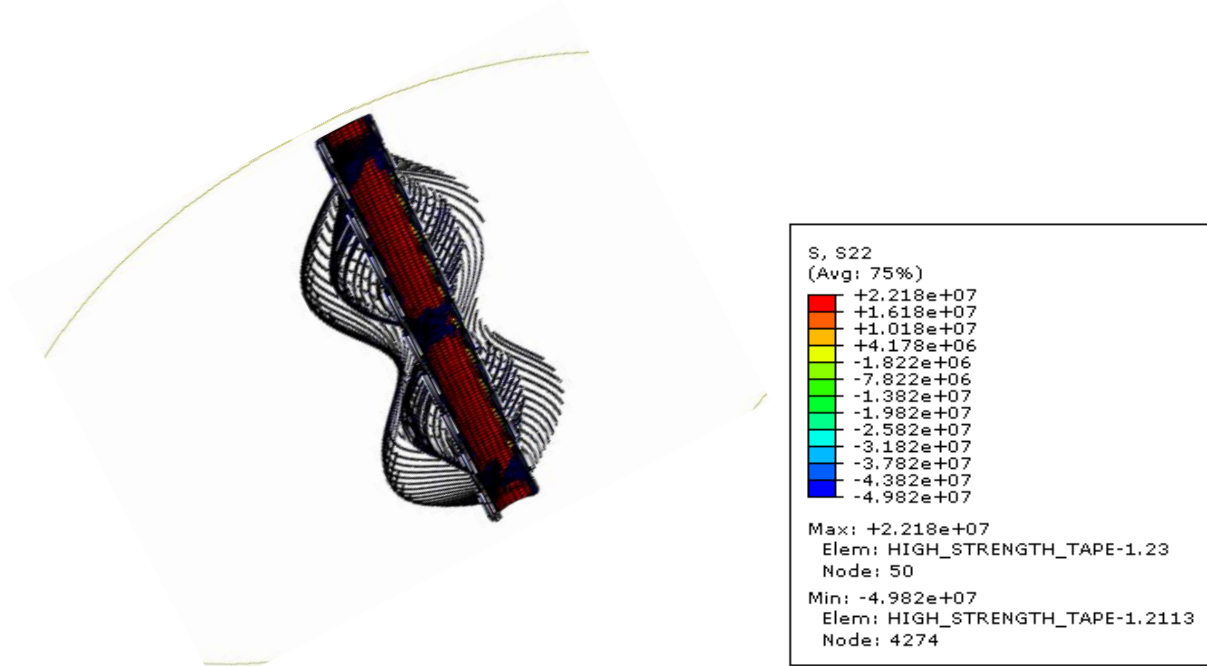


Figure 5-7: Stress contours under damage pull and comprehensive forces

5.3.2.3 Internal Pressure + Compressive Load

In this case, the combined load of internal pressure and compressive force from 22.7 to 65.4 MPa and 1747.79 kN were applied under the same conditions. The results were significant as they show a considerable difference as expected in sample A than sample B. The pressure given by the manufacturer was applied on the inner surface of the flexible carcass in addition to a 1747.79 kN concentrated load placed at the free end of the flexible pipe. In contrast, the bottom end and the blockage/plug were constrained in all directions, and the other end was free. The deformation of the pipe was greater than when only internal pressure was applied. Table 5-8 shows the overall results.

5.3.2.4 External Pressure:

The hydrostatic collapse pressure 11.7 MPa was applied, and both pipes' samples A and B were deformed similarly with the same stress concentration. This happens because the collapse pressure is higher than the normal hydrostatic pressure generally acting on the pipe due to environmental factor which is given as:

$$P = \rho gh \quad \text{Equation 5-1}$$

$$P = 1000 \times 9.81 \times 590$$

$$P = 5.8 \text{ MPa}$$

where h is the water depth, ρ is density, and g represents the gravitational constant y

The external pressure, 11.7 MPa, acting on the outer sheath layer, created deformation in the pipe. It is observed that the application of external pressure caused a similar deformation in both sample A and sample B with the same displacement values and stress concentration. This means that the external pressure transmits from the outer structure to the internal structure layer by layer through contact. Still, the presence of a plugin in the pipe does not generate any significant effect. Table 5-8 shows the external pressure with frictionless based on the stiffness constant of 0.00001, with resulting misse stress, hoop stress, and displacement for Sample A and Sample B layers.

**Table 5-8: Hoop stress, Displacement and Reaction force for Sample A and Sample B layers
Frictionless when coefficient of friction (μ) =0 and for μ =0.1-0.5, stiffness constant=0.00001**

| Load type | Sample A | | | Sample B | | |
|----------------------|--------------------------|-----------------------|--------|--------------------------|-----------------------|--------|
| | S _{mises} (MPa) | S ₂₂ (MPa) | U (mm) | S _{mises} (MPa) | S ₂₂ (MPa) | U (mm) |
| Carcass | 0.1027 | *8.56e-4 | 1.726 | 0.1027 | *8.56e-4 | 1.726 |
| Pressure Sheath | 0.5884 | 0.1532 | 1.726 | 0.5884 | 0.1532 | 1.726 |
| Zeta Pressure Armour | 85.23 | *3.67e-4 | 1.726 | 85.23 | *3.67e-4 | 1.726 |
| First Tensile | 0.451 | 0.161 | 1.728 | 0.451 | 0.161 | 1.728 |
| Second Tensile | 1.20 | 0.208 | 2.513 | 1.20 | 0.208 | 2.513 |
| High Strength Tape | 72.11 | 8.493 | 1.726 | 72.11 | 8.493 | 1.726 |
| External Sheath | 245.9 | -15.29 | 0.380 | 245.9 | -15.29 | 0.380 |

The stress concentration and reaction forces decrease as the coefficient of friction increases while the stiffness constant remains the same value.

5.3.2.5 Co-efficient of Friction

The coefficient of friction for the interaction and surface contact was varied from 0.1 to 0.5, and the contact stiffness was kept constant throughout the simulation. The results obtained showed that the higher the coefficient of friction, the lower the stress concentration or, the lower the coefficient of friction, the higher the stress when the coefficient of friction μ =0.5, the stress values obtained for Sample A is higher than sample B and same applicable to displacement and reaction force, which were due to the hydrate presence.

The values obtained for sample A is higher than sample B for stress, displacement, and reaction force due to the hydrate being blocked for all the load conditions.

5.4 Blockage Simulation

Hydrate blockage ranges from diameters 0.1 to 1 m length were introduced into sample B and simulated with tangential behaviour, penalty, and normal behaviour of stiffness constant 10^{-5} . The results show a significant decrease in the displacement and high-stress concentration in all directions in the flexible pipe.

The impact of the blockage/plugin reflected more in the values of mises stress, reacting force, and hoop stress on the entire structure, especially the carcass and the tensile wires. The plug is constrained at point RP-1 with

the other two sides fixed, so there is no significant movement. The relocation vis-à-vis movement started with an increase in internal pressure. Table 5-9 shows the applied plug parameters.

Table 5-9: Simulated Blockage (Plug) Sizes

| Length (m) | Inner diameter (mm) |
|------------|---------------------|
| 0.1 | 0.00762 |
| 0.5 | 0.0381 |
| 1.0 | 0.0762 |

5.5 Conclusion

The numerical models detailed in Chapter 3 have been simulated using the available data. The models have been subjected to various load conditions and defined boundary factors as prescribed by the real-world physical condition. The results obtained from the non-bonded flexible pipe samples A and B showed a general effect of blockage on the flexible pipe, which no research has mentioned. While sample A is blocked pipe, sample B is unblocked pipe, and the results obtained varied significantly along the length and the wall thickness of the two samples, as shown in Figure 5-8 for the reaction force and displacement. The concentration of stress is much more in Sample A compared to Sample B. The presence of blockage/plug in the flexible pipe creates more stress in the layers. The stress and reaction force increased with an increase in the internal pressure from operating pressure to burst pressure. The operating pressure is considered the pipe normal behaviour and could only be experienced, verified, and validated under pressure ranges from 22.4-25.4 MPa. The stress distribution along the length of the pipe and the wall thickness showed higher values in Sample A than in Sample B. However, it is noted that the plug absorbs part of the stress in Sample A. The pipe ruptured mainly due to the block trying to adjust the stress level. In addition, the coefficient of friction impacts significantly on sample A, compared to sample B for stress, displacement, and reaction force due to the hydrate being blocked. The lower the coefficient of friction, the higher the stress values. This shows that the pipe responds to the coefficient of friction. The summary is presented in Table 5-10.

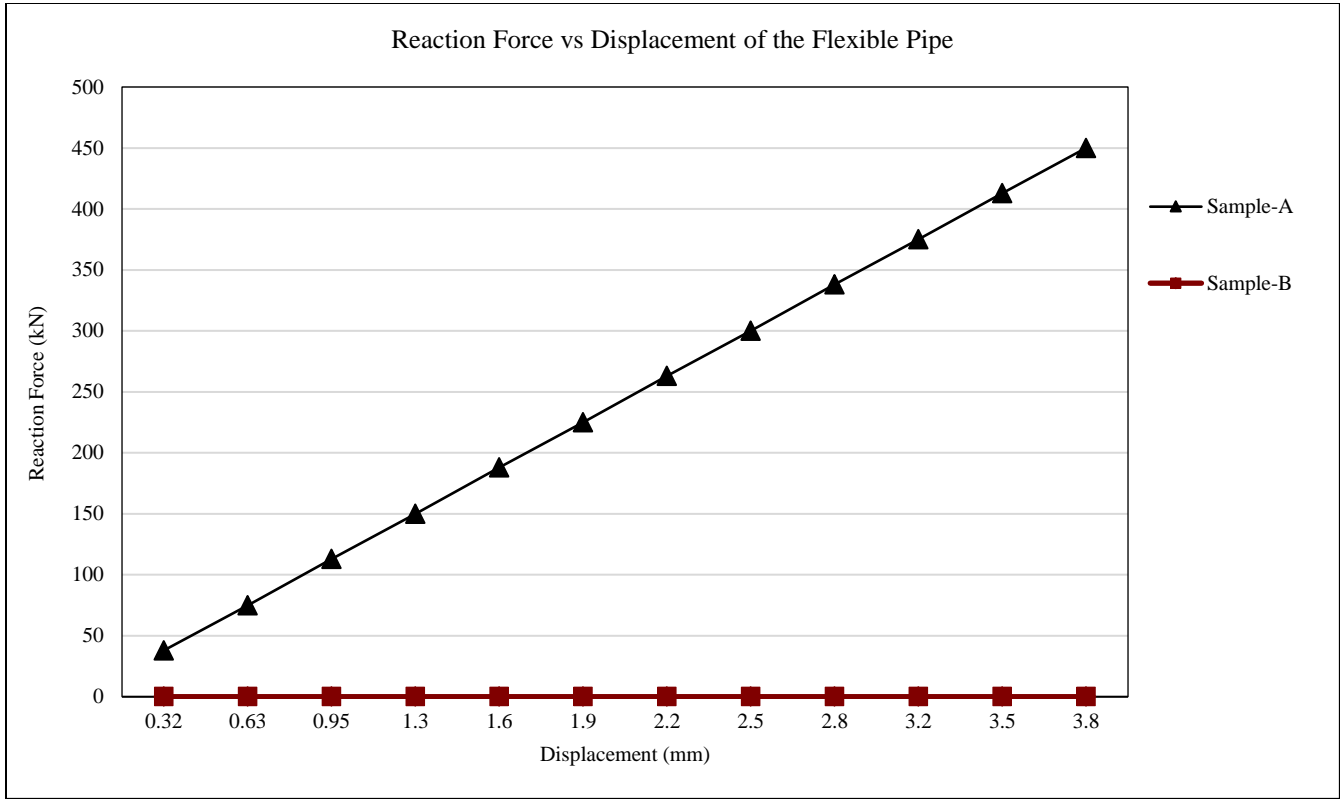


Figure 5-8: Reaction Force and Displacement in Samples A and B

Table 5-10: Numerical stress values under various load conditions-Designed and Experimental

| Layers | SAMPLE A | | | | | SAMPLE B | | | |
|-----------------------|-----------|--------------------|-------|------|--------------------|----------|------|------|-------|
| | UTS (MPa) | Stress Mises (MPa) | | | Stress Mises (MPa) | | | | |
| | | Designed | Exp | IP | CF+IP | EP | Exp | IP | CF+IP |
| Carcass | 550 | 860.7 | 1926 | 2315 | 0.103 | 853.7 | 1844 | 2206 | 0.103 |
| Pressure Sheath | *48 | 56.3 | 0.029 | 4.34 | 0.588 | 52.7 | - | 3.45 | 0.588 |
| Zeta-Pressure Armour | 1000 | 1036.5 | - | 628 | 85.23 | 1032.0 | - | 50 | 85.23 |
| First Tensile Armour | 1400 | 1537.3 | 0.304 | 3.33 | 0.451 | 1541.5 | - | 2.65 | 0.451 |
| Second Tensile Armour | 1400 | 1545.8 | 0.084 | 8.86 | 1.20 | 1534.8 | - | 7.05 | 1.20 |
| High Tensile Strength | *3400 | 476.3 | 5.714 | 532 | 72.11 | 510.3 | - | 423 | 72.11 |
| External Sheath | *34 | 32.7 | 0.059 | 3.86 | 245.9 | 32.9 | - | 3.07 | 245.9 |

* Source from the internet; Abbreviation: Exp- Experiment, Num- Numerical; IP-Internal Pressure, CF-Compressive Force, EP- External Pressure.

CHAPTER 6: RESULTS AND DISCUSSIONS

6.1 Results

This chapter presents the overall research results of a model 6” 7 layers non-bonded flexible pipe. The flexible pipe was designed to the specification of a case study sample, modelled, and investigated under two (2) scenarios, namely damaged pipes, pipe with blockage (Sample A) and undamaged pipe, intact (Sample B). Experimental and numerical investigations using ABAQUS were performed on the two samples, A and B, to confirm the behaviours of the samples under different load conditions. Hence, the outcomes from the studies were compared. It was essential to state that the experimental results described in chapter 4 used in this research were carried out at two locations on the main flexible pipe retrieved from the deepwater Gulf of Guinea. It was in use for a long time, damaged, and eventually used replaced. This is with full participation, while the results were not published but submitted for review. However, a separate sample of flexible pipe retrieved from North Sea deepwater available for analysis was also investigated, the result obtained and formed part of this research work. Numerical analysis was carried out to demonstrate the accuracy and computational suitability of the results and the experimental investigation. A numerical study was carried out as described in Chapter 5. Comparisons were made between the results obtained for samples A and B; however, there are scenarios where computational analyses were used to validate the obtained results mainly for stress and reacting force. The stress analysis was performed on the hydrate blocked flexible pipe specimens detailed under the experimental investigation and supplied by the manufacturer [5]. In addition to the experimental results, the numerical analysis confirmed those failure modes that had led to the rupture of the flexible pipe are investigated. The concentration of stress in the layers, mainly the two tensile wires, are critically studied while applying the loads, such as the internal pressure to the inner surface of the carcass and on the hydrate plug. The same compressive force and external pressure were applied at the reference point RP-1 for force and on the outer sheath for external hydrostatic pressure.

Concisely, the analyses show that the layers of the flexible pipe under investigation, especially the tensile wires are susceptible to the applied loads. The response of the pipe to the subjected loads shows significant deformation, which indicates the presence of a plug in the pipe triggers the failure modes stated by API [1]. The results from hydrate blocked and unblocked flexible pipe, sample A and sample B, respectively, are presented therein based on the load conditions. The numerical investigation confirmed the real behaviour of the flexible pipe under certain conditions and response to anomalies in the pipe during depressurisation and pressurization processes. The response of the pipe to the load shows a significant deformation which indicates the presence of the plug in the pipe triggers the failure modes stated in API 17B [1].

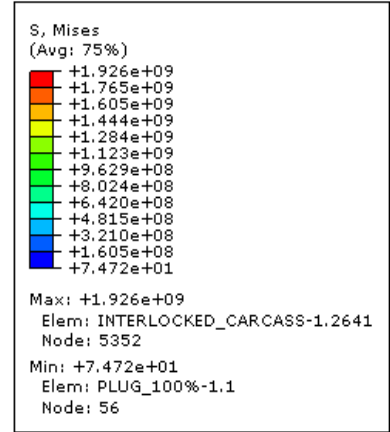
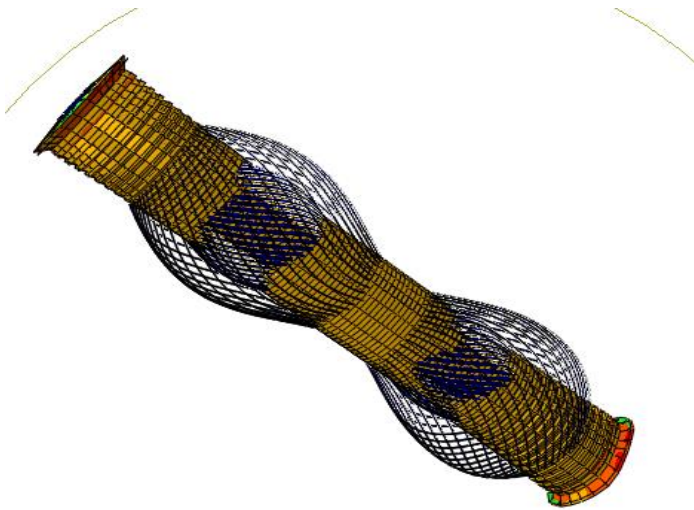
6.2 Numerical investigation Results Analysis

The results are analysed for von-mises stress, hoop stress, displacement, reaction force and other stress components (MPa) for various load cases applied to the flexible pipe.

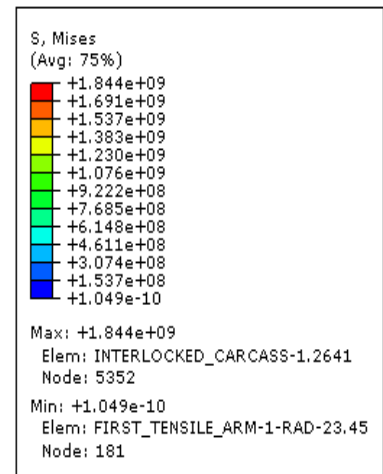
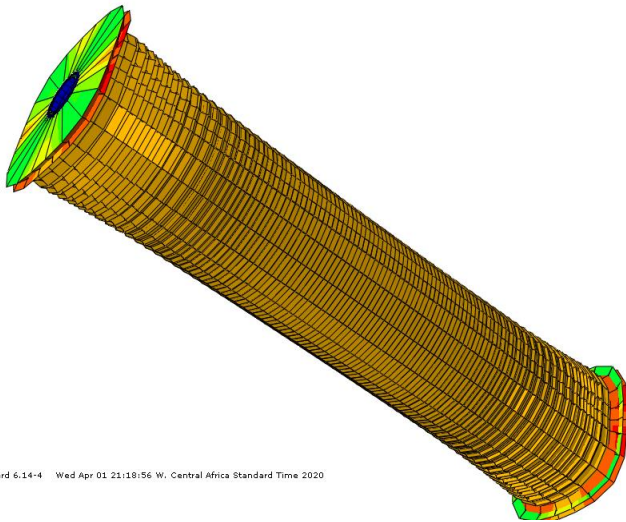
6.2.1 Load case 1: Internal Pressure

A load of 22.7 MPa is applied on the inner surface of the carcass, and the hydrate plug of about 1 m long. However, the deformation of the hydrate blocked flexible pipe Sample A was conspicuous. The first tensile wire was twisted at the middle, and the ends, the deformation at the two points of the first tensile wire resembles a birdcage that is ready to burst. The second tensile wire looks like a balloon ready to burst and compares the first tensile wire deformation shown in Figures 6-1 (b, g and h).

The maximum stress distribution on each layer, S_{mises} and S_{22} , are recorded, where 1930 MPa and 1840 MPa are the maximum stress on Sample A and Sample B while the maximum displacements stand at 3.798 mm and 2.028 mm, respectively. The displacement values represent 0.14% and 0.07% of the original flexible pipe, and sample A is about 1.77 mm deformed more than sample B. Further information about the stress and displacement on the individual layer are shown in Tables 6-1 and 6-2. It is good to see that Sample B values of stresses and displacement reflect good results that indicate a good condition of a pipe under operating pressure. Hence, the measured values of Sample B are negligible, as shown in Figures 6-1 and 6-2.

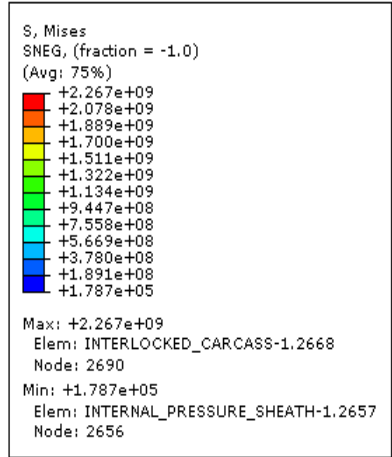
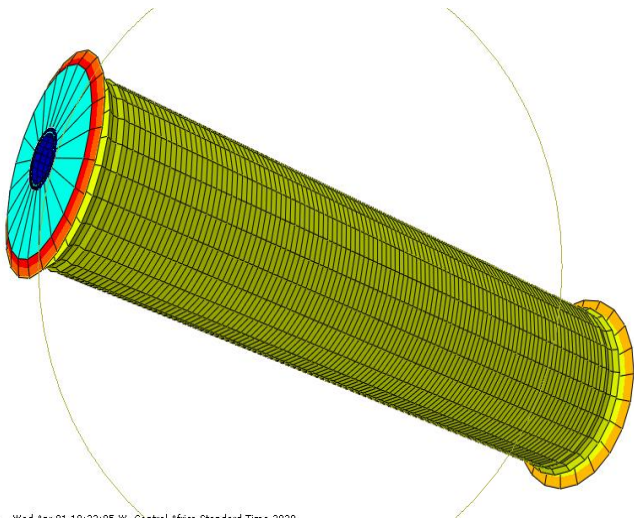


(a) Solid

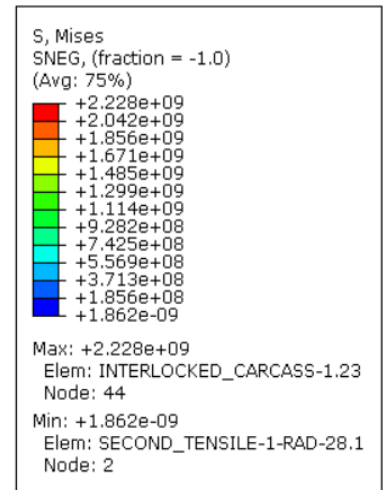
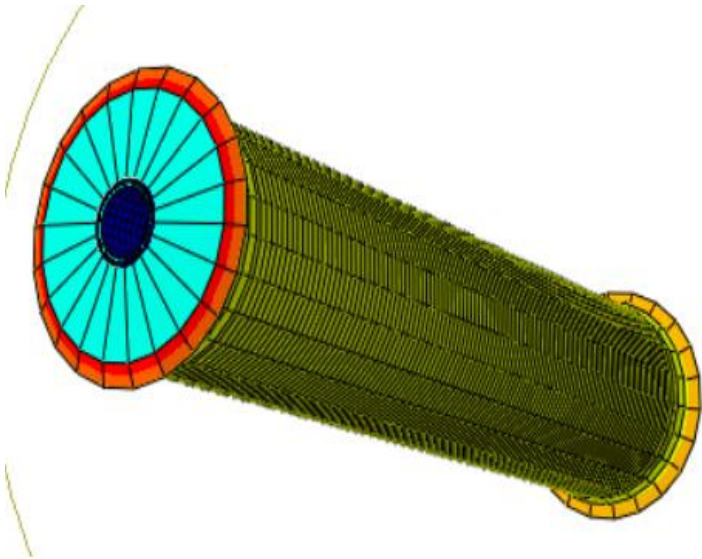


(b) Solid

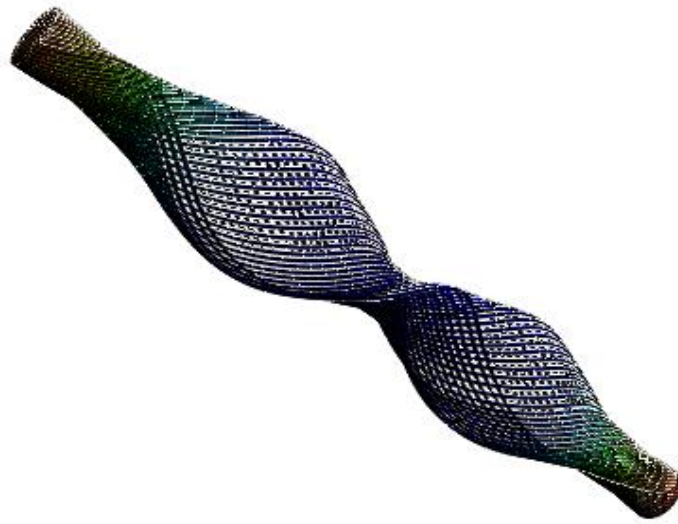
andard 6.14-4 Wed Apr 01 21:19:56 W. Central Africa Standard Time 2020



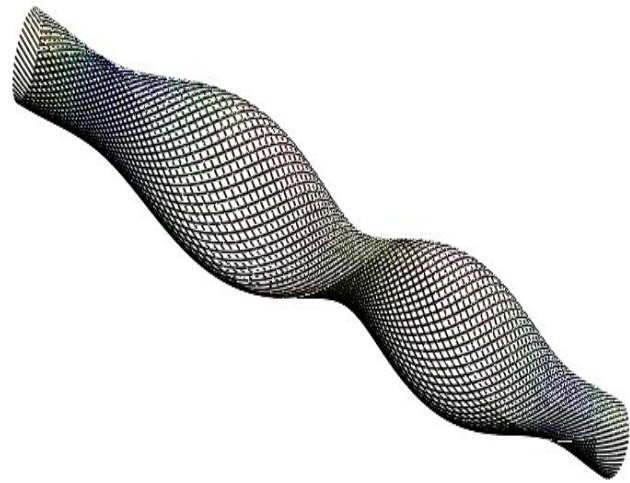
(c) Shell



(d) Shell

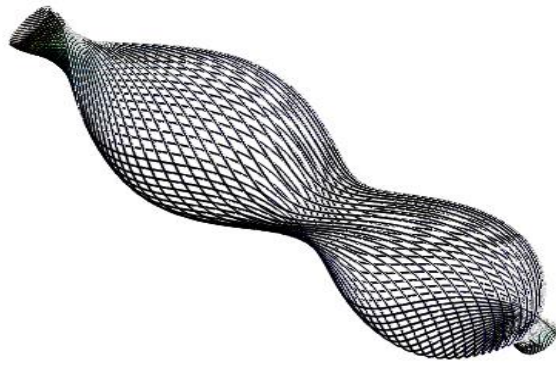


Solid

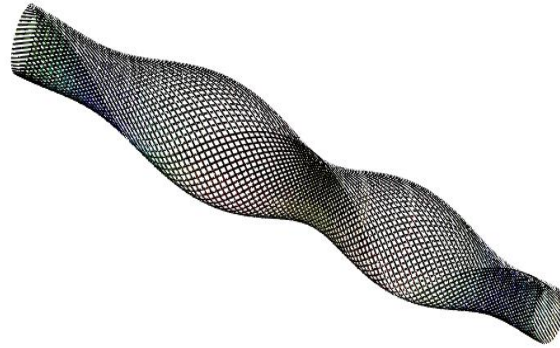


Shell

(e) First Tensile for blocked



Solid



Shell

(f) Second Tensile for unblocked



Solid



Shell



Solid



Shell

(g) First Tensile for blocked

(h) Second Tensile for unblocked

Figure 6-1: Pipe deformations-blocked (a), (c), (e) & (g); unblocked layers; (b), (d), (f) &(h)



Figure 6-2: Pipe Understudy-Similar deformation with Sample A and B [5]

Table 6-1: Hoop stress and the Reaction force



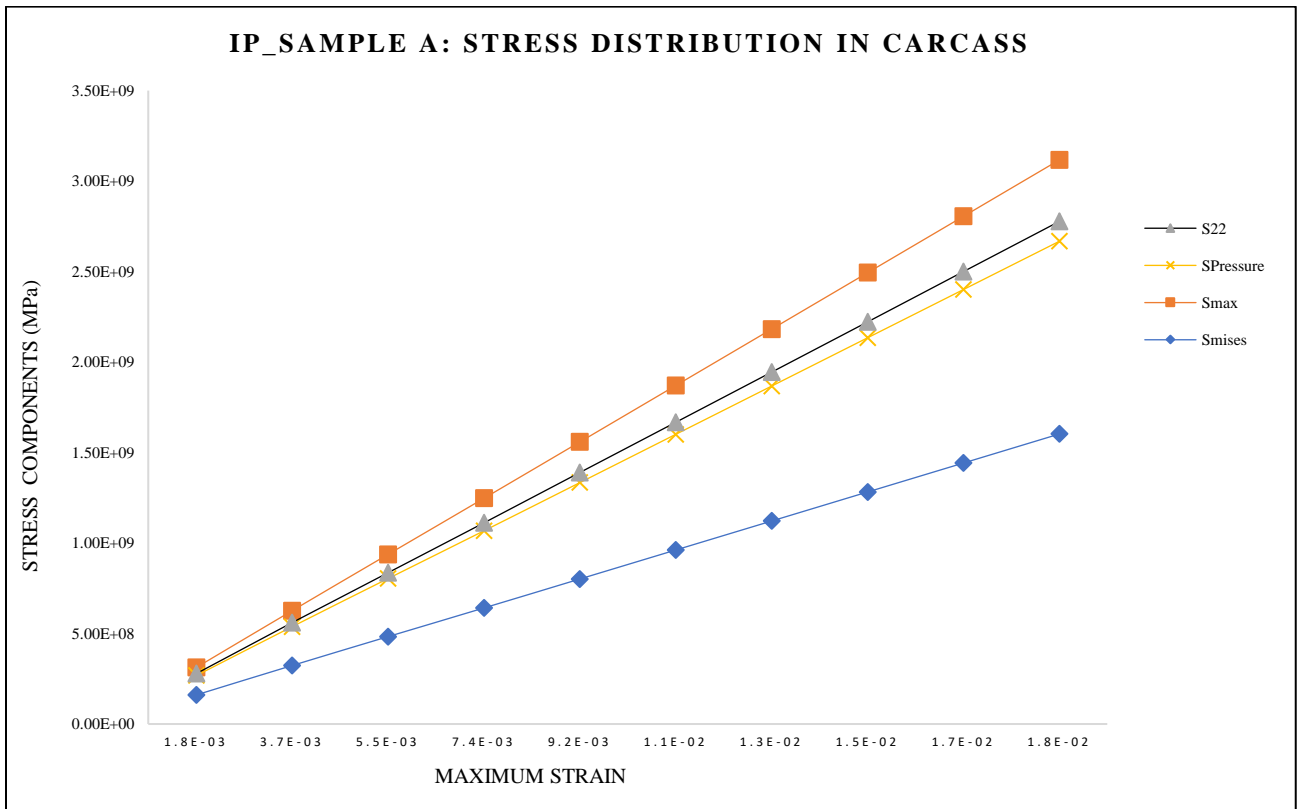
| Sample A | | Sample B | | | |
|---|--|--|---|---|--|
|  | <p>S, S22 (Avg: 75%)</p> <ul style="list-style-type: none"> +1.574e+09 +1.445e+09 +1.316e+09 +1.188e+09 +1.059e+09 +9.304e+08 +8.017e+08 +6.731e+08 +5.444e+08 +4.158e+08 +2.871e+08 +1.585e+08 +2.982e+07 <p>Max: +1.574e+09 Elem: INTERLOCKED_CARASS-1.2619 Node: 5286</p> <p>Min: +2.982e+07 Elem: INTERLOCKED_CARASS-1.5 Node: 26</p> | <p>RF, Magnitude</p> <ul style="list-style-type: none"> +4.502e+05 +4.127e+05 +3.752e+05 +3.377e+05 +3.002e+05 +2.626e+05 +2.251e+05 +1.876e+05 +1.501e+05 +1.126e+05 +7.504e+04 +3.752e+04 +0.000e+00 <p>Max: +4.502e+05 Node: ASSEMBLY.2</p> <p>Min: +0.000e+00 Node: EXTERNAL_SHEATH-1.1</p> |  | <p>S, S22 (Avg: 75%)</p> <ul style="list-style-type: none"> +1.574e+09 +1.442e+09 +1.311e+09 +1.180e+09 +1.049e+09 +9.179e+08 +7.868e+08 +6.557e+08 +5.245e+08 +3.934e+08 +2.623e+08 +1.311e+08 -7.442e-07 <p>Max: +1.574e+09 Elem: INTERLOCKED_CARASS-1.2619 Node: 5286</p> <p>Min: -7.442e-07 Elem: HIGH_STRENGTH_TAPE-1.2 Node: 5</p> | <p>RF, Magnitude</p> <ul style="list-style-type: none"> +1.113e-09 +1.020e-09 +9.277e-10 +8.349e-10 +7.422e-10 +6.494e-10 +5.566e-10 +4.638e-10 +3.711e-10 +2.783e-10 +1.855e-10 +9.277e-11 +0.000e+00 <p>Max: +1.113e-09 Node: ASSEMBLY.2</p> <p>Min: +0.000e+00 Node: EXTERNAL_SHEATH-1.1</p> |

Table 6-2: Mises's stress, Hoop stress and Displacement for Sample A and Sample B layers

| Internal Pressure | Frictionless, stiffness constant=0.00001 | | | | | |
|----------------------|--|-----------------------|--------|--------------------------|-----------------------|--------|
| | Sample A | | | Sample B | | |
| Load type | S _{mises} (MPa) | S ₂₂ (MPa) | U (mm) | S _{mises} (MPa) | S ₂₂ (MPa) | U (mm) |
| Carcass | 1926 | 1574 | 3.373 | 1844 | 1574 | 2.028 |
| Pressure Sheath | 0.889 | 0.029 | 2.609 | 0 | 0 | 0 |
| Zeta Pressure Armour | 128.8 | 0 | 2.609 | 0 | 0 | 0 |
| First Tensile | 0.682 | 0.304 | 2.612 | 0 | 0 | 0 |
| Second Tensile | 1.815 | 0.084 | 3.798 | 0 | 0 | 0 |
| High Strength Tape | 109.0 | 5.714 | 2.609 | 0 | 0 | 0 |
| External Sheath | 0.790 | 0.059 | 2.609 | 0 | 0 | 0 |

The linearity in Sample A indicates an inconsistency in the behaviour of the flexible pipe layers, such that the stress built up to the peak values when internal pressure (IP) is applied. This affected the pipe functionality and led to eventual failure mode as recommended in [1]. However, the sinusoidal behaviour (stress/strain distribution) in Sample B denotes the normal functionality under operating conditions. Except for the carcass layer with the same behaviour in samples A and B. Figure 6-3 shows the behaviour of the carcass when internal pressure is applied; the plot looks similar because the pressure was directly applied to the inner surface of the carcass. However, the measured values differ, with some values being negligible, making their zeros. Other layers show a significant change in the behaviour, as shown in Figures 6-4 to 6-6.



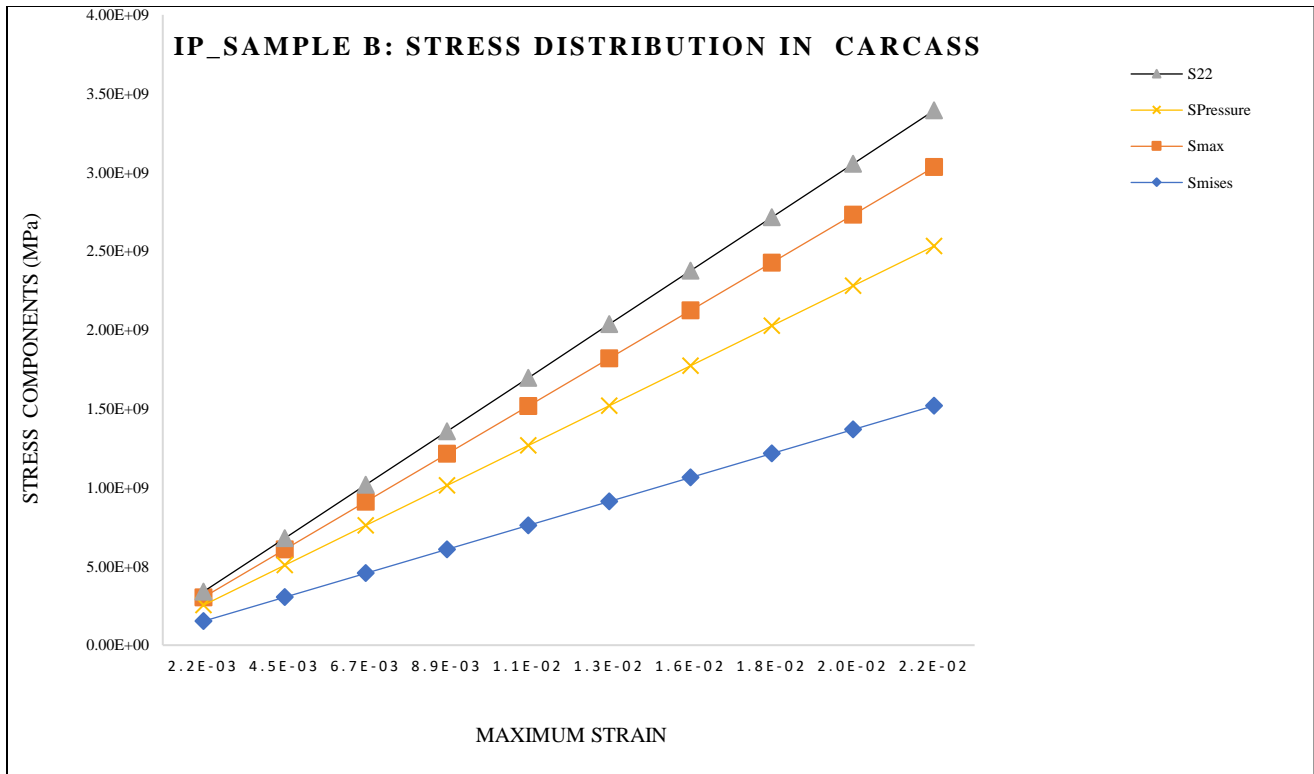
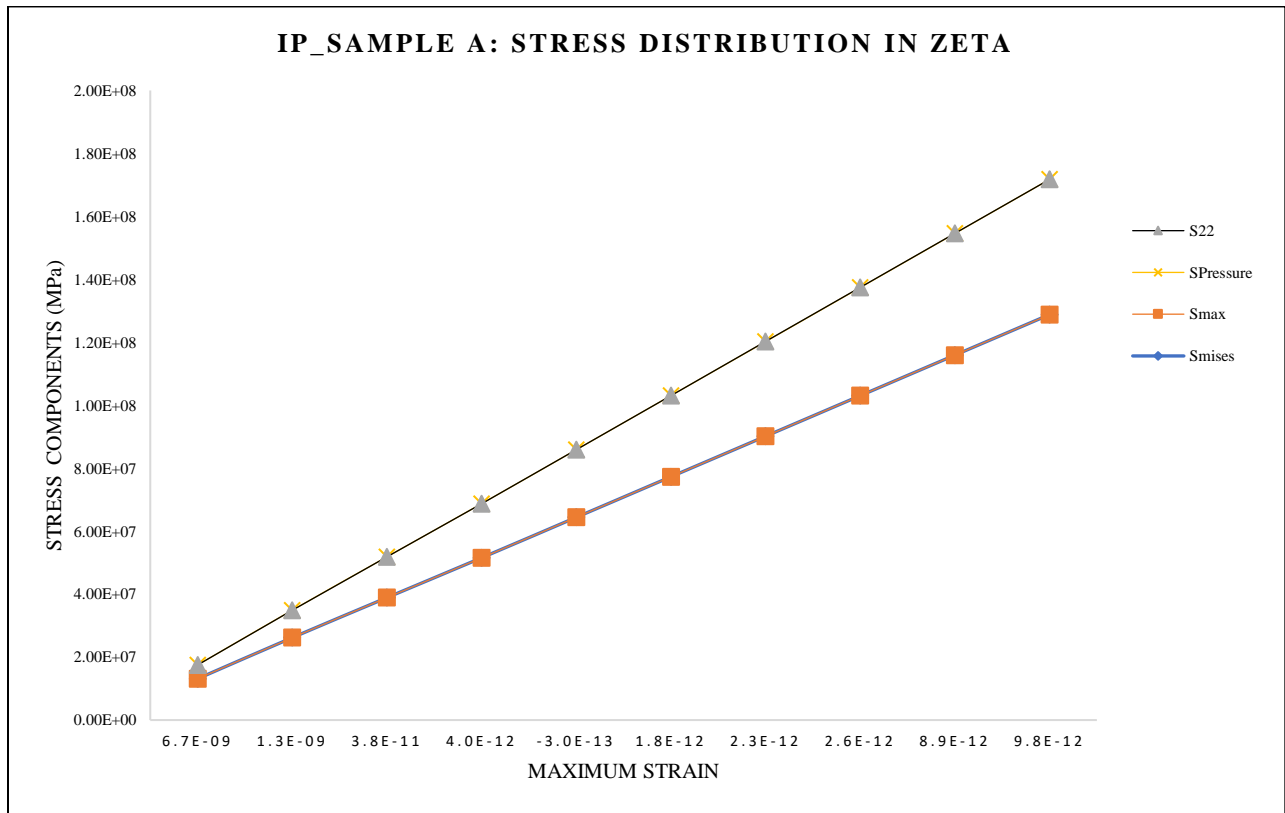


Figure 6-3: Samples A and B: Stress Distribution in Carcass layer



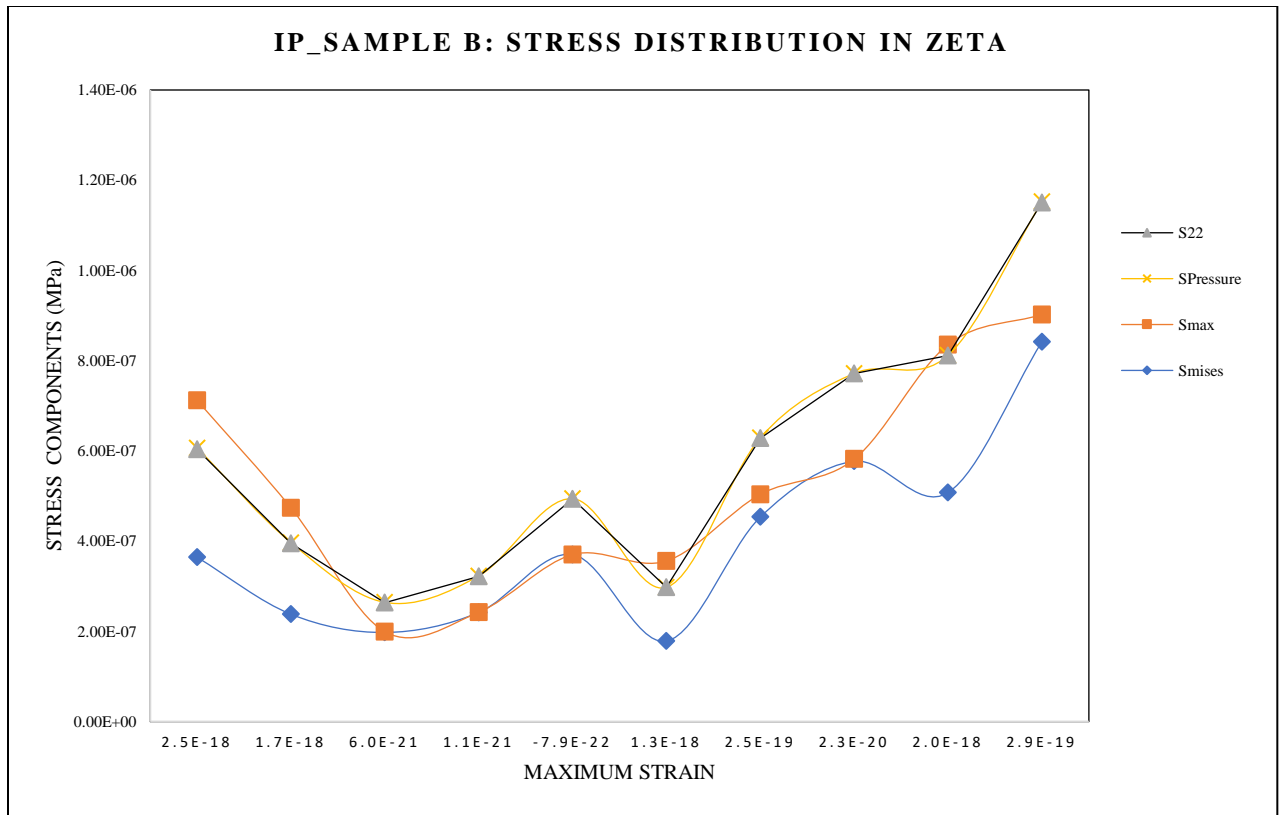


Figure 6-4: Samples A and B: Stress Distribution in Zeta layer

The behaviour of Zeta/Pressure armour varied significantly for sample A and sample B when applied the internal pressure. It is noted that the zeta layer has the functionality to protect the pipe from the effects of internal pressure, as shown in Figures 6-4, where the same behaviour is noted in the other layers in Figures 6-5 to 6-6.

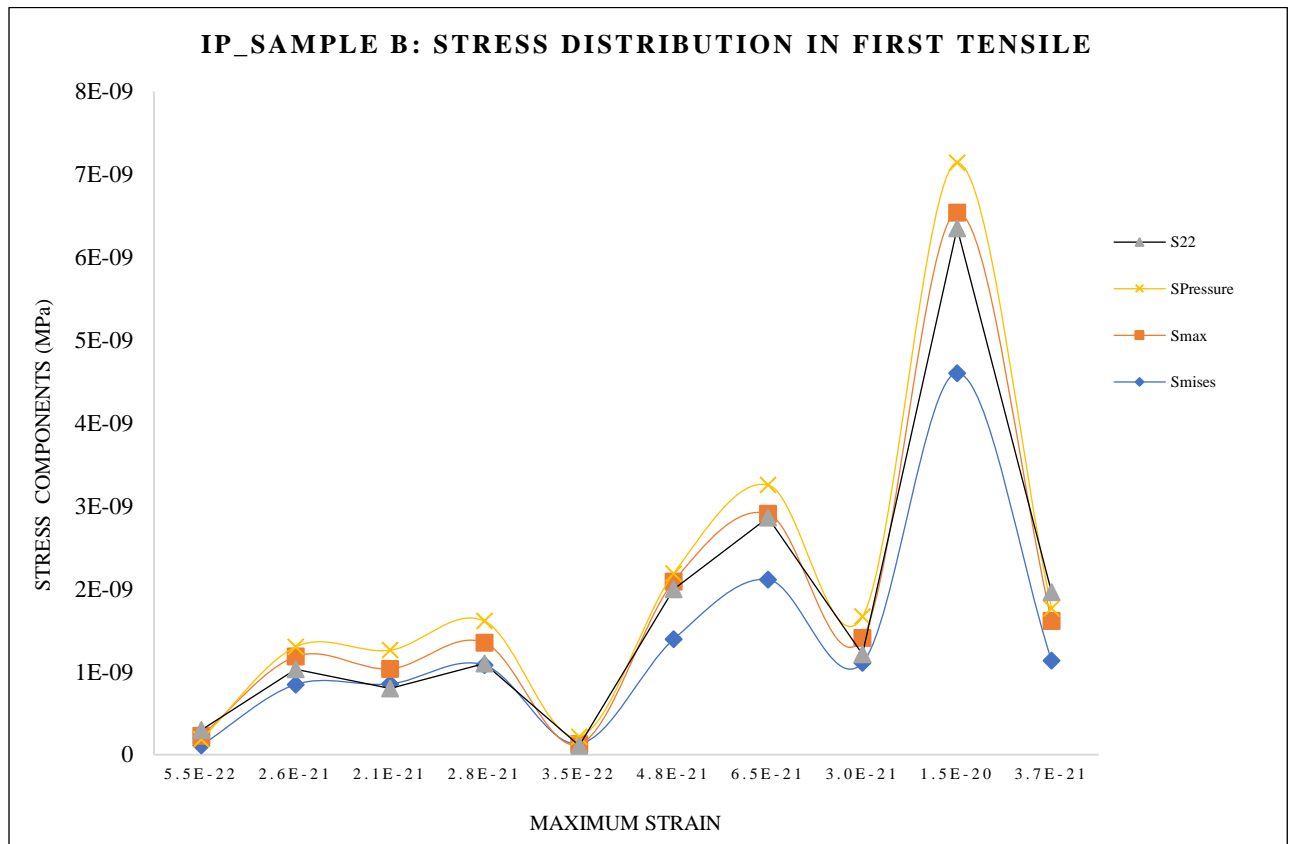
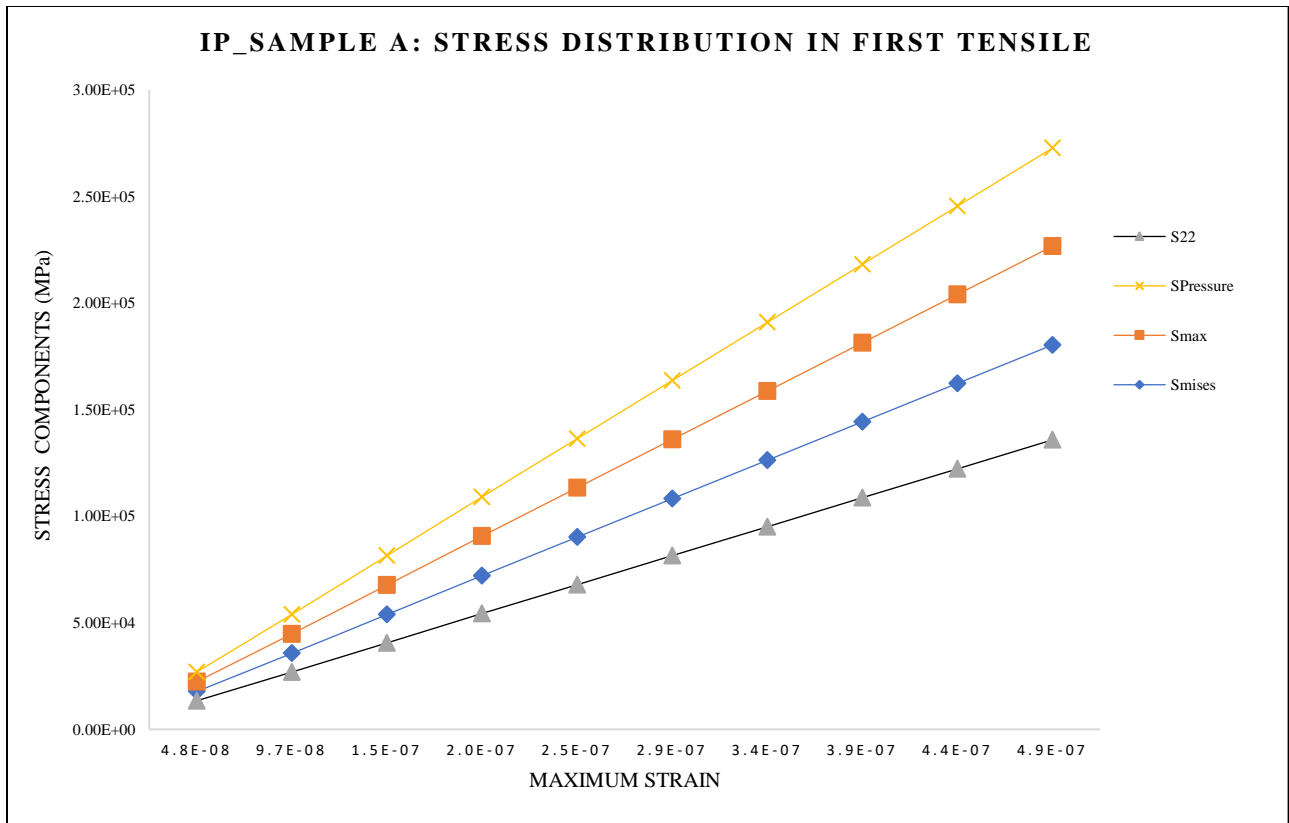


Figure 6-5: Sample A and B: Stress Distribution in First Tensile Wire layer

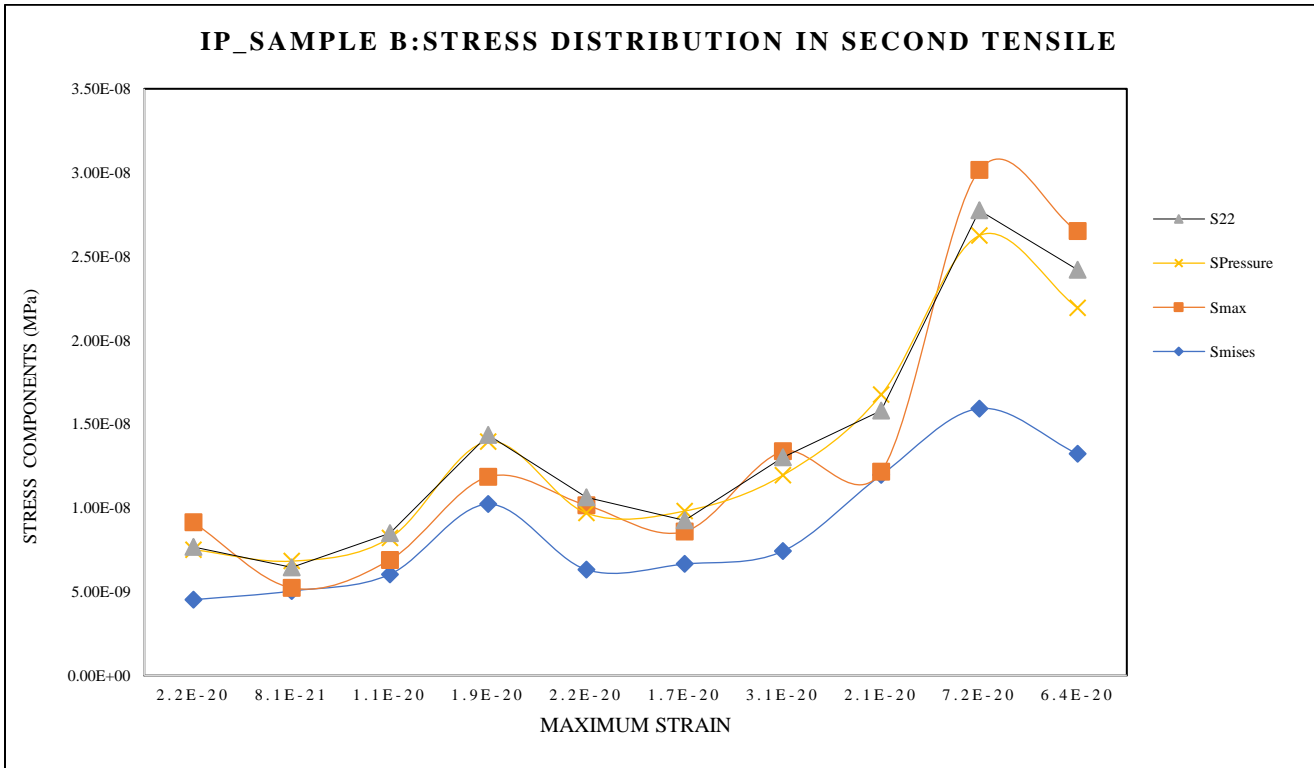
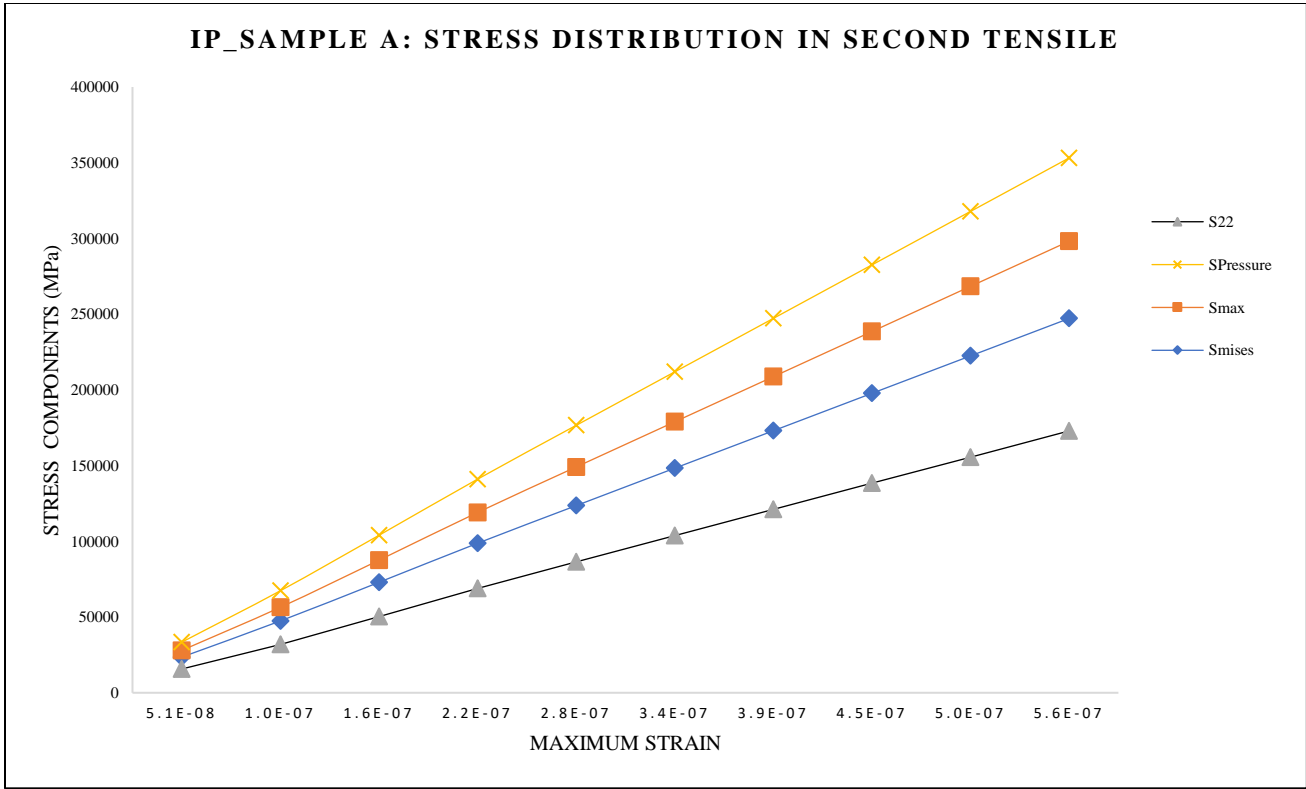


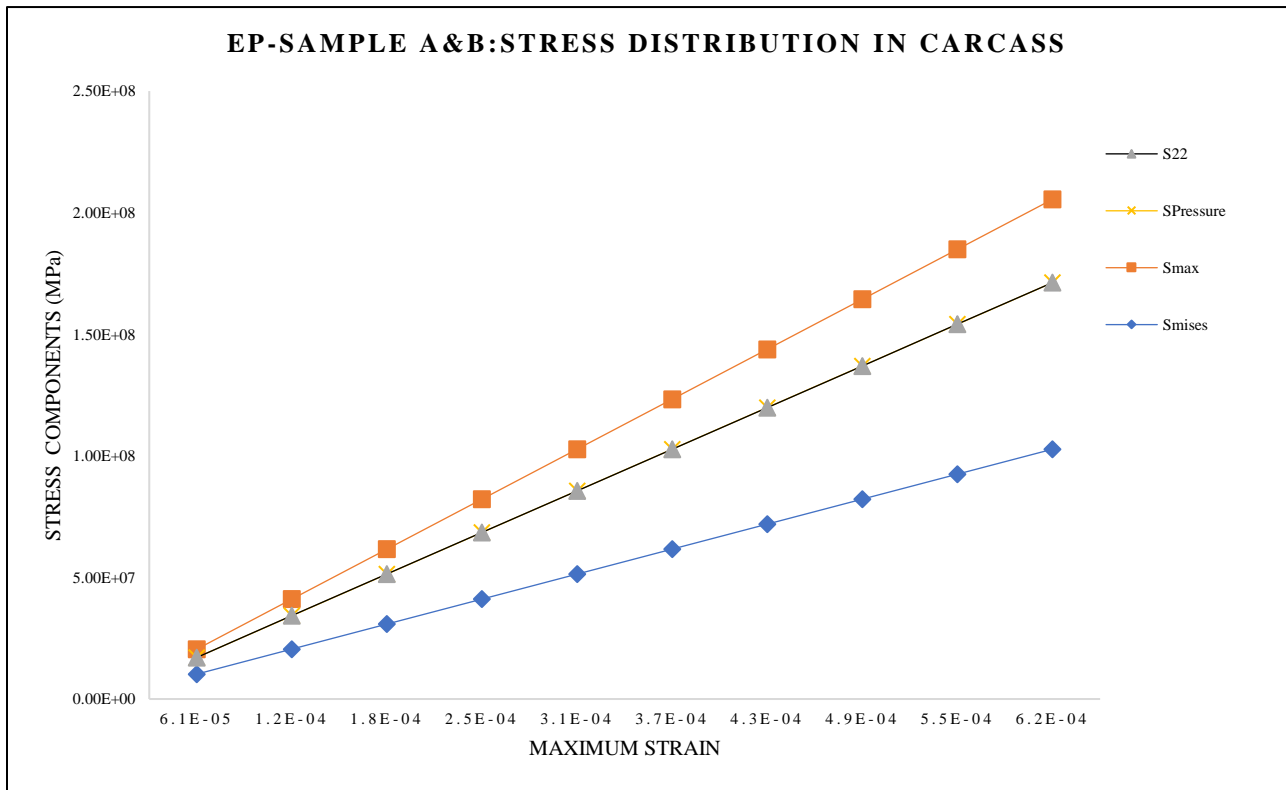
Figure 6-6: Sample A and B: Stress Distribution in Second Tensile Wire layer

6.2.2 Load case 2: External Pressure

There is no observable difference in the stress and deformation on the individual layer when external pressure 11.7 MPa is applied on the external sheath of the flexible pipe. This clearly shows that external pressure has the same effect on the flexible pipe being hydrate blocked or not; the results are only shown on the blocked pipe when it is combined with other loads. The maximum stress distribution on each layer, S_{mises} and S_{22} , are shown in Table 6-3, where 246 MPa on the external sheath and 8.49 MPa on high strength tape are the maximum mises stress and hoop stress, respectively. The stress and strain behaviour of the carcass is shown in Figure 6-7, with Samples A and B behaviour looking similar except for S_{22} .

Table 6-3: Hoop stress, Displacement and Reaction force for Sample A and Sample B layers

| | Frictionless, stiffness constant=0.00001 | | | | | |
|----------------------|--|----------------|--------|-------------------|----------------|--------|
| | Sample-A | | | Sample-B | | |
| Load type | S_{mises} (MPa) | S_{22} (MPa) | U (mm) | S_{mises} (MPa) | S_{22} (MPa) | U (mm) |
| Carcass | 0.1027 | 0 | 1.726 | 0.1027 | 0 | 1.726 |
| Pressure Sheath | 0.5884 | 0.1532 | 1.726 | 0.5884 | 0.1532 | 1.726 |
| Zeta Pressure Armour | 85.23 | 0 | 1.726 | 85.23 | 0 | 1.726 |
| First Tensile | 0.451 | 0.161 | 1.728 | 0.451 | 0.161 | 1.728 |
| Second Tensile | 1.20 | 0.208 | 2.513 | 1.20 | 0.208 | 2.513 |
| High Strength Tape | 72.11 | 8.493 | 1.726 | 72.11 | 8.493 | 1.726 |
| External Sheath | 245.9 | 0 | 0.380 | 245.9 | 0 | 0.380 |



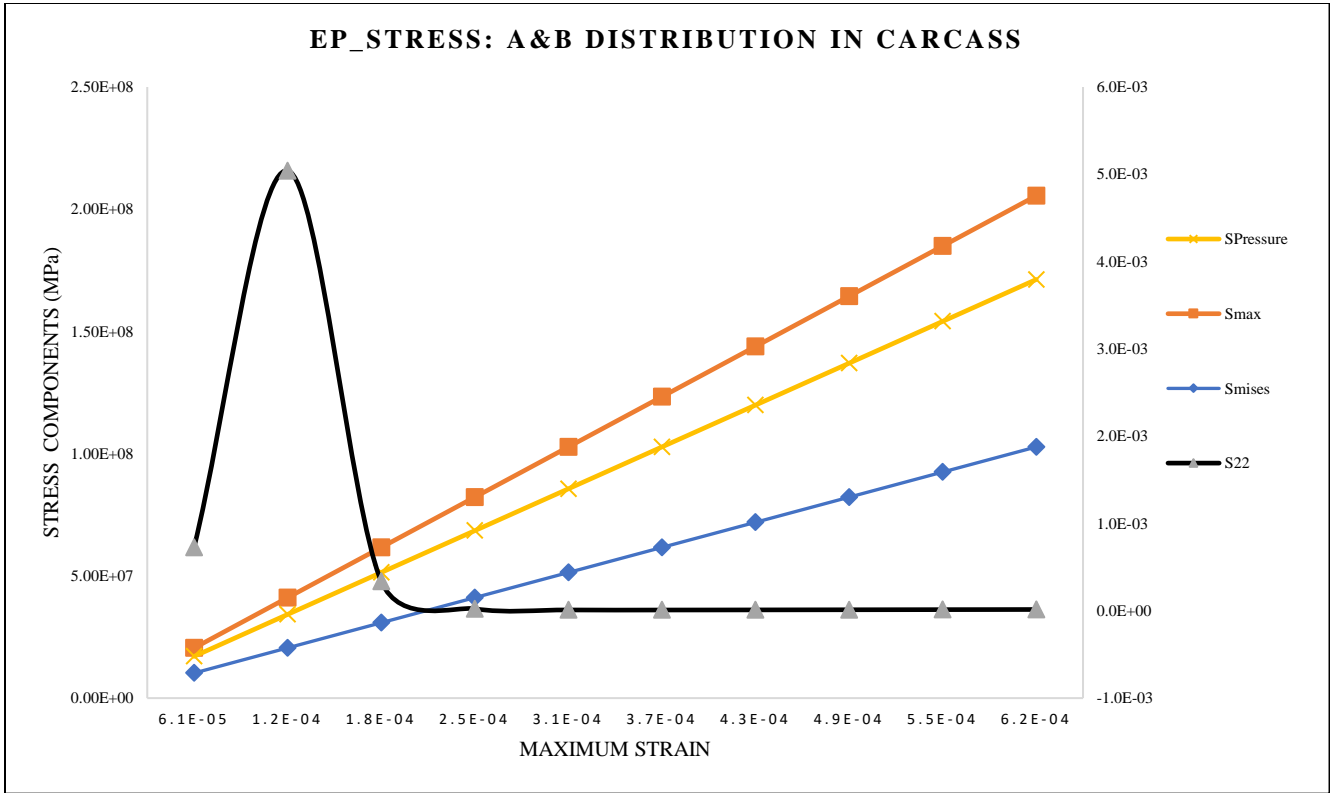


Figure 6-7: Samples A and Sample B: Stress Distribution-Carcass/External Pressure (EP)

6.2.3 Load case 3: Internal Pressure and Compressive Force

22.7 MPa internal pressure was applied to the inner surface of the carcass, and a 1m long hydrate plug, a 1747.79 kN compressive load, was simultaneously applied to the reference point RP-1. However, the deformation in Sample A, a hydrate blocked flexible pipe, was higher than expected. The first tensile wire was twisted at the middle, and the ends narrowed in diameters; the deformation at the two points of the first tensile wire resembled a birdcage that is ready to burst. The second tensile wire looks like a balloon ready to burst and resembles the first tensile wire deformation presented in Figures 6-8. The reacting force is 25.76% greater than the applied tension value, which shows that the hydrate blockage created much more load in the pipe, resulting in its deformation. The average deformation of 0.1852 mm, approximately 0.66% of the original length, is due to the higher value of the hoop stress, which was earlier confirmed by lame's and normal equations and the reaction force. The deformation is higher than the flexible pipe without blockage, which stands at an average of 0.1474 mm, representing 0.53% of the pipe's original length of 2.8 m. The stress components (MPa) and the strain are shown in the graph, with the stress pressure having a higher value than the von mises and maximum stress. The hoop stress is negative, which denotes that the stress is acting outwardly on the circumferential part of the pipe.

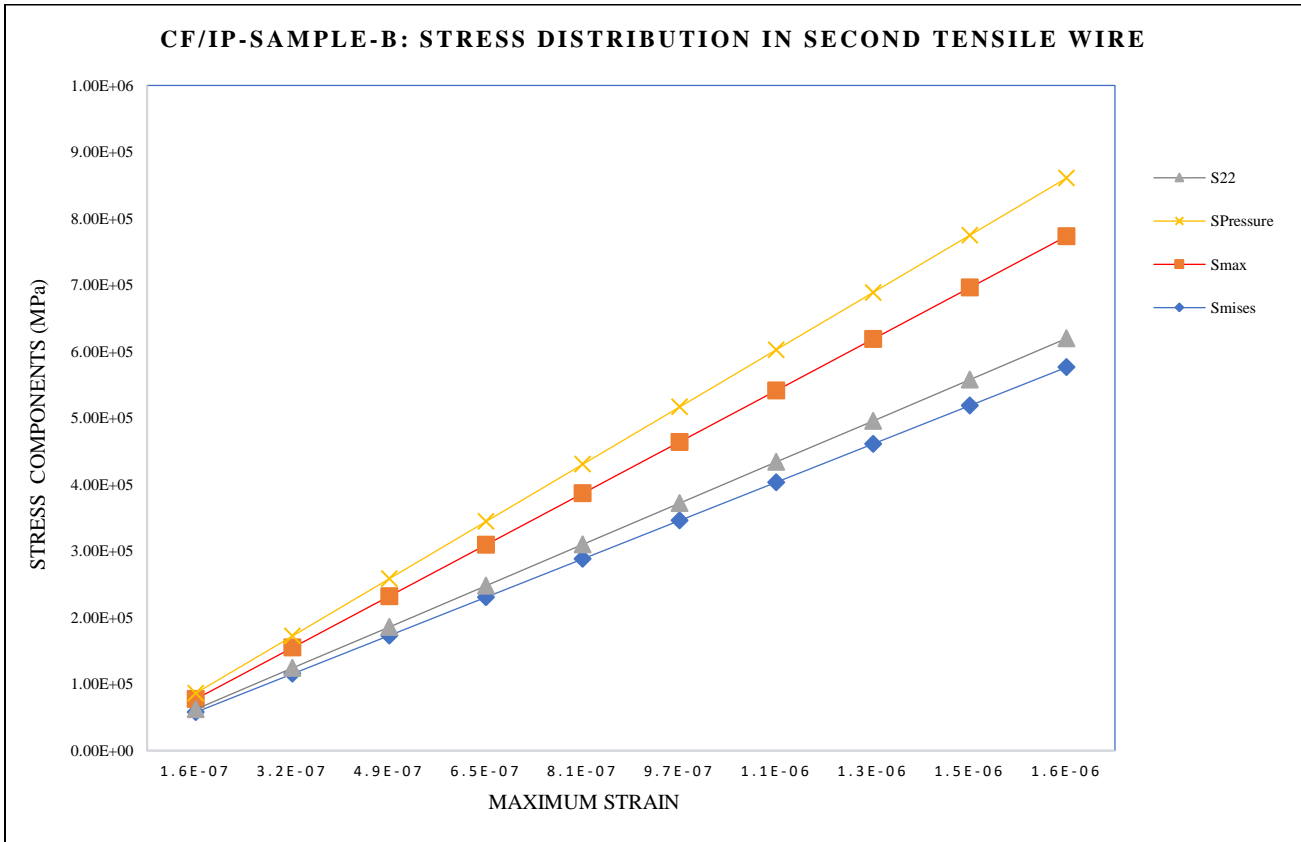
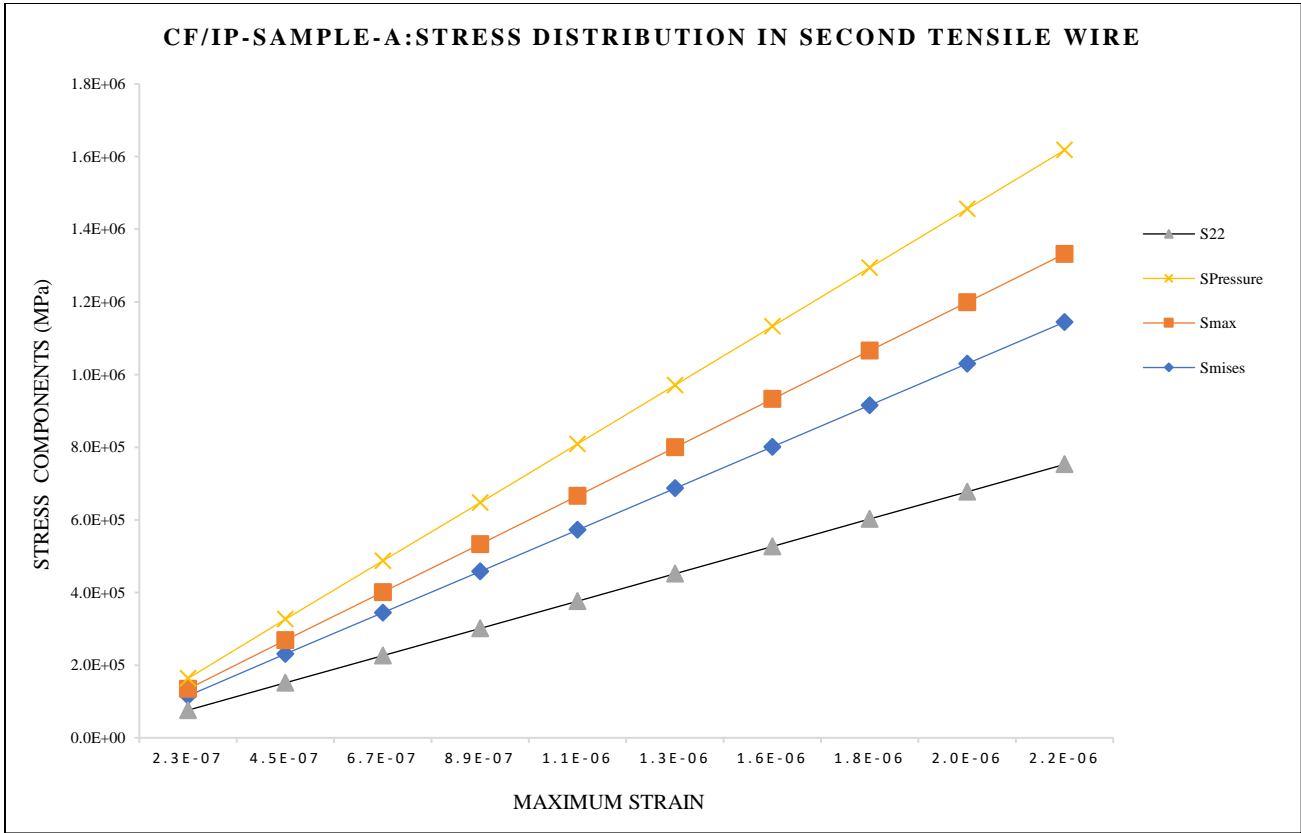


Figure 6-8: Samples A & B: Stress Distribution in Second Tensile Wire layer

The internal pressure and compressive force application showed a complete deformation of the flexible pipe already sensitive to load force. The linearity of the stress/strain distribution shown in Figure 6-8 showed the unusual behaviour of pipe under a combined load of tension and internal pressure. Therefore, whether it is blocked or not, the application of tension can lead to several failure modes and should be avoided in all cases.

Consequently, when considering three (3) load conditions, it is observed that the deformation and stress distribution is more significant when the pipe is under a combined load most often occurs under internal pressure and compressive and perhaps pulling force. The simulation has shown that apart from being sensitive to load, blocked flexible pipes are also liable to damage or failure modes as recommended in API 17B [1].

Table 6-4: Hoop stress, Displacement and Reaction force for Samples A & B layers

| Internal Pressure + Compressive Force | Frictionless, stiffness constant=0.00001 | | | | | |
|---------------------------------------|--|-----------------------|--------|--------------------------|-----------------------|--------|
| | 2198 | | | 1748 | | |
| Reacting Force (kN) | Sample A | | | Sample B | | |
| Load type | S _{mises} (MPa) | S ₂₂ (MPa) | U (mm) | S _{mises} (MPa) | S ₂₂ (MPa) | U (mm) |
| Carcass | 2315 | 1574 | 0.129 | 2206 | 1574 | 0.1035 |
| Pressure Sheath | 4.341 | 0.1435 | 0.127 | 3.452 | 0.114 | 0.1013 |
| Zeta Pressure Armour | 628.8 | *0.00271 | 0.1274 | 50 | *0.00215 | 0.1013 |
| First Tensile | 3.328 | 1.484 | 0.1275 | 2.647 | 1.180 | 0.1014 |
| Second Tensile | 8.861 | 0.410 | 0.1854 | 7.046 | 0.326 | 0.1474 |
| High Strength Tape | 532 | 27.89 | 0.1274 | 423.1 | 22.18 | 0.1013 |
| External Sheath | 3.857 | 0.288 | 0.1274 | 3.067 | 0.229 | 0.1013 |

* the unit is in Pa

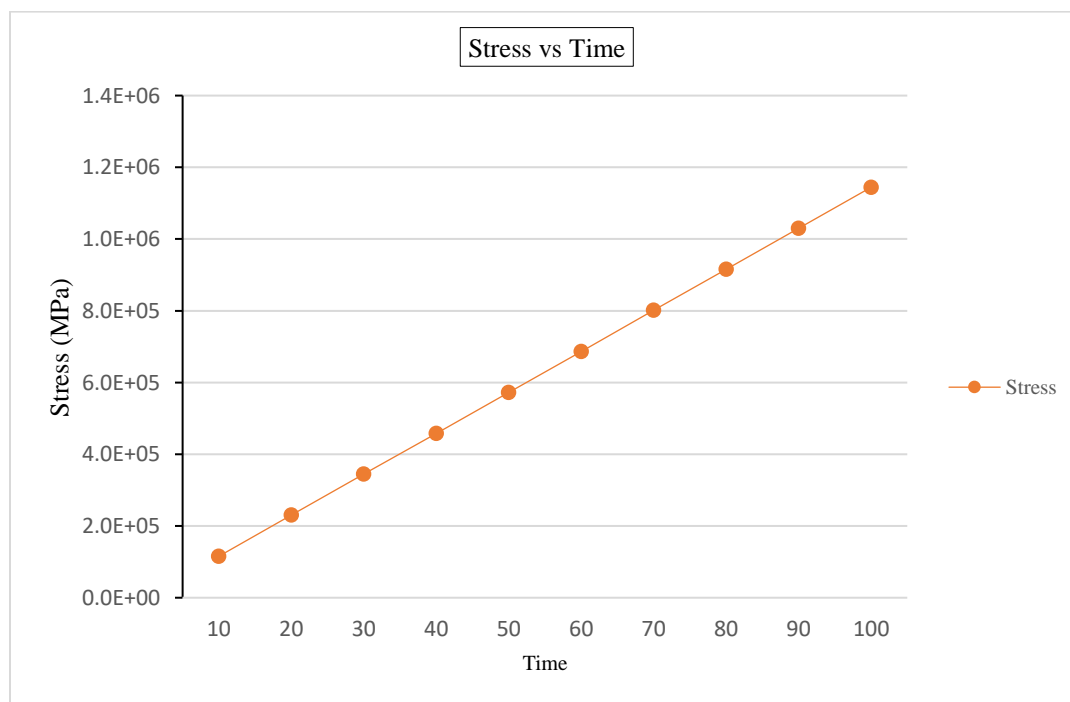


Figure 6-9: Stress vs Time showing an increase in stress value over the set time duration

6.2.4 Load Case 4: (a) Compressive Force (b) Pulling Force

The tension was mainly on the tensile wires, which are meant to withstand the compressive or pulling axial load. The deformation of the tensile wires is like the birdcage formed in the specimen, representing the ruptured pipe. They are described in Figures 6-10 and 6-11.

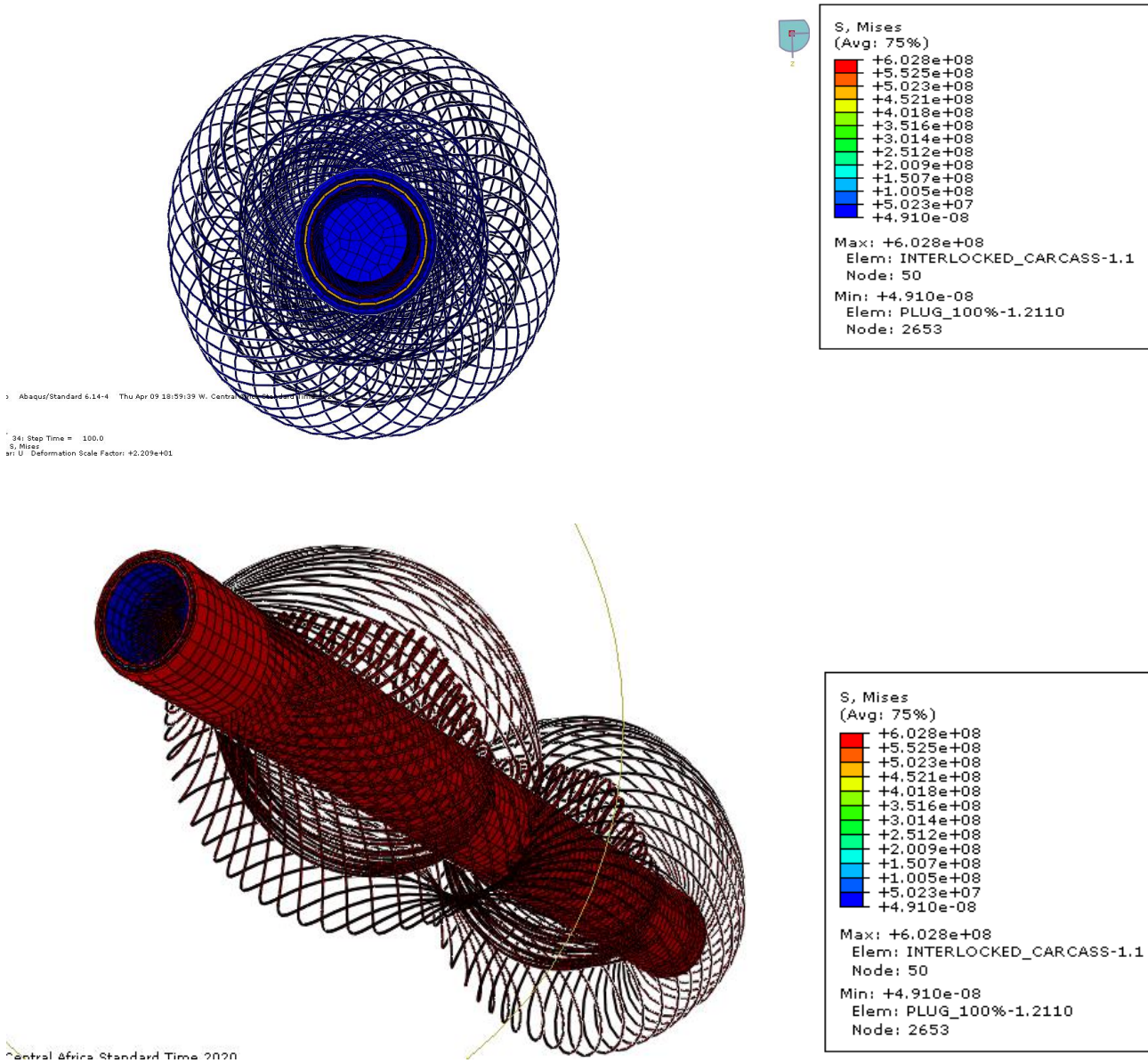


Figure 6-10: The deformation when applied a compressive force

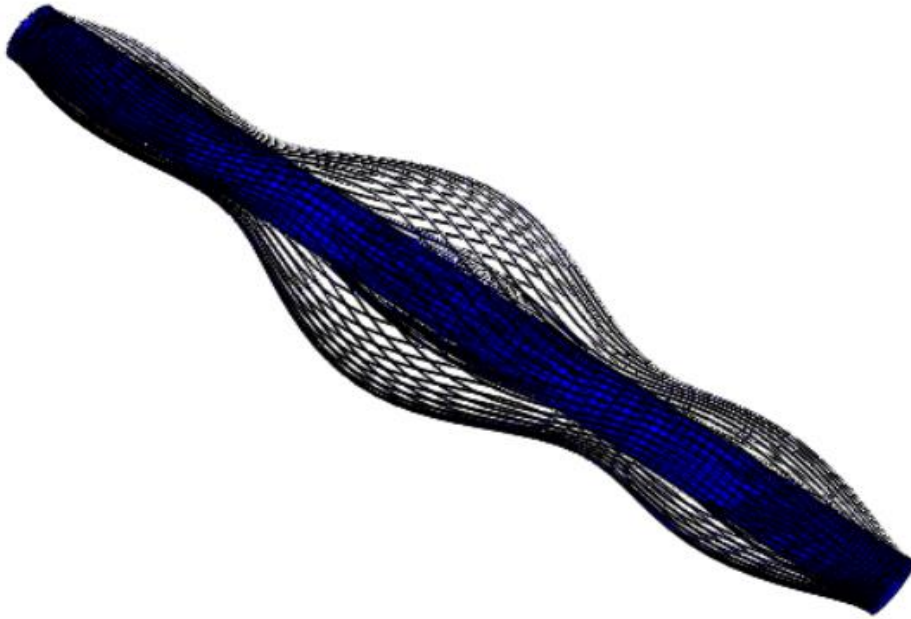


Figure 6-11: The deformation of the flexible when pulling force was applied

Pulling force: The stresses and displacement values are the same, except the reaction force is higher in sample A than sample B because of excess load created by the presence of the hydrate along the pipe axis, as shown in Figure 6-11.

6.2.5 Load Case 5: Variation of co-efficient of friction

The coefficient of friction (μ) was varied from 0.1 to 0.5 for all the load conditions. This is to confirm the effect that the contact friction has on the pipe with the hydrate blockage. It is observed that the values of stress and deformation of the flexible pipe increase with a lower coefficient of friction, keeping the contact stiffness constant.

The value is higher for 0.0, 0.1 and start to decrease for 0.2, 0.3, 0.4, 0.5 with further decrease for higher values. This shows that the pipe responds to the coefficient of friction and a limit is to be considered during flexible pipe design. Therefore, the coefficient of friction required should be greater than 0 but less than 0.5 for effective interaction between the layers; greater than 0.5 may not be suitable for non-bonded flexible pipes but may be good for bonded pipes where there is no interaction between the layers.

6.3 Experimental Investigation Results Analysis

The experimental results in Chapter 4 show that the investigated pipe behaviours are similar, and stress values are in line with numerical investigation results. That pointed to the same reasons that led to the damage of the

flexible pipe under investigation with the percentage deviation for the experiment and design values shown in Table 6-5.

Therefore, the overall stress values from the experiment are compared with the numerical values, most especially the metallic layers such as the Carcass with 36% and 35.6% deviation from designed values for Sample A and Sample B, respectively. The non-metallic values by the manufacturer were missing and thus sourced from the internet. The variations were significantly low, as shown in Table 6-6 for metallic and non-metallic layers.

Table 6-5: The layer-by-layer stress and strain outcome

| Layers | UTS as Designed (MPa) | SAMPLE A | | SAMPLE B | | Deviations from designed UTS | |
|-----------------------|-----------------------|-----------|------------|-----------|------------|------------------------------|------------|
| | | UTS (MPa) | Strain (%) | UTS (MPa) | Strain (%) | Sample A % | Sample B % |
| Carcass | 550 | 860.7 | 31.4 | 853.7 | 30.6 | 36.10 | 35.57 |
| Pressure Sheath | *48 | 56.3 | 312.3 | 52.7 | 308.2 | 14.74 | 8.92 |
| Zeta-Pressure Armour | 1000 | 1036.5 | 8.7 | 1032.0 | 8.2 | 3.52 | 3.10 |
| First Tensile Armour | 1400 | 1537.3 | 3.9 | 1541.5 | 5.8 | 8.93 | 9.18 |
| Second Tensile Armour | 1400 | 1545.8 | 4.8 | 1534.8 | 5.5 | 9.43 | 8.78 |
| High Tensile Strength | *3400 | 476.3 | 700.0 | 510.3 | 698.0 | -613.84 | -566.27 |
| External Sheath | *34 | 32.7 | 709.7 | 32.9 | 700.3 | -3.98 | -3.34 |

*Sourced from the internet.

Table 6-6: Numerical stress values under various load conditions

| Layers | SAMPLE A | | | | | SAMPLE B | | | |
|-----------------------|-----------|--------------------|-------|-------|-------|--------------------|------|-------|-------|
| | UTS (MPa) | Stress Mises (MPa) | | | | Stress Mises (MPa) | | | |
| | | | IP | CF+IP | EP | | IP | CF+IP | EP |
| | Designed | Exp | Num | | | Exp | Num | | |
| Carcass | 550 | 860.7 | 1926 | 2315 | 0.103 | 853.7 | 1844 | 2206 | 0.103 |
| Pressure Sheath | *48 | 56.3 | 0.029 | 4.34 | 0.588 | 52.7 | - | 3.45 | 0.588 |
| Zeta-Pressure Armour | 1000 | 1036.5 | - | 628 | 85.23 | 1032.0 | - | 50 | 85.23 |
| First Tensile Armour | 1400 | 1537.3 | 0.304 | 3.33 | 0.451 | 1541.5 | - | 2.65 | 0.451 |
| Second Tensile Armour | 1400 | 1545.8 | 0.084 | 8.86 | 1.20 | 1534.8 | - | 7.05 | 1.20 |
| High Tensile Strength | *3400 | 476.3 | 5.714 | 532 | 72.11 | 510.3 | - | 423 | 72.11 |
| External Sheath | *34 | 32.7 | 0.059 | 3.86 | 245.9 | 32.9 | - | 3.07 | 245.9 |

*Sourced from the internet; Abbreviation: Exp- Experiment, Num- Numerical; IP-Internal Pressure, CF-Compressive Force, EP-External Pressure.

The actual ultimate tensile stress for the non-metallic layers was evaluated by carrying out an iteration test on different pieces of pressure sheath and external sheath layers. It was performed under two scenarios for pressure sheath when the specimen was dry and wet and only one test for the external sheath. Slight deviations in the design and experimental results were recorded except for the carcass with 36.1% and 35.6% for samples A and B, majorly for the designed ultimate tensile stress. The measurement of stress and strain for the pressure sheath when dry and wet is presented in Figures 6-12 and 6-13, while Figures 6-14 and 6-15 show the external sheath. The stress and strain vary with various samples' lengths and thicknesses.

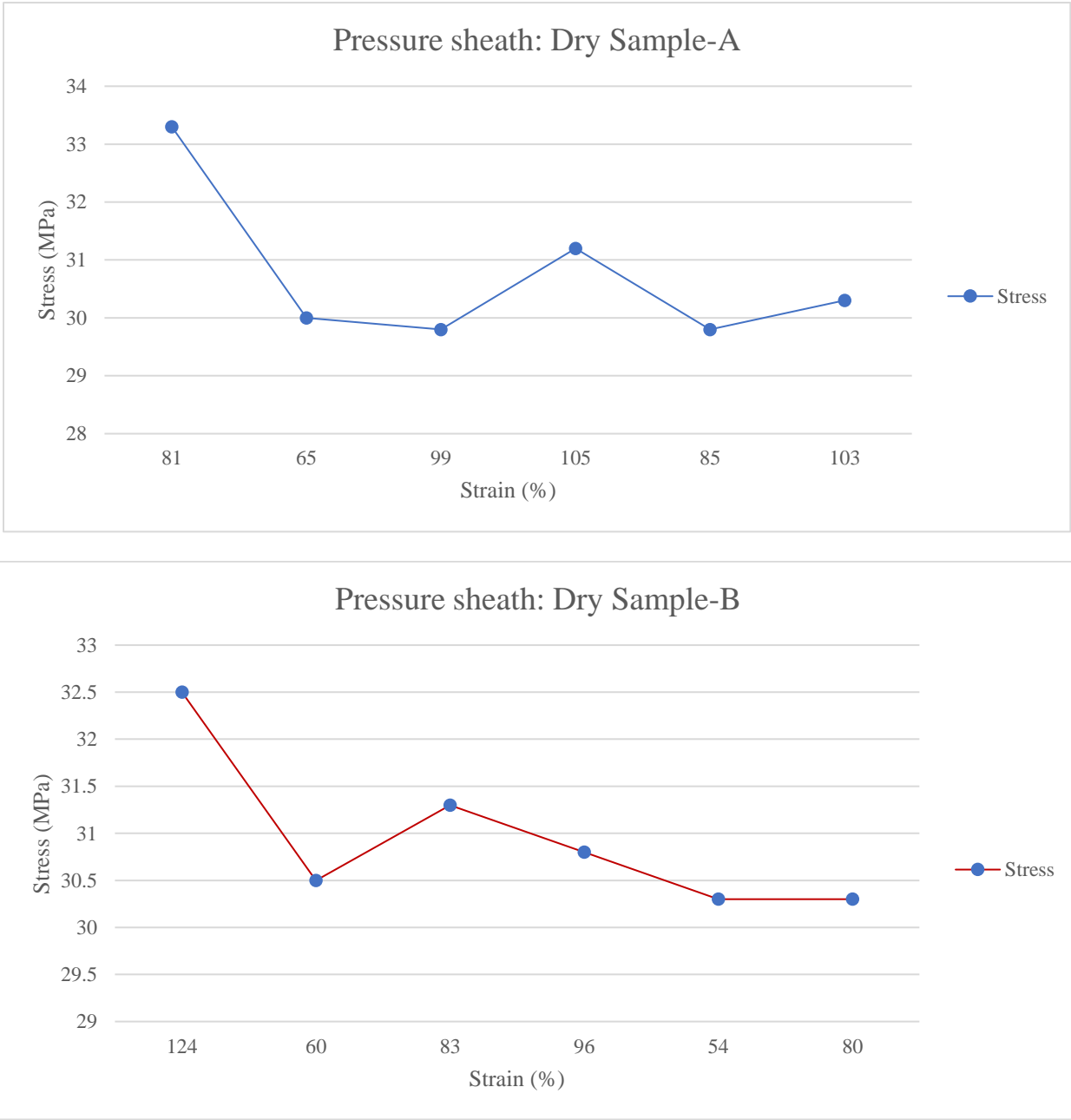


Figure 6-12: Experimental value of stress and strain for pressure sheath layer

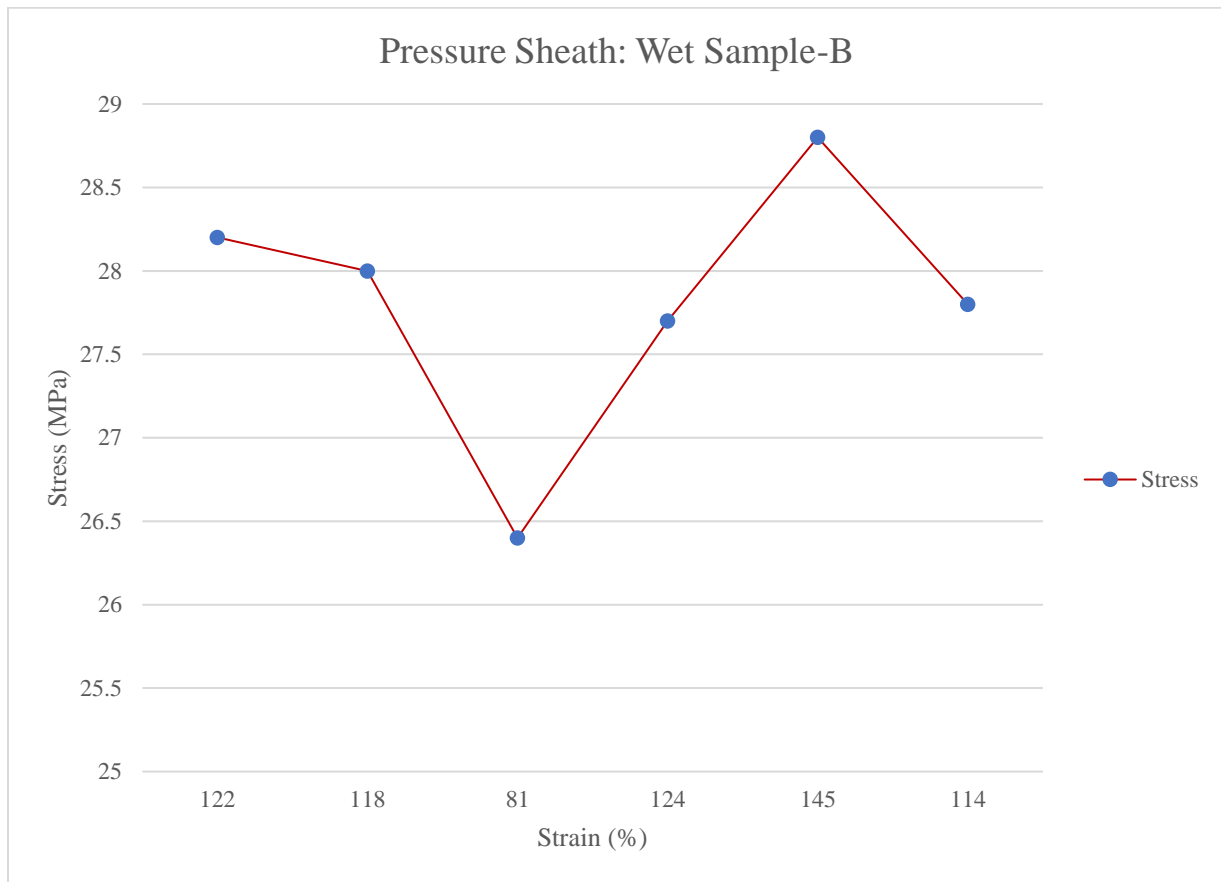
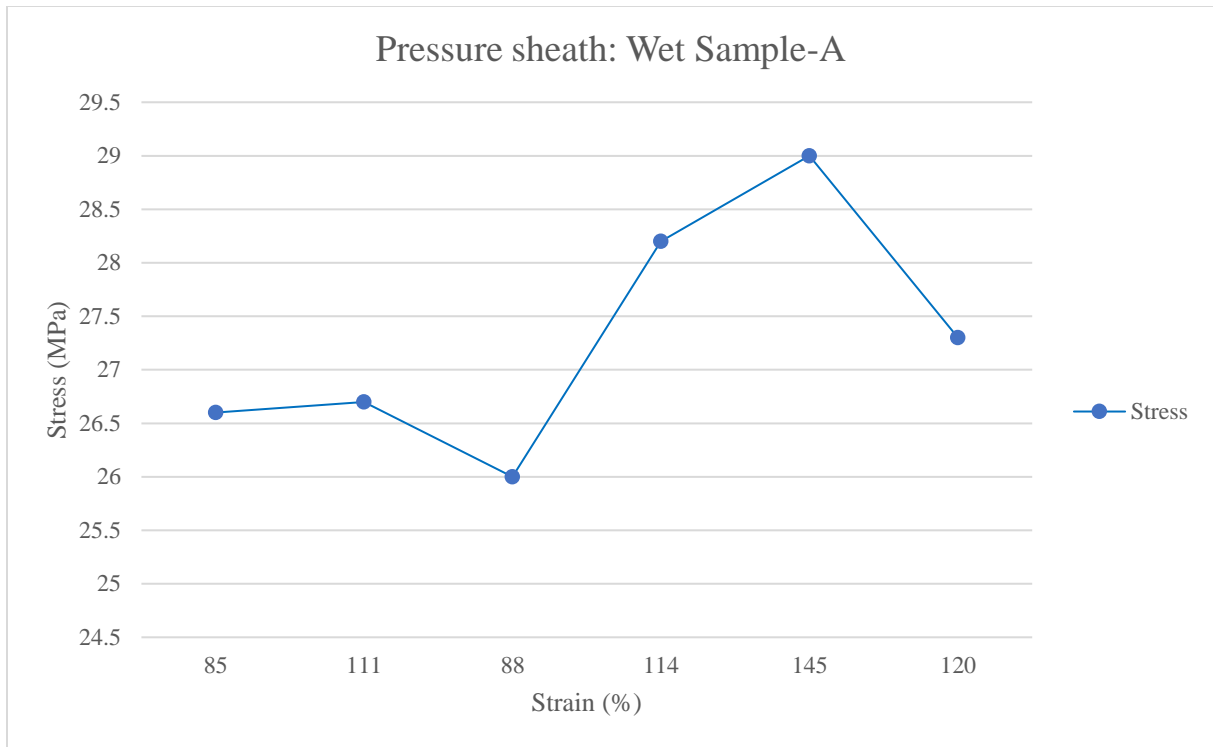


Figure 6-13: Experimental Value of stress and strain for Pressure Sheath layer

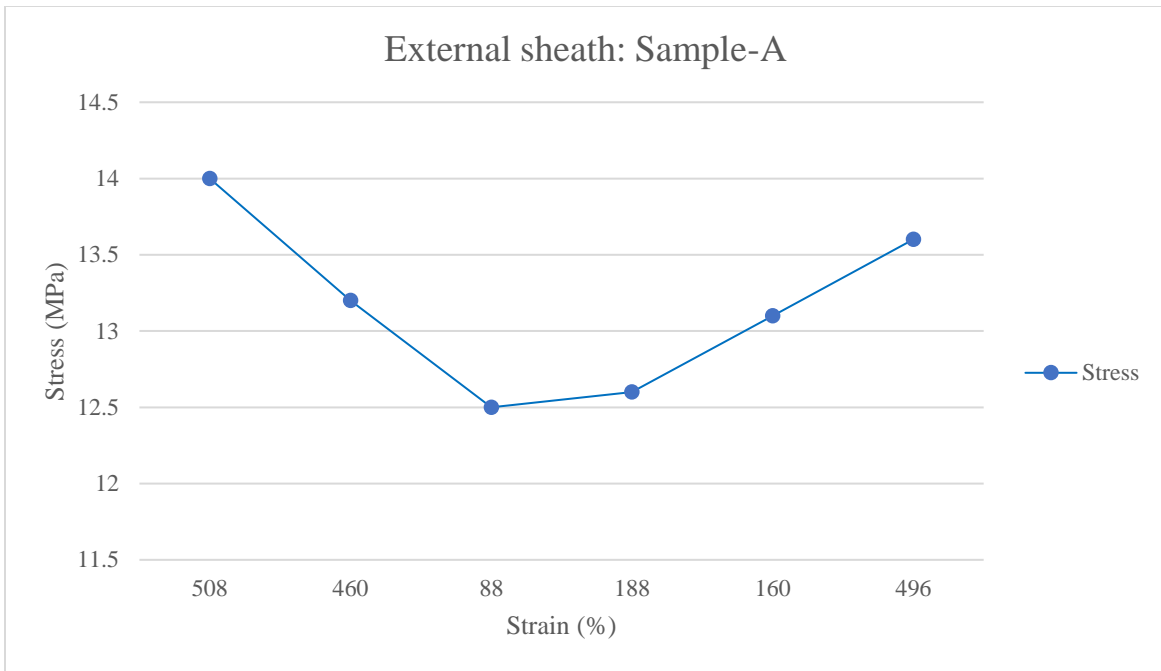


Figure 6-14: Experimental value of stress and strain for external sheath layer

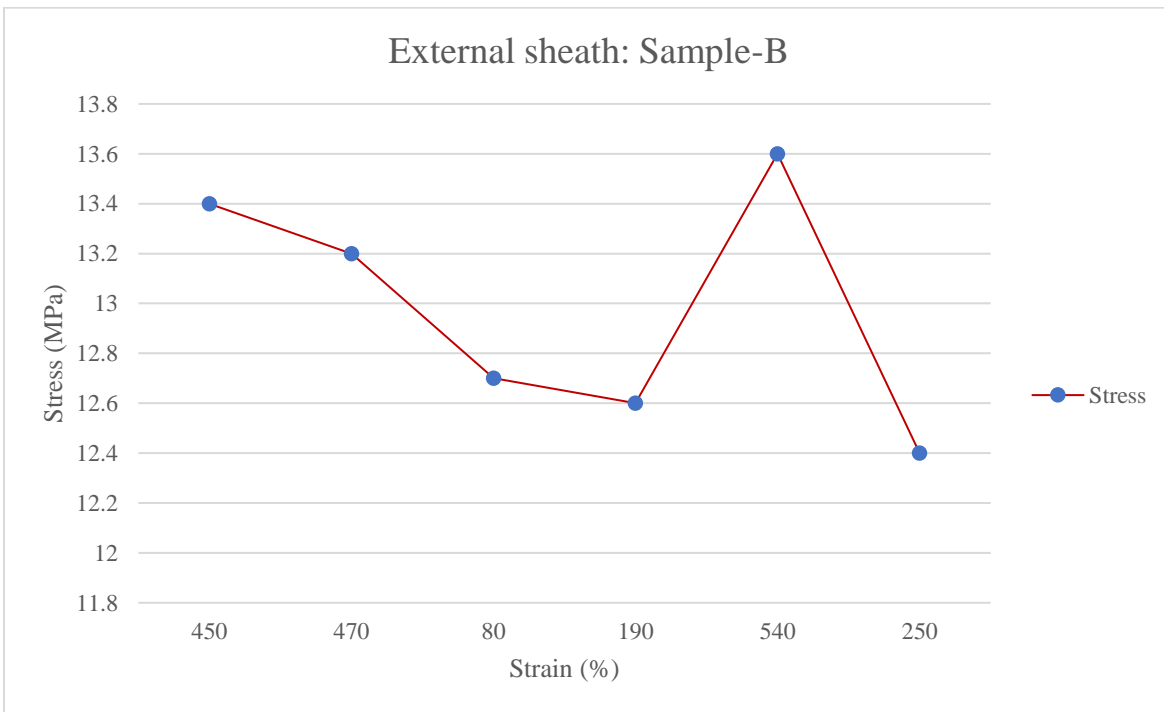


Figure 6-15: Experimental Value of stress and strain for external sheath layer

Accordingly, the average stress and strain values obtained for Pressure and External sheath layers to get the final values of each sample are compared with numerical results to assess the overall reasons for the pipe failure.

6.4 Validation and Verification

6.4.1 Interlocked Carcass

A simple static structural analysis was run on the carcass to check that the results obtained were in the computation region. Hoop Stress in a pipe was calculated using Lames and normal hoop stress equations as earlier used by Li, which considers both carcass and pressure armour instead of the only carcass being the layer where the pressure was applied.

6.4.1.1 Lamé's Equation

The Three (3) primary mechanical stresses that are applied to a flexible pipe being a cylindrical object are:

- Hoop Stress
- Radial Stress
- Axial Stress

If the object/vessel has walls with a thickness greater than one-tenth of the overall diameter, then these objects can be assumed to be 'thick-walled. The general equations to calculate the stresses are:

Hoop Stress

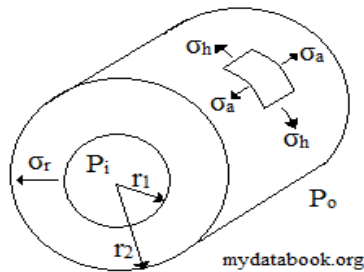
$$\sigma_h = A + \frac{B}{r^2} \quad \text{Equation 6-1}$$

Radial Stress

$$\sigma_r = A - \frac{B}{r^2} \quad \text{Equation 6-2}$$

From a thick-walled cylinder, the boundary conditions are shown below:

$$\sigma_r = -p_{oat} \text{ at } r = r_o \text{ and } \sigma_r = -p_i \text{ at } r = r_i$$



To simplify the two equations, hoop and axial stresses, the boundary conditions are applied and then solve simultaneously,

$$A = \frac{p_i r_i^2 - p_o r_o^2}{r_o^2 - r_i^2} \quad \text{and} \quad B = \frac{(p_i - p_o) r_o^2 r_i^2}{r_o^2 - r_i^2} \quad \text{Equation 6-3}$$

Finally, solving the general equations with A and B gives rise to Lamé's equations:

Hoop Stress

Equation 6-4

$$\sigma_h = \frac{p_i r_i^2 - p_o r_o^2}{r_o^2 - r_i^2} + \frac{(p_i - p_o) r_o^2 r_i^2}{(r_o^2 - r_i^2) r^2}$$

Radial Stress

Equation 6-5

$$\sigma_r = \frac{p_i r_i^2 - p_o r_o^2}{r_o^2 - r_i^2} - \frac{(p_i - p_o) r_o^2 r_i^2}{(r_o^2 - r_i^2) r^2}$$

The axial stress for a closed-ended cylinder is calculated by means of the equilibrium, which reduces to:

Axial Stress

$$\sigma_a = p_i \frac{r_i^2}{r_o^2 - r_i^2}$$

Equation 6-6

- σ_a = Hoop stress,
- P_i = internal pressure,
- P_o = external pressure
- r_o = external radius,
- r_i = internal radius,
- r = radius at point of interest (usually r_i or r_o)

Table 6-7: Computation Results of Hoop Stress using (a) Lamé's (b) Normal Equations

| A. Lamé's | | | | |
|---------------------|-----------------------------|------------------------|-----------------------|-------------------------------------|
| Layer description | Internal Pressure (P) (MPa) | Inner Radius (Ri) (m) | Outer Radius (Ro) (m) | Hoop Stress (H _s) (MPa) |
| Interlocked carcass | 22.7 | 0.0800 | 0.0812 | 1559 |
| B. Normal | | | | |
| Layer description | Internal Pressure (P) (MPa) | Inner Diameter (d) (m) | thickness (t) (m) | Hoop Stress (H _s) (MPa) |
| Interlocked carcass | 22.7 | 0.1601 | 0.0012 | 1514 |

Table 6-8: Comparison of Hoop Stress in Table 6-7 A and B

| Layer description | Internal Pressure (P) (MPa) | Hoop Stress (H _s) (MPa) | | |
|----------------------------|-----------------------------|-------------------------------------|-----------------|-----------------|
| | | Abaqus Model | Lamis' Equation | Normal Equation |
| Interlocked carcass | 22.7 | 1574 | 1559 | 1514 |

Tables 6-7 A and B, and the summary in Table 6-8 shows relative hoop stress values for the carcass layer. The result of the model is approximately the same as the calculated values of the hoop stress, and the model values are valid with the margins of 0.95% and 3.81% between Abaqus and Lamis' normal equations, respectively. It is worth noting that further refining the mesh quality will give a more accurate result that may even be closer to the theoretical values.

6.4.1.2 Axial Stiffness for the Carcass and Pressure Armour

The axial stiffness of the model, C3D8R, was calculated by dividing the applied force by the displacement caused when applied the compressive load. The flexible pipe length is 2.8 m (2800 mm), and a tensile load of 250 kN as used by De Sousa was placed at the free end of the model.

However, the axial stiffness measure on the physical pipe in the De Sousa study is 153000 kN. The deformation because of the axial load and calculated axial stiffness (EA) of the FE model is derived from Hooke's law, and the result is shown in Table 6-7:

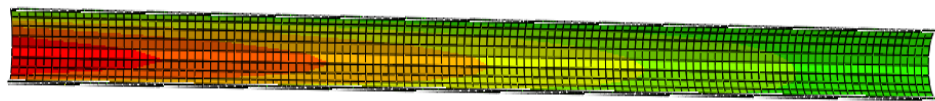
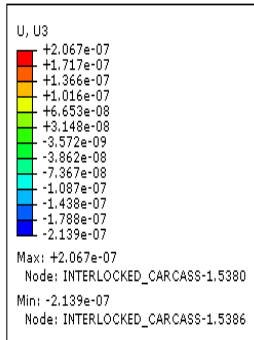
$$E = \frac{\text{Stress}}{\text{Strain}} = \frac{F}{A} / \frac{D}{L} \quad E = \text{Young Modulus}; F = \text{Applied Force} \quad \text{Equation 6-7}$$

$$EA = \frac{F}{D/L} \quad D = \text{Elongation or Compression}; L = \text{Original Length} \quad \text{Equation 6-8}$$

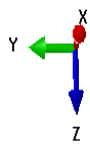
Table 6-9: Axial Stiffness for the Carcass and Pressure Armour

| COMPUTATION OF AXIAL STIFFNESS | | | | | | |
|--------------------------------|---------------|-----------|-----------|---------------------|-----------------|----------|
| De Sousa value – 153000kN | | U (m) | | Original Length (m) | Axial Stiffness | |
| Layer description | Applied Force | Sample A | Sample B | | Sample A | Sample B |
| Carcass | 2.50E+05 | 2.067E-07 | 4.233E-07 | 2.800 | 3.39E+12 | 3.39E+12 |
| Pressure Armour | 2.50E+05 | 2.331E-07 | 4.77E-07 | 2.800 | 3.00E+12 | 1.47E+12 |

The values varied significantly with the De Sousa physical pipe axial stiffness, perhaps because of many reasons, such as the flexible pipe parameters. Nonetheless, the exact value of force 250 kN was applied, resulting in the above results in Table 6-9. The variation reduces with increased applied force and the axial displacement of the carcass shown in Figures 6-16.



ODB: CF.odb Abaqus/Standard 6.14-4 Fri Apr 10 08:35:06 W. Central Africa Standard Time 2020



Step: Step-1
Increment 15: Step Time = 100.0
Primary Var: U, U3
Deformed Var: U Deformation Scale Factor: +1.545e+02

Figure 6-16: Carcass layer with axial displacement

6.5.2 Tensile wires

The computational result of tension in the tensile wire by recommended practice for flexible pipe API 17B is shown in Table 6-10.

$$\delta = \frac{T}{2te\pi D \cos^2\theta}; \quad \text{Equation 6-9}$$

where δ is the tensile stress,

T is Tensile Load, te is equivalent armour thickness, and D is the mean d

Table 6-10: Tension in the Tensile Wire

| COMPUTATION OF TENSILE STRESS | | | | | |
|-------------------------------|--------------------|------------------------|-------------------|------------------------|----------------------|
| Layer description | Applied Force (kN) | Inner Diameter (d) (m) | thickness (t) (m) | Cos ² (35°) | Tensile Stress (MPa) |
| First Tensile Armour | 1747.79 | 0.1828 | 0.002 | 0.671 | 1130 |
| Second Tensile Armour | 1747.79 | 0.1868 | 0.002 | 0.671 | 1110 |

The tensile stress compared with the hoop stress is 39% more than the computed value.

6.5.3 Behaviours of Flexible Pipe Layers when subjected to a combined Load

Figures 6-17 to 6-22 and 6-23 to 6-25 present the behaviour of Sample A and Sample B flexible pipe layers under a combined load of internal pressure and compressive force as components of stress against strain, respectively. The components show the increase in mises stress, hoop stress, pressure stress and maximum stress as the deformation of flexible pipe increases. Please note that all STRESS COMPONENTS are in MPa as shown in Figures 6-17 to 6-26.

6.5.3.1 Sample A

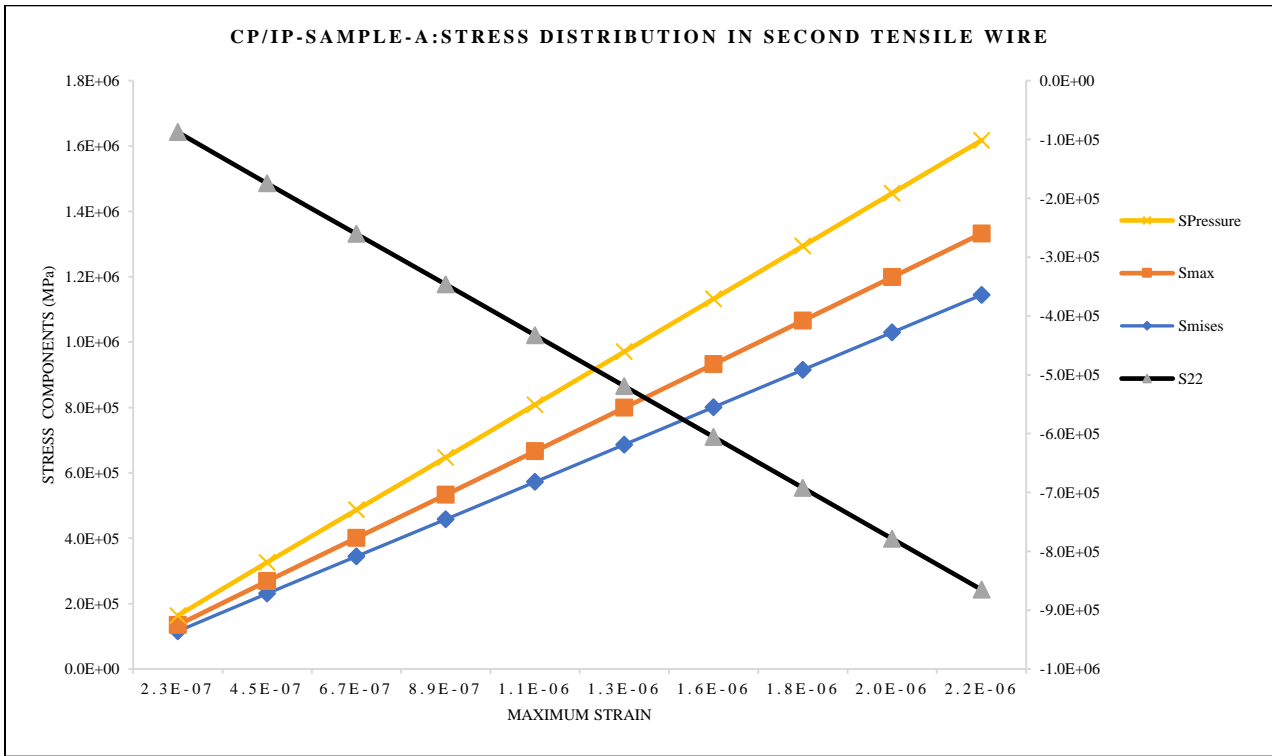


Figure 6-17:Sample A- Stress distribution in Second Tensile Wire layer

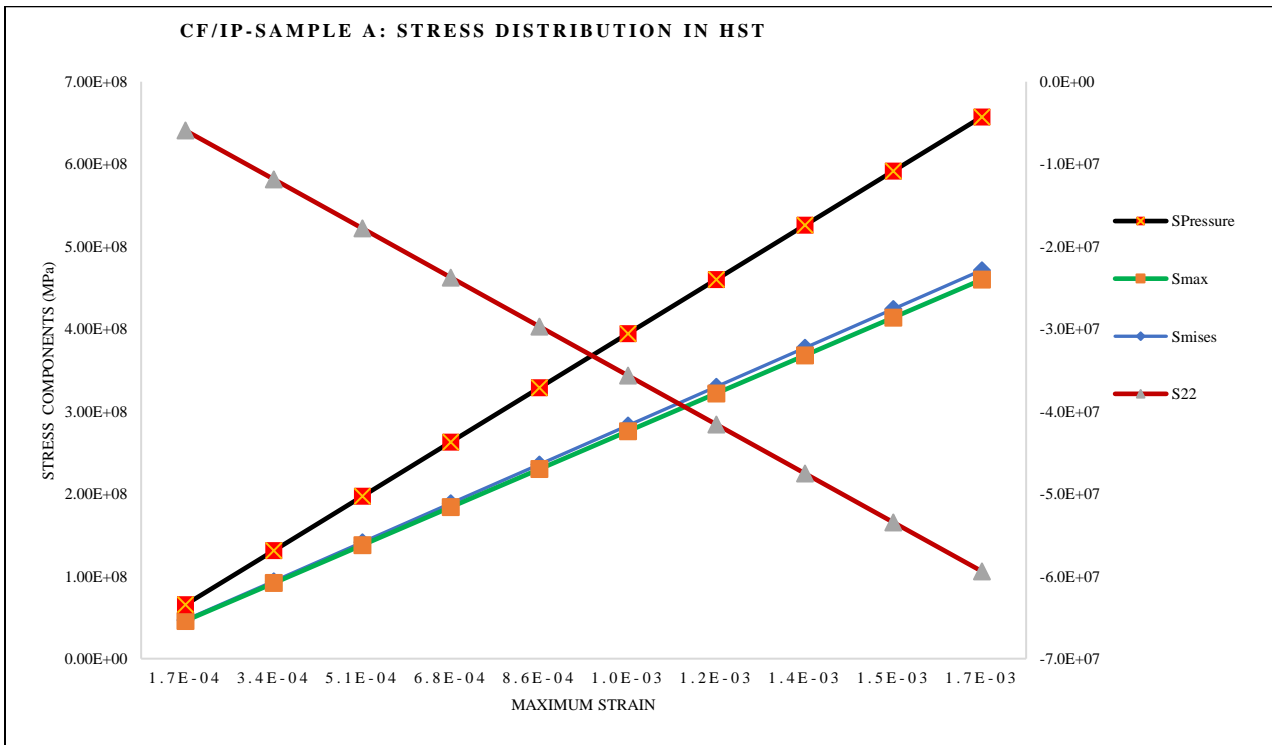


Figure 6-18: Sample A- Stress distribution in High Strength Tape (HST) layer

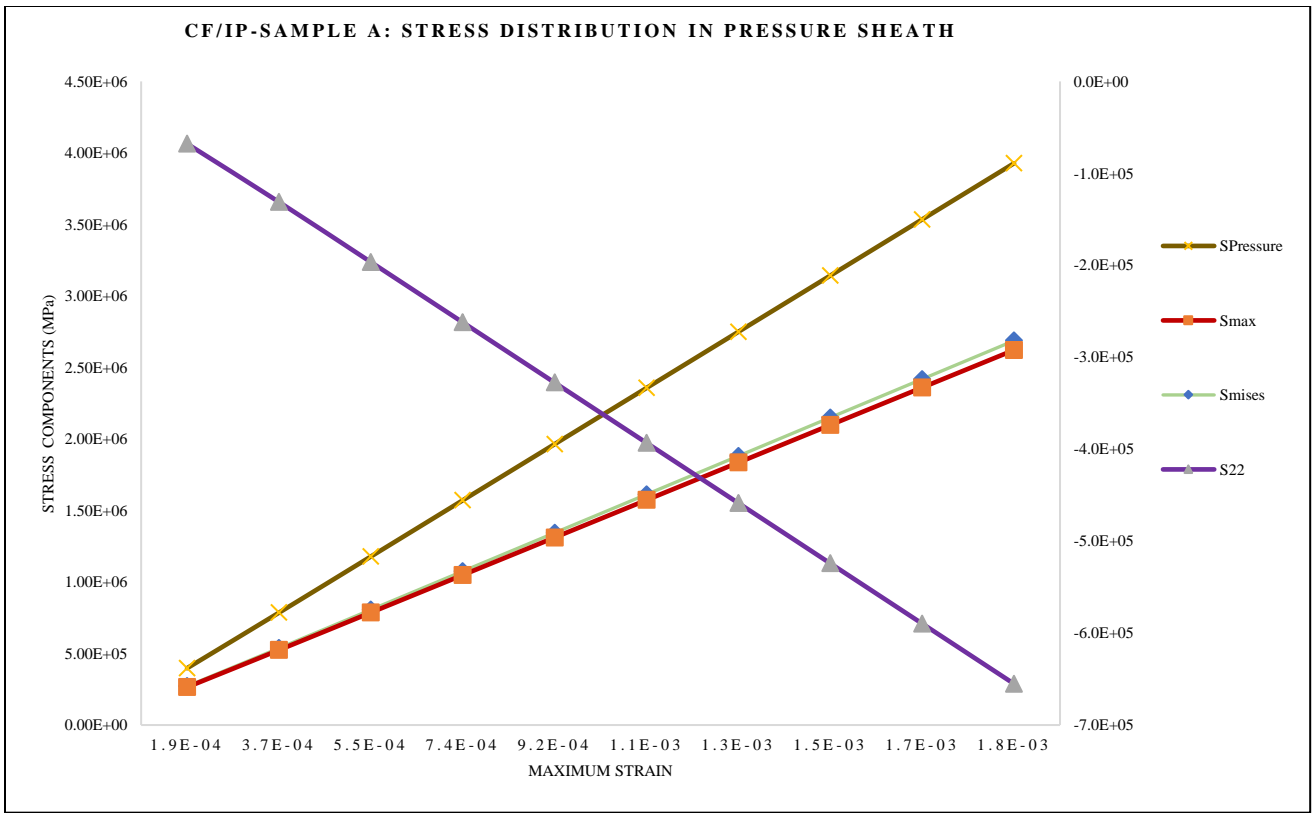


Figure 6-19: Sample A- Stress distribution in Pressure Sheath layer

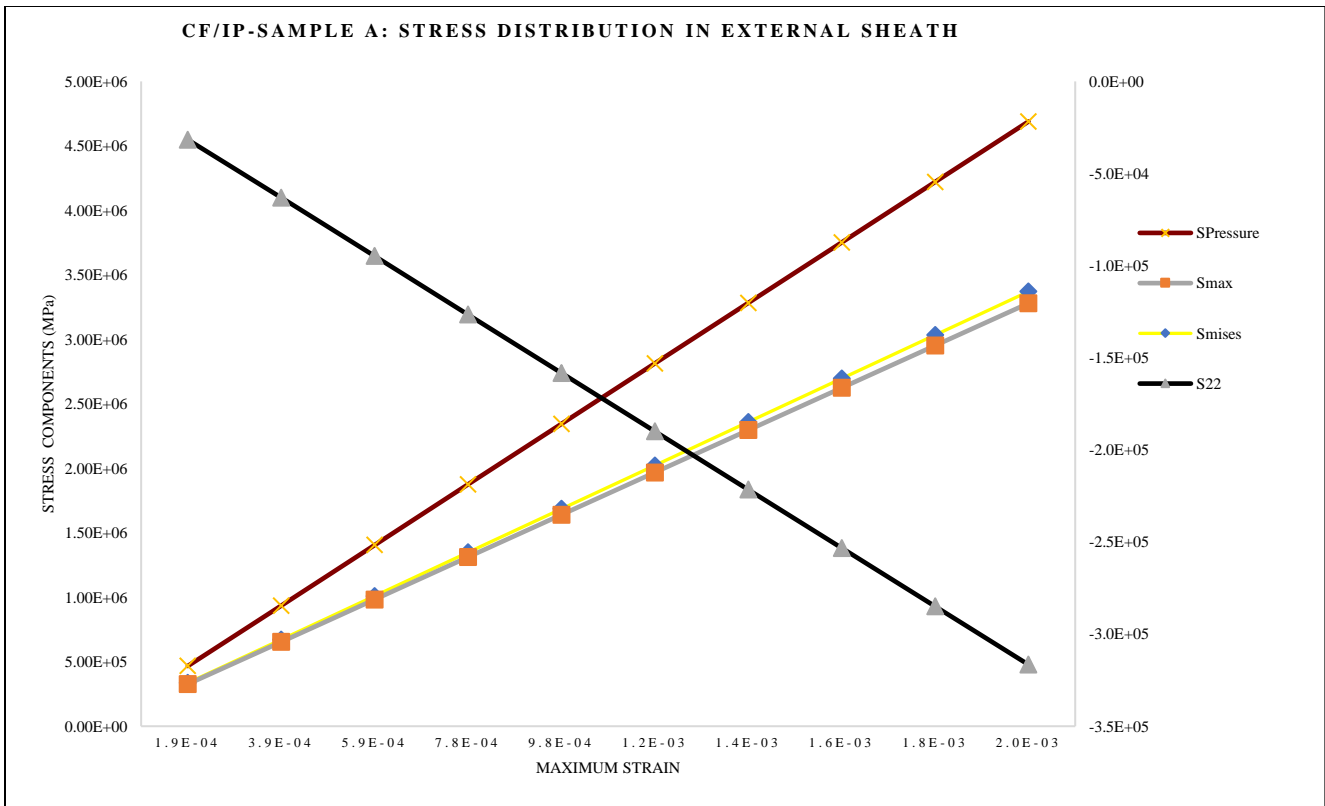


Figure 6-20: Sample A- Stress distribution in External Sheath layer

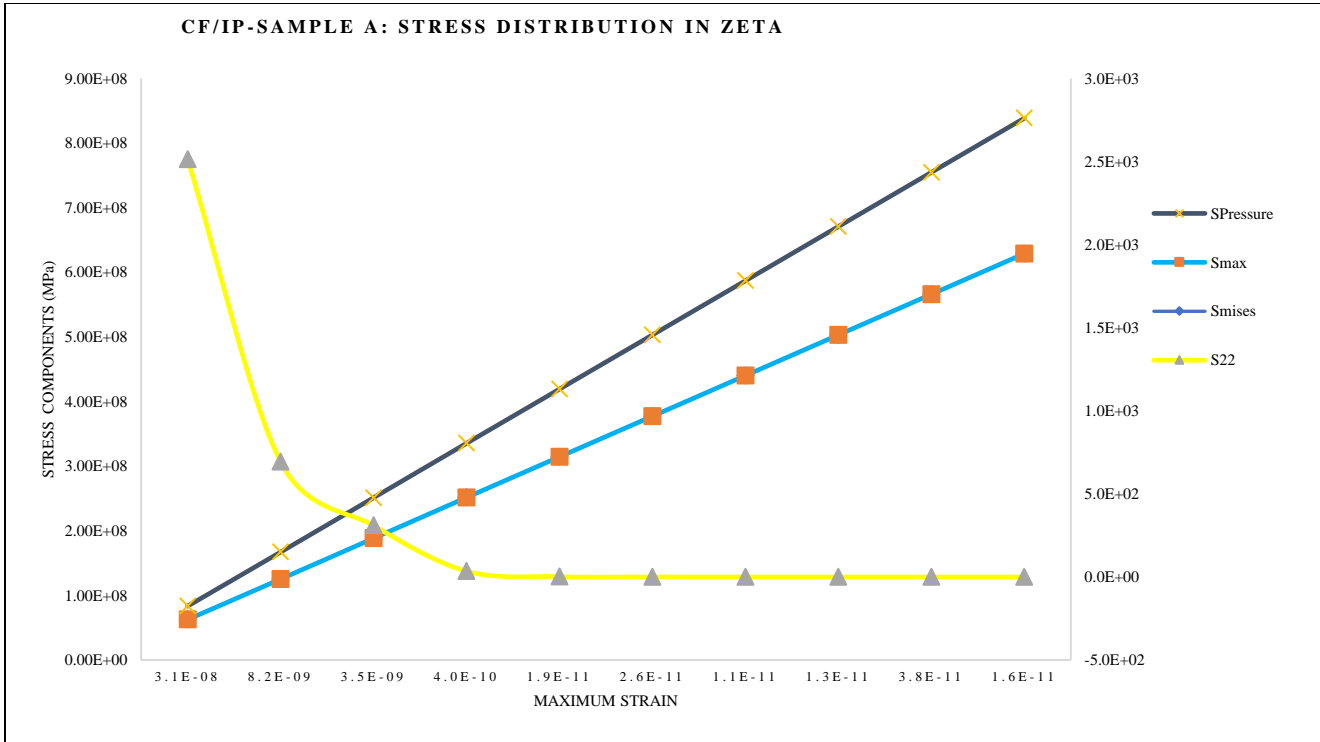


Figure 6-21: Sample A- Stress distribution in Zeta or Pressure Armour Wire layer

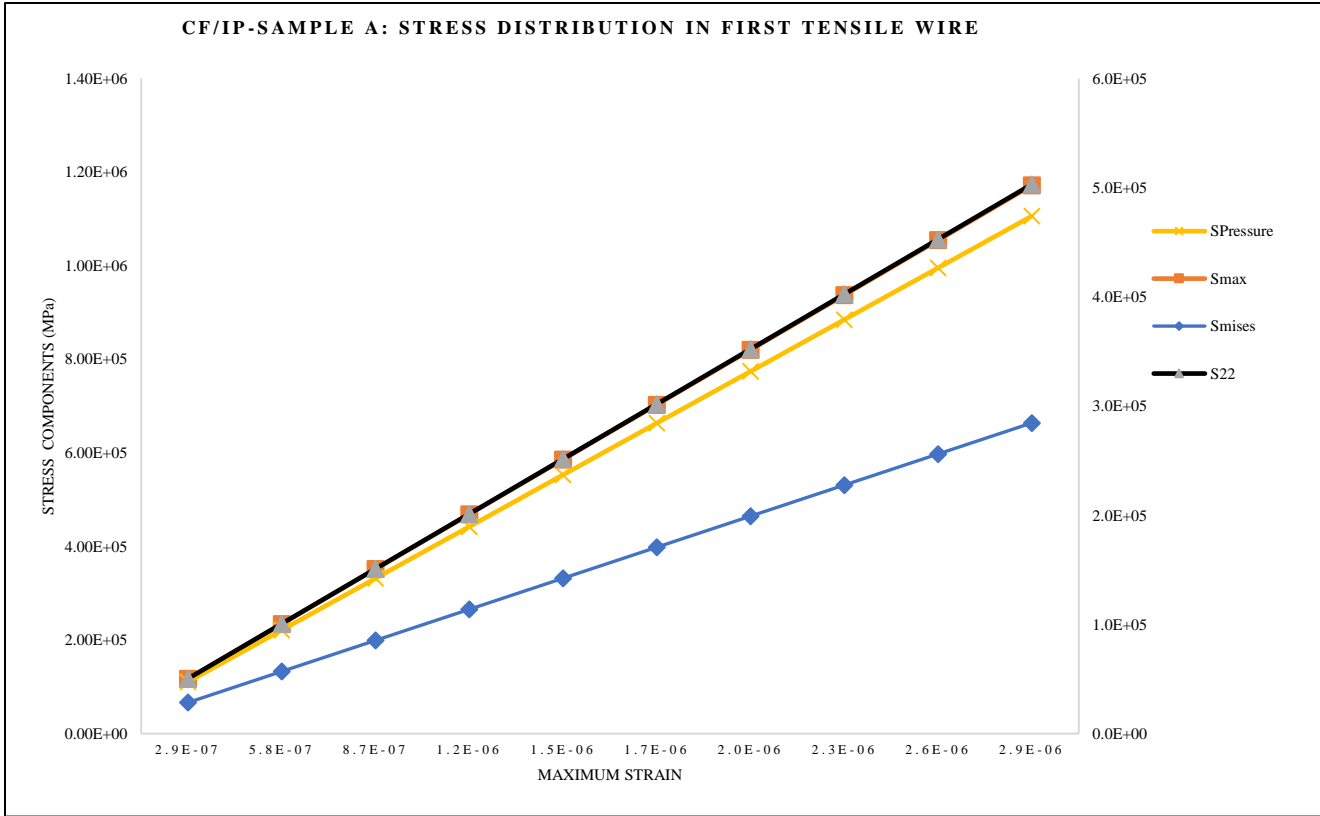


Figure 6-22: Sample A- Stress distribution in First Tensile Wire layer

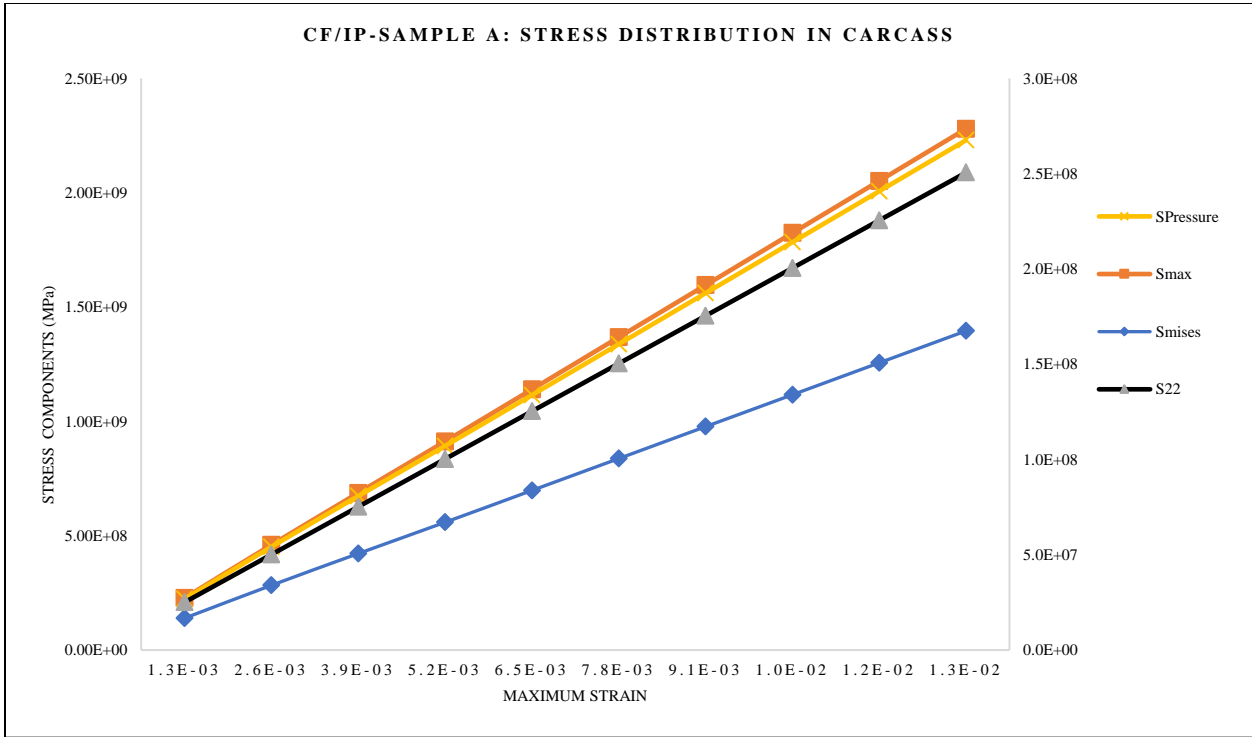


Figure 6-23: Sample A- Stress distribution in Carcass layer

6.5.3.2 Sample B

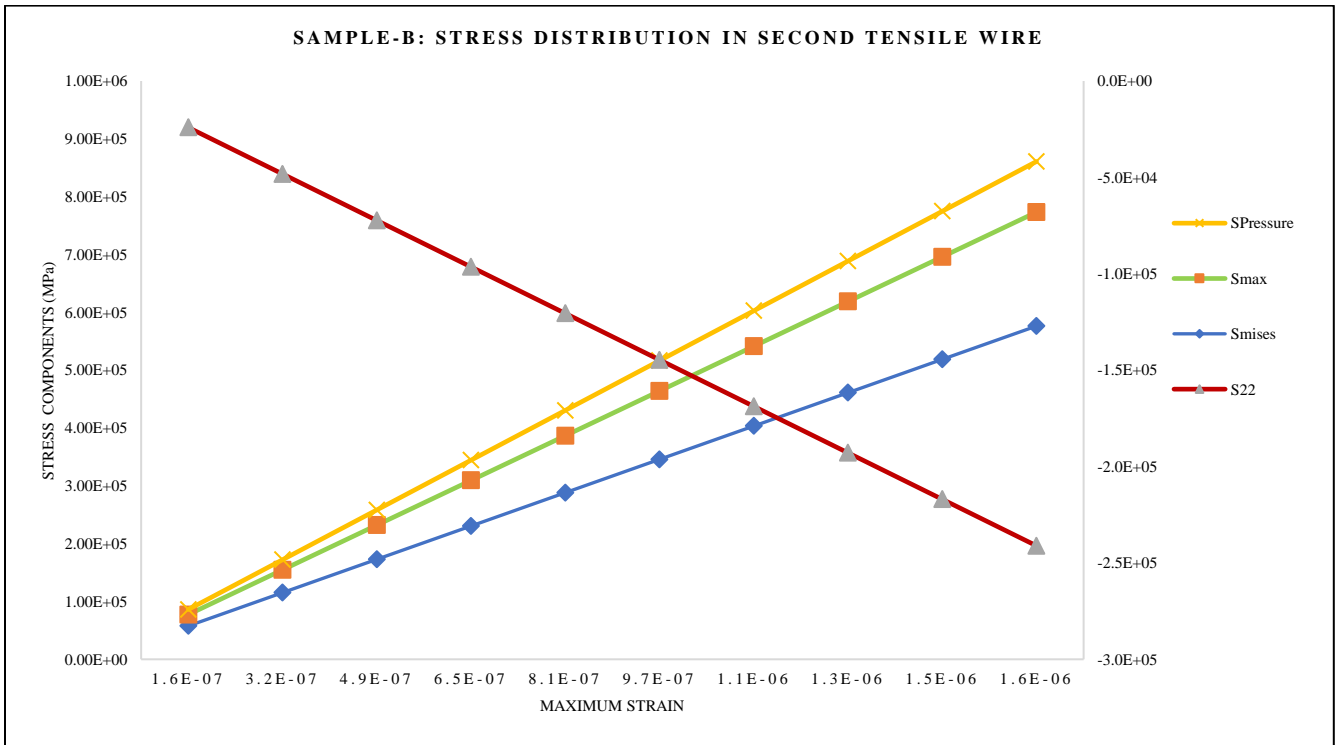


Figure 6-24: Sample B- Stress distribution in Second Tensile Wire layer

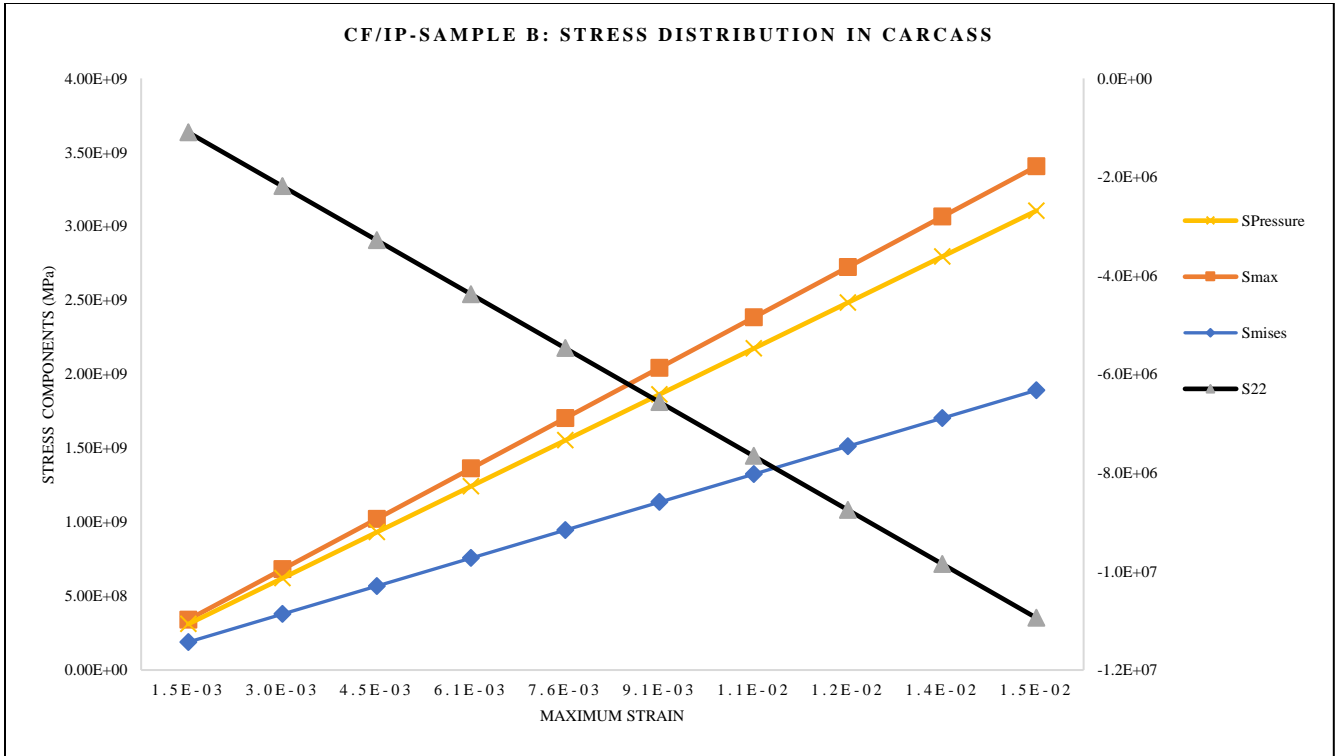


Figure 6-25: Sample B- Stress distribution in Carcass layer

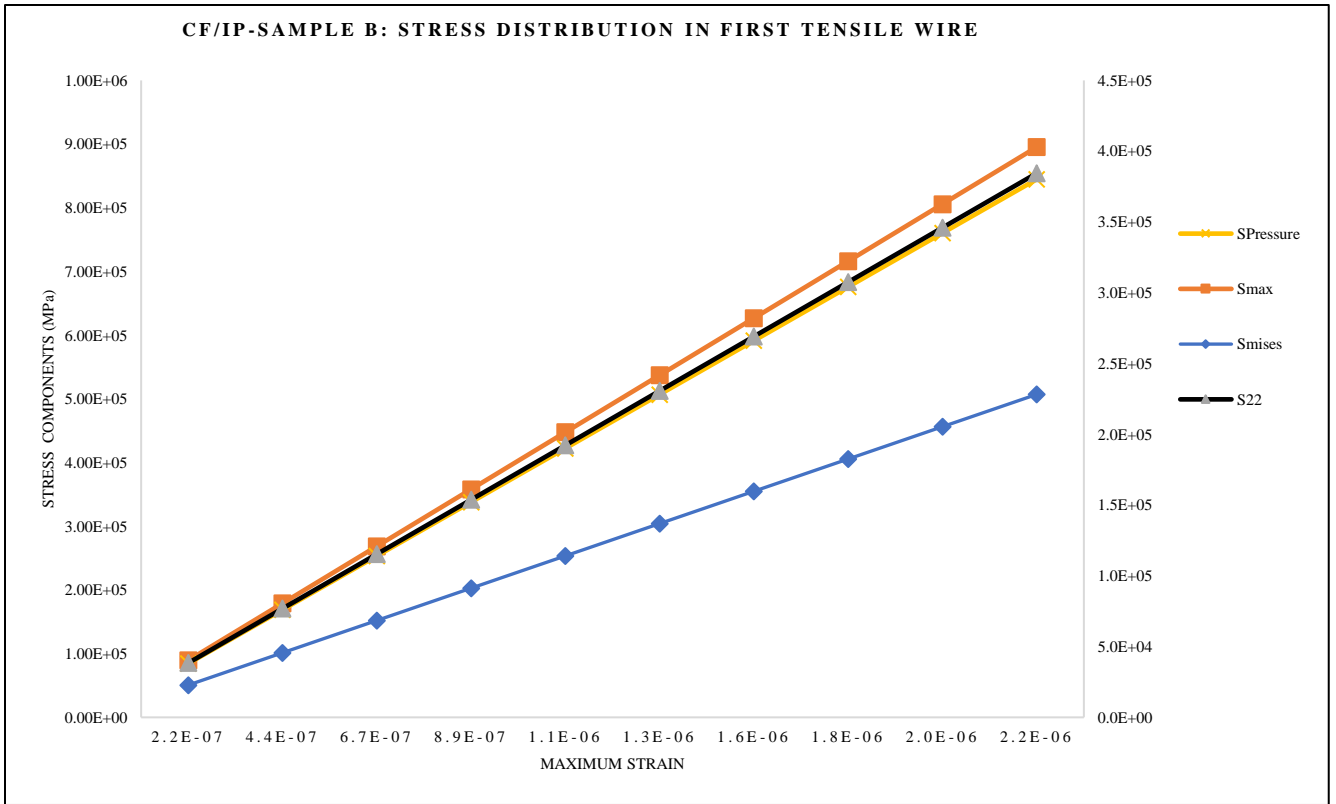


Figure 6-26: Sample B- Stress distribution in First Tensile Wire layer

Consequently, with three (3) load conditions considered, it is observed that the deformation and stress distribution is more significant when the pipe is under a combined load, most especially under internal pressure and compressive and perhaps pulling force.

The simulation has shown that a blocked flexible pipe, apart from being sensitive to load, is also prone to damage or failure modes as recommended in [1] as shown in Figure 6-27.

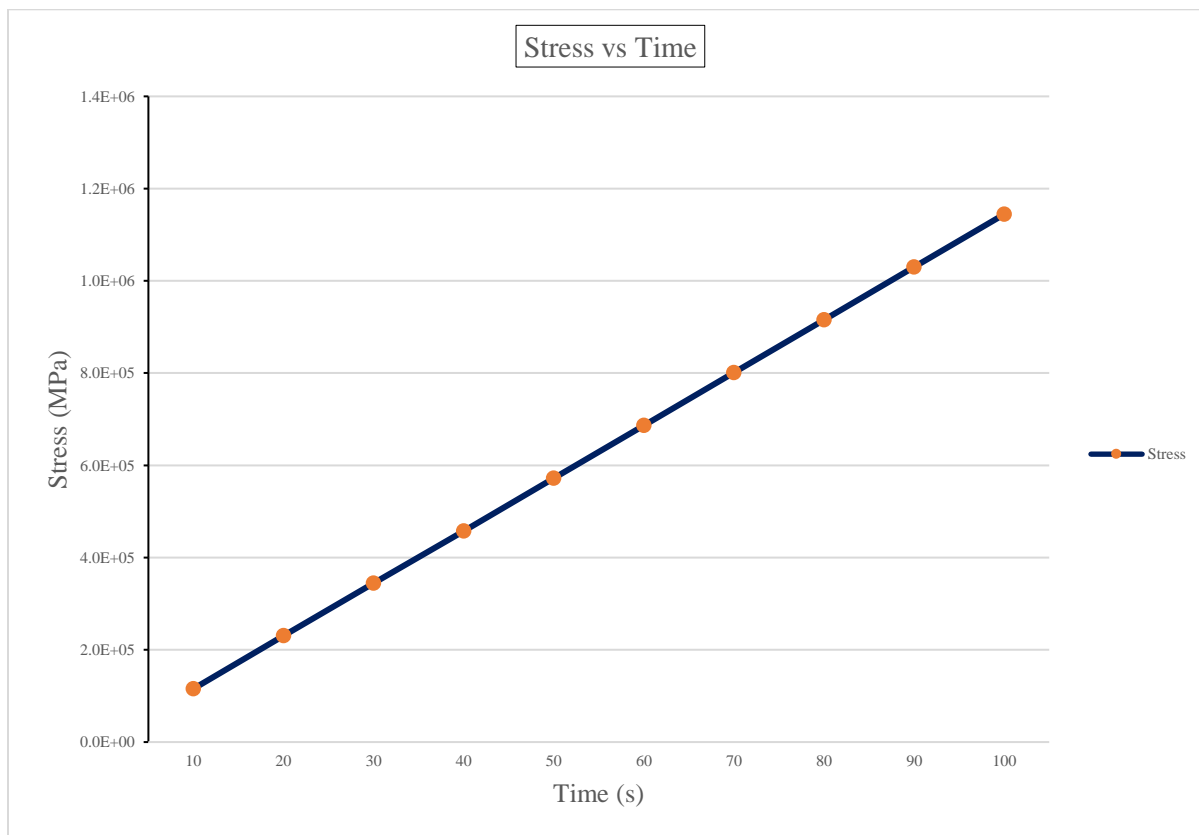


Figure 6-27: Stress vs Time showing the increase in stress value over set time duration

6.6 Effects of Reaction Force on the Flexible Pipe Layers

The deformation of the flexible pipe in all directions in the presence of methane hydrate and any other blockages is due to excess load created on the pipe surface layers that are usually greater than the load required to damage the pipe. The radial and axial deformation are due to reacting force and excess stress due to hydrate blockage, which depends on the applied load internal pressure and compressive or pulling force. The higher the values, the more deformed the flexible pipe when the load is applied and, conversely, does not occur in an unblocked flexible pipe. Though the force is node dependent, it is higher at the constraint point. Sample A has a maximum value of 450 kN, and sample B is 1.113×10^{-9} N. This is 100% higher, making it almost zero value and thereby negligible. It is much higher under the combined load of internal pressure and compressive force. The reaction load is 2198 kN, 80% higher than when only internal pressure is applied and 20.5% more

than the manufacturer's recommended pulling/compressive force. However, the value is expected in sample B as the flexible pipe operates under normal conditions as recommended by the manufacturer. Figure 6-28 shows the relationship between the two samples investigated under internal pressure, which is bound to be higher under a combined load. The Sample A gradient can easily be calculated due to the inclined nature as the displacement increases with force; however, the inclination tends to be almost zero for Sample B.

$$\text{The gradient} = \frac{\Delta \text{Force (f)}}{\Delta \text{Displacement (d)}} \qquad \text{Equation 6-10}$$

Gradient, according to Hooke's law, represents the pipe stiffness constant (k)

$$k = \frac{\Delta f}{\Delta d}$$

$$k = \frac{(450-75)*1000}{(3.8-0.63)*0.001}$$

$$=118300 \text{ kN/m}$$

The reaction force is higher in the blocked flexible pipe that eventually led to the deformation, while Sample B is almost zero without any significant change in the flexible pipe when a load is applied. The action is supported by equation 6-10 with the stiffness constant k, 118300 kN/mm

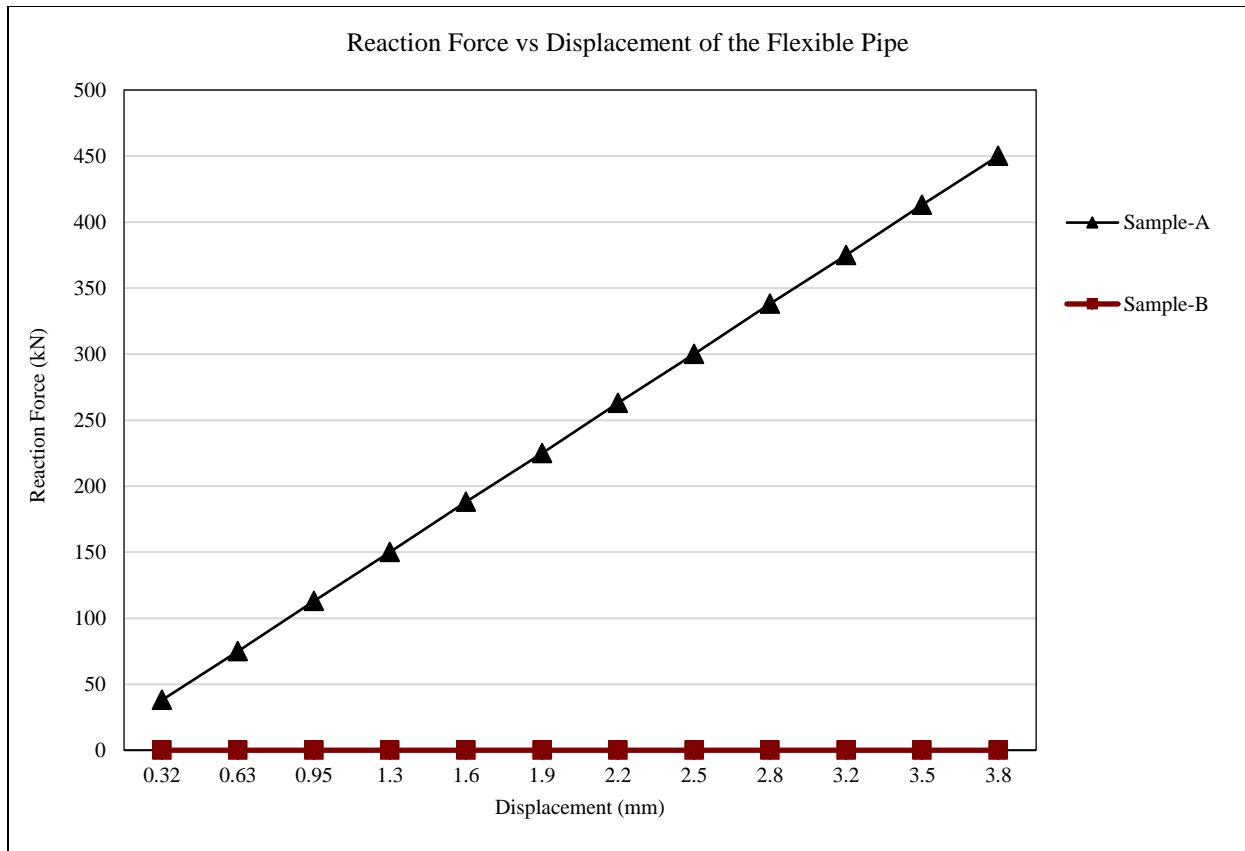


Figure 6-28: Reaction Force vs Displacement of the Flexible Pipe

6.7 Conclusions

The result showed the hydrate formation or any blockage/plug generates excess loads on the non-bonded flexible pipes wall in static and dynamic positions, as shown in Figure 6-6. This produces unnecessary stress that damages the flexible layers. The deformation of tensile wires in birdcage form is because of these excess loads created and impacted by the hydrate plug/blockage. As observed in the experiment, the estimated load to tear the layers is carcass- 77 kN, pressure sheath- 63 kN, and others swell up with an additional 10 kN. However, the numerical analysis shows the reaction force in the hydrate blocked pipe to be 450 kN, which is much more than the load impacted during the 1st, 2nd, and 3rd pressurisation at 87 kN, 269 kN 318 kN, respectively.

Subsequently, the loads induced by the hydrate plug are higher than the compressive load that can lead to birdcage of the tensile wires and tears the carcass and the pressure sheath, with an indication in the models. The rupture of the non-bonded flexible pipe under investigation is due to the process (continuous pressurization and depressurization) that lead to the removal of the hydrate. It is essential to mention that the investigated flexible pipe is susceptible to load. The pipe's collapse or deformity was because of the compressive axial load generated by the pressure created during the pigging process. Table 6-9 shows the

values of numerical tensile stresses are lower in all the layers except for the carcass. It connotes that the load transmits from the inner layer to the outer layer; however, these loads with the excess reaction force generated, which for internal pressure is 450 kN and for a combined load is 2198 kN damaged the flexible pipe. In conclusion, the applied internal pressure and perhaps combined with other environmental loads damaged the non-bonded flexible pipe, being that the research work investigated. This shows that loads during operation can have adverse effects on the pipe layers and can eventually lead to damage if not carefully handled.

It is recommended that the blocked pipe be handled with utmost care while pigging or during any attempt to remove the plug/blockage, which could be hydrate formation or wax. This, if not well handled, could permanently deform the flexible pipe and perhaps damage it.

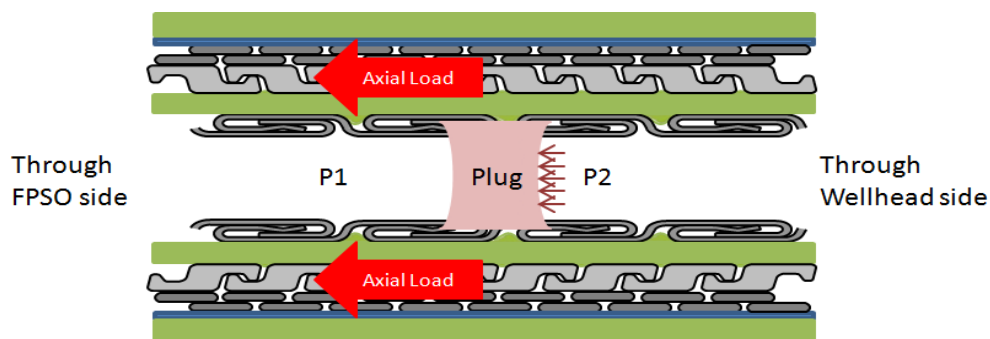


Figure 6-29: General effects of plug in the investigated pipe (I Clement, E Godefroy et.

Summarily, the presence of the plugin in the flexible pipe resulted in the differential pressure at the plug location (depressurization) and created an axial load in the flexible pipe layers, as shown in Figure 6-29. The failure analysis is entirely consistent with experimental investigations and supported by additional assessments. Failure was not due to manufacturing, material properties, installation, ageing, or corrosion. The failure mechanism based on the analysis are as follow:

1. Birdcage of armour wires was because of the presence of hydrate plug
2. Unlocking of the Zeta layer during pressurization was due to hydrate dissolution
3. Tearing of the carcass linked to the presence of a hydrate plug
4. Attempt to pressurize the line following hydrate dissolution leading to failure of pressure sheath

CHAPTER 7: CONCLUSION AND RECOMMENDATION FOR FURTHER WORKS

7.1 Conclusion

This present research work considered and analysed a methane hydrate blocked multi-layer non-bonded flexible pipe under different load conditions. It determined the root causes of ruptured flexible pipe, the associated challenges, and remedial measures in deepwater operations in the Gulf of Guinea.

The following objectives were achieved at the end of the simulation and after critically analysing the investigated flexible pipes, divided into two different samples, A and B.

1. Understood the subject and available research through literature review
2. Carried out a review of the experimental investigation on a 6", 7-layers blocked and unblocked pipe; determined the stress values and analysed according to the failure modes in API 17B/17J standard.
3. Developed a robust and comprehensive nonlinear finite element model for the investigated flexible pipe samples
4. Undertook a comparison analysis with experimental results and numerical results for specific cases with verification.
5. Combined the models and undertook a parametric study and analysed the effects of hydrate blockage and predicted the impact on the flexible pipe, which included but was not limited to pipe under the influence of internal pressure, compression force and combined loads.
6. Compared the results of both the experimental and numerical investigations of the hydrate blocked flexible pipe in line with API standards
7. The analysed results were combined and developed to guide the pipes with hydrate formation with suitable removal and manage industrial challenges associated with focus on the vital information on flexible pipes failure modes during operation and life extension.

The above objectives were achieved by representing non-bonded flexible pipes components with equivalent materials, sizes, and conditions. They were modelled, analyzed, and validated numerically using Abaqus by subjecting it to mechanical loading.

The material constituent of the flexible pipe was, as stated by the pipe manufacturer and in some cases leveraged on other related materials sourced from similar vendors. In addition, the design limits of all modelled flexible pipes were predicted based on von-mises failure criteria.

Lastly, parametric studies of the flexible pipe configurations (different layers configuration) and various material combinations were performed. This gave insight into the most optimal configuration and material combination for the service conditions.

The deformation of the blocked flexible pipe is the effect of depressurization and pressurization activities, which should not be ignored. The operations have a tremendous impact on the structure's lifespan. The layers, primarily external and internal tensile wires, are too sensitive to load, particularly to the internal pressure, which is the significant load applied during the pigging operations. The stress concentrations have higher values in the blocked pipe while almost negligible in the unblocked pipe under normal operating and factory test loads.

It is not far from the facts and figures in the experimental data that the pipes under investigation ruptured due to pigging operation. The operations involve a series of pressurization and depressurisation activities and are supported by comparing the numerical analyses results with experimental and, in some cases, computational values. Categorically, most people may not be aware of the effects of hydrate formation and its aftermath on the flexible pipe layers, perhaps due to less research in the area.

The result has shown that hydrate formation or any blockage/plug will generate excess load in static and dynamic conditions. This, in turn, causes unnecessary stress and later damage the layers. The deformation on the tensile wires inform of birdcage is because of the excess load created and impacted by the hydrate plug/blockage.

7.2 Experimental Investigation

The tensile tests conducted on the seven (7) layers non-bonded flexible pipe showed good results like the predicted failure modes in the API 17B and with similar loading conditions specified in the API 17 J. The results presented the spread of stress from layer to layer based on the properties and function of the individual pipe layers. The summary of the findings and conclusion of the experimental investigation was presented in chapter 4. Compared with Abaqus results in terms of stress and displacement, the results obtained were around 85% similar in values and 99.9% deformations and plots. Again, further verification of the obtained outcomes, tensile and compressive tests was conducted on a nine (9) layers non-bonded flexible pipe from an unspecified field in the North Sea, UK. The layers were subjected to similar loading conditions specified in the API 17 J with tensile load (0-110 KN) while the compressive load (0-250 KN). There was a similarity in the results but with limited applied loads due to the unavailability of some key equipment.

7.3 Numerical Investigation

Several prototype flexible pipes ranging from 3 to 14 layers were modelled using solid and shell parts for the blocked and unblocked configurations. Finite element analysis (FEA) used the Abaqus Finite Element system to represent typical flexible pipe with the physical behaviour of a series of offshore piping systems configurations. The numerical models were simulated using available papers and manufacturer data for the pipe under investigation. The models were subjected to different conditions and defined boundary factors as prescribed by the real-world physical conditions. The overall results clearly showed the effect of blockage in pipes with the numerical yield stress values are more significant than the ultimate tensile stress (UTS) of the original materials. The highest value was recorded in the carcass layer, and it is above 30% for Sample A and Sample B compared to the designed values. There is significant variation in the values obtained for the reaction force and displacement for sample A (blocked) and sample B (unblocked), and it varied along the length and the wall thickness of the two samples. The concentration of stress is much more in Sample A than Sample B due to blockage and creates enormous stress in the layers. The stress and reaction force increase with the increase from operating pressure to burst pressure. The operating pressure is considered an applied working pressure under which the pipe possesses exhibited normal behaviour with the value circa 22.4 MPa. The stress distribution indicates the significant differences between a pipe under normal operating conditions and those with anomalies such as Sample A. The hydrate plug absorbs part of the stress as it tries to adjust to the stress level under normal conditions, the reason for the investigated pipe rupture. In addition, the coefficient of friction impacts samples A more than sample B for stress, displacement, and reaction force due to the hydrate presence. The lower the coefficient of friction, the higher the stress values. This shows that the pipe responds to the coefficient of friction which is recommended to be within the allowable value of 0.1 to 0.5 μ . Any values above the allowable 0.5 μ may cause erosion of the layers as they slide over each other. Again, the estimated load to tear the layers is put at carcass: 77 kN, pressure sheath layer: 63 kN and different layers will swell up with an additional 10 kN. However, in the analysis, the reaction force in the hydrate blocked pipe is 450 kN which is also more than the load observed during the 1st, 2nd, and 3rd pressurisation that the blockage impacted 87 kN, 269 kN and 318 kN, respectively.

Subsequently, the loads induced by the hydrate plug are higher than the compressive load that can lead to birdcage of the tensile wires and tears the carcass and the pressure sheath, which is clearly shown in the models. Therefore, the rupture of the non-bonded flexible pipe under investigation is due to the process (continuous pressurization and depressurization) that lead to the removal of the hydrate, which presence has already created a danger to the pipe. It is important to mention again that the flexible pipe being investigated is very sensitive to load and that the collapse or deformity of the pipe was because of compressive axial load

generated by internal pressure; however, it gets worse when combined with compressive or pulling force and external pressure.

7.4 Recommendation

The outcome shows that the blockage inside the flexible pipe exerts more loads on the layers, which can damage the pipe and lead to eventual failure. The pipe with blockage is handled with caution by following the operation guideline during the removal process or during an attempt to remove the plug/blockage, such as hydrate or wax formation. Without laid down procedures, any attempt could permanently deform the flexible pipe and perhaps result in a replacement or dump on the seabed. The problem can be avoided based on the outcome of this research work, with identified ways to avert damage to the flexible pipes should there be a blockage.

7.5 Suggestion for Future Works

The recommendations are premised on the limitation of adopting a numerical analysis approach and limited experimental data due to the unavailability of adequate equipment throughout the entire study. And this could be further improved if the modelled non-bonded blocked flexible pipes are further validated through other approaches in future studies, most especially detailed experimental investigation with higher loads. As a result, the following future researches are suggested.

Additional studies are recommended to determine other conditions that could affect the pipes when operating under higher load conditions and exceeding the burst pressure. This is to eliminate those factors that can cause damage to the pipe. Therefore, suitable methods be adopted for the removal and cleaning of flexible pipes. This is to avoid burst and collapse of the pipes under environmental and internal conditions. Furthermore, the interaction and contacts of the layers should be improved, and finer mesh should be adopted for the model. At the same time, a higher coefficient of friction should be applied.

Again, this present work is based on limited numerical and experimental results; further studies can also be performed based on mathematical approaches to close all assumptions and gaps between the numerical and experimental results. In the process, other load conditions such as torsion, bending, and fatigue of the flexible pipe can be considered to understand non-bonded flexible pipes better.

REFERENCES

1. API. Recommended Practice for Flexible Pipe, API RP 17B. American Petroleum Institute. July 2008;(4th ed).
2. Gonzalez G. M., De Sousa J. R. M., Sagrilo L.V.S. An unbonded flexible pipe finite element model. In Proceedings of 36th Ibero-Latin America Congress on Computational Methods in Engineering, 22-25 November 2015. In; 2015; Rio de Janeiro.
3. Braestrup, M., Andersen, J. B., Andersen, W. L., Bryndum, M. B., Rishøj Nielsen, N.J. Design and Installation of Marine Pipelines, Blackwell Science Ltd. 2005; 278-316.
4. Barltrop, Nigel. Simplified Static Analysis of Pipelaying: Subsea System and Installation Glasgow: University of Strathclyde; 2016.
5. I Clement, E Godefroy et. al, 2014. Abo 5 6” GI flowline expertise and failure analysis. Technip; 2014.
6. Custodio AB, Vaz MA. A nonlinear formulation for the axisymmetric response of umbilical cables and flexible pipes. Applied Ocean Res. 2002; 24: 9-21.
7. Fergestad D., Løtveit S.A. Handbook on Design and Operation of Flexible Pipes; 2014.
8. API. Specification for Unbonded Flexible Pipe, API RP 17J. American Petroleum Institute. July 2008; 3rd ed.
9. DNV. C205 Environmental conditions and environmental loads. Recommended Practice. ; 2010.
10. PSA. Un-bonded Flexible Risers – Recent Field Experience and Actions for Increased Robustness 0389-26583-U-0032. Norway: 2013.
11. T.A. Anderson and M.E. Vermilyea, GE Global Research, and V. Jha, N. Dodds, D. Finch and J.R. Latto. OTC 24160 Qualification of Flexible Fiber-Reinforced Pipe for 10,000-Foot Water Depths. In GE Oil & Gas; 2003; Texas, Houston.
12. Liu, Zhijian. Study Of Hydrate Deposition And Sloughing Of Gas-Dominated Pipelines Using Numerical And Analytical Models PhD Thesis. Colorado: 2017.
13. ABAQUS. Simulia ABAQUS 16.4-4 Online Documentation <http://abaqus.software.polimi.it/v6.14>. 1644th ed.: Online Documentation.
14. De Sousa, J. R. M., Viero, P. F., Magluta, C., Roitman, N. Motta, A. M. R. An Experimental and Numerical Study on the Axial Compression Response of Flexible Pipes. In; June 6-11, 2010; Shanghai: ASME 2010 29th International Conference on Ocean, Offshore and Arctic Engineering OMAE 2010.

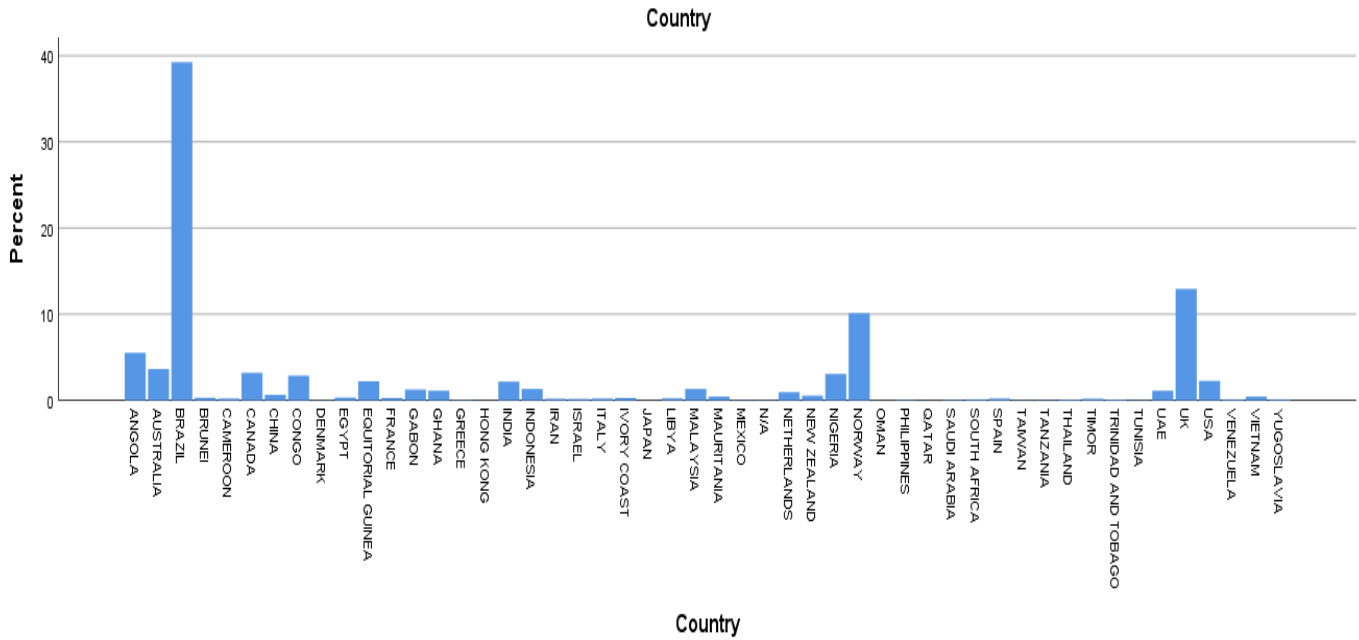
15. TechnipFMC. TechnipFMC. [Online]. [cited 2018. Available from: <https://www.technipfmc.com/en/what-we-do/subsea/subsea-systems/Subsea-infrastructure/Flexible-pipes>].
16. Beaudoin, Y. C., Waite, W., Boswell, R. and Dallimore, S. R. Frozen Heat: A UNEP Global Outlook on Methane Gas Hydrates. United Nations Environment Programme, GRID-Arendal. 2014; 1(ISBN: 978-92-807-3429-4): 1-80.
17. Nagham Amer Sami, Jitendra Sangwai and Bala Subramanian. Gas hydrate applications and problems in the oil and gas industry. In; 2013.
18. O.A. Adeyanjua, , O.A. Olafuyi. Experimental studies of sand production from unconsolidated sandstone petroleum reservoirs in Niger-Delta. Nigerian Journal of Technology. 2011; Volume 30(2): 19-20.
19. Ben Edmans, Dinh Chi Pham, Zhiqian Zhang, Tianfu Guo, Sridhar Narayanaswamy, G. S. Multiscale Finite Element Analysis of Non bonded Flexible Risers. In; 2014: Proceedings of the ASME 2014 33rd International Conference on Ocean, Offshore and Arctic Eng.
20. Ben Edmans, Dinh Chi Pham, Zhiqian Zhang, Tianfu Guo, Sridhar Narayanaswamy, G. S. Multiscale Finite Element Analysis of Non bonded Flexible Risers', Proceedings of the ASME 2014 33rd International Conference on Ocean, Offshore and Arctic Engineering OMAE2014. 2014; 14(2): 1-9.
21. Li, J. Y., Qiu, Z. X. and Ju, J. S. (2015). Numerical Modelling and Mechanical Analysis of Flexible Risers. In; 2015.
22. Xie, P., Zhao, Y., Yue, Q. and Palmer, A.C. Dynamic loading history and collapse analysis of the pipe during deepwater S-lay operation. Marine Structures. Marine structures. 2015; 40: 183-192.
23. De Sousa, J. R. M. Numerical Analysis of a Flexible Pipe With Damaged Tensile Armor. 28th International Ocean, Offshore and Arctic Engineering Conference., Honolulu. 2009;: 829-839.
24. Xu Yang, Svein Saavik, Liping Sun. Numerical analysis of buckling failure in flexible pipe tensile armour wires. Ocean Engineering, (2015),Elsevier Ltd. 2015; 108: 594-605.
25. D. B McIver. A Method of Modelling the Detailed Component and Overall Structural Behaviour of Flexible Pipe Sections. Engineering Structures. 2015; 7(14): 254–266.
26. Roberto Ramos Jr., Alexandre Kawano. Local structural analysis of flexible pipes subjected to traction, torsion and pressure loads. Marine Structures. 2015; 42: 95-114.
27. R. Cuamatzi-Melendez, O. Castillo-Hernández, A.O. Vázquez-Hernández, M.A. Vaz. Finite element and theoretical analyses of bisymmetric collapses in flexible risers for deep waters developments. Ocean Engineering. 2017; 140: 195-208.

28. Niels Højen Østergaard, Anders Lyckegaard, Jens H. Andreasen. A method for predicting the equilibrium state of a long and slender wire on a frictionless toroid was applied to analyse flexible pipe structure. *Materials Science and Engineering*. 2011; 34(1): 391-399.
29. Witz, J. A. A case study in the cross-section analysis of flexible risers. Elsevier BV. 1995; 9(9): 885-904.
30. M.T. Rahmati, B.S. Norouzia, H. Bahaia, G. Alfanoa. Experimental and numerical study of the structural behaviour of a flexible riser model. *Applied Ocean Research*. 2017; 67: 162-168.
31. Péronne, S. et al. (2015). Flexible Pipe Hysteretic Bending Behaviours: Comparison with Experimental Characterization and Finite Element Method. 34th International Conference on Ocean, Offshore and Arctic Engineering. Volume 5A: Pipeline and Riser. 2015; 5A.
32. E Dendy Sloan, Carolyn Ann Koh et al. Fundamentals and Applications of Gas Hydrates. *Annual Review of Chemical and Biomolecular Engineering*. 2011; 2(1): 237-57.
33. Samim, Soroush Zarinabadi and Amir. Problems of Hydrate Formation in Oil and Gas Pipes Deals. *Australian Journal of Basic and Applied Sciences*, 5(12). 2011; 5(12): 741-745.
34. Sloan, E. Dendy. Introductory overview: Hydrate knowledge development. Center for Hydrate Research, Colorado School of Mines, Golden, Colorado 80401, U.S.A. 2004; 89: 1155-1161.
35. Total, Nigeria. AKPO Field Devekopment Plan (FDP). Lagos: 2008.
36. SHELL, Nigeria. Bonga Field Devekopment Plan (FDP). Lagos: 2005.
37. ESSO, Nigeria. Erha Field Devekopment Plan (FDP). Lagos:; 2005.
38. Bai Y., Bai Q. *Subsea Pipelines and Risers*. 497499th ed.: ELSEVIER Ltd; 2005.
39. DNV-OS-F101. Submarine Pipeline system. Worldwide: 2013.
40. ASME/ANSI. Pipe schedules according to ASME/ANSI B36.10M.; 2000.
41. ISO. ISO 13628-2 (Design and operation of subsea production systems- Part 2: Non-bonded flexible pipe systems for subsea and marine applications). , <https://www.iso.org/obp/ui/#iso:std:iso:13628:-2:ed-2:v1:en>; 2006/2007.
42. Bhatui, Ali. Development of a Constitutive Model to Simulate Unbonded Flexible Riser Pipe Elements. United Kingdom: 2008.
43. Leroy, Jean-Marc et al. Stress assessment in armour layers of flexible risers. In; 2010: Proceedings of the ASME 2010 29th International Conference on Ocean, Offshore and Arctic Engineering (ASME).

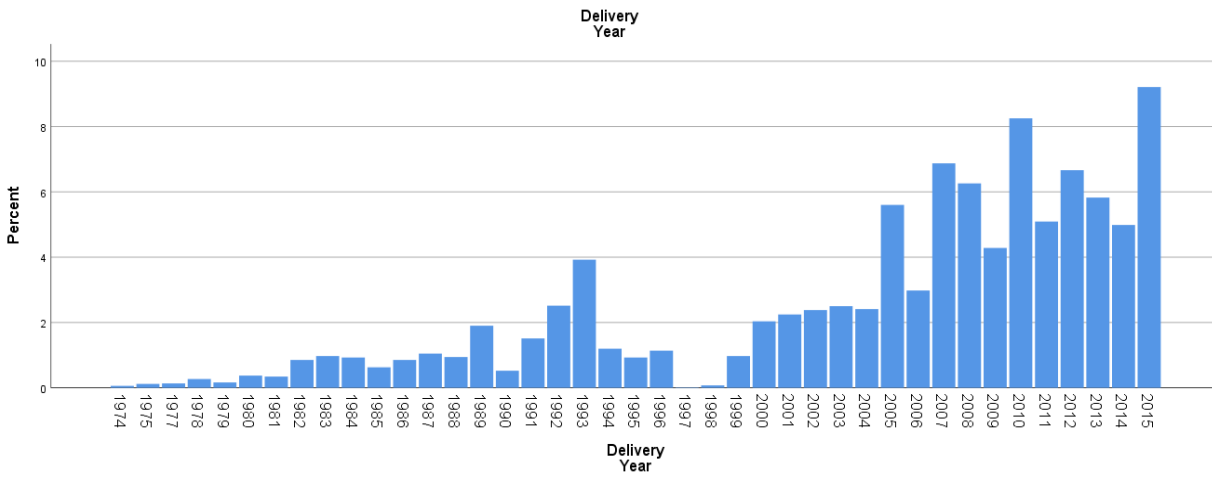
44. Lapidus, L. and Pinder, G.F. Numerical solution of partial differential equations in science and engineering. In; 1982; New York: John Wiley & Sons.
45. Nguyen et.al, Ngoc Linh. Analysis of thin-walled beam-shell structures for concept modelling based on higher-order beam theory. In ; 2017; Korea: Elsevier.
46. José R.M. deSousa, Carlos Magluta, Ney Roitman, Gilberto B. Ellwanger, Edison C.P. Lima Arnaldo Papaleo. On the response of flexible risers to loads imposed by hydraulic collars. Applied Ocean Research. 2009; 31: 157-170.
47. Xiaohua Zhu, Qinglong Lei. Effect of Axial Compression and Wet Collapse Loads on Torsional Response of Flexible Pipe. Arabian Journal for Science and Engineering (2019). 2019; 44: 10397–10408.
48. F. Bolzoni, R. Frassine. ABO 5 - Failure Analysis Flexible Pipe. Final Workshop. Milan: Politecnico di Milano, Dipartimento di Chimica, Materiali e Ingegneria Chimica “Giulio Natta”; 2014.
49. De Sousa, J. R. M. et al. An Experimental and Numerical Study on the Axial Compression Response of Flexible Pipes. Journal of Offshore Mechanics and Arctic Engineering. 2012; 134(3): 31703.
50. OSPAR. The Convention for the Protection of the Marine Environment of the North-East Atlantic OSPAR Decision 98/3 on the Disused Offshore Installations. ; 2013.
51. Bond, A.J., Hight, D.W. and Jardine, R.J. Design of Piles in Sand in the UK Sector of the North Sea. Offshore Technology Report. 1997.

APPENDIX A

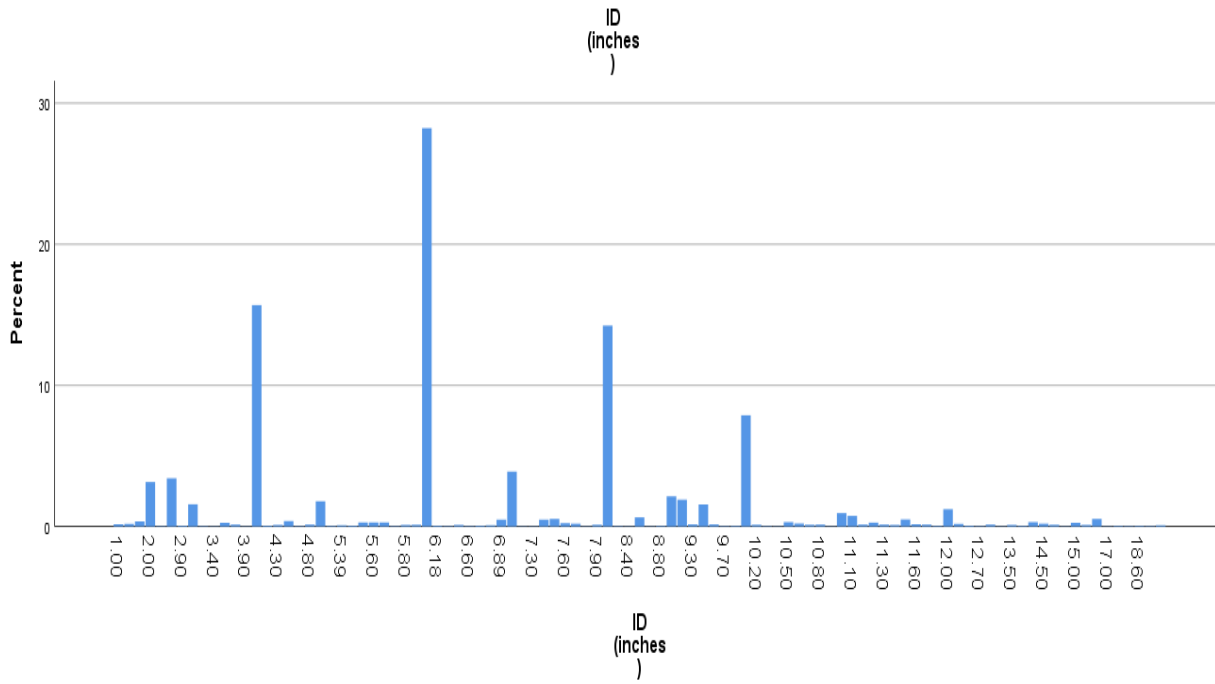
The outlook of flexible pipes usage globally and on a continent basis



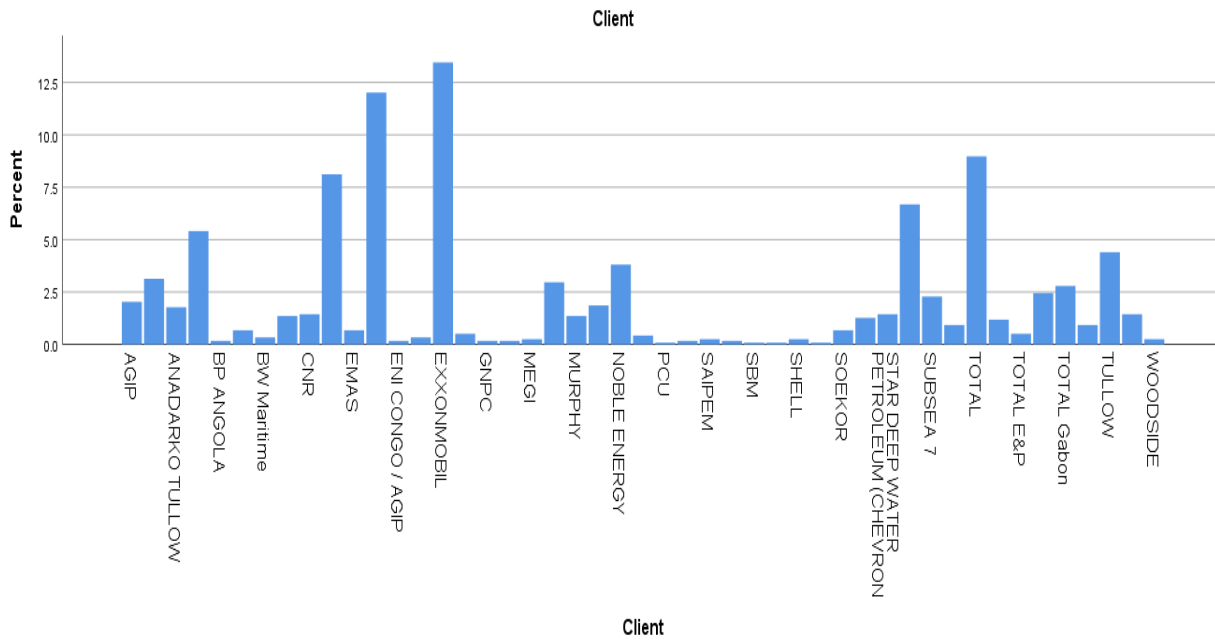
Flexible pipe usage



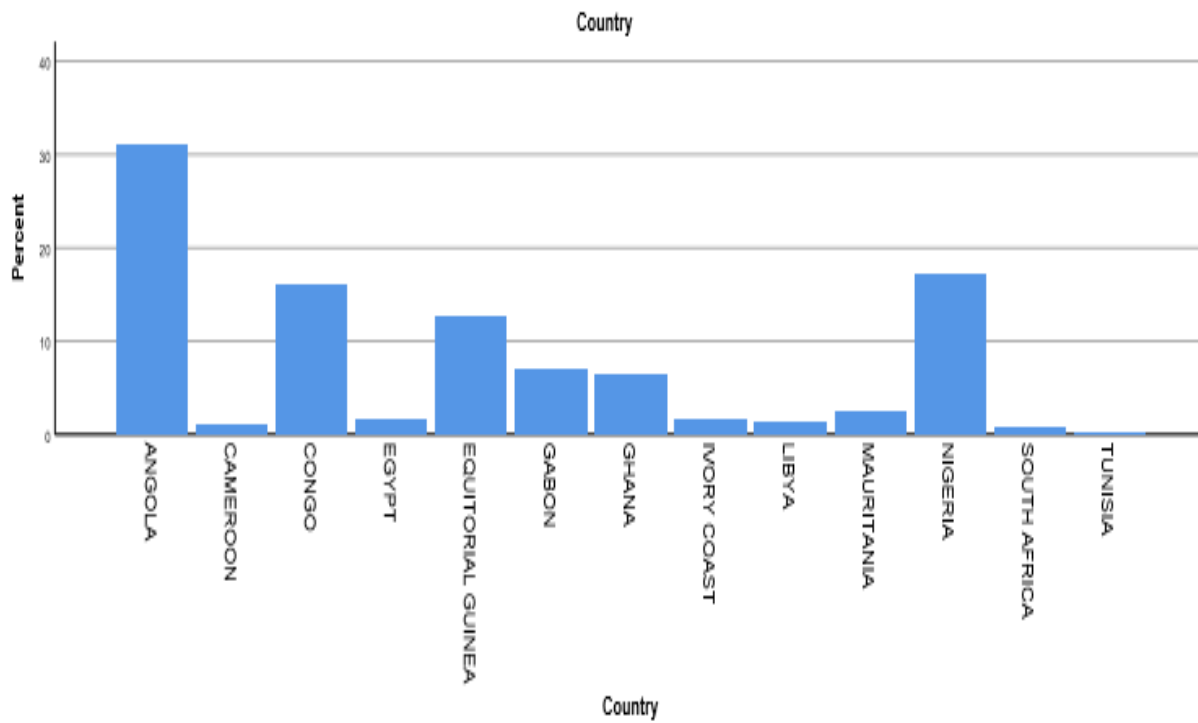
Flexible pipe annual usage



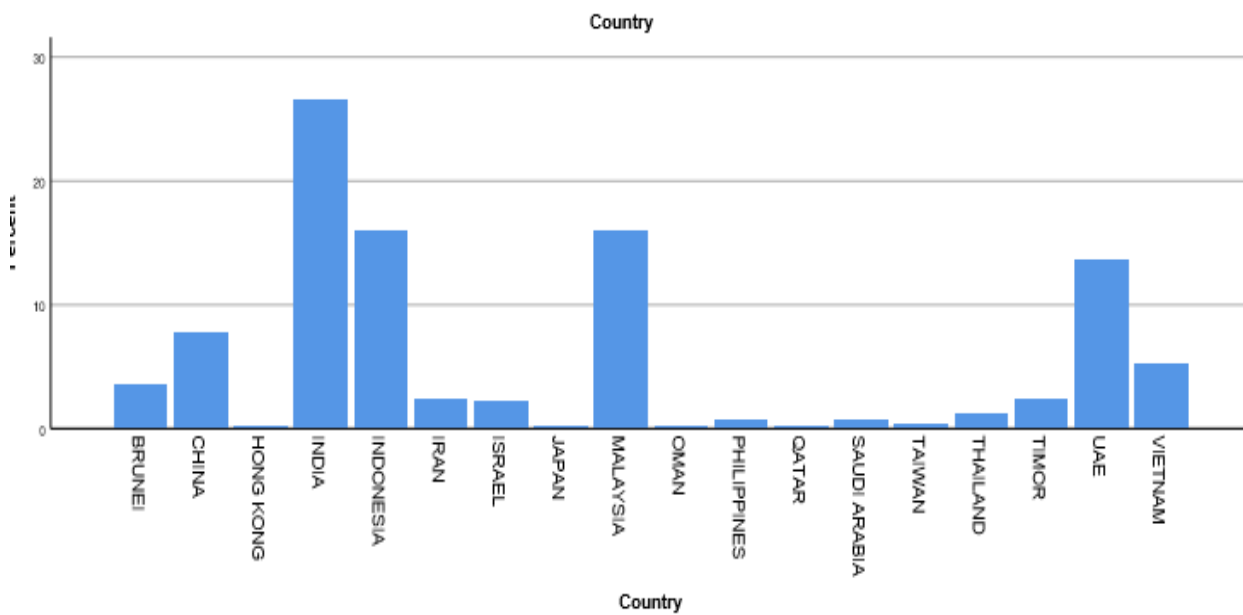
Flexible pipe size distribution and usage



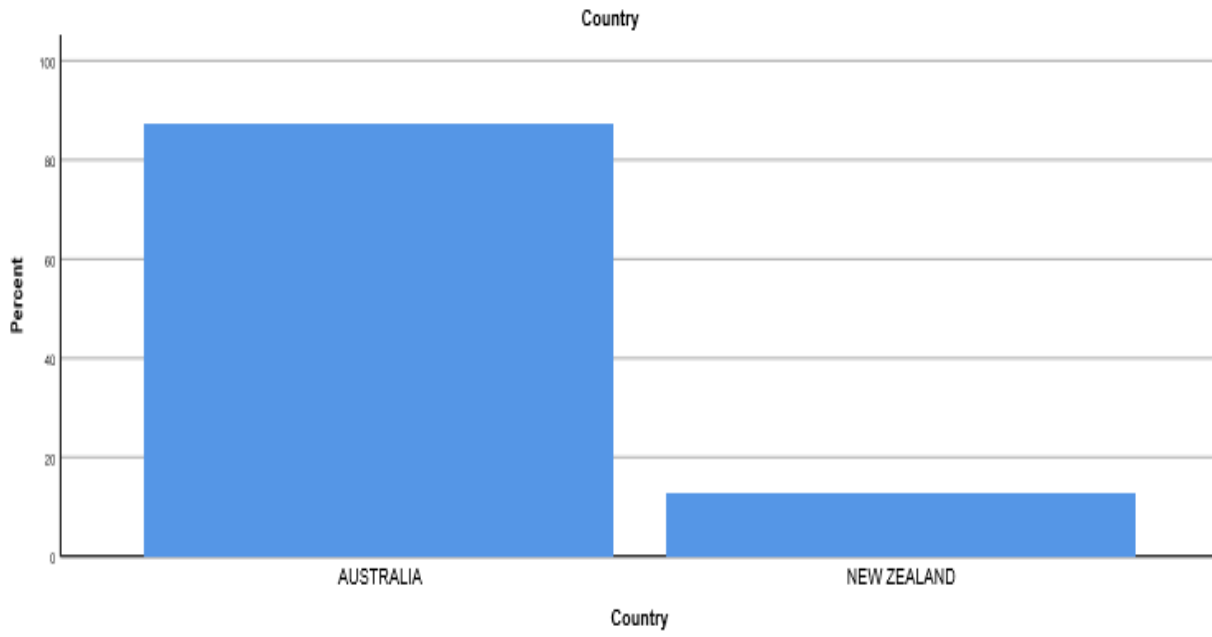
Flexible pipe usage based on Companies



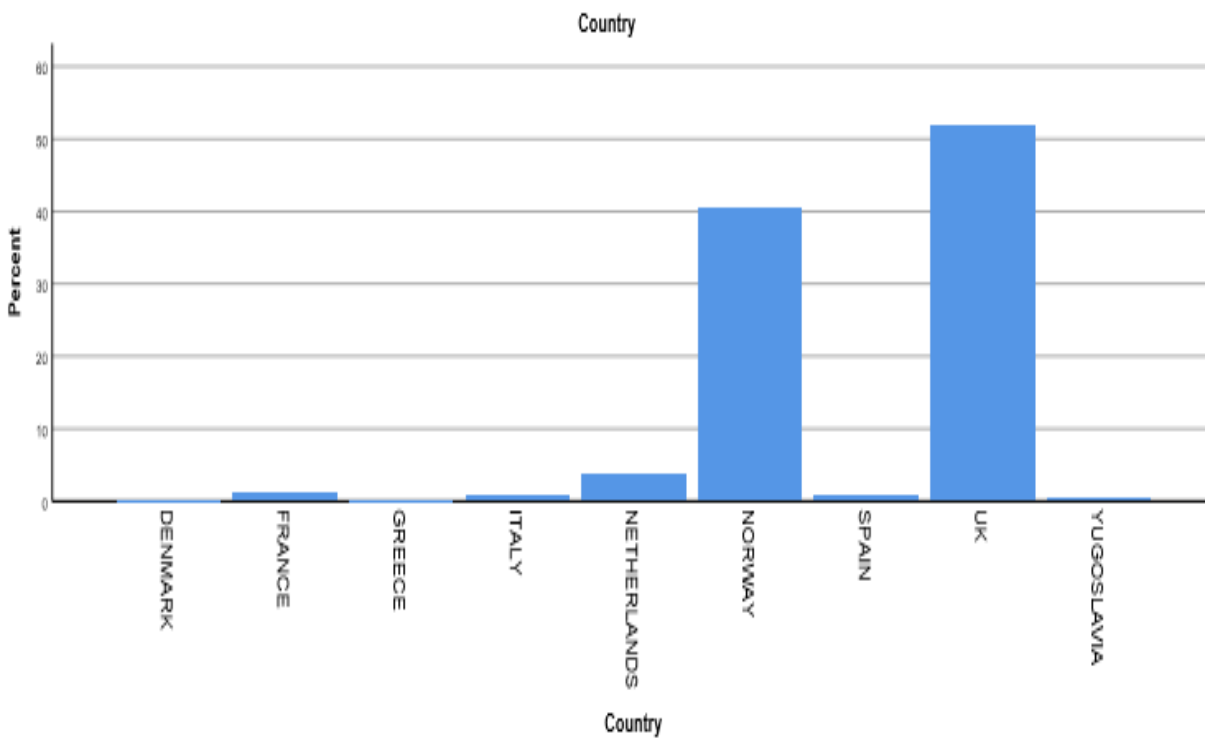
Flexible pipe usage in Africa



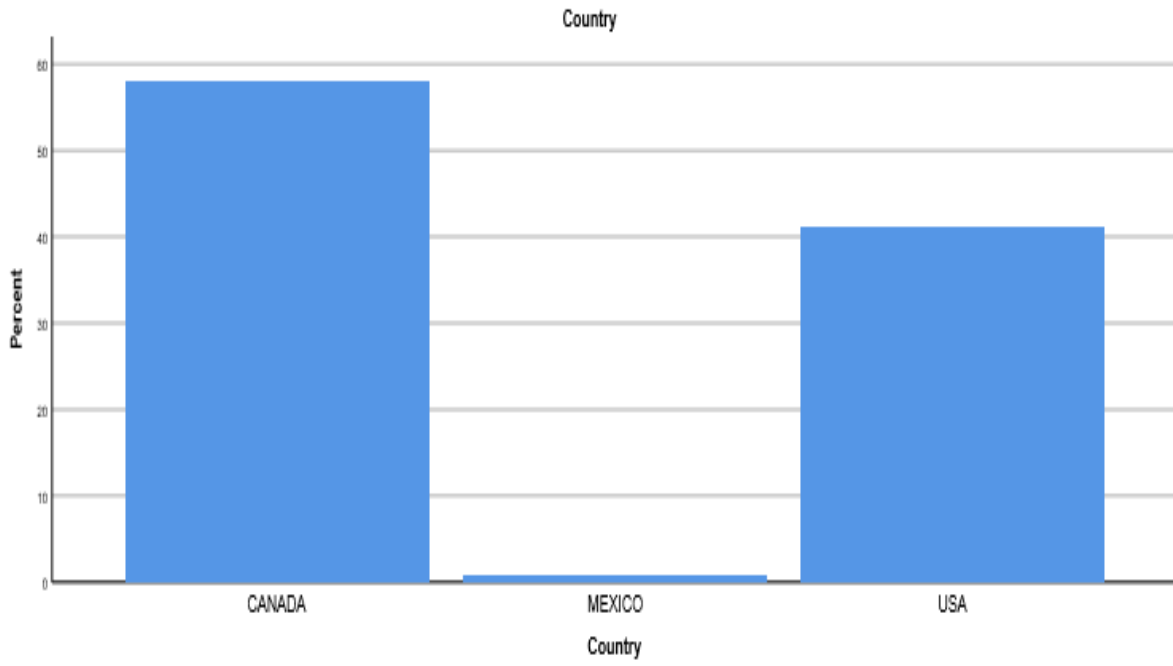
Flexible pipe usage in Asia



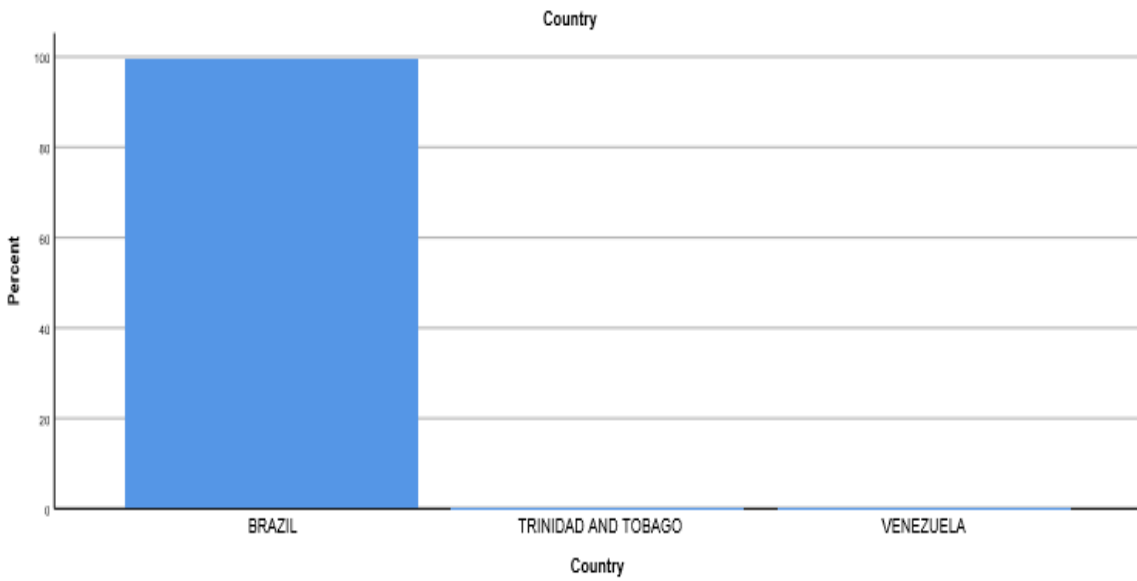
Flexible pipe usage in Australia



Flexible pipe usage in Europe



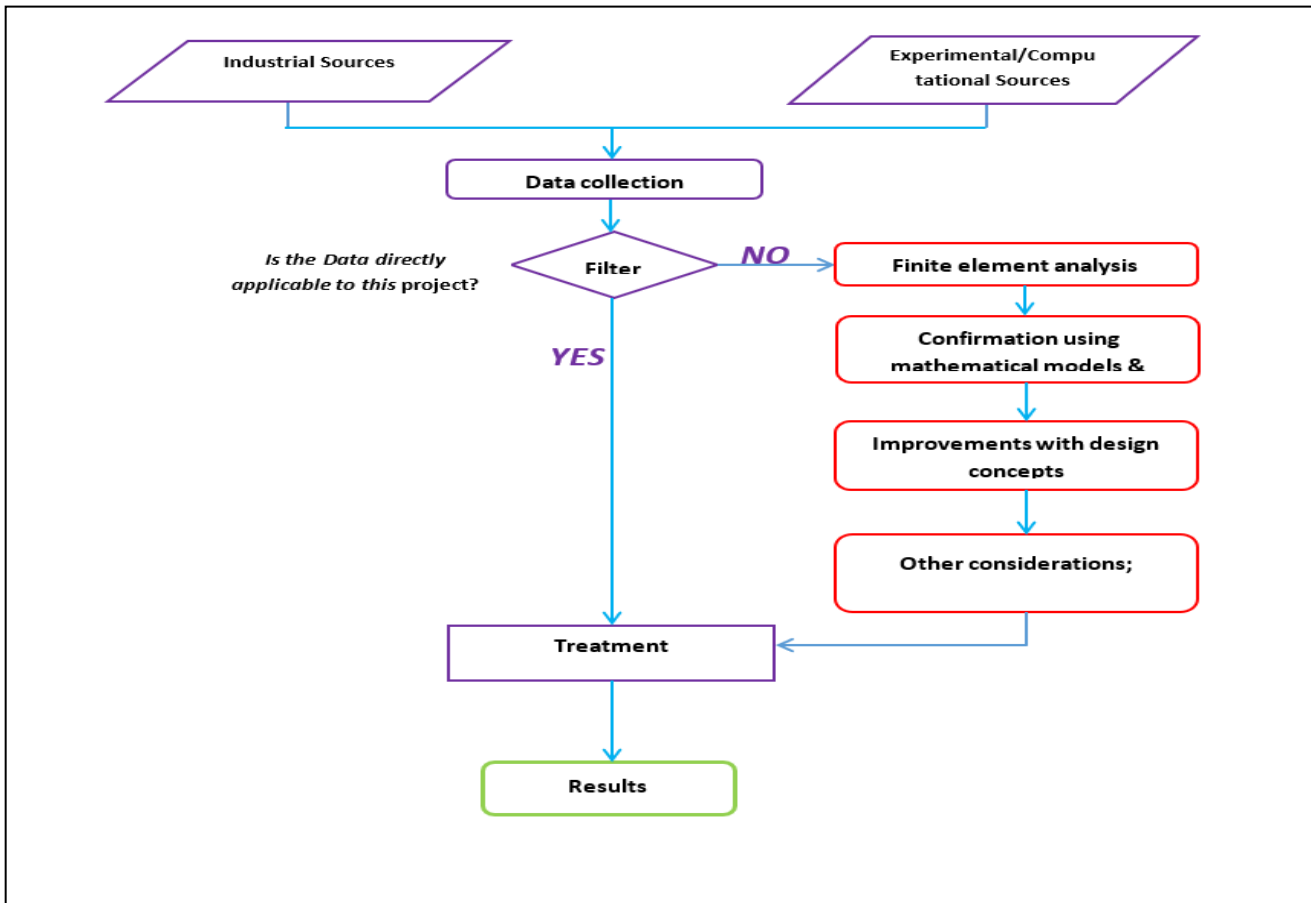
Flexible pipe usage in North America



Flexible pipe usage in South America

APPENDIX B

Adopted Approach- Flow Chart



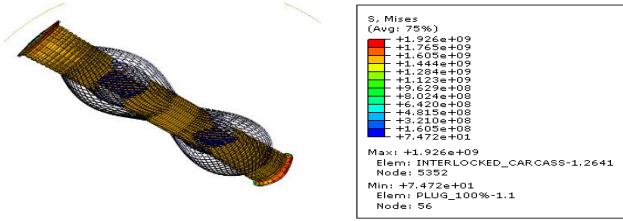
The

approach used in this research

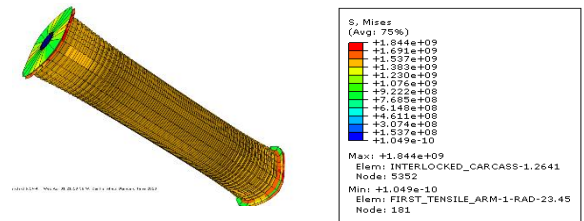
APPENDIX C

LOAD CONDITIONS CONSIDERED

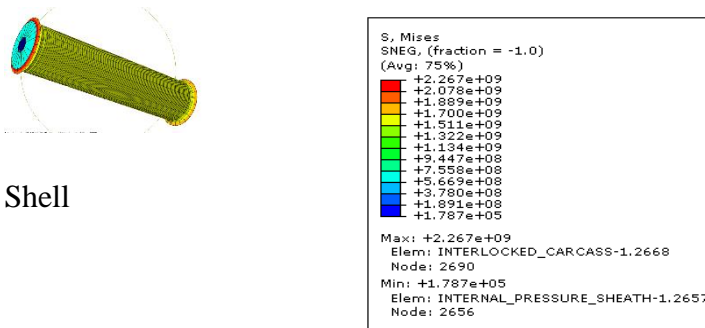
Load case 1: Internal Pressure



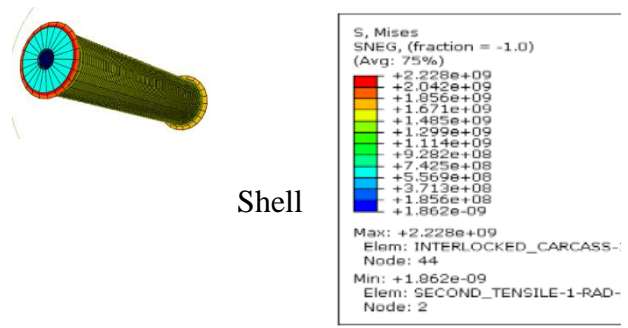
(a) Solid



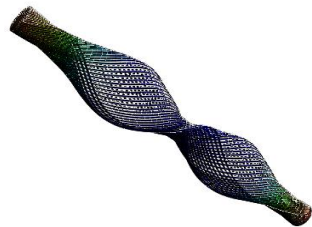
(b) Solid



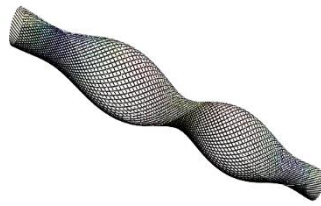
Shell



Shell



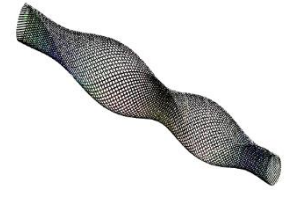
Solid



Shell



Solid



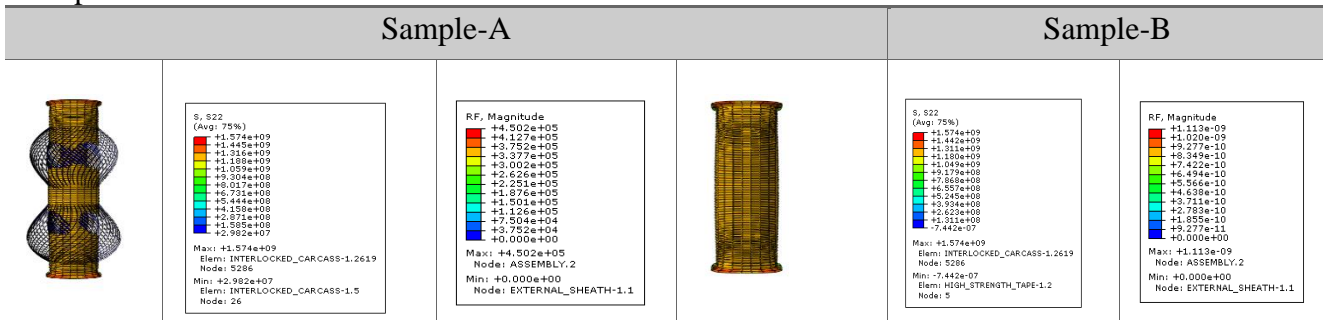
Shell

First Tensile

Second Tensile

The pipe under investigation shows similar deformation with Sample A and B

Hoop stress and the Reaction force



** 0.0005588 Pa and not measured in MPa

Load case 2: External Pressure

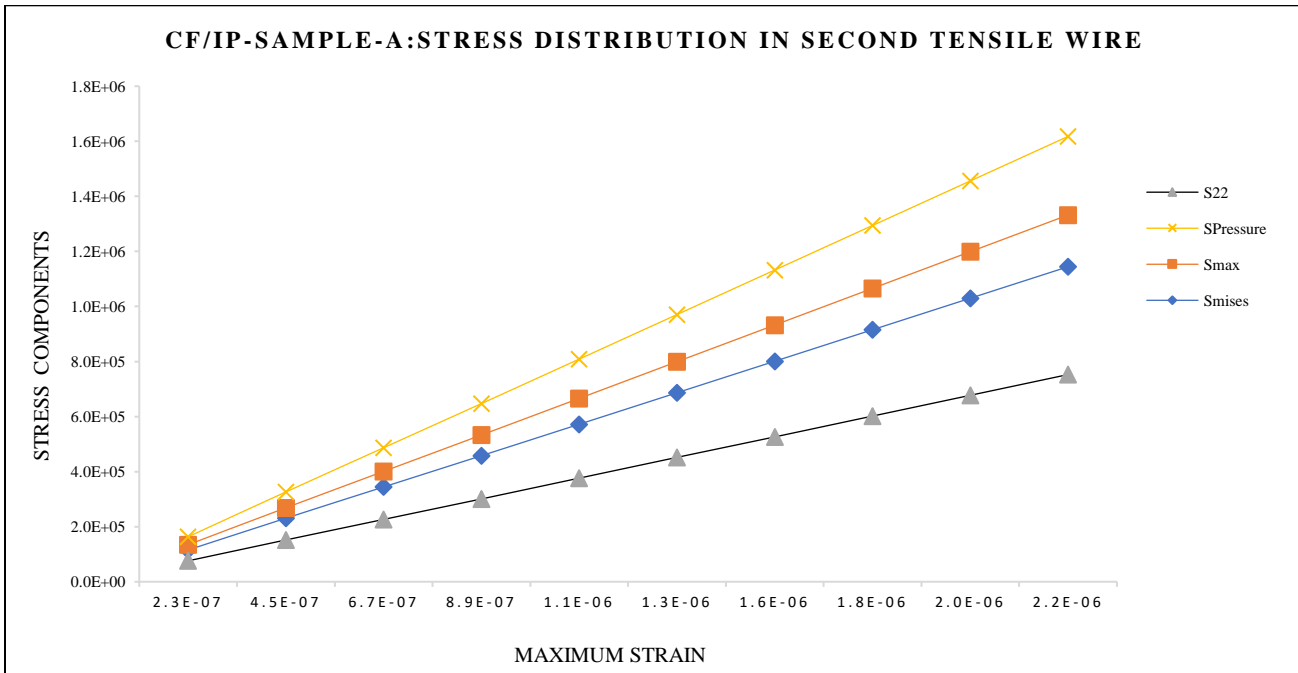
Hoop stress, Displacement and Reaction force for Sample-A and Sample-B layers

| Load type | Frictionless, stiffness constant=0.00001 | | | | | |
|----------------------|--|-----------------------|--------|--------------------------|-----------------------|--------|
| | Sample-A | | | Sample-B | | |
| | S _{mises} (MPa) | S ₂₂ (MPa) | U (mm) | S _{mises} (MPa) | S ₂₂ (MPa) | U (mm) |
| Carcass | 0.1027 | *8.56e-4 | 1.726 | 0.1027 | *8.56e-4 | 1.726 |
| Pressure Sheath | 0.5884 | 0.1532 | 1.726 | 0.5884 | 0.1532 | 1.726 |
| Zeta Pressure Armour | 85.23 | *3.67e-4 | 1.726 | 85.23 | *3.67e-4 | 1.726 |
| First Tensile | 0.451 | 0.161 | 1.728 | 0.451 | 0.161 | 1.728 |
| Second Tensile | 1.20 | 0.208 | 2.513 | 1.20 | 0.208 | 2.513 |
| High Strength Tape | 72.11 | 8.493 | 1.726 | 72.11 | 8.493 | 1.726 |
| External Sheath | 245.9 | -15.29 | 0.380 | 245.9 | -15.29 | 0.380 |

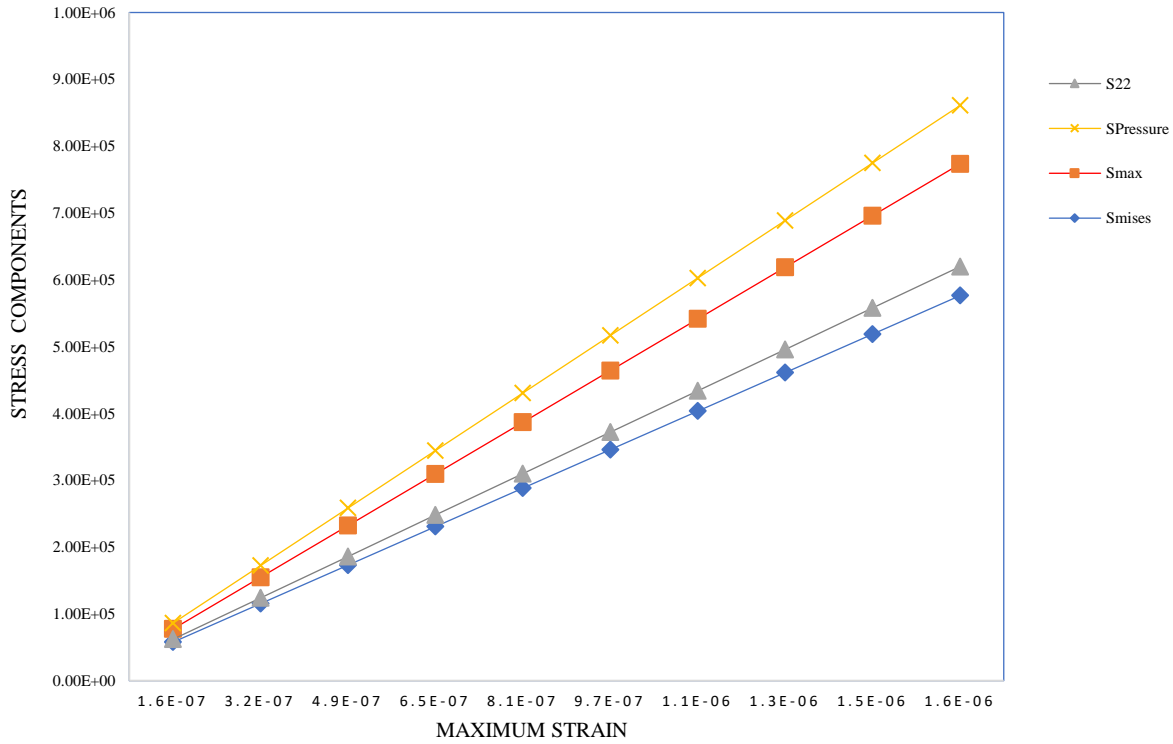
*Measured in Pascal (Pa)

Load case 3: Internal Pressure and Compressive Force

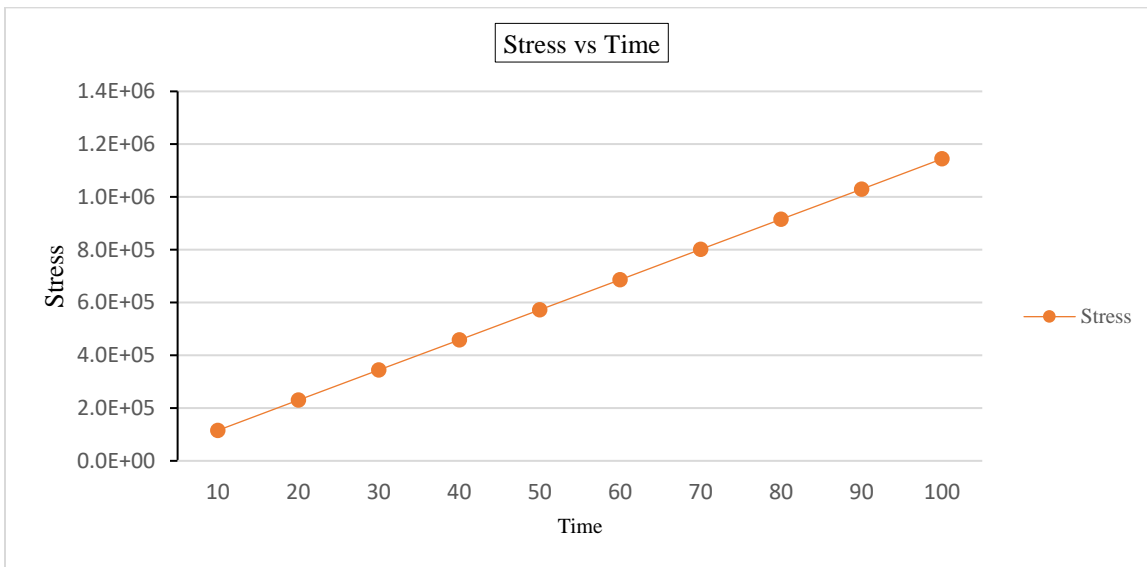
Sample-A & B: Stress Distribution in Second Tensile Wire layer



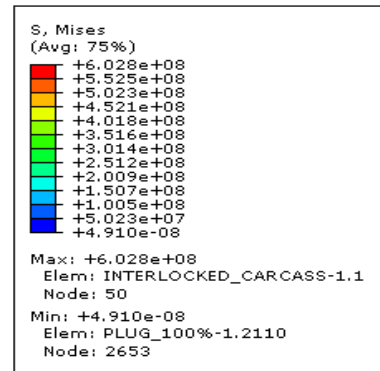
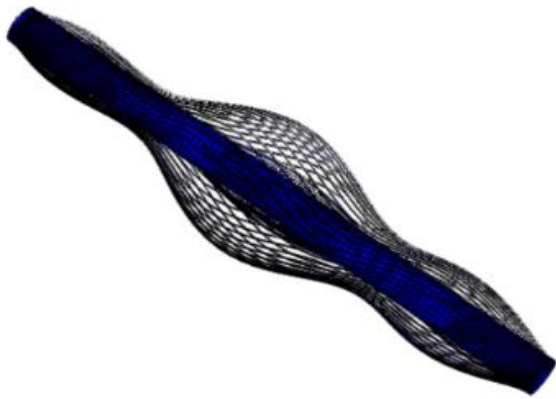
CF/IP-SAMPLE-B: STRESS DISTRIBUTION IN SECOND TENSILE WIRE



Stress vs Time showing an increase in stress value over the set time duration



Load Case 4: Compressive Force



The deformation of the flexibility when pulling force was applied

APPENDIX D

VALIDATION OF JOURNALS

Journal: **Finite Element Investigation on the Tensile Armour Wire Response of Flexible Pipe for Axisymmetric Loading Conditions Using an Implicit Solver**

Authors: Alireza Ebrahimi, Shawn Kenny, and Amgad Hussein

Introduction: The cross-section investigated in this study include the 1) carcass, 2) interior plastic sheath, 3) pressure armour, 4) anti-wear tape, 5) interior tensile armour wires, 6) outer tensile armour wires, 7) anti-bird caging tape, and 8) exterior plastic sheath.

Layer Modelling:

Carcass and Pressure Armour Layer

The carcass layer and pressure armour layer were modelled as hollow pipes putting into consideration their orthotropic nature; thus, engineering constant was used in their material properties and composition, thereby finding their equivalent shear modulus, poisons ratio and Young's Modulus in all three directions of x, y and z.

Please consult the previous report for a method of determining Equivalent materials; Lay angles, shear modulus, Young's modulus and equivalent Poison's ratios

After modelling the carcass and pressure armour layers, orientation angles were assigned to it (see figure 2)

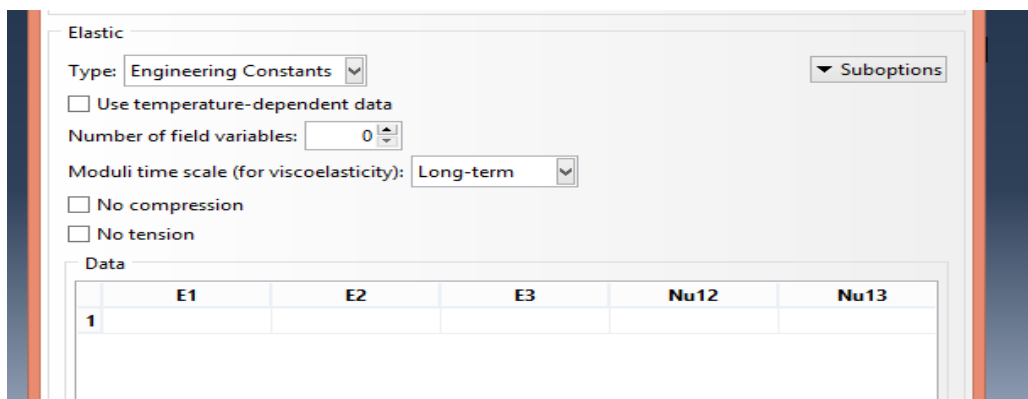


Figure 1: Assigning Orthotropic (Engineering Constant) Material Properties

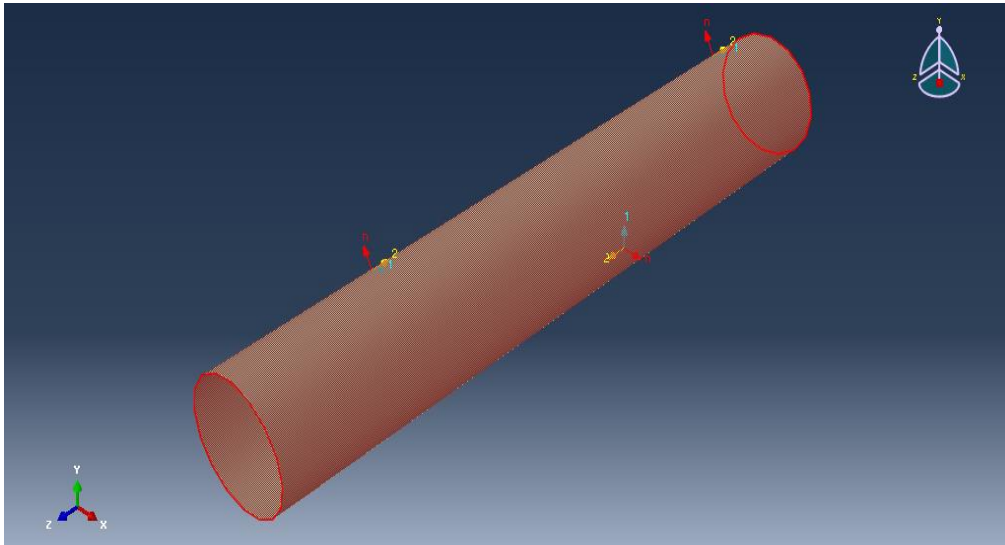


Figure 2: Sample of Carcass layer and Pressure armour layer with orientation assigned

Pressure Sheath, Anti-Wear and Plastic Sheath

These layers were modelled as simple shell (CD4R) hollow pipes with Isotropic materials using the material properties as provided. The cylindrical hollow pipelayers were modelled using extrusion as should in figure 3 below.

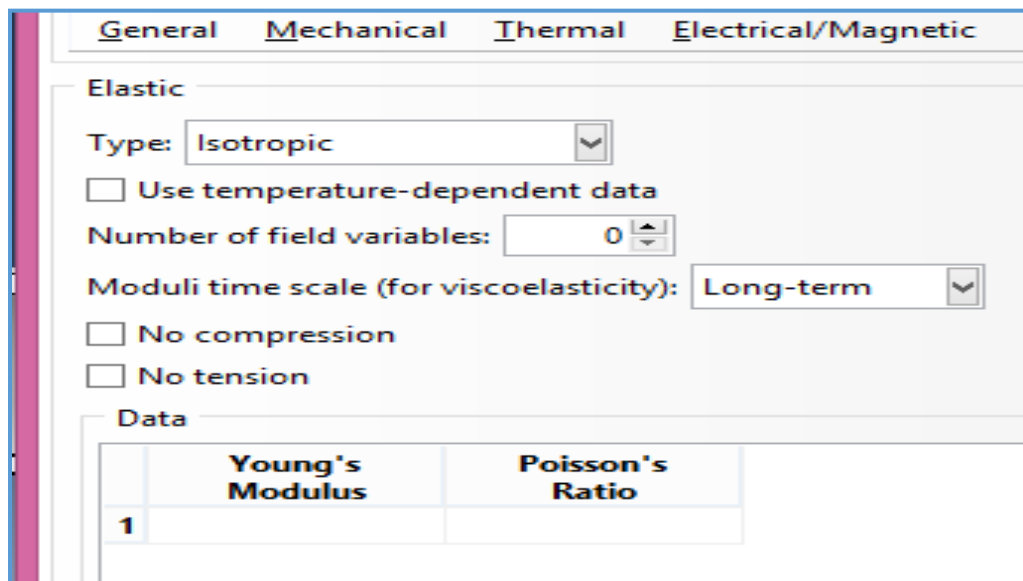


Figure 3: Modelling simple cylindrical hollow pipes

Inner and Outer Tensile Armour layers

The tensile layers were modelled a shell wire using revolution considering the following;

1. Pitch; this is naturally half of the total length of the sample.
2. Angle of revolution

3. Materials orientations were also assigned for tensile wires, as shown in figure five for the following

- Primary axis
- Normal axis

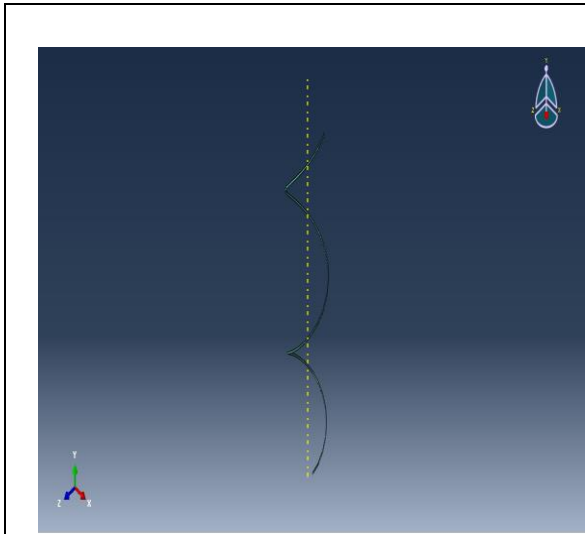


Figure 4: Tensile Wire Pitch

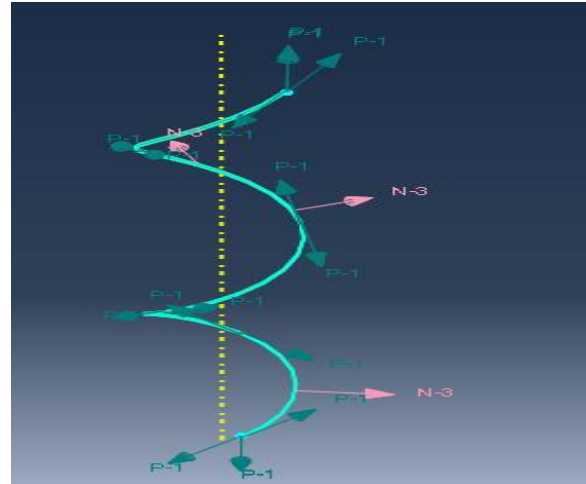
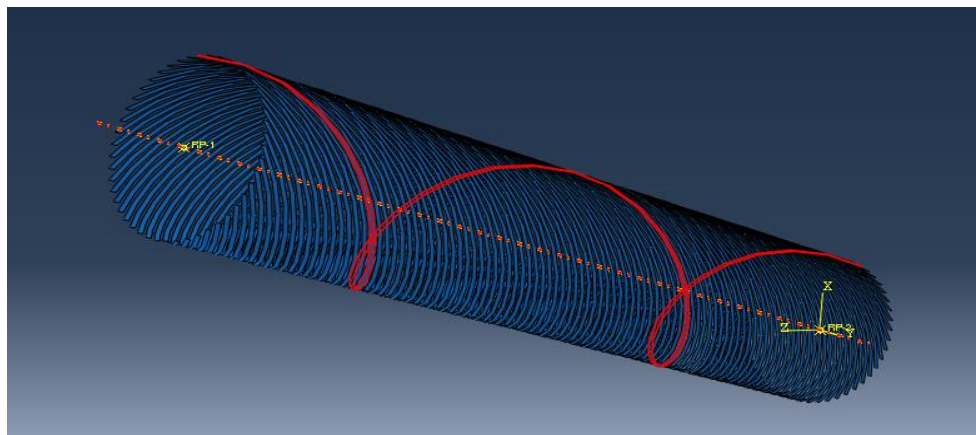
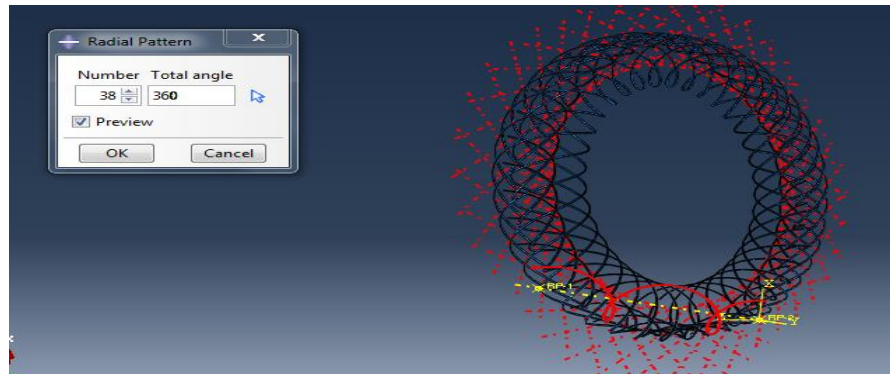
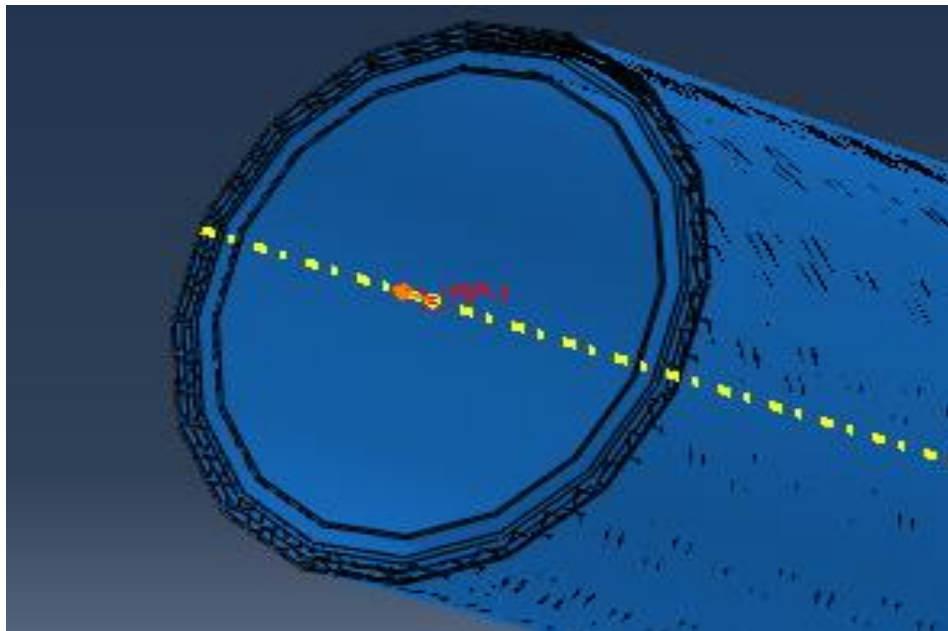
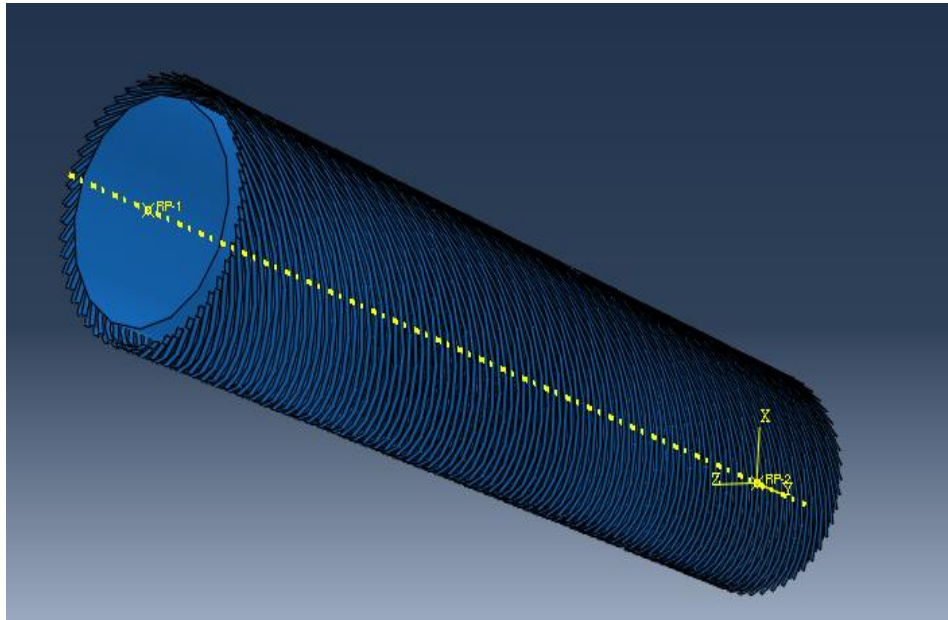


Figure 5: Tensile Wire with Orientation



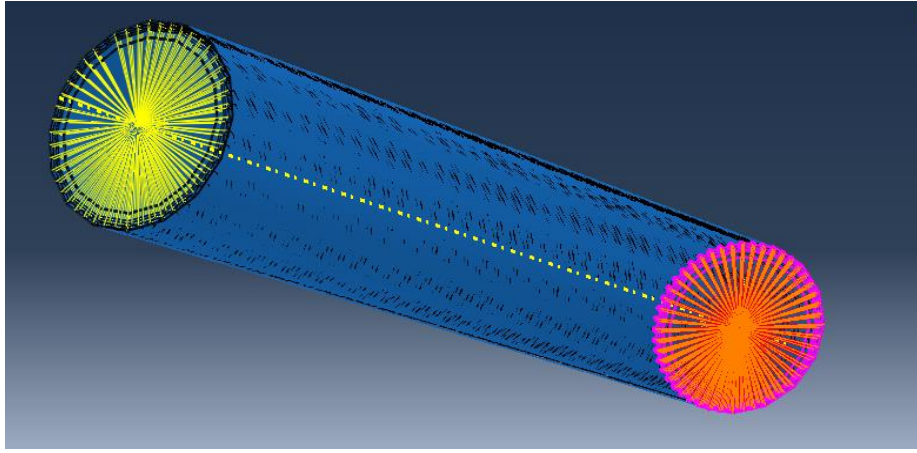
Assembled Layers



Constrains

To apply boundary conditions and loading in uniform distribution, all layers were constrained to a reference point at the Centre, as shown in the figure below.

The kinetic coupling method was used.



Boundary Conditions

The end boundary conditions were imposed through a reference node located at each end of the pipe segment. Coupling the end nodes of the elements in six degrees of freedom with the reference node simulated the axial and radial constraint of the end fitting.

Loading Conditions

Load case investigates the influence of external (5 MPa) and internal pressure (10 MPa) with torsion (± 8 kN.m) on the mechanical pipe response. For these load cases, the essential boundary conditions were to define one end fixed while the other pipe end was free to rotate with the axial degree of freedom restrained or free to elongate.

Contact Mechanics and Frictional Coefficient.

For the numerical simulations, normal hard contact with varying frictional coefficients in the tangential direction was defined. The penalty algorithm was used for both normal and tangential directions in which the contact stiffness factor is calculated (i.e., in the normal direction) based on penetration of the master surface into the slave surface. A frictional coefficient of 0.2 was used to create interaction for this numerical analysis. The interactions were considered for all layers in exclusion of the tensile armour layers due to the complexity. It is therefore presumed that all works on flexible pipes considered no contact between the tensile armours.

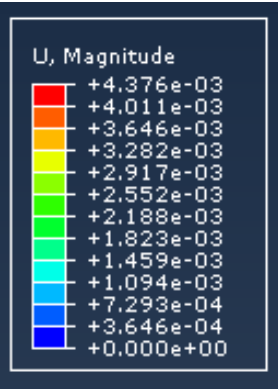
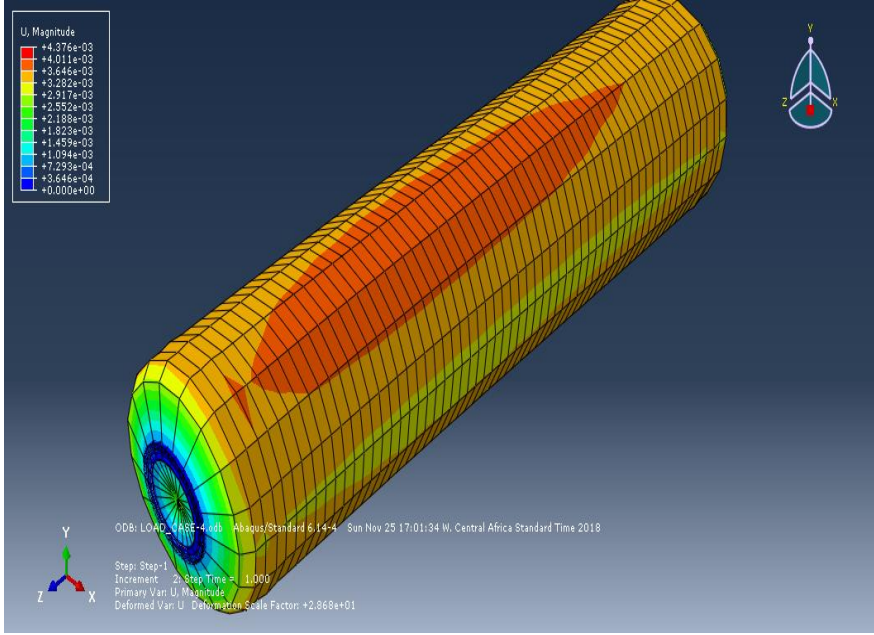
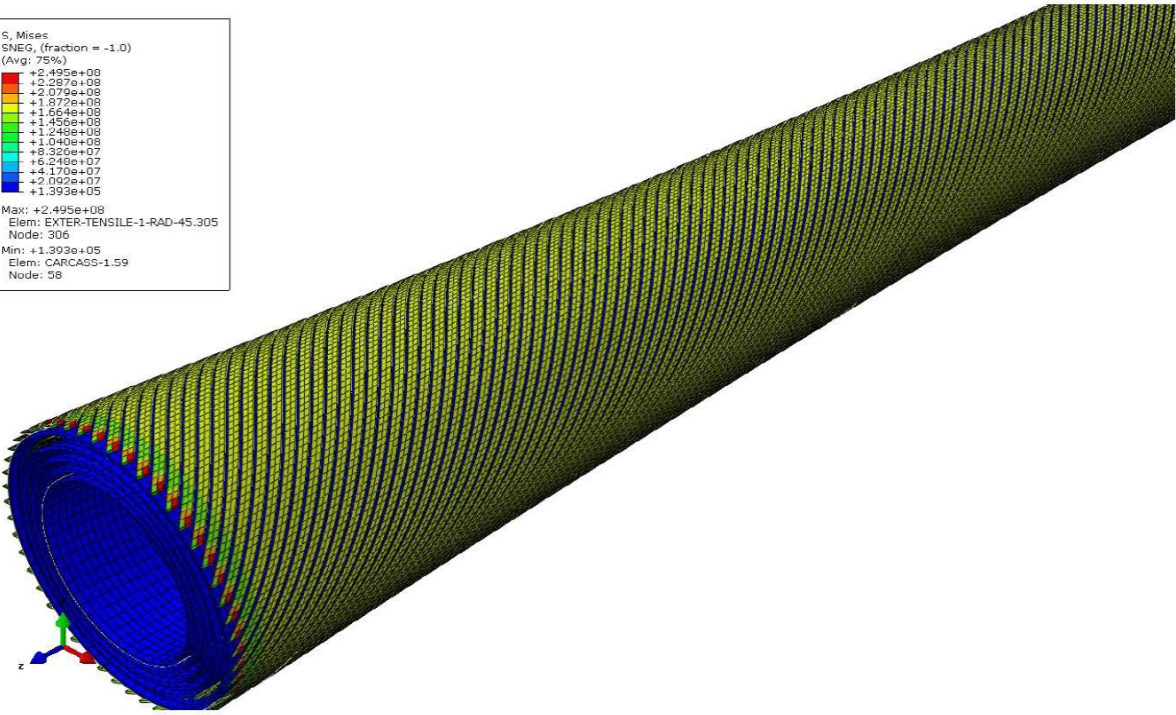
Result and Discussions

S_e Mises
 SNEG, (fraction = -1.0)
 (Avg: 75%)

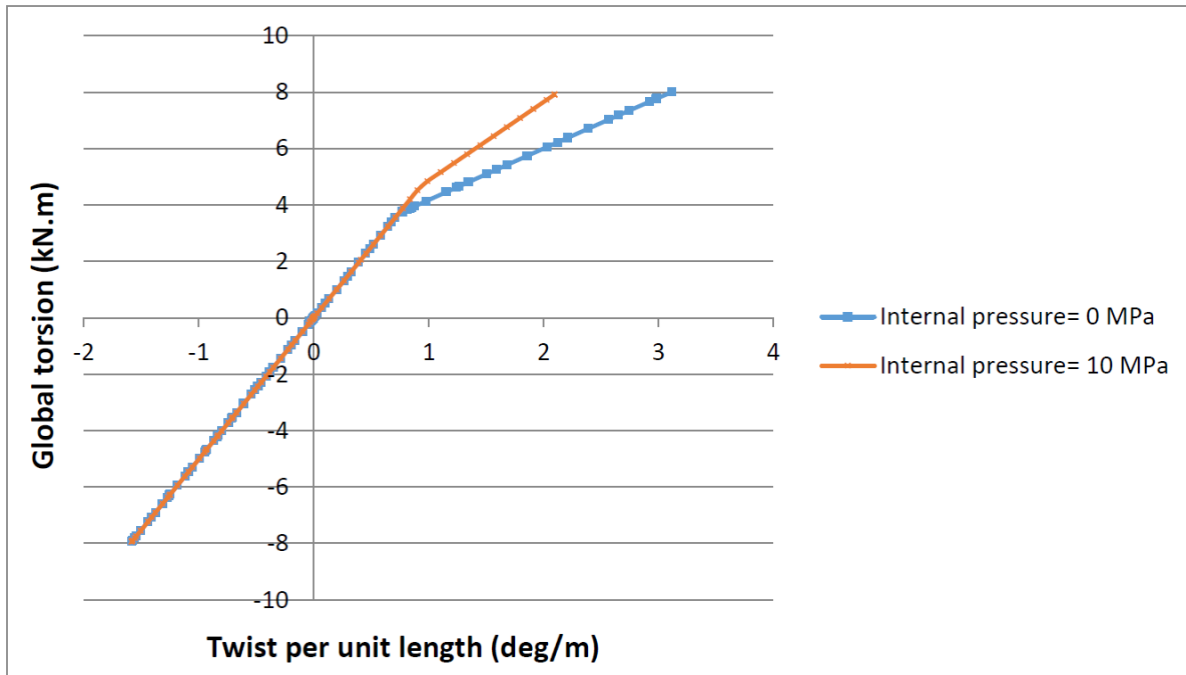
| | |
|---|-----------|
| + | 2.495e+08 |
| + | 2.297e+08 |
| + | 2.079e+08 |
| + | 1.872e+08 |
| + | 1.654e+08 |
| + | 1.456e+08 |
| + | 1.248e+08 |
| + | 1.040e+08 |
| + | 8.320e+07 |
| + | 6.240e+07 |
| + | 4.170e+07 |
| + | 2.090e+07 |
| + | 1.393e+05 |

Max: +2.495e+08
 Elem: EXTER-TENSILE-1-RAD-45.305
 Node: 306

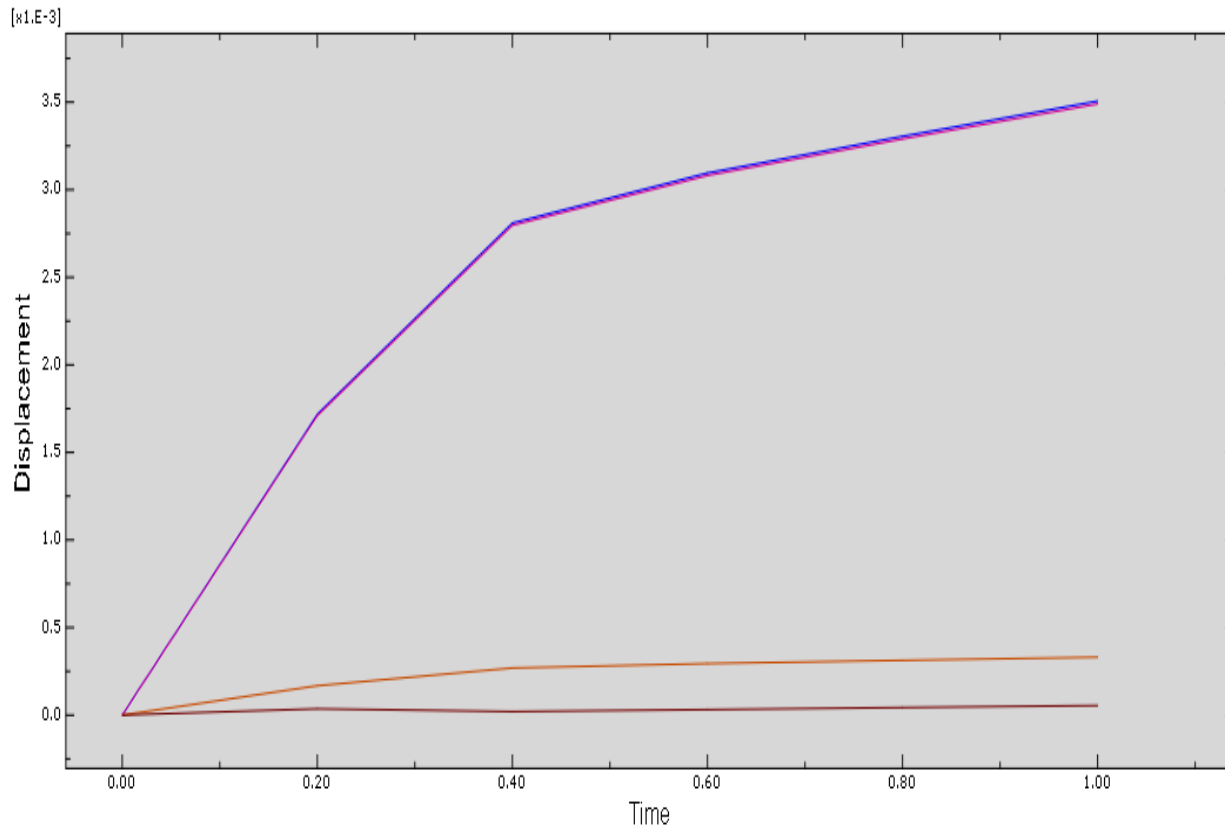
Min: +1.393e+05
 Elem: CARCASS-1.59
 Node: 58



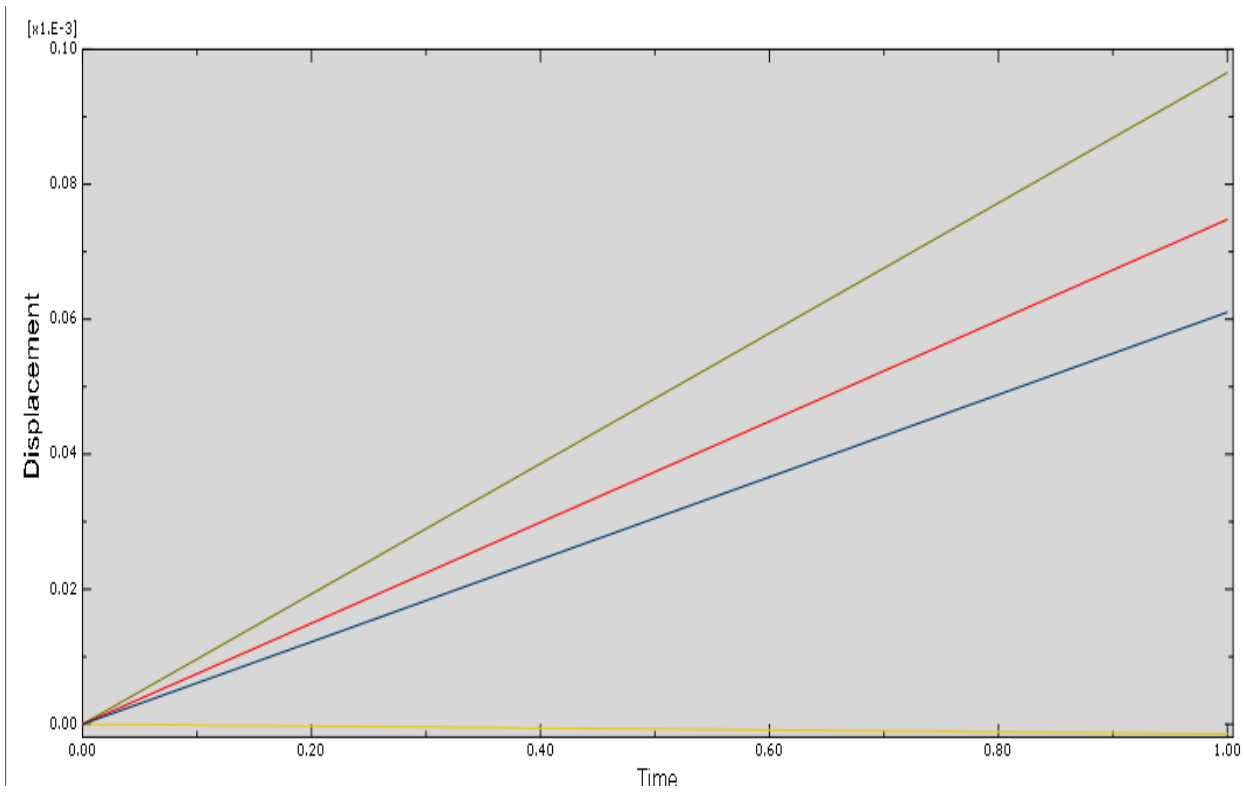
DISPLACEMENT WITH INTERNAL PRESSURE, TORQUE AND EXTERNAL PRESSURE



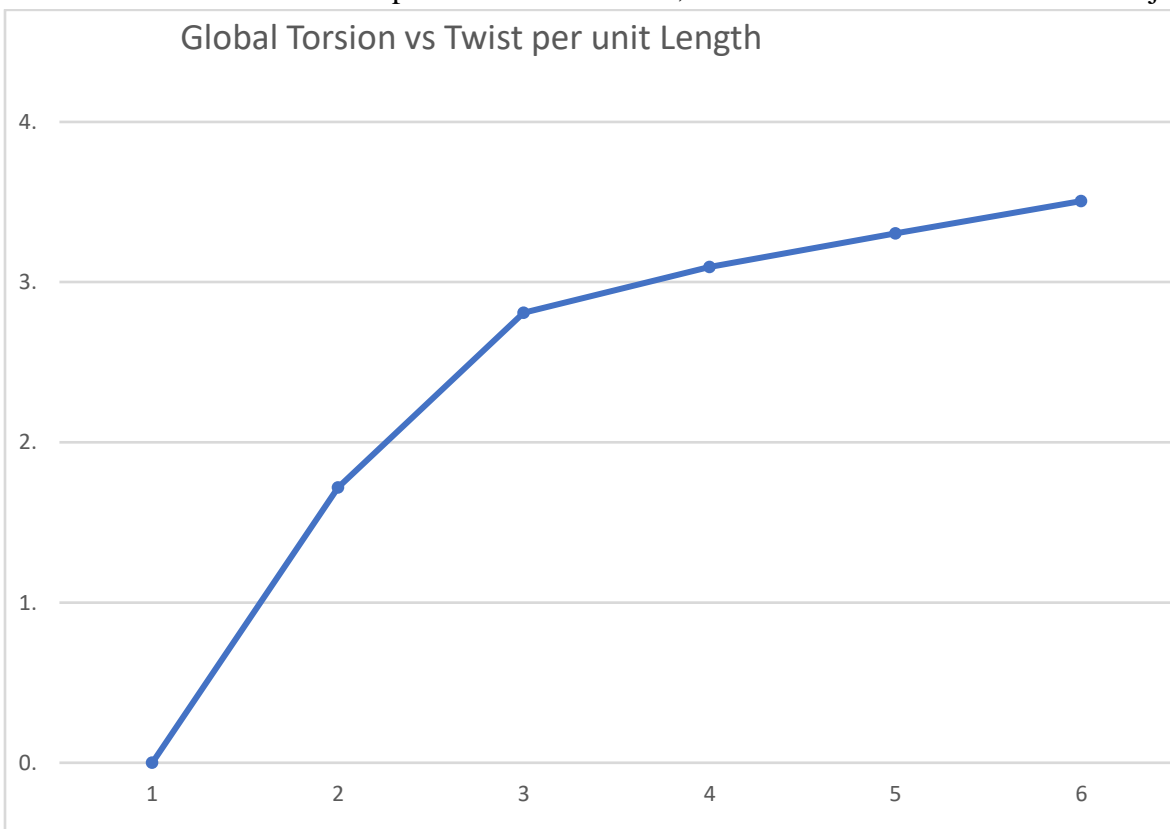
PRESENT WORK ABAQUS VERIFICATION



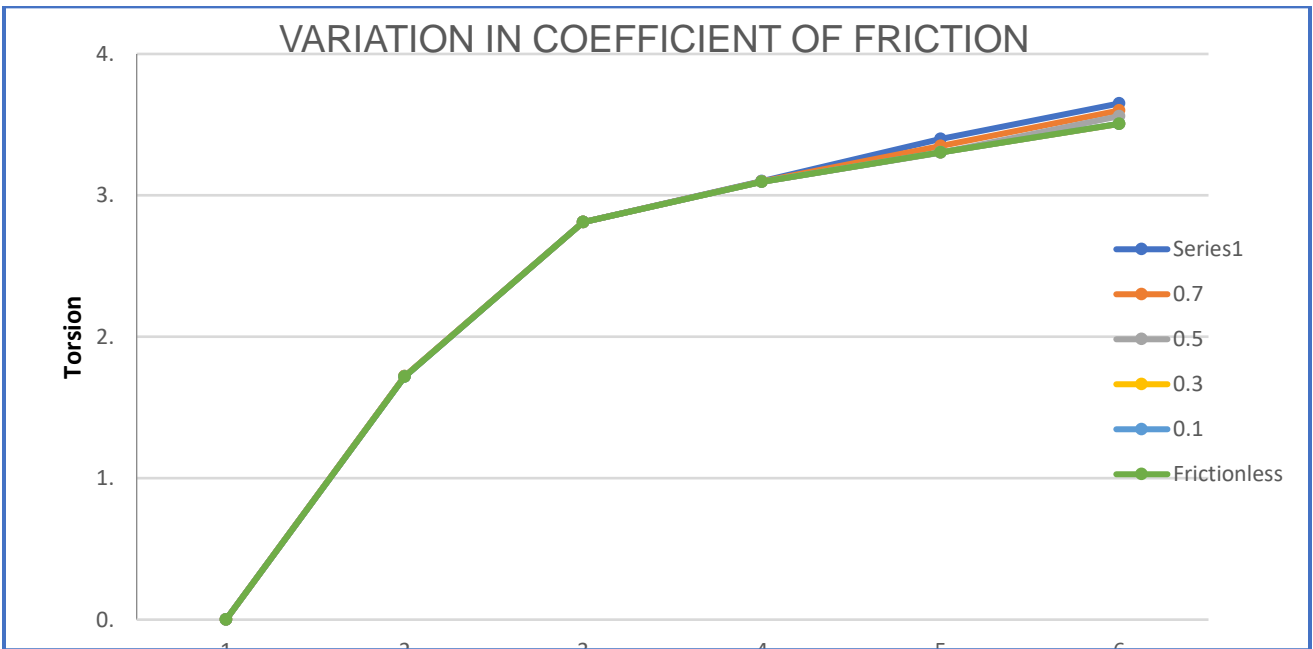
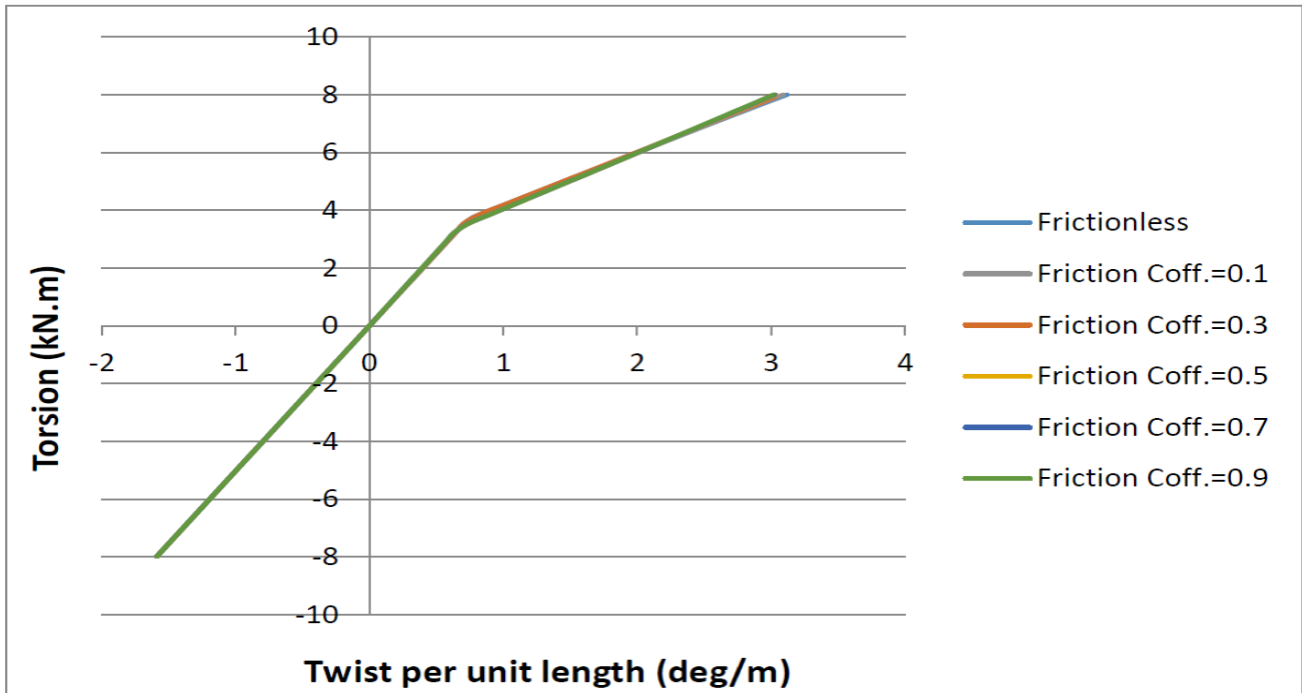
Burification occurred at about 1.5mm in conformance with the journal



No burification when internal pressure was removed, and this is in conformance with the journal result.



Frictional Coefficient Variation



The result showed close conformance with the journal. Frictional coefficient variation showed a minimal effect in displacement resulted. It is worthy to note that the graphs are only considered for positive or clockwise torsion.

Conclusion

The entire results conform with the Journals recommendations

APPENDIX E

DATASHEET

```

INTERNAL DIAMETER      : 6.00"          STRUCTURE REFERENCE : 152.11175
                                JOB REFERENCE : 11658
DESIGN PRESSURE       : 4003 psi ( 276 bars)
FACTORY TEST PRESSURE : 6005 psi ( 414 bars)          SWEET SERVICE
Ratio : FTP/DP =1.50
DESIGN TEMPERATURE   : 80 deg.C
    
```

--- CONFIDENTIAL ---

| ! No | ! LAYER DESCRIPTION | ! UTS | ! MYS | ! Mass | ! I.D | ! Th. | ! SDP |
|--------------------------------|----------------------------------|------------|------------|-----------|---------|--------|-------|
| | | ! MPa | ! MPa | ! kg/m | ! mm | ! mm | ! MPa |
| ! 1 | ! INTERLOCKED CARCASS 48.0 x 1.0 | ! 550 | ! - | ! 11.70 | ! 152.4 | ! 5.0 | ! |
| ! ! | ! AISI 304 (FE 02) | ! ! | ! ! | ! ! | ! ! | ! ! | ! ! |
| ! 2 | ! RILSAN P40TL TP01 PRESSURE SH. | ! ! | ! ! | ! 2.31 | ! 162.4 | ! 4.0 | ! ! |
| ! ! | ! ! | ! ! | ! ! | ! ! | ! ! | ! ! | ! ! |
| ! 3 | ! ZETA WIRE th. 6.2 | ! 1000 | ! - | ! 22.73 | ! 170.4 | ! 6.2 | ! 380 |
| ! ! | ! FM 35 (FI 11) | ! ! | ! ! | ! ! | ! ! | ! ! | ! ! |
| ! 4 | ! FIRST ARMOUR LAY 35.0 deg. | ! 1400 | ! - | ! 8.27 | ! 182.8 | ! 2.0 | ! 403 |
| ! ! | ! High charact.FI41 | ! ! | ! ! | ! ! | ! ! | ! ! | ! ! |
| ! 5 | ! SECOND ARMOUR LAY -35.0 deg. | ! 1400 | ! - | ! 8.39 | ! 186.8 | ! 2.0 | ! 461 |
| ! ! | ! High charact.FI41 | ! ! | ! ! | ! ! | ! ! | ! ! | ! ! |
| ! 6 | ! HIGH STRENGTH TAPE | ! ! | ! ! | ! 0.40 | ! 190.8 | ! 1.25 | ! ! |
| ! ! | ! 1 TAPE (BA09 KV 400daN;130 mm) | ! ! | ! ! | ! ! | ! ! | ! ! | ! ! |
| ! 7 | ! EXTERNAL SHEATH | ! ! | ! ! | ! 2.81 | ! 193.3 | ! 4.8 | ! ! |
| ! ! | ! FINATHENE (TP 04) | ! ! | ! ! | ! ! | ! ! | ! ! | ! ! |
| ! THEORETICAL CHARACTERISTICS | | ! IMPERIAL | | ! METRIC | | | |
| ! DIAMETER | ! inside | ! 6.00 | ! in | ! 152.40 | ! mm | ! ! | ! ! |
| ! ! | ! outside | ! 7.99 | ! in | ! 202.90 | ! mm | ! ! | ! ! |
| ! VOLUME | ! internal | ! 0.207 | ! cf/ft | ! 19.22 | ! l/m | ! ! | ! ! |
| ! ! | ! external | ! 0.348 | ! cf/ft | ! 32.33 | ! l/m | ! ! | ! ! |
| ! WEIGHT | ! in air empty | ! 38.05 | ! lbf/ft | ! 56.61 | ! kgf/m | ! ! | ! ! |
| ! ! | ! in air full of sea water | ! 51.29 | ! lbf/ft | ! 76.31 | ! kgf/m | ! ! | ! ! |
| ! ! | ! in sea water empty | ! 15.77 | ! lbf/ft | ! 23.47 | ! kgf/m | ! ! | ! ! |
| ! ! | ! in sea water full of sea water | ! 29.02 | ! lbf/ft | ! 43.17 | ! kgf/m | ! ! | ! ! |
| ! SPECIFIC GRAVITY | ! in sea water empty | ! ! | ! ! | ! 1.71 | ! ! | ! ! | ! ! |
| ! PRESSURE | ! Nominal bursting | ! 9490 | ! psi | ! 654 | ! bars | ! ! | ! ! |
| ! ! | ! Hydrostatic collapse | ! 1700 | ! psi | ! 117 | ! bars | ! ! | ! ! |
| ! DAMAGING PULL | ! in straight line | ! 392865 | ! lbf | ! 1747.79 | ! kN | ! ! | ! ! |
| ! MINIMUM BENDING RADIUS | ! for STORAGE | ! 4.33 | ! ft | ! 1.32 | ! m | ! ! | ! ! |
| ! BENDING STIFFNESS | ! at 20 deg.C | ! 32739 | ! lb.ft2 | ! 13.53 | ! kN.m2 | ! ! | ! ! |
| ! RELATIVE ELONGATION | ! at design pressure | ! ! | ! ! | ! 0.233 | ! % | ! ! | ! ! |
| ! RELATIVE ELONGATION | ! for 50 kN | ! ! | ! ! | ! 0.027 | ! % | ! ! | ! ! |
| ! THERMAL EXCHANGE COEFFICIENT | ! at 20 deg.C | ! 8.09 | ! Btu/hftF | ! 14.00 | ! W/m.K | ! ! | ! ! |

Summary of the Research Analyses on Non-bonded flexible Pipe

| 1st Author | 2nd Author | 3rd Author | Date | Publisher | Paper Name/Title | Summary of the Paper |
|-------------------------|-----------------------|------------------------|------|--|---|--|
| Anders Simonsen | | | 2014 | Master's Thesis | Inspection and monitoring techniques for unbonded risers and pipelines | Master's paper on the inspection and monitoring of non-bonded flexible risers. There are a few mentions of hydrates forming in the pipes and problems these can cause (erosion, blockage, etc.). Attractive section from experimental data from Norway breaking down all the different layers, the possible defects in these layers, the consequence of these defects and the possible causes. Hydrates probable cause for hole/ crevice/ pitting/ thinning and unlocking deformation of the carcass layer. |
| R. Cuamatzi-Melender | O. Castillo-Hernandez | A.O. Vazquez-Hernandez | 2017 | Ocean Engineering | Finite element and theoretical analyses of bisymmetric collapses in flexible risers for Deepwater's development | This work presents analytical and finite elements modelling strategies to study both types of collapse risers fabricated with an "S" carcass profile to predict collapse failure. The developed methodologies were applied to a 50.8 mm (2 in.) non-bonded flexible riser. The results showed the importance to performs 3D finite element modelling for a proper carcass design and collapse assessment, calibration of the length of the finite element models and boundary conditions defined to obtain reliable results and computer time optimization. It was also found a difference in collapse loads for each type of collapse: for ovality type collapse, the development of a finite element of the carcass only is sufficient, but for the eight types of failure, it is necessary to develop a finite element model including carcass, internal polymer sheath and pressure armour. Furthermore, it was found that the analytical formulations developed to date can only evaluate the collapse properties of the carcass. Still, they are limited to be used for the design of the carcass for flexible risers. |
| Xu Yang | Svein Sarvik | Liping Sun | 2015 | Ocean Engineering | Numerical analysis of buckling failure in flexible pipe tensile armour wires | Flexible pipes may be exposed to high axial compression and bending during deep-water installation. The compression force is mainly sustained by the tensile armour layers, which may result in localized lateral or radial buckling failure in these layers. In this paper, a finite element model was created to evaluate the critical instability load of tensile armour wires under external pressure and compression. The tensile armour wires are modelled by curved beam elements under loxodromic assumptions. Other layers' contribution was simplified by spring elements and equivalent beams. The buckling load capacity and associated failure modes are obtained. The results are also compared with the results based on 3D Euler beam elements and results published in the literature. Parametric analyses were further included concerning external pressure, friction modelling and the influence of initial imperfections. |
| Jose Renato M. de Sousa | Paulo F. Viero | Carlos Magluta | 2010 | Researchgate/offshore Mechanics and Arctic Engineering | An experimental and numerical study on the axial compression response of flexible pipes | This paper deals with a nonlinear three-dimensional finite element (FE) model capable of predicting the mechanical response of flexible pipes subjected to axisymmetric loads focusing on their axial compression response. Moreover, to validate this model, experimental tests carried out at COPPE/UFRJ are also described. In these tests, a typical 4" flexible pipe was subjected to axial compression until its failure was reached. Radial and axial displacements were measured and compared to the model |

| | | | | | | |
|---------------|--------------|-------------|------|---------------------------------|--|--|
| | | | | | | predictions. The good agreement between all obtained results points that the proposed FE model is efficient to estimate the response of flexible pipes to axial compression and has the potential to be employed in the identification of the failure modes related to excessive axial compression as well as in the mechanical analysis of flexible pipes under other types of loads. |
| Minggang Tang | Chan Yang | Qianjin Yue | 2015 | Ocean Research | Validity and limitation of analytical models for the bending stress of a helical wire in non-bonded flexible pipes | An analytical model for the prediction of bending behaviour is essential for understanding the mechanism of the local stress distribution in the helical wires of the tension armour layers under alternative curvatures and rapid estimation of the service life of flexible pipes for designers in engineering practice. In this paper, seven analytical models available in the literature are selected and summarized. Although the experimental results reported in the literature are limited, a three-dimensional finite element model is developed for investigation of the seven models, and the validity and limitations of these models for different structural parameters of helical wire are discussed, i.e., the width-thickness ratio of the wire section and helical angle. The analytical model based on spring theory resulted in a satisfactory estimation of bending stress for most cases and is recommended as a tool for the basic design of the helical armour wire structures in flexible pipes. |
| M. T. Rahmati | S. Norouzi | H. Bahai | 2017 | Applied Ocean Research/Elsevier | Experimental and numerical study of the structural behaviour of a flexible riser model | Experimental tests and detailed finite element analyses were carried out on a model of the flexible riser to evaluate the capability of the finite element method to predict its nonlinear structural response. The riser consists of four layers, which include two cylindrical polycarbonate tubes and two steel helical layers. One helical layer represents the carcass layer in a flexible riser, whilst the other represents the riser tendon armour layer. First, bending load experiments on the model are described, which provide some insight regarding the fundamental behaviour of flexible pipe structures. This is followed by the description of the FE models in which all layer components are individually modelled, and a surface-to-surface frictional contact model is used to simulate their interaction. Finally, the FE numerical results were compared with the test data to outline the capacity of the numerical method to predict the response of flexible riser structures. |
| M.A. Vaz | N.A.S. Rizzo | | 2011 | Marine Structure/Elsevier | A finite element model for flexible pipe armour wire instability | In this work, a finite element model is developed to estimate the critical instability load and failure modes. An axisymmetric model is constructed employing a complex combination of beam and spring elements. For each armour layer, only one wire needs to be modelled. Hence the computational cost is minimized without compromising the phenomenon characterization. A parametric case study is performed for a typical flexible pipe structure, where the friction coefficient between the wire armours and the external pressure is varied, and the critical instability loads and failure modes are obtained, and results are discussed. |

| | | | | | | |
|----------------------|------------------|------------------|------|--------------------|--|---|
| E.O. Obanijesu | V. Pareek | R. Gubner | 2011 | NAFTA | Hydrate formation and its influence on natural gas pipeline internal corrosion | This study establishes the ability of hydrate formation to initiate internal corrosions along natural gas pipelines. The identified corrosion types, which are cavitation's, erosion and corrosions by chemical reactions, are capable of individually or collectively initiating pitting and stress cracking corrosions which are also dangerous to gas pipelines. The impacts of these corrosion types are classified as an economic, environmental and human loss with the economic loss of as much as US\$3 trillion depending on the pipe length, location, sea depth, wave function, climatic conditions and political situations. Various predictive measures to minimize hydrate formations are finally recommended. |
| J. Y. Li, Z. X. Qiu, | J. S. Ju | | 2015 | Hindawi | Numerical Modelling and Mechanical Analysis of Flexible Risers | Abaqus CAE is used to create a detailed finite element model for a 10-layer non-bonded flexible riser to simulate the riser's mechanical behaviour under three load conditions: tension force and internal and external pressure. It presents a technique to create a detailed finite element model and to analyse flexible risers. In the FEM model, all layers are modelled separately with contact interfaces; interaction between steel trips in certain layers has been considered as well. FEM model considering contact interaction, geometric nonlinearity, and friction has been employed to accurately simulate the structural behaviour of the riser. The model includes the main features of the riser geometry with very few simplifying assumptions. The model was solved using a fully explicit time-integration scheme implemented in a parallel environment on an eight-processor cluster and 24G memory computer. There is a very good agreement obtained from numerical and analytical comparisons, which validates the use of the numerical model here. The results from the numerical simulation show that the numerical model considers various details of the riser. It has been shown that the detailed finite element model can be used to predict the riser's mechanics behaviour under various load cases and bound conditions |
| Nagham Amer Sami | Jitendra Sangwai | Bala Subramanian | 2013 | ResearchGate/Ijser | Gas hydrate applications and problems in the oil and gas industry | This paper presents a brief account of different applications and problems of gas hydrate in the oil and gas industry. Broadly, gas hydrate is a physical clathrate compound in which the molecules of gas are trapped in crystalline cells, formed from hydrogen bonds of water molecules. Gas hydrates can be formed from all the gases in the presence of water under different conditions of high pressures and low temperatures. The oil and gas industry for many years has taken strict measures to prevent gas from forming hydrates because of their annoying tendency to plug pipelines. However, natural gas hydrates that exist on earth in colder regions, such as permafrost, or sea bottom areas, are an unconventional energy resource available for mankind. The other positive applications are carbon dioxide sequestration, gas separation, and natural gas storage and transportation. Finally, the use of hydrate dissociation energy can be applied in refrigeration processes and cool storage. |

| | | | | | | |
|------------------|------------------------------|-----------------|------|--------------------------|---|---|
| Ali Bahtui | | | 2008 | PhD Thesis | Development of a Constitutive Model to Simulate Non-bonded Flexible Riser Pipe elements | The results of several numerical simulations for a riser of small-length, obtained with a very detailed (small-scale) non-linear finite-element model, are used to identify the parameters of the constitutive law, bridging in this way the small scale of the detailed finite-element simulations with the large scale of the beam model. The effectiveness of the proposed method is validated by the satisfactory agreement between the results of various detailed finite-element simulations for a short riser, subject to internal and external uniform pressures and cyclic bending and tensile loadings, with those given by the proposed constitutive law. The merit of the present constitutive law lies in the capturing of many important aspects of the riser's structural response, including the energy dissipation due to frictional slip between layers and the hysteretic response. This privilege allows one to accurately study the cyclic behaviour of non-bonded flexible risers subject to axial tension, bending moment, internal and external pressures. |
| Djihad Rial | Hocine Kebir | Eric Wintrebert | 2014 | Material&Design/Elsevier | Multiaxial fatigue analysis of a metal flexible pipe | In this paper, hydroformed metal corrugated tubes were subjected to a series of fatigue tests in which the amplitude of the mechanical fatigue load is constant, in addition to a constant inner pressure similar to the work conditions, which generate a three dimensional stress-strain states, then, the life of the structure was extracted in term of number of cycles at the crack initiation for different load configurations, further, a finite element model was created taking into account the residual stresses resulted from the hydroforming process, moreover, the numerical simulations were used to estimate and compare with the experiment the fatigue life by using different approaches: a stress-strain life approach which is widely used in commercial codes, a critical plane approach, an energy approach and a continuum damage based approach, then, it is shown that for these type of structures the critical plane model and the continuum damage model are more convenient to predict the fatigue life when the residual stresses are taken into account. |
| Gabriel Gonzalez | Jose Renato Mendes des Sousa | Luis Sagrilo | 2015 | Researchgate | A non-bonded flexible pipe finite element model | This paper presents a finite element model, entirely developed in ABAQUS® environment, fully capable of calculating stresses and strains in those several layers when subjected to different types of loads. The finite element model employs four nodes reduced integration shell elements. The inner layers, located below the first tensile armour, are condensed into a unique cylinder with its distinct properties well assured. The same assumption is applied to the layers placed above the second tensile armour. Moreover, rebar elements were considered for the carcass and pressure armour modelling. As for the tensile armours, each steel tendon is modelled individually by shell elements. The interactions between tensile armours tendons and between the tensile armours and the adjacent layers are handled with tangential and normal contact formulations. As a case study, a 2.5" non-bonded flexible pipe is considered under pure tension. The results obtained are compared to an existing analytical model as well as from previously |

| | | | | | | |
|-------------------|------------------|--------|------|----------------------------|---|---|
| | | | | | | published experimental data. All results agreed quite well. |
| Roberto Ramos Jr. | Alexandre Kawano | | 2015 | Marine Structures/Elsevier | Local structural analysis of flexible pipes subjected to traction, torsion and pressure loads | Helically armoured cables or pipes find a wide range of applications as structural members in engineering. An example of this is the increasing use of flexible pipes in oil offshore production. Although keeping a geometrical similarity with other helically armoured structures such as wire ropes and ACSR conductors, and borrowing from them a useful methodology for the structural analysis, some care must be taken in order not to indiscriminately use an approach which was not thought for a flexible pipe: internal and external pressures, for instance, are a great concern in the analysis of flexible pipes, but not for wire ropes. This work aims at giving some additional contribution to the structural response of flexible pipes when subjected to axisymmetric loads, including the effect of both internal and external pressure in pipe displacements. Derivation of linear operators, relating the stress resultants to their related displacements or deformations in each of the layers of the pipe, as well as the process of deriving an analogous linear operator to represent the behaviour of the pipe as a whole, are presented, highlighting interesting mathematical aspects and their associated physical meaning. A numerical case study of a 2.500 flexible pipe subjected to traction and internal pressure is also presented and discussed. |
| T.A. Anderson | M.E. Vermilyea | Vineel | 2013 | OTC | Qualification of Flexible Fibre-Reinforced Pipe for 10,000-Foot Water Depths | The combination of ultra-deep-water applications and large pipe diameter requirements presents severe engineering challenges for rigid pipe technology and remains outside the current flexible pipe qualification scope. To address those needs, General Electric, with the support of the Research Partnership to Secure Energy for America (RPSEA), has recently embarked on a development program to qualify flexible pipe with an internal diameter of greater than seven inches for ultra-deep-water applications. The program is based on a novel hybrid flexible riser technology that will be developed and qualified by a combination of design, analysis of performance, material and subcomponent testing, and finally a field trial. |

| | | | | | | |
|----------------------|------------|----------------|------|-------------------|--|---|
| Amadeu K. Sum | Carolyn A. | E. Dendy Sloan | 2012 | Energy and Fuels | Developing a Comprehensive Understanding and Model of Hydrate in Multiphase Flow: From Laboratory Measurements to Field applications | Gas hydrates pose a major flow assurance problem in the production and transportation of oil and gas. Managing the formation of gas hydrates is central for safe and continuous operation. In this paper, we will provide an overview of the Centre for Hydrate Research and its efforts toward a better understanding of the formation, agglomeration, and accumulation of hydrates in multiphase flow. This paper will discuss the projects in the Centre for Hydrate Research aimed at quantifying how hydrates can be managed by first understanding the fundamental processes for nucleation, growth, agglomeration, deposition, and plugging, knowledge in these areas that has been accumulated over decades of research. While still a work in progress, significant advances have been made in describing the hydrate formation in oil-dominated, water-dominated, and gas-dominated systems. One of the end goals of our effort is to develop the knowledge and tools to manage hydrates, as opposed to avoidance, in the production and transportation of oil and gas. It is recognized that the ideas and concepts introduced here are solely based on the efforts at the Centre for Hydrate Research with direct input from industry leaders in the field over decades; as such, there may be alternative views on the problem, but these are not considered here. However, the authors do not know of any published models that provide transient, multiphase prediction of hydrates in a flowline. |
| Zhijian Liu | | | 2017 | Publication | Study of hydrate deposition and sloughing of gas dominated pipelines using numerical and analytical models | To investigate the sloughing phenomenon in pipelines, the finite element method (FEM) is applied to study the internal stress distribution inside the hydrate deposit. The compact force induced by the momentum of upstream gas molecules will result in the collapse of hydrate deposits from the wall. This work also investigated the methods to characterize hydrate deposits: (1) pressure-temperature profile method, (2) back-pressure method, (3) average pressure method, and (4) pressure transient method. The combination of these methods can provide more detailed information about the deposit. |
| R. Cuamatzi-Melendez | | | 2017 | Ocean Engineering | Finite element and theoretical analysis of bisymmetric collapses in flexible risers for deep-water developments | Paper presents analytical and finite element strategies looking at ovality and eight mode collapses in the carcass layer. Paper found a difference in collapse loads for the ovality and eight mode collapse. For ovality, the development of a finite element model of the carcass only is enough, but for eight modes it is necessary to develop a finite element model including the carcass, internal polymer sheath, and pressure armour. Critical load for eight type collapse is higher because displacements are restricted by the pressure armour. The reports on analytical and finite element modelling strategies to predict carcass collapse failure. Two types of failure mode were presented - Ovality and eight types of collapse. The former occurs when the external pressure overcomes the carcass' structural collapse capacity and the latter when the external polymeric sheath is damaged, and water enters the annulus region. This creates hydrostatic pressure around the internal polymer sheet which transmits pressure to the carcass. This paper |

| | | | | | | |
|---------|--|--|------|-------------------|--|---|
| | | | | | | <p>highlights that non-metallic layers and tensile armours do not contribute to the collapse resistance and can therefore be neglected when predicting such failure modes. However, it should be noted that the internal polymer sheath and the pressure armour must be included in the model is to predict 8 type failure accurately. This is relevant to the work done in this paper as it provides an efficient way of cutting cost and computational time if these modes of failure are the desired results predicted by a finite element model. The loading and boundary conditions described in these papers could be mirrored on to the finite element model created here to validate that the model created the correct structural response. The papers described here are also of great value and relevance as they highlight conditions that are not expected and predict modes of failure when the external sheath is compromised which is neglected in the API 17B recommendations</p> |
| X. Yang | | | 2015 | Ocean Engineering | Numerical Analysis of buckling failure in flexible pipe tensile armour testing | <p>Paper presents a finite element model to evaluate critical instability load of tensile armour wires under external pressure and compression. The buckling load capacity and associated failure modes were obtained. Paper found critical load and failure mode strongly depend on friction and external pressure. Critical loads decrease with reduction of friction and external pressure. Four buckling modes identified:</p> <ol style="list-style-type: none"> 1. Lateral instability failure with very low friction when the critical load is sensitive with friction coefficient. 2. Lateral instability failure and the relationship between critical load and friction coefficient is linear. 3. Radial buckling without tape failure. 4. Failure of anti-buckling tape. He made a finite element model that was created to calculate the value of the critical instability load of tensile armour wires under external pressure and compression. The FEM employed in this research looks to reduce computational time by simplifying the interaction of other layers to spring element and equivalent beams. During installation, when the pipe is not in use and therefore not subject to internal pressure, the pipes are likely to be exposed to a high compressive force as well as cyclic bending which can induce local instability of the tensile armour layers. The armour wires are likely to experience large radial and lateral movement which in turn may result in buckling failure. Some pipes make use of high strength tapes which is introduced to provide resistance to the radial buckling mode (bird-caging). However, this can fail and in cases where it does not, lateral instability may still exist. In short, there are two types of failure that this paper underlines and they are dependent on the whether the annulus condition is wet or dry. In other words, when the external sheath is still intact the water pressure can provide extra support in terms of contact pressure and friction. The former condition applies when no pressure exists around the wires thus providing less contact pressure and friction resistance. Four modes of failure were detected and upon comparison to another FEM created on ABAQUS the use of curved beam elements provided increased |

| | | | | | | |
|---------------|--|--|------|-------------------------------|---|--|
| | | | | | | computation efficiency to a factor between 10 & 20. |
| J. De Sousa | | | 2010 | Journal of Offshore Mechanics | An experimental and numerical study on the axial compression response of flexible pipes | Paper deals with a nonlinear finite element model capable of predicting the mechanical response of flexible pipes subjected to axisymmetric loads focusing on their axial compression response. To validate this, experimental tests were also carried out. The paper also showed the response of the pipe to pure axial compression is linear. Axial compression stiffness, tension stiffness, but the pipe is torque balanced. Finite element analysis predicted the failure of the pipe by excessive radial expansion of the tensile armour wires, i.e. bird-caging. Finite element estimations were corroborated by experimental tests. It also explains clearly how different layers of a finite element model can be represented. In this case, he used the model to observe the effects of compression on the tensile armour of a 4" flexible pipe. A brief description of the carcass and pressure armours is included later in this work as the same theory is employed in the FEM used in this paper |
| M. Tang | | | 2015 | Applied Ocean Research | stress of a helical wire in non-bonded flexible pipes | Paper deals with seven analytical models available in the literature. 3D finite element model is developed for investigation of the seven models, the validity and limitations of these models were discussed. The paper shows good agreement between Costello's model and the 3D finite element model |
| M. T. Rahmati | | | 2017 | Applied Ocean Research | Experimental and numerical study of the structural behaviour of a flexible riser model | Paper carries out experimental tests and finite element analysis on a flexible riser model to evaluate the capability of the FEA to predict its non-linear structural response. Paper showed that the finite element bending moment-curvature relationship predicted captures several aspects of the experimental data. However, the amount of hysteresis predicted by the finite element model is lower than the measured one. Good agreement was found between axial strains at most locations. For transverse strains at the same locations, some good agreement was found, and some discrepancies. This may be due to inaccuracy in the modelling contact. |

| | | | | | | |
|---------------|--|--|------|-----------------------------|---|--|
| R. Ramos Jr | | | 2015 | Marine Structures | Local structures analysis of flexible pipes subjected to traction, torsion and pressure loads | The paper aims to give some additional contributions to the structural response of flexible pipes when subjected to axisymmetric loads. Paper found that the reduced (2x2) linear operator of a flexible pipe can only be obtained with the complete (4x4) linear operator. |
| D. Rial | | | 2013 | Materials and Design | Multiaxial fatigue analysis of a metal flexible pipe | General paper on metal flexible pipes. Not much relation to subsea usage. |
| M. A. Vaz | | | 2011 | Marine Structures | A finite element model for flexible pipe armour wire instability | Paper develops a finite element model to estimate the critical instability load and failure modes. A parametric case study is performed for a typical flexible pipe structure, where the friction coefficient between the wire armours and the external pressure is varied. Paper found both friction coefficient and external pressure influence the friction forces between the armour wires. The most critical condition is when the annulus is flooded, even though the net compressive force reduces because the friction coefficient substantially decrease, and hydrostatic pressure doesn't support the wires. Instability load and failure mode strongly depend on the friction coefficient and external pressure. Four instability modes were identified, two related to lateral instability, and the other two related to radial instability. |
| N. A. Sami | | | 2015 | Research Gate | Gas hydrate applications and problems in the oil and gas industry | Paper presents briefly the applications and more important problems of gas hydrates in the oil and gas industry. Explains what hydrates are, how they form, and the different types and structures |
| Y. Guo | | | 2016 | Petroleum | A prediction method of natural gas hydrate formation in deep-water gas wells and its application | Paper compares 5 prediction methods of hydrate formation with experimental data. A method based on OLGA and PVTsim for predicting the hydrate formation area was proposed. The paper shows hydrate formation area decreases with the increase of gas production, inhibitor concentrations and thickness of insulation materials, and increase in area with an increase of thermal conductivity of insulation materials. |
| Amadeu K. Sum | | | 2012 | Centre for Hydrate Research | Developing a comprehensive understanding and model of hydrate in multiphase flow: From the laboratory, measurements to field applications | The Paper gives an overview of the centre for Hydrate Research and its current research to provide a better understanding of the formation, agglomeration and accumulation of hydrates in multi-phase flow. The Paper discusses fundamental processes for nucleation, growth, agglomeration, deposition and plugging. Comparing oil-dominated, water-dominated and gas-dominated flows. The paper shows that for a gas-dominated system the main hydrate formation mechanism is deposition on the pipe wall, caused by water condensate. |

| | | | | | | |
|--------|--|--|------|-----------------|---|--|
| Z. Liu | | | 2017 | Doctoral Thesis | <p>Study of hydrate deposition and sloughing of gas dominated pipelines using numerical and analytical models</p> | <p>A very in-depth paper discussing hydrate formation mechanism and prediction models. An equation is developed to predict hydrate deposit thickness growth. The growth of hydrate deposits is mainly due to (1) water condensation on the pipe wall, and (2) direct hydrate deposition from the gas phase. The model is unverified using published experimental data.</p> <p>Investigation of hydrate sloughing risk, the mechanical properties of hydrate deposits are studied. Four different packing patterns are proposed.</p> <p>FEM was used to investigate the sloughing phenomenon in pipelines, to study internal stress distribution inside the hydrate deposit.</p> <p>The work in the report makes good progress in the area of hydrate deposition and sloughing mechanisms for gas dominated systems.</p> <p>Gas hydrates classify into 3 main types based on their crystalline structure. The structure I (usually found in nature), Structure II (usually found in pipelines) and structure H.</p> <p>Structure II is described by formula $8X \cdot 136H_2O$, where X could be N_2, C_3H_8, or $i-C_4H_{10}$.</p> |
| Witz | | | | | | <p>Witz conducted a study into the response of flexible pipelines under various loading conditions.²³ He then compared his results with the analytical solutions provided by 10 well-known institutions including Lloyds Register, Statoil and University College London. Some institutions chose to use purely mathematical models while others used computer simulation software. The pipe used in the study was a 2.5" version of the pipe used in this project</p> |